state-of-the-art magnetic resonance imaging IN THE WORK-UP OF PRIMARY HEPATOCELLULAR TUMORS

Indra Céline van den Bos

State-of-the-art MR Imaging in the Work-up of Primary Hepatocellular Tumors

Indra C van den Bos

State-of-the-art MR Imaging in the Work-up of Primary Hepatocellular Tumors

Magnetische kernspinresonantie in de diagnostiek van primaire levertumoren

PROEFSCHRIFT

ter verkrijging van de graad van doctor aan de
Erasmus Universiteit Rotterdam
op gezag van de
rector magnificus

Prof.dr. S.W.J. Lamberts

en volgens besluit van het College voor Promoties.

De openbare verdediging zal plaatsvinden op
woensdag 16 mei 2007 om 11.45 uur

Door

Indra Céline van den Bos
geboren te Rotterdam

ISBN: 978-90-9021644-7
Cover design and lay-out: Ton Everaers
Printed by: Print Partners Ipskamp

Illustrations: I.C. van den Bos
The figures in chapter 1.1 were provided by A. van den Bos and M.H.B van den Bos - van den Berg.

The printing of this thesis was financially supported by the department of Radiology of the Erasmus MC, University Medical Center Rotterdam, the Netherlands.

PROMOTIECOMMISSIE

Promotoren:

Prof.dr. S.M. Hussain
Prof.dr. G.P. Krestin

Overige leden:

Prof.dr. P.M.T. Pattynama
Prof.dr. J.N.M. IJzermans
Prof.dr. C. van Kuijk

Co-promotor:

Dr. R.A. de Man

For my parents
ANTONIE AND MEREL

CONTENTS

chapter1
INTRODUCTION

chapter1.1
general introduction

For accurate interpretation of MR imaging findings of hepatic diseases, UNDERSTANDING OF THE LIVER ANATOMY IS OF PARAMOUNT IMPORTANCE.

In this chapter, fundamentals of the liver anatomy and fundamentals of MR imaging of the hepatobiliary system will be discussed, followed by an overview of the research questions that are addressed in this dissertation.

Anatomy of the liver

The liver, located in the upper right abdomen, develops very early in embryogenesis. It is of endodermal origin, and arises from the hepatic diverticulum which is a midline outgrowth form the ventral wall of the future duodenum (foregut). The connective tissue of the liver on the other hand, is of mesenchymal origin. The liver has remarkable potential for regulation of its size, as is demonstrated in patients after partial liver surgery[1].

The high level metabolism within the liver is directly related to the hepatic blood flow, which comes from two main hepatic vessels: the hepatic artery which originates in the abdominal aorta; and the portal vein, which originates within the bowel wall as mesenteric vein (Fig. 1, overview of the liver anatomy). The hepatic artery accounts for approximately 25% of the blood flow to the liver, while the portal vein contributes to the remaining 75% of the hepatic flow[2].

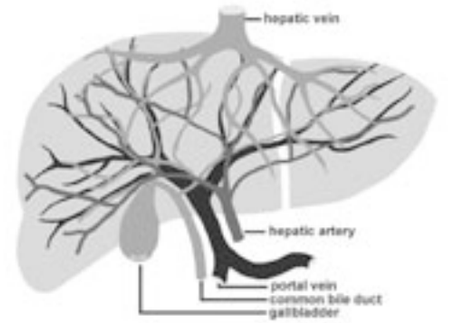

Figure 1: Overview of the liver anatomy

The metabolic function of the liver is facilitated by this dual blood supply. The total blood supply may vary considerably, depending on the feeding status and amount of exercise. Also, the proportions of blood supply divided among hepatic artery and portal vein may vary considerably. The inflowing blood is distributed and flows through the hepatic sinusoids, which are aligned in a columnar fashion. These columns of hepatocytes, which radiate from a central vein, are contained within a three-dimensional hexagonal unit (liver lobule) (Fig. 2). The hepatic vein is located in the center of the hexagonal liver lobule, for the outflow of metabolized blood into the caval vein (Fig. 3)[2].

Figure 2: Overview of the hexagonal liver lobule, with organization in sinusoids; six sets of three tubules surrounding the lobule (hepatic artery, portal vein and bile duct); and the hepatic vein in the center.

The liver has an important role in detoxification processes, including clearance of bilirubin resulting from breakdown of hemoglobin and other hem-containing substances; lipoprotein metabolism; cholesterol homeostasis; amino acid metabolism; protein synthesis; carbohydrate metabolism; and others. Many medications are absorbed within the liver, where an extensive set of enzyme systems are activated for metabolism of these agents. In addition, the liver is important in immune systems, as it contains a large pool of mononuclear phagocytes and natural killer cells. Kupffer cells, which are part of the reticuloendothelial system, provide an important role in the initiation of immunological responses as they act as the first line of defense against gut-derived foreign material. The bile duct system, including the intra- and extrahepatic bile ducts and the gallbladder, regulates bilirubin excretion, cholesterol homeostasis and absorption of dietary lipid in the intestine[2].

The liver is routinely divided in eight segments, according to Couinaud (Fig. 4)[3,4]. He described eight segments: one for the caudate lobe (segment I), three on the left (segments II, III and IV) and four on the right (segments V, VI, VII and VIII). The caudate lobe receives vessels both from the left and right branches of the portal vein and hepatic artery, its hepatic veins are independent and drain directly into the inferior vena cava. Recent studies suggest that the caudate lobe could be divided into a left part or Spiegel's lobe or segment I and the right part or segment IX or paracaval portion[5]. Identification of Couinaud's segments on cross-sectional imaging as well as during surgery is important for determination of the location of intrahepatic tumors relative to the intrahepatic vessels, for evaluation of respectability and extent of potential surgery. Even though this classification is sometimes questioned for its accuracy, it is routinely used in daily practice until an improved classification system becomes available[6].

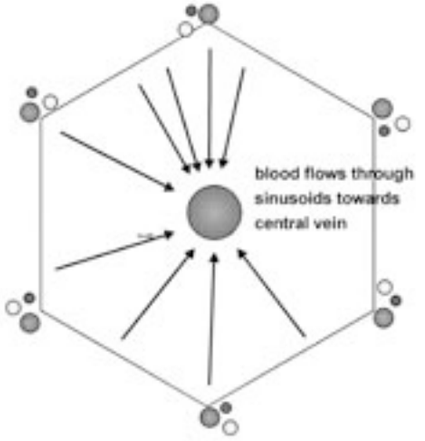

Figure 3: Schematic representation of intrahepatic blood flow

Many of the disease processes in the liver result in profound changes in the hepatic hemodynamics. In addition, almost all liver diseases are accompanied by damage to the hepatocytes, which can be observed as steatosis, atrophy, or cell death[2]. Liver diseases can be categorized as focal, or diffuse; and they can be congenital or acquired, including infections, auto-immune diseases, or (nodular) neoplasm's (primary or secondary). Diffuse liver diseases include a wide variety of metabolic (storage) diseases, including accumulation of iron within the liver (hemochromatosis or hemosiderosis), accumulation of copper, or fat (non-alcoholic fatty liver disease (NAFLD)); and hepatitis which may be either acute or chronic, associated with either an auto-immune etiology or with an infectious agent (hepatitis B and C virus are most common)[7]. Several of these disease entities may lead to fibrosis and cirrhosis and give rise to various types of hepatic nodules. According to an International Working Party, liver nodules are characterized by the regenerative, or dysplastic nature of the lesion. In addition, the characteristics of the surrounding liver parenchyma are considered[8]. The most important primary liver lesions are focal nodular hyperplasia (FNH), hepatocellular adenoma (HCA) and hepatocellular carcinoma (HCC), including the precursor nodules in the step-wise development of HCC: regenerative nodules (RN) and dysplastic nodules (DN).

MR imaging of the hepatobiliary system

An historical perspective

In 2003, Paul Lauterbur and Peter Mansfield were awarded the Nobel prize for Medicine for their pioneer work in the fundamentals of magnetic resonance imaging[9]. The potential of nuclear magnetic resonance (NMR), which was later called magnetic resonance imaging (MRI), was already known for many decades, since the publication of Walter Gerlach and Otto Stern in 1924. In this publication, they described the quantum nature of magnetic moment of silver atoms, by molecular beam deflection in an inhomogeneous magnetic field[9,10]. In 1952, Bloch and Purcell jointly received the Nobel Prize in Physics, for their independent description in 1946 of a physico-chemical phenomenon which was based upon the magnetic properties of certain nuclei in the periodic system. Their discoveries entailed that nuclei within a magnetic field absorbed energy, and re-emitted this energy when they returned to their normal state. The strength of the magnetic field matched the radiofrequency according to the so-called "Larmor" relationship. This was nuclear magnetic resonance, or NMR[11,12]. However, the exact origin of the NMR signal could not be determined within the sample, as all experiments had been one-dimensional and therefore lacked spatial information. In 1973, both Paul Lauterbur and

Peter Mansfield independently published a method for spatial localization of the NMR signals, by means of local magnetic field gradients[9,13,14]. Their discoveries laid the foundations of modern MR imaging.

Modern MR imaging

In today's daily practice, MR imaging is routinely applied in patients with a wide variety of abnormalities of the hepatobiliary system. MR imaging has evolved in a versatile imaging modality that allows adequate characterization of intrinsic tissue characteristics, by means of several imaging sequences based on different T1- and T2-weighting. In addition, multiple vascular phases can be imaged after intravenous contrast administration in a dynamic fashion, allowing characterization of focal or diffuse disease processes[15].

The currently used state-of-the-art MR imaging protocol typically consists of T1-weighted sequences with in- and opposed-phase (chemical shift) imaging; single-shot T2-weighted fast spin-echo (FSE) sequences; fat-suppressed T2-weighted sequences and dynamic multiphasic gadolinium-enhanced imaging. In addition, a heavily T2-weighted sequence may be added for evaluation of the biliary tree (magnetic resonance cholangiopancreatography, MRCP)[7].

Essentially, T1-weighted gradient-echo sequences provide information for characterization purposes, including information on material with high protein, fibrotic or fatty components. Fat-suppressed T2-weighted sequences are important for detection of liver nodules, because most nodules depict high signal intensity compared to the surrounding hepatic stroma. Dynamic contrast-enhanced multiphasic sequences demonstrate the enhancement pattern of the lesion, including amount of arterial enhancement, distribution of contrast within the lesion, washout characteristics and delayed enhancement of fibrotic components within or surrounding the lesion. The combination of these sequences results in adequate diagnosis in most cases, obviating the need for more invasive diagnostic strategies including percutaneous needle biopsy[7].

Aims of the study

The aim of the research projects described in this dissertation was to investigate and improve knowledge on MR imaging findings of primary hepatocellular tumors. Emphasis was put on non-invasive diagnostic possibilities in young women with focal nodular hyperplasia or hepatocellular adenoma and improved early diagnosis of developing hepatocellular carcinoma in cirrhosis. In addition, the potential of imaging on higher field MR imaging systems as well as post-processing of dynamic gadolinium-enhanced imaging data is assessed for the work-up of hepatobiliary diseases.

REFERENCES

1. MacSween FNM, Desmet VJ, Roskams T, Scothornej RJ. Developmental anatomy and normal structure. In: MacSween RNM, Burt AD, Portmann BC, ed. Pathology of the liver Churchill Livingstone 2002.
2. Burt AD, Day CP. Pathophysiology of the liver. In: MacSween RNM, Burt AD, Portmann BC, ed. Pathology of the liver. Churchill Livingstone 2002 67-104.
3. Couinaud C. Le foie: etudes anatomique et chirurgicales. Paris, 1957.
4. Couinaud C. Liver anatomy: portal (and suprahepatic) or biliary segmentation. Dig Surg 1999; 16:459-467.
5. Abdalla EK, Vauthey JN, Couinaud C. The caudate lobe of the liver: implications of embryology and anatomy for surgery. Surg Oncol Clin N Am 2002; 11:835-848.
6. Fischer L, Cardenas C, Thorn M, et al. Limits of Couinaud's liver segment classification: a quantitative computer-based three-dimensional analysis. J Comput Assist Tomogr 2002; 26:962-967.
7. Hussain SM. Liver MRI - correlation with other imaging modalities and histopathology. Berlin, Heidelberg, New York: Springer-Verlag, 2007.
8. International Working Party. Terminology of nodular hepatocellular lesions. Hepatology 1995; 22:983-993.
9. Geva T. Magnetic resonance imaging: historical perspective. J Cardiovasc Magn Reson 2006; 8:573-580.
10. Gerlach W, Stern O. Uber die richtungsquantelung im magnetfeld. Ann Phys 1924; 74:673.
11. Bloch F, Hanson W, Packard M. Nuclear Infraction. Phys Rev 1946; 69:127.
12. Purcell E, Torrey H, Pound R. Resonance absorption by nuclear magnetic moments in a solid. Phys Rev 1946; 69:37-38.
13. Mansfield P, Grannel PK. NMR "diffraction" in solids? J Phys C: Solid State Phys 1973; 6:422-426.
14. Lauterbur PC. Image formation by induced local interactions: examples of employing nuclear magnetic resonance. Nature 1973; 242:190-191.
15. Hussain SM, Semelka RC. Liver masses. Magn Reson Imaging Clin N Am 2005; 13:255-275

chapter1.2 outline

Outline of THE THESIS

This thesis describes the imaging findings of primary hepatocellular tumors on magnetic resonance imaging.

In **chapter 1**, a general introduction is provided, with an overview of the anatomy of the liver, fundamentals of MR imaging and current state-of-the-art MR imaging. In **chapter 2**, the imaging findings of focal nodular hyperplasia are discussed, including imaging findings before and after administration of two different contrast agents. In **chapter 3**, hepatocellular adenoma is reviewed and discussed, with special emphasis on imaging findings on MR imaging in correlation with histology findings of both liver and lesions. In addition, recent literature concerning a potential pathway for development of malignancy within hepatocellular adenoma is discussed. In **chapter 4**, hepatocellular carcinoma is discussed, with special emphasis on step-wise carcinogenesis in cirrhosis, and MR imaging findings in relation to the size of the tumor. In **chapter 5**, two optimization strategies for hepatobiliary imaging on higher magnetic field strength are discussed, including the application of variable-rate selective excitation and black-blood echo-planar imaging. In **chapter 6**, post-processing techniques including generation of color-encoded images and time-intensity curves are discussed, for improved analysis of multiphasic dynamic contrast-enhanced imaging. **In chapter 7**, a general discussion is provided with conclusions and recommendations for future research, followed by an overview article illustrating the current status of MR imaging of primary hepatocellular lesions. In **chapter 8**, the findings of this project are summarized.

introductionOUTLINE OF THE THESIS

chapter2
MR IMAGING OF FOCAL NODULAR HYPERPLASIA

Focal nodular hyperplasia: LESION CHARACTERISTICS AT STATE-OF-THE-ART MR IMAGING

including dynamic gadolinium-enhanced and superparamagnetic iron-oxide-uptake sequences in a prospective study.

ABSTRACT

Purpose: To image a cohort of patients with pathology-proven focal nodular hyperplasia (FNH) in order to assess which of the characteristics on state-of-the-art magnetic resonance (MR) imaging of the liver are most useful for improved detection and characterization of FNH.

Materials and Methods: In fourteen patients, pathology-proven FNH (n=33) were prospectively examined, using gadolinium and superparamagneticiron-oxide (SPIO) contrast media. All lesions were evaluated for signal intensity, fatty infiltration, central scar, mode of enhancement with gadolinium and uptake of SPIO. Percentages of dynamic contrast-enhancement in arterial, portal and delayed phases were assessed. Contrast-to-noise ratio (CNR) before and after administration of SPIO contrast was calculated.

Results: Signal intensity of the lesions was low to isointense on T1-weighted and intermediate to isointense on T2-weighted imaging. Fatty infiltration of the lesions was present in 6%. Percentage of enhancement in liver and lesion respectively were 110, 115, 95% and 151, 182, 160% (p<0.001). All lesions showed uptake of SPIO with improved conspicuity of central scar and septa. The CNR values pre-contrast and post-gadolinium/SPIO were significantly different for T1-weighted in- and opposed-phase and black-blood echo planar imaging.

Conclusion: Combination of dynamic gadolinium-enhanced imaging with T1- and T2-weighted sequences after administration of SPIO facilitates comprehensive evaluation of FNH.

Türkan Terkivatan, MD, PhD[1], Indra C. van den Bos, MD[2], Shahid M. Hussain, MD, PhD[2, 3], Piotr A. Wielopolski, PhD[2], Robert A. de Man, MD, PhD[4], Jan N.M. IJzermans, MD, PhD[1]

Departments of [1]Surgery, [2]Radiology, and [4]Gastroenterology and Hepatology, Erasmus MC, University Medical Center Rotterdam, The Netherlands, [3]Department of Radiology, University of Nebraska Medical Center, Omaha, NE, USA

Journal of Magnetic Resonance Imaging, 2006 Aug; 31;24(4): 864-872.

INTRODUCTION

Although focal nodular hyperplasia (FNH) of the liver is a well-described lesion in the literature, considerable diagnosis problems regarding this lesion still remain. Given the fact that FNH is the second most common benign liver tumor after hemangioma and has a reported prevalence of approximately 1%[1], definitive distinction between this benign liver lesion and other benign and malignant hepatic masses is a common dilemma. Since FNH is usually observed in young to middle-aged women and most often is asymptomatic, the main goal of imaging in these patients is to firmly establish the diagnosis in order to avoid unnecessary biopsy or surgical resection and to suggest a conservative approach to therapy[2,3].

Since morphology and radiological enhancement patterns of FNH is strongly determined by its histological composition, it is important to realize that this lesion is divided into two types: classic and non-classic[1]. According to one large pathology study, the non-classic type contains three subtypes (a) teleangiectatic FNH, (b) FNH with cytologic atypia, and (c) mixed hyperplastic and adenomatous FNH. More recently, a study based on DNA micro-array analysis suggested that teleangiectatic FNH had more similarities with hepatocellular adenomas than with FNH[4]. Classic FNH is characterized by the presence of (a) abnormal nodular architecture, (b) malformed vessels, and (c) cholangiolar proliferation. Nonclassic FNH lacks one of the following classic features – nodular abnormal architecture or malformed vessels – but always shows bile duct proliferation.

Typical magnetic resonance (MR) imaging features of FNH – that is iso- or hypointensity on T1-weighted images, slight hyper- or isointensity on T2-weighted images, and a hyperintense central scar on T2-weighted images – are seen in up to 84-100% of these lesions (Fig. 1)[5,6]. However, in our experience these imaging features alone are not diagnostic for FNH and have been observed in a number of benign and malignant lesions[7,8].

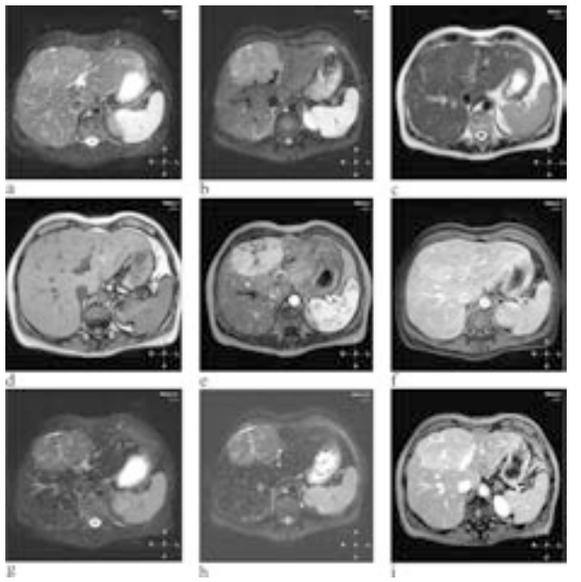

Figure 1: State-of-the-art MR imaging of classical FNH; signal intensity, enhancement patterns and uptake of SPIO. (a) Fat-suppressed T2-weighted fast spin-echo (FSE): large, well-circumscribed FNH in the left liver lobe, just slightly hyperintense to the liver, with a faint hyperintense septa. (b) Black-blood T2-weighted echo planar imaging (BBEPI): hyperintense signal intensity, with hyperintensity of central scar and septa. (c) Single-shot T2-weighted fast spin-echo (SSFSE): the lesion is isointense with the liver. (d) Opposed-phase T1-weighted gradient-echo (GRE): the lesion is isointense, with hypointense central scar, septa and pseudocapsule composed of compressed vessels. (e) Arterial phase gadolinium-enhanced T1-weighted GRE: immediate, homogeneous enhancement with sparing of central scar and septa. (f) Delayed phase gadolinium-enhanced 3D T1-weighted GRE: the signal intensity has faded to isointensity with the liver, with faint delayed enhancement of central scar, septa and pseudocapsule. (g) Post-SPIO fat-suppressed T2-weighted fast spin-echo (FSE): the liver and spleen have dropped in signal intensity after SPIO. The lesion is hyperintense, with slightly improved conspicuity of central scar and septa. (h) Post-SPIO diffusion T2-weighted black-blood echo planar imaging (BBEPI): better conspicuity of central scar and septa, with high signal intensity. (i) Post-SPIO opposed-phase T1-weighted gradient-echo (GRE): high signal of central scar and septa, especially when compared to delayed phase 3D dynamic gadolinium-enhanced imaging (f).

Dynamic gadolinium-enhanced MR imaging enables evaluation of the hemokinetics of contrast distribution during the first few minutes after injection. Related to the hypervascularity of the tumor, during the arterial phase of hepatic enhancement, FNH typically shows an immediate and intense enhancement, with the exception of the central scar, which has delayed enhancement caused by the presence of abundant fibrous stroma (Fig. 1)[9,10]. During portal or delayed venous phases the hyperintensity of the tumor fades, which results in an isointense lesion, with gradual diffusion of the contrast material into the fibrous central scar. On delayed phase imaging, the central scar shows high signal intensity because of the accumulation of contrast material.

Atypically, FNH may present as a large lesion, which is sometimes multiple in localization[5]. Rare imaging features include nonvisualization or nonenhancement of the central scar, and pseudocapsular enhancement on delayed images[9]. In these cases it may be difficult to differentiate an atypical FNH from other benign and malignant hypervascular liver lesions such as hepatocellular adenoma (HCA), hepatocellular carcinoma (HCC) and hypervascular metastases[11-13].

At our institute, we apply a state-of-the-art comprehensive MR imaging, which provides information concerning the soft tissue characteristics of the lesion besides the vascularity of the lesion at gadolinium-enhanced multiphasic dynamic imaging. In addition, in selected cases specific MR imaging contrast agents such as SPIO particles can provide information concerning the primary nature of the lesion[14,15].

Previous studies have described imaging features of FNH using both non-specific and specific contrast agents such as manganodipir[16] and superparamagnetic iron-oxide (SPIO) particles. In a few studies, uptake of SPIO and imaging characteristics of FNH were assessed using conventional MR sequences[17-21]. To our knowledge, none of the previous studies have evaluated lesion characteristics of pathology-proven FNH using both dynamic gadolinium-enhanced imaging and multiple T1- and T2-weighted sequences after gadolinium/SPIO.

The purpose of our prospective study was to image a cohort of patients with pathology-proven FNH in order to assess which of the characteristics derived from the state-of-the-art comprehensive MR imaging of the liver (including T1-weighted imaging, T2-weighted imaging with short and long TE-values, dynamic gadolinium-enhanced, multi-phasic imaging, and imaging after SPIO-uptake) were most useful for improved detection and characterization of FNH.

MATERIALS AND METHODS

Patients

The study was performed in a tertiary referral center

with large experience in hepatobiliary surgery and transplantation. Liver pathology reports of percutaneous needle biopsies that were performed between 1990 and 2003 were reviewed for the diagnosis of FNH. These data were matched with the hospital database to retrieve patients who were managed conservatively by observation of the lesion. Fifty-one patients had been evaluated for therapy by a hepatobiliary surgeon. In none of these patients a surgical treatment was indicated because of the absence of complaints. All of these 51 patients were contacted to take part in this prospective cohort study with the state-of-the-art MR imaging. Of those, 14 replied and provided informed consent. The local ethics committee granted approval for the study.
A total of 33 lesions were detected in 14 patients. The patients were all women with a mean age of 45 years (range, 30-68 years). Analysis of data was based on evaluation of each single lesion. The mean size of all lesions was 2.6 cm (range, 0.6-10.0 cm). Twenty-two lesions were located in the right lobe and 11 in the left lobe. A single lesion was depicted in 7 patients, and multiple lesions were present in the other 7 patients (2 lesions in 2 patients, 3 in 3 patients, 4 in 1 patient, and 9 in 1 patient).

MR imaging technique

The MR examinations were performed using a 1.5T unit (Philips Medical Systems, Best, The Netherlands or General Electrics, Signa, Milwaukee, WI, USA; identical scan protocols). A four-channel body-array coil with capability of sensitivity encoding (SENSE) was used. Scan sequences included single-shot fast spin-echo (SSFSE) (repetition-time (TR) msec/ echo-time (TE) msec 832/80-120; flip-angle 90º) with varying TE values (short and long TE, 80 and 120 msec respectively), fat-suppressed T2-weighted fast spin-echo (FSE) (3000/80, flip-angle 90º), diffusion T2-weighted black-blood echo-planar imaging (BBEPI) (shortest/60, flip-angle 90º) and T1-weighted in- and opposed-phase gradient-echo sequences (shortest/4.6 and 2.3 respectively, flip-angle 80º). In each patient, a timing bolus technique using 2ml of the same contrast agent followed by 15ml saline was used to accurately capture the arterial phase after the administration of gadolinium. After administration of an intravenous bolus of 30ml of non-liver specific gadolinium chelate (Magnevist [gadopentetate dimeglumine], Schering, Berlin, Germany), dynamic imaging with 2D T1-weighted gradient-echo sequences in at least 4 phases (pre-contrast, arterial, portal and delayed phases) was performed. The total dose of administered gadolinium was slightly increased in part to compensate for some signal loss due to the implementation of the parallel imaging. The portal phase was acquired 45 seconds, and delayed at least 120 seconds after the acquisition of the arterial phase. In addition, a delayed phase 3D T1-weighted gradient-echo sequence was performed at least 4 minutes after contrast injection, in which the evaluation of central scar and septa was done. A slice thickness of 7 mm was used in all sequences.
After completion of the gadolinium-enhanced imaging, a SPIO contrast agent (Ferrocarbutan, Schering AG, Berlin, Germany) was administered intravenously as a bolus of 1.4ml (>60 kg body weight). Ten minutes after the administration of SPIO imaging was performed using fat-suppressed T2-weighted FSE (3000/80, flip-angle 90º), BBEPI (shortest/60, flip-angle 90º), and T1-weighted in- and opposed-phase GRE sequences (shortest/4.6 and 2.3 respectively, flip-angle 80º) were performed. No adverse reactions were reported during the study.
The MR scan sequences, including SSFSE with short and long TE values, fat-suppressed T2-weighted FSE, diffusion T2-weighted BBEPI and T1-weighted in- and opposed-phase GRE sequences were complete for at least 29 lesions. In the following sequences, a few lesions were too small to visualize: 2 lesions on SSFSE sequences with short and long TE values (n=31) and 2 lesions on T1-weighted in- and opposed-phase GRE sequences (n=31). Because of technical problems with data acquisition, the following lesions were excluded for the following sequences: SSFSE with long TE values in one patient (2 lesions, n=29), fat-suppressed T2-weighted FSE sequence in 1 patient (3 lesions, n=30) and diffusion T2-weighted BBEPI in 2 patients (with 1 and 2 lesions, respectively; n=30). The dynamic series were available for 28 of 33 lesions after contrast enhancement with gadolinium and for 30 lesions after enhancement with a SPIO contrast agent. For post-enhancement evaluation of signal intensities of both the liver and the lesion, analysis was based on 30 lesions for T1-weighted in- and opposed-phase GRE sequences, 27 lesions for fat-suppressed T2-weighted FSE, and 23 lesions for BBEPI sequences.
Histologic proof of FNH was obtained in 14 of the 33 lesions (14 patients). In case of multiple lesions, a percutaneous needle biopsy was performed in the largest one. Nineteen lesions not confirmed at histology were at (follow-up) MR imaging identical to the biopsy-pathology-proven FNH. This is a common clinical practice, and it would have been unnecessary and unethical to biopsy all the lesions. The appearance of the lesions without biopsy remained unchanged at imaging during a period of at least 12 months.

Image analysis

All MR imaging exams were transported digitally using a picture archiving and communication system to a viewing station. The analysis of all liver lesions was performed by two radiologists in consensus and with the knowledge of the diagnosis of FNH.

The following MR items were assessed qualitatively and/or quantitatively: 1) liver surrounding the focal lesions (presence or absence of normal parenchyma, 2) diffuse and focal fatty infiltration, 3) focal non-steatosis, 4) iron deposition); 5) lesion localization according to the hepatic segment numbering system of Couinaud; 6) number and diameter of lesions; 7) signal intensity of lesions compared with normal parenchyma before and after intravenous administration of gadolinium and SPIO at T1- and T2-weighted images; 8) signal intensity characteristics of the lesions at unenhanced and contrast-enhanced T1-weighted images with regard to the surrounding liver parenchyma; 9) homogeneous or heterogeneous appearance; 10) presence of fatty infiltration within the lesion (in- and opposed-phase); 11) presence of a central scar, 12) presence of a pseudocapsule; 13) the uptake of SPIO, and 14) the conspicuity of the central scar and septa after the uptake of SPIO.
For quantitative image analysis, the signal intensity of the lesion and liver parenchyma was measured using operator-defined regions of interest (ROI). For the lesions, the largest possible region of interest in the lesion that excluded fibrotic areas was selected for measurement of signal intensity. For the liver, a region of interest that excluded vessels and artifacts was used to measure the signal intensity of the liver adjacent to the tumor. The ROI's were placed identically for both the unenhanced and contrast-enhanced images.
In dynamic gadolinium-enhanced imaging, enhancement patterns in arterial, portal en delayed phase imaging were subjectively evaluated. The lesion-to-liver contrast-to-noise ratio (CNR) was calculated as the difference in signal intensity between the lesion and the liver scaled to the standard deviation of background noise. The percentage of contrast enhancement was calculated for gadolinium-chelates and the SPIO agent as follows:$[(SI_{enhanced} - SI_{unenhanced}) / SI_{unenhanced}] \times 100$, where SI is signal intensity.

Statistical analysis

Statistical parameters (mean, median, standard deviation, and range) were calculated using the Statistical Package for the Social Sciences (SPSS) program. Significance levels were determined by two-tailed Mann-Whitney test analysis. The unit of measure in our statistical analysis was number of lesions, rather than number of patients.

RESULTS

Signal intensity of the lesions

At T1-weighted imaging, signal intensity of the lesions compared to the surrounding liver parenchyma was slightly lower to isointense at both in-phase T1-weighted GRE (30 of 31 lesions (96.8%)) and opposed-phase T1-weighted GRE (21 of 31 lesions (67.8%)) images. The lesions appeared relatively brighter to much brighter to the liver at opposed-phase T1-weighted GRE in 24.5% (8 of 31 lesions). This was caused by fatty infiltration of the liver parenchyma in those cases.
At T2-weighted imaging, the lesions showed an isointense to slightly higher signal intensity of the lesions at SSFSE T2-weighted images with short and long TE respectively (18 of 31 lesions (90.4%) and 26 of 29 lesions (89.6%)). This implied that the lesion and the liver behaved very similar on both sequences, most likely because of the solid nature as well as comparable tissue composition.
At fat-suppressed T2-weighted FSE and diffusion T2-weighted BBEPI, the lesions showed a slightly higher to much higher signal intensity in 28 of 30 lesions (93.3%) and 30 of 30 lesions (100%), respectively. In FSE, fat-suppression and fewer numbers of refocusing pulses per TR than SSFSE, most likely improved the liver-to-lesion contrast. In BBEPI, several factors improved the liver-to-lesion contrast, including 1) fat-suppression; 2) less magnetization transfer contrast effect than in FSE and SSFSE images due to the lack of refocusing pulses; 3) black-blood imaging based on the low diffusion-weighted gradient that dephased the signal from intrahepatic vessels; and 4) the application of the diffusion gradients was applied in all three orthogonal directions, and the composite image was a sum of three individual images. This improved the signal-to-noise ratio (SNR) of BBEPI.

Enhancement after gadolinium

In arterial phase imaging after the administration of gadolinium, an intense enhancement was observed in 27 of 28 lesions (95%). The enhancement was either completely homogeneous in 15 of 28 lesions (53.6%) or intensely homogeneous with sparing of septa and the central scar in 12 of 28 lesions (42.8%).
In the portal phase, most lesions remained higher or slightly higher in signal intensity compared to the surrounding liver parenchyma (18 of 28 lesions (64.2%)). The remaining lesions became almost isointense in 9 of 28 lesions (32.1%).
In the delayed phase, 11 of 28 (39.3%) lesions remained higher in signal intensity, whilst 14 of 28 (50%) lesions now showed an almost isointense signal intensity compared to the surrounding liver parenchyma. Enhancement of central scar and septa was noted in delayed phase imaging.
A quantitative analysis of the enhancement in the different phases showed a percentage increase of enhancement in liver parenchyma in arterial, portal and venous phases respectively of 110, 115 and 95%, and in the lesion this was 151, 182 and 160% ($p<0.001$) (Fig. 2). This shows that the lesions are typically hypervascular in the arterial phase, but behave in a similar

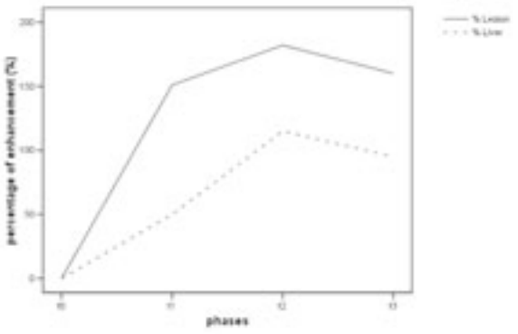

Figure 2: Percentage of enhancement of liver parenchyma and the lesion in arterial, portal and venous phases (p<0.0001). ((t0; pre-contrast phase, t1; arterial phase, t2; portal phase, t3; venous phase)

pattern as the surrounding liver parenchyma in the portal and delayed phases.

Signal intensity after SPIO-uptake

After administration of SPIO marked decrease in the signal intensity of the liver and spleen was observed at T2-weighted sequences, which indicated the accumulation of iron particles in the Kupffer cells. When compared to the same sequence before and after SPIO-uptake, all lesions showed loss of signal intensity. This finding, in fact, revealed the presence of Kupffer cells within the lesions and hence their hepatocellular origin. The lesions showed a marked uptake in 17 of 30 lesions (56.7%) and slight, but certainly present uptake in 13 of 30 lesions (43.3%). Conspicuity of specific lesion characteristics such as presence of a central scar and septa had improved in 90% (27 of 29) of the lesions.

A qualitative, subjective evaluation of signal intensity of the lesion compared to the surrounding liver parenchyma was repeated. At T1-weighted imaging, signal intensity was slightly higher to isointense at in-phase T1-weighted GRE (23 of 30 lesions (76.7%)) and slightly higher to much higher at opposed-phase T1-weighted GRE (30 lesions, 100%). This can be explained based on improved T1-weighting and less susceptibility artifacts due to relatively shorter TE value. At T2-weighted imaging, signal intensity of the lesions was slightly to much higher at both fat-suppressed T2-weighted FSE and diffusion T2-weighted BBEPI (26 of 27 lesions (96.3%) and 22 of 23 lesions (95.7%)).

Contrast-to-noise ratio before and after SPIO-uptake

Based on the measurements of signal intensity of lesion and surrounding liver parenchyma, CNR values of the lesions before and after SPIO-uptake were calculated. These values were as follows: T1-weighted in-phase -2.8 and 6.95 (p<0.0005), T1-weighted opposed-phase -0.44 and 1.65 (p<0.0005), fat-suppressed T2-weighted FSE 6.45 and 16.4 (p=0.9) and BBEPI 5.64 and 9.25 (p<0.05) (Figure 3). The values for T1-weighted in- and opposed-phase and BBEPI were significantly different. High CNR values in BBEPI demonstrated a more pronounced uptake in the liver parenchyma compared to the lesion, with sensitive detection through susceptibility (T2*) effects of iron particles in SPIO.

Miscellaneous findings

The liver parenchyma surrounding the lesions was normal in magnitude, shape and contour in 12 out of 14 cases (85.7%). Diffuse fatty infiltration of the liver was present in 3 out of 14 cases (21.4%), and focal fatty infiltration in 4 out of 14 cases (28.6%). Focal non-steatosis was seen in 2 of 14 cases (14.3%). Fatty infiltration within the lesion was noted in 2 of 33 lesions (6.1%). Visibility of a central scar and pseudocapsule varied between 3 and 15% of the lesions for different sequences, but was best in post-gadolinium sequences. Low detection rate of these characteristics can be explained by the relatively large amount of small lesions in this study.

DISCUSSION

In this study, a cohort of patients with pathology-proven FNH were examined to assess which of the characteristics derived from the state-of-the-art MR imaging of the liver are most useful for improved detection and characterization of FNH. The results of our study indicated that 1) the signal intensity of FNH was only slightly different from the surrounding liver on pre-contrast T1- and T2-weighted images; 2) chemical shift imaging showed fatty infiltration in a minority of FNH (6%) whereas the surrounding liver showed focal or diffuse fatty infiltration in up to 50% of the cases; 3) almost all lesions showed intense homogeneous enhancement (with or without intra-tumoral septal sparing) in the arterial phase after the administration of gadolinium; 4) the lesions faded almost to isointensity on the delayed phase; 5) the central scar and septa were visible only in a minority of patients; 6) all lesions showed uptake of SPIO with improved conspicuity of the central scar and septa; 7) most sensitive sequences to detect the SPIO-uptake were in- and opposed-phase T1-weighted GRE and diffusion T2-weighted BBEPI.

The results of our study indicate that the following characteristics are significant for the diagnosis of FNH. First, the similarity of the signal intensity with the surrounding (non-cirrhotic) liver should be considered

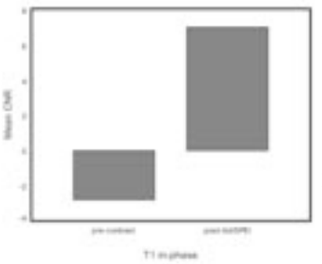

Figure 3: Contrast-to-noise ratio (CNR) before and after gadolinium and superparamagnetic iron-oxide (SPIO)-uptake in in-phase T1-weighted GRE, showing a significant increase in CNR after contrast enhancement (p<0.0005).

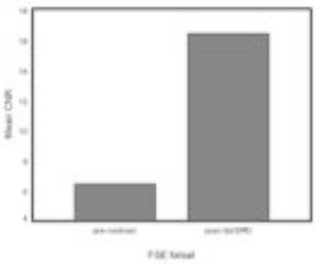

Figure 4: Contrast-to-noise ratio (CNR) before and after gadolinium and superparamagnetic iron-oxide (SPIO)-uptake in opposed-phase T1-weighted GRE, showing a significant increase in CNR after contrast enhancement (p<0.0005).

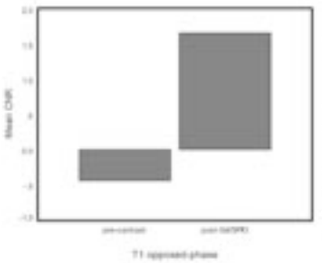

Figure 5: Contrast-to-noise ratio (CNR) before and after gadolinium and superparamagnetic iron-oxide (SPIO)-uptake in fat-suppressed T2-weighted FSE (FSE fatsat), showing a non-significant increase in CNR after contrast enhancement (p=0.9).

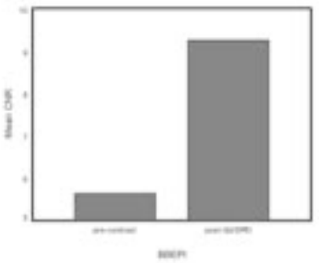

Figure 6: Contrast-to-noise ratio (CNR) before and after gadolinium and superparamagnetic iron-oxide (SPIO)-uptake in diffusion-weighted black-blood echo planar imaging (BBEPI), showing a significant increase in CNR after contrast enhancement (p<0.05).

as a strong indicator that the lesion is most likely of hepatocellular origin. Second, the presence of fatty infiltration in a relatively small number of lesions as well as in the surrounding liver is important. In our study, the lesions demonstrated fatty contents in only 6% of all lesions, confirming the fact that accumulation of fat inside FNH does occur but it is not a common finding. Other primary liver lesions that contain fat include HCA, and HCC. HCA may have fatty contents in up to 35-77% and HCC in 35%[22]. Third, the enhancement pattern at dynamic gadolinium-enhanced imaging is essential in the work-up of focal liver lesions. As shown in this study, in the case of FNH, lesions show intense enhancement in the early arterial phase, but show almost similar enhancement in the later phases; the lesions remain slightly more enhanced than the surrounding liver. This enhancement pattern is typical for primary solid liver lesions, such as FNH, HCA, and HCC. Particularly, HCA in which early arterial enhancement is often observed[23], but is often less intense compared to enhancement patterns observed in FNH[24]. As in FNH, HCA fades to near isointensity with the surrounding liver parenchyma in delayed phase imaging[23,24]. HCA, though, does not show any enhancing central scar and septa. In FNH, central scar and septa show high signal intensity at T2-weighted imaging, with enhancement in delayed phase imaging. Enhancement patterns in small HCC may show almost homogeneous enhancement in the arterial phase, but will often become heterogeneous (partial washout) or even homogeneously lower than the liver (complete washout). In addition, HCCs often shows enhanced tumor capsule in the delayed phase, and occurs in livers with parenchymal disease such as fibrosis and cirrhotic livers. HCC in non-cirrhotic liver are often single lesions with a large size and strong heterogeneous enhancement in the arterial phase. Other lesions such as hemangiomas and metastases have quite different signal intensities and enhancement patterns[24]. Hemangiomas typically enhance in a peripheral nodular fashion, with slow centripetal enhancement over time, to become and remain isointense with the liver in delayed phase imaging. Enhancement patterns in metastases may vary according to the origin of the malignancy. Colorectal metastases typically demonstrate ring-like arterial enhancement, with filling of the central areas of the lesion over time and washout of contrast material in the active peripheral border of the lesion[24]. Fourth, after administration of SPIO, all lesions showed uptake of contrast which caused signal loss in the lesion, the liver, and spleen on sequences with T2*-weighting, such as T2-weighted FSE, SSFSE, and BBEPI, and T1-weighted GRE sequences. The signal loss in the liver was most pronounced, followed by

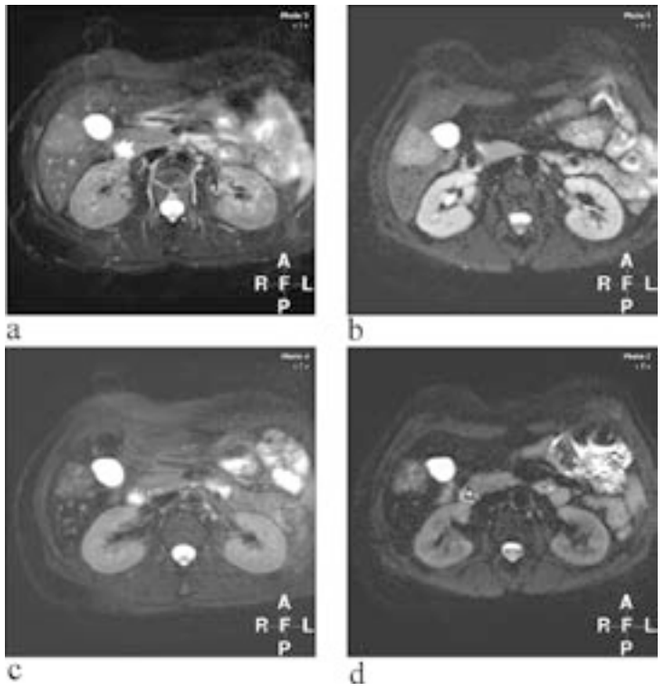

Figure 7: Improved conspicuity of central scar and septa after SPIO-uptake (a and b). Axial fat-suppressed T2-weighted fast spin echo (FSE) and axial T2-weighted black-blood (based on low diffusion gradients) echo planar imaging (BBEPI): images prior to SPIO-uptake show a slightly hyperintense lesion without any recognizable central scar. (c and d). Axial fat-suppressed T2-weighted FSE and T2-weighted diffusion BBEPI: the same images after SPIO-uptake show an improved visibility of the central scar, mainly due to loss of signal within the solid parts of the tumor.

the spleen and the lesions. It should be noticed that relatively more signal loss in the normal liver rendered FNH lesions brighter to the liver, which may improve the detection rate of FNH. The intratumoral signal loss was mainly present in areas with hepatocytes that were mostly arranged in small nodules. The septa and the central scar surrounding the intralesional nodules therefore appeared brighter with improved conspicuity (Fig. 7). This finding may improve the characterization of FNH, and may facilitate distinction from HCA.
In our study, a central scar was visible in only a minority of patients on standard dynamic gadolinium-enhanced imaging, which may well be explained by the relatively large amount of small lesions included. Since most classic FNH will show a central scar and septa on MR imaging, lack of these characteristics is likely to occur in a minority of cases only in daily practice. Our observation in this study was that in cases in which no clear central scar was visible, evaluation of additionally performed SPIO-enhanced images was often helpful for detection of this feature. It should be noted that even though lack of central scar may very well require biopsy, MR imaging provides complementary information concerning the morphology of both lesion and liver, including fatty content and vascularity. Also, in our experience, biopsies of especially smaller lesions may be inconclusive due to sampling variability and technical difficulties because many of these lesions may be difficult to see on ultrasound and/or CT for imaging guidance.
In our study, the most sensitive sequences in SPIO-enhanced imaging were BBEPI and T1-weighted GRE sequences. As demonstrated in the calculated CNR, T1-weighted sequences may be useful in analysis of lesions after gadolinium/SPIO. In particular, the opposed-phase T1-weighted sequence is useful, because of its shorter TE in combination with T2* effects of the administered SPIO. Although T1-weighted sequences are not commonly used in evaluation after gadolinium/SPIO, the ability of detection of intrinsic details, less artifacts in combination with high resolution compared to T2-weighted sequences make it a useful additional sequence, as has been demonstrated before[20,25]. In addition, high SNR and CNR in these sequences may allow a smaller amount of SPIO, which may facilitate further reduction of side effects.
The results of our study indicate that FNH may show complete homogeneous enhancement (without any septal sparing), especially in smaller lesions. It may also be difficult to assess the intensity of enhancement for differentiation from HCA. In such cases, T2-weighted images and gadolinium-enhanced T1-weighted images in the delayed phase should be carefully assessed for the presence of central scar and septa. In addition, SPIO-uptake may reveal the presence of central scar and septa, making the distinction between FNH and HCA. Also, in a recent study it is suggested that delayed imaging, 1-3 hours after administration of non-specific contrast material, may be helpful in differentiation between FNH and HCA[26].
Distinction between FNH and HCA is very important: 1) follow-up in pregnancy or use of oral anticonceptive medication; 2) risk for hemorrhage and malignancy; and 3) assessment of need of surgical or endovascular embolization treatment. At our institution, an asymptomatic single HCA of less than 5 cm in diameter or multiple HCA with variable diameters are subject to intensive follow-up with imaging and laboratory tests because of the risk of hemorrhage and malignancy. Whereas a single HCA larger than 5 cm or HCA with signs of malignancy at imaging (increasing size, changing density of signal intensity, changing enhancement, washout of contrast, enhancing fibrous tumor capsule) often will need surgical removal or at least biopsy. It is also important to know that HCA can present with intrahepatic or intraperitoneal hemorrhage that can be life threatening and may need intervention, including surgery or embolization.
Several studies have described imaging characteristics of focal liver lesions after administration of both specific and non-specific liver contrast agents. As has been described by Kim et al[20], Ba-Ssalamah[19] and Precetti et al[17], use of ferumoxide contrast agents may aid in better delineation of central scar and septa in FNH. Also, Paley et al[18] have shown a significant uptake of SPIO in pathology-proven FNH at T2-weighted imaging compared to other focal liver lesions. Recently, Scharitzer et al[16] have described the improved accuracy for differentiation between surgical and non-surgical liver lesions with mangafodipir-enhanced imaging. Few studies have evaluated the combined use of both gadolinium- and SPIO-enhanced imaging for focal liver lesions[19,21]. Ba-Ssalamah et al describe the imaging results of several focal liver lesions in separate imaging sessions for specific and non-specific contrast agents[19]. In addition to this study, we combine the use of dynamic gadolinium-enhanced imaging with T1- and T2-weighted imaging after administration of SPIO in one imaging session, to illustrate imaging findings of FNH using modern state-of-the-art MR sequences.
Our study has a limitation because of the relatively small cohort of patients. Only patients with an FNH lesion that was confirmed by percutaneous needle biopsy were included because histological proof is still considered to be the gold standard for diagnosis. However, since the introduction of state-of-the-art MR imaging at our department in 1999, FNH has been diagnosed non-invasively. Diagnosis of FNH is confirmed with at least one follow-up MR imaging examination at 6-12 months. Consequently, the small amount of patients that are included in this cohort were diagnosed with a needle biopsy before the availability of MR imaging or during analysis elsewhere before being admitted to our clinic.
In conclusion, our study indicates that combination of dynamic gadolinium-enhanced imaging with T1- and T2-weighted imaging after administration of SPIO facilitates detection and characterization of FNH. It is shown that: 1) signal intensity of FNH prior to contrast differs only slightly from the surrounding liver; 2) accumulation of fat is present in a minority of FNH; 3) enhancement of FNH is intense homogeneous in arterial phase imaging with fading to near isointensity in delayed phase imaging; 4) uptake of SPIO in FNH is pronounced with improved conspicuity of the central scar and septa. Most sensitive sequences to detect the SPIO-uptake are in- and opposed-phase T1-weighted GRE and diffusion T2-weighted BBEPI.

REFERENCES

1. Nguyen BN, Flejou JF, Terris B, Belghiti J, Degott C. Focal nodular hyperplasia of the liver: a comprehensive pathologic study of 305 lesions and recognition of new histologic forms. Am J Surg Pathol 1999; 23:1441-1454.
2. Charny CK, Jarnagin WR, Schwartz LH, et al. Management of 155 patients with benign liver tumors. Br J Surg 2001; 88:808-813.
3. Terkivatan T, de Wilt JH, De Man RA, et al. Indications and long-term outcome of treatment for benign hepatic tumors: a critical appraisal. Arch Surg 2001; 136:1033-1038.
4. Paradis V, Benzekri A, Dargere D, et al. Telangiectatic focal nodular hyperplasia: a variant of hepatocellular adenoma. Gastroenterology 2004; 126:1323-1329.
5. Mortele KJ, Praet M, Van Vlierberghe H, Kunnen M, Ros PR. CT and MR imaging findings in focal nodular hyperplasia of the liver: radiologic-pathologic correlation. AJR Am J Roentgenol 2000; 175:687-692.
6. Martin DR, Semelka RC. Imaging of benign and malignant focal liver lesions. Magn Reson Imaging Clin N Am 2001; 9:785-802.
7. Semelka RC, Martin DR, Balci C, Lance T. Focal liver lesions: comparison of dual-phase CT and multisequence multiplanar MR imaging including dynamic gadolinium enhancement. J Magn Reson Imaging 2001; 13:397-401.
8. Mahfouz AE, Hamm B, Taupitz M, Wolf KJ. Hypervascular liver lesions: differentiation of focal nodular hyperplasia from malignant tumors with dynamic gadolinium-enhanced MR imaging. Radiology 1993; 186:133-138.
9. Hussain SM, Zondervan PE, IJzermans JN, Schalm SW, De Man RA, Krestin GP. Benign versus malignant hepatic nodules: MR imaging findings with pathologic correlation. Radiographics 2002; 22:1023-1036.
10. Hussain SM, Terkivatan T, Zondervan PE, et al. Focal nodular hyperplasia: findings at state-of-the-art MR imaging, US, CT, and pathologic analysis. Radiographics 2004; 24:3-17.
11. Marti-Bonmati L, Casillas C, Dosda R. Enhancement characteristics of hepatic focal nodular hy-

focal nodular hyperplasiaLESION CHARACTERISTICS

perplasia and its scar by dynamic magnetic resonance imaging. MAGMA 2000; 10:200-204.
12. Mathieu D, Vilgrain V, Mahfouz AE, Anglade MC, Vullierme MP, Denys A. Benign liver tumors. Magn Reson Imaging Clin N Am 1997; 5:255-288.
13. Motohara T, Semelka RC, Nagase L. MR imaging of benign hepatic tumors. Magn Reson Imaging Clin N Am 2002; 10:1-14.
14. Semelka RC, Helmberger TK. Contrast agents for MR imaging of the liver. Radiology 2001; 218:27-38.
15. Helmberger T, Semelka RC. New contrast agents for imaging the liver. Magn Reson Imaging Clin N Am 2001; 9:745-766.
16. Scharitzer M, Schima W, Schober E, et al. Characterization of hepatocellular tumors: value of mangafodipir-enhanced magnetic resonance imaging. J Comput Assist Tomogr 2005; 29:181-190.
17. Precetti-Morel S, Bellin MF, Ghebontni L, et al. Focal nodular hyperplasia of the liver on ferumoxides-enhanced MR imaging: features on conventional spin-echo, fast spin-echo and gradient-echo pulse sequences. Eur Radiol 1999; 9:1535-1542.
18. Paley MR, Mergo PJ, Torres GM, Ros PR. Characterization of focal hepatic lesions with ferumoxides-enhanced T2-weighted MR imaging. AJR Am J Roentgenol 2000; 175:159-163.
19. Ba-Ssalamah A, Schima W, Schmook MT, et al. Atypical focal nodular hyperplasia of the liver: imaging features of nonspecific and liver-specific MR contrast agents. AJR Am J Roentgenol 2002; 179:1447-1456.
20. Kim JH, Kim MJ, Suh SH, Chung JJ, Yoo HS, Lee JT. Characterization of focal hepatic lesions with ferumoxides-enhanced MR imaging: utility of T1-weighted spoiled gradient recalled echo images using different echo times. J Magn Reson Imaging 2002; 15:573-583.
21. Takahama K, Amano Y, Hayashi H, Ishihara M, Kumazaki T. Detection and characterization of focal liver lesions using superparamagnetic iron oxide-enhanced magnetic resonance imaging: comparison between ferumoxides-enhanced T1-weighted imaging and delayed-phase gadolinium-enhanced T1-weighted imaging. Abdom Imaging 2003; 28:525-530.
22. Prasad SR, Wang H, Rosas H, et al. Fat-containing lesions of the liver: radiologic-pathologic correlation. Radiographics 2005; 25:321-331.
23. Elsayes KM, Narra VR, Yin Y, Mukundan G, Lammle M, Brown JJ. Focal hepatic lesions: diagnostic value of enhancement pattern approach with contrast-enhanced 3D gradient-echo MR imaging. Radiographics 2005 25:1299-1320.
24. Hussain SM, Semelka RC. Liver masses. Magn Reson Imaging Clin N Am 2005; 13:255-275.
25. Oudkerk M, van den Heuvel AG, Wielopolski PA, Schmitz PI, Borel R, I, Wiggers T. Hepatic lesions: detection with ferumoxide-enhanced T1-weighted MR imaging. Radiology 1997; 203:449-456.
26. Grazioli L, Morana G, Kirchin MA, Schneider G. Accurate differentiation of focal nodular hyperplasia from hepatic adenoma at gadobenate dimeglumine-enhanced MR imaging: prospective study. Radiology 2005; 236:166-177.

chapter3
MR IMAGING OF HEPATO-CELLULAR ADENOMA

chapter3.1
hepatocellular adenoma, a review of imaging findings

Hepatocellular adenoma: FINDINGS AT ULTRA-SOUND, COMPUTED TOMOGRAPHY,

MR imaging and pathologic analysis

ABSTRACT

The purpose of this paper is to describe the most recent concepts and pertinent findings of hepatocellular adenomas, including clinical presentation, gross pathology and histology, pathogenesis and transformation into hepatocellular carcinoma, and imaging findings at ultrasound, computed tomography, and magnetic resonance (MR) imaging.

INTRODUCTION

Before the introduction of oral contraceptives (OC) in the 1960s, hepatocellular adenoma (HCA) was a rare hepatic tumor[1]. In fact, only two cases of HCA were found in a review of 50.000 autopsies performed during the 36 years before 1954[2]. During the late 1960s, Edmondson and colleagues observed a sudden increase in presented patients with HCA. In their study, a significant difference between cases and matched controls in mean months of OC use was found: 73.4 as compared to 36.2 ($p<0.001$)[3]. In 1979, a more extensive epidemiological survey was performed in 79 women with HCA and 220 matched controls, which also confirmed a relationship between OC use and HCA[4]. In addition, this study showed that in women who had never used OC or used them for less than 24 months, HCA developed at an annual rate of about 1.0-1.3 per million, whereas long-term users of OC had an estimated annual incidence of HCA of 3.4 per 100,000 which is 25-fold higher[4]. It should be noted that these figures are based on OC with much higher hormonal levels compared to new generation OC's. Later studies suggest that modern OC's are safer with less tendency to developing HCA[5]. Non-OC-related causes of HCA include glycogen storage diseases or hormonal stimulation from other sources, for instance anabolic steroid use by body builders, gynecological tumors, and pregnancy. Rarely, HCA is reported in men[6,7], probably related to use of anabolic steroids or based on abnormal stimulus from an endogenous source. It is important to note that HCA may present with potentially life-threatening hemorrhage, and some HCA may develop or present with a hepatocellular carcinoma (HCC)[4].

On ultrasound (US) and computed tomography (CT), distinction of HCA from other hepatic abnormalities may be difficult because these modalities, unlike MR imaging, lack information concerning tissue characteristics of the lesions. Currently, CT is increasingly applied for assessment of liver lesions. However, it should be kept in mind that in case of a mono-phasic CT or incorrect timing of the arterial phase, HCA can easily be misdiagnosed, exposing patients to unnecessary delay in diagnosis and proper management. Familiarity with clinical presentation, pathology and imaging findings of HCA, particularly at state-of-the-art MR imaging, facilitates distinction from other hepatic lesions and ensures proper treatment[8]. The purpose of this paper is to describe the most recent concepts and pertinent findings of hepatocellular adenomas, including the clinical presentation, gross pathology and histology, pathogenesis and transformation into hepatocellular carcinoma (HCC), and imaging findings at US, CT, and MR imaging.

Shahid M. Hussain, MD, PhD[1*], Indra C. van den Bos, MD[1], Roy S. Dwarkasing, MD[1], Jan-Willem Kuiper, MD[1], Jan den Hollander, MD[2]

Departments of [1]Radiology and [2]Pathology, Erasmus MC, University Medical Center Rotterdam, The Netherlands, [*]Department of Radiology, University of Nebraska Medical Center, Omaha, NE, USA

European Radiology, 2006 Sep; 16(9): 1873-86

Gross pathology and histology

In 1995, the International Working Party classified HCA as neoplastic lesions, composed of hepatocytes which show histological characteristics of abnormal growth caused by presumed or pathology-proven genetic alteration[9]. Hepatic adenomas are well-circumscribed solitary lesions, often with hemorrhage and/or necrosis, in a majority of cases (Fig. 1). At histology, HCA solely consists of liver cells, arranged in plates that are not thicker than two to three cells. The plates are arranged in sheets and cords, devoid of lobular pattern due to absence of portal areas, and separated by slit-like sinusoids lined by epithelium. Lack of bile ductules facilitates distinction from focal nodular hyperplasia (FNH). Mitosis in HCAs are absent or few. In contrast to most HCC, the normal reticulin pattern is well preserved[10]. Despite earlier reports, Kupffer cells are present in liver cell adenomas[11]. These Kupffer cells are reduced in number and perhaps also less functional, which explains the diminished uptake of technetium-99m sulfur colloid. In a recent study, fat within HCA was observed in up to 70% of the cases[12]. Large tortuous arteries and dilated, thin-walled veins are often present, with large veins draining the lesions, which denotes the hypervascular nature of HCA. In addition, HCAs lack a true, fibrous, tumor capsule, which is a characteristic sign of larger HCC[13]. Therefore, hemorrhage may spread into the liver or abdominal cavity.

Histologically, there is no difference among the adenomas arising as single lesions, multiple lesions (2-6 lesions), and liver adenomatosis (>10 lesions)[9,10,14]. Previously, some reports suggested that liver adenomatosis occurred in a different population and the changes in size of these adenomas did not depend on OC use[15]. Recent reports as well as our own experience contradict this. Therefore, it is likely that "hepatocellular adenomas" and "liver adenomatosis" are two manifestations of the same underlying disease.

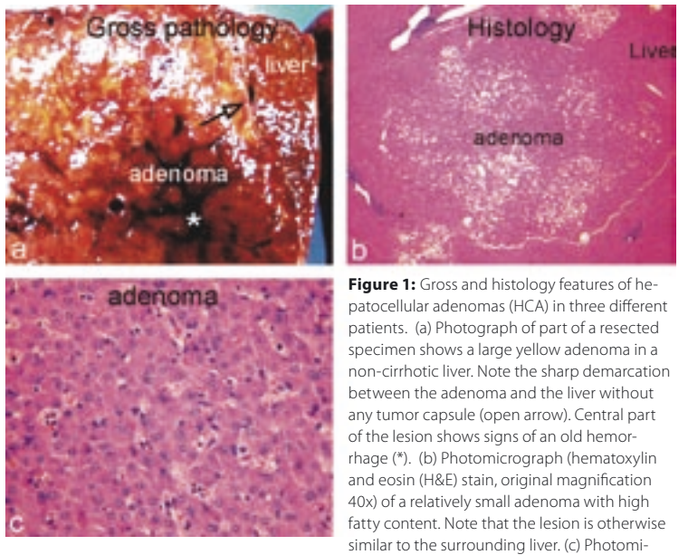

Figure 1: Gross and histology features of hepatocellular adenomas (HCA) in three different patients. (a) Photograph of part of a resected specimen shows a large yellow adenoma in a non-cirrhotic liver. Note the sharp demarcation between the adenoma and the liver without any tumor capsule (open arrow). Central part of the lesion shows signs of an old hemorrhage (*). (b) Photomicrograph (hematoxylin and eosin (H&E) stain, original magnification 40x) of a relatively small adenoma with high fatty content. Note that the lesion is otherwise similar to the surrounding liver. (c) Photomicrograph (H&E stain, original magnification 200x) of an adenoma shows almost normal hepatocyte with increased cellularity and normal cytoplasm-to-nuclear ratio. Note that most plates are not thicker than two cells and the sinusoids are slit-like and variable in shape.

Lesions formerly known as "teleangiectatic focal nodular hyperplasia (TFNH)" are now considered to be a variant of HCA, since a recent study[16] showed the molecular profile is much closer to the profile of hepatocellular adenomas than typical FNH. However, more recently, Bioulac and colleagues have illustrated molecular patterns and morphologic features of TFNH which suggest that these lesions do in fact show similarities with HCA and should therefore be treated in the same way, but probably be regarded as a separate entity[17].

Pathogenesis of HCA and transformation into HCC

The exact pathogenesis of HCA is not known. Based on a detailed pathologic analysis of various types of lesions that occur in patients with liver adenomatosis, the following sequence of events was hypothesized: focus → group of foci → nodule → micro-adenoma → adenoma[14]. Malignant transformation of HCA into HCC has been described in the literature by several groups[18-22]. Most authors have reported transformation of an existing HCA into HCC. Gordon and colleagues, however, reported a case of HCC after complete regression of HCA at the same anatomic location[18]. At this point in time, it is not quite clear if all HCAs eventually can transform into HCCs. Also, the exact characteristics of HCAs that eventually may undergo malignant transformation are not well known. Currently, most authors consider increase in size of the lesion at imaging, increased serum alfa-fetoprotein, and suspicious findings at fine-needle-aspiration-biopsy (for histological criteria of HCA versus HCC, please see text below) as signs of malignant transformation of HCA.

In this context, Tao recently published remarkable findings of his study based on 1673 patients who had undergone a fine-needle-aspiration-biopsy of liver mass or masses between 1976 and 1990[20]. In this study, 99 of 1973 (5.9%) patients were diagnosed with HCC[20]. Among them, three patients were long-term (> 10 years) OC users. Another 9 of 1673 (0.54%) were diagnosed with HCA. Two of these 9 patients (OC use: 8 and 10 years respectively) showed foci of liver cell dysplasia (LCD) within HCA at histological analysis. LCD was defined as a) cytoplasmic and nuclear enlargement, b) nuclear pleomorphism as well as prominent nuclei, c) hyperchromasia and multinucleation. The cytological features strikingly mimic HCC. Therefore, the author suggested that LCD should be considered the missing link between HCA and HCC[20]. In addition, the author also suggested that HCA is not pre-malignant and may undergo reversible change

after withdrawal of OC, whereas LCD is an irreversible, pre-malignant change and will eventually progress to HCC (HCA-LCD-HCC sequence) (Fig. 2).
The concept of Tao[20] can explain some of the issues

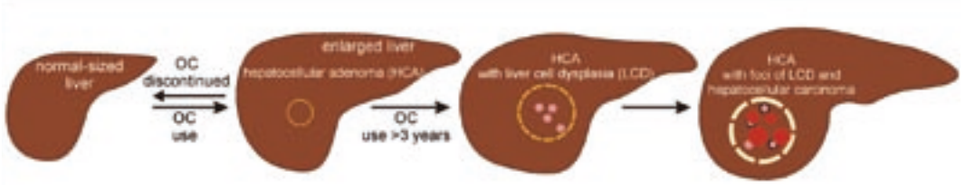

Figure 2: HCA-HCC sequence. Drawing illustrates recently discovered various steps in hepatocellular adenoma (HCA) and hepatocellular carcinoma (HCC) sequence. After the use of oral contraceptives (OC) for a certain period, the liver shows altered shape and enlargement with the development of one or more HCA. This step is considered to be reversible if OC use is discontinued. Therefore, most recently HCA is not considered as a pre-malignant lesion. During this phase, fatty infiltration within the lesion(s) as well as in the liver may concur and coexist. With the continuous use of OC (probably longer than three years), liver cell dysplasia (LCD) develops within HCA. HCA with foci of LCD is considered as a pre-malignant lesion. The areas with LCD gradually transform into foci of HCC. Eventually, the foci of HCC coalesce to form a large HCC. After the development of LCD, the sequence of events is thought to be irreversible. Therefore, HCC may also develop at the location of a HCA, even if that particular HCA has regressed or disappeared at imaging. In addition to OC, other (genetic) factors play a role in the HCA-HCC sequence.

regarding the malignant transformation of HCA, including 1) HCA-LCD-HCC sequence has two important similarities with the previously described stepwise carcinogenesis of HCC in cirrhotic liver[13, 23] in the sense that LCD plays a crucial role in both pathways, and LCD in HCA is histologically identical to LCD in dysplastic nodules in cirrhosis; 2) why not all HCAs undergo malignant transformation; and 3) why HCC can occur at the same anatomic location even after complete regression of an HCA as described by Gordon and colleagues[18].

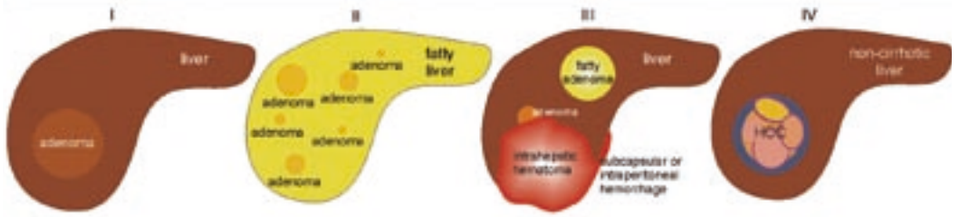

Figure 3: Many faces of hepatocellular adenomas. I) A non-fatty single lesion in a non-fatty liver: the lesion appears very similar to the surrounding liver. II) Multiple HCAs within a fatty liver. III) Fatty HCA and small HCAs associated with intra- and extra-hepatic hematomas. IV) Hepatocellular carcinomas (HCC) may arise from HCAs or at the same anatomic location after regression of HCA. Note the confluent nodules of HCC contained within a thick fibrous tumor capsule.

The distinction between HCA and well-differentiated HCC at times may be impossible at histology[10]. The following findings may indicate HCC: a) liver-cell plates more than three cells thickness; b) decreased nuclear/cytoplasm ratio; c) prominent nucleoli; d) mitosis; e) loss of reticulin pattern; f) absence of Kupffer cells; g) presence of vascular invasion; and h) stainable alfa-fetoprotein. However, none of these features can be relied upon with certainty as some may rarely be seen in HCA and others are common in well-differentiated HCC[10]. For pathologists, the most helpful, perhaps, are the thickness of the cell plates, amount of reticulin, and vascular invasion. This is one of the important reasons why a US-guided biopsy of a primary liver lesion with suspicion of malignancy may not be the solution, and either follow-up with (MR) imaging or even resection of the lesion may be preferred to biopsy depending on the level of suspicion.

IMAGING OF HCA

At imaging, hepatocellular adenomas (HCAs) may appear heterogeneous reflecting the histological nature, the complex anatomy and composition of the lesions, and the mode of presentation at the time of the diagnosis (Fig. 3). Heterogeneity is most likely associated with relatively larger lesions containing hemorrhage, necrosis, fibrosis and malignant transformation. Patients with such lesions are more likely to be symptomatic with higher chance of getting an imaging examination. This may explain the fact that in most publications based on imaging HCAs are large (> 5 cm) and complex in nature[24-31]. Some authors therefore consider "heterogeneity" as the hallmark of HCAs at imaging.

In our experience, relatively small HCAs without hemorrhage and necrosis are often asymptomatic, discovered as incidental findings at cross-sectional imaging, and are more likely to appear as homogenous lesions, particularly at CT and MR imaging.

Ultrasound

HCAs without abundant necrosis, hemorrhage or malignant degeneration, will most likely have a homogenous appearance with somewhat variable echogenicity, which depends on the structural composition of the lesions as well as the surrounding liver (Fig. 4). Mathieu and colleagues described the US appearance in 27 HCAs as follows: 11 of 27 (41%) hypoechoic, 8 of 27 (30%) hyperechoic, 6 of 27 (22%) isoechoic, and 2 of 27 (7%) with mixed echogenicity[32]. In another study, five patients underwent US: 4 of 5 (80%) lesions had mixed echogenicity and in 1 of 5 (20%) the lesion was clearly hypoechoic[32]. The sensitivity and specificity of US for HCA is not well-known. In general, the sensitivity of US for liver lesions is about 50%[33, 34]. In liver adenomatosis, using US, fewer lesions were detected than using CT or MRI, and most of the lesions were somewhat heterogeneous but predominantly hypoechoic[23]. Echogenicity of liver lesions in general and of HCAs in particular depends on two main factors: 1) architecture of the lesions, and particularly solid versus non-solid components as well as the number of interfaces that influence sound transmission, etc.); 2) architecture of the surrounding liver (normal parenchyma versus parenchyma with diffuse (depositional) disease). Therefore, HCA with abundant fat, fibrosis, or hemorrhage will appear as echogenic lesions compared to the surrounding liver. However, HCAs within fatty liver are likely to appear hypoechoic compared to the surrounding liver tissue.

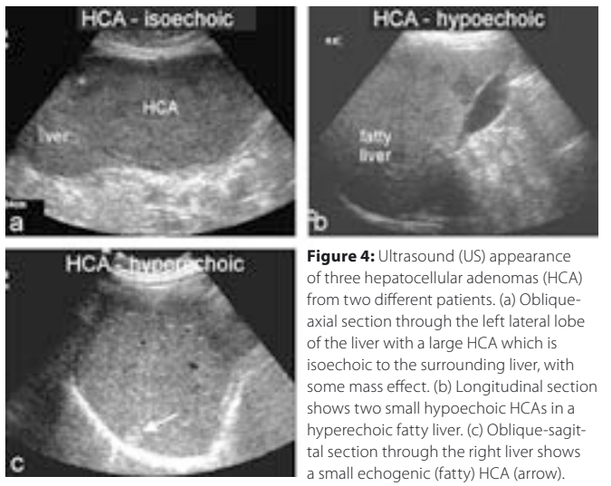

Figure 4: Ultrasound (US) appearance of three hepatocellular adenomas (HCA) from two different patients. (a) Oblique-axial section through the left lateral lobe of the liver with a large HCA which is isoechoic to the surrounding liver, with some mass effect. (b) Longitudinal section shows two small hypoechoic HCAs in a hyperechoic fatty liver. (c) Oblique-sagittal section through the right liver shows a small echogenic (fatty) HCA (arrow).

According to Mathieu et al, at US, HCAs and FNHs are indistinguishable with all echo-structural patterns observed in both types of lesions[32]. Based on Doppler, several authors[25,35] have demonstrated a continuous (venous) wave form in a majority of HCAs as opposed to the pulsatile wave within malignant tumors like HCC. In these studies, relatively larger HCAs (mean diameter > 5 cm) were examined. In smaller lesions with small vessels, it may be technically difficult to visualize reproducible Doppler signal findings. In our experience with various imaging modalities for hepatic imaging, it is often challenging - if not impossible - to diagnose HCA at US with confidence[33].

Several developments, including tissue harmonics, contrast harmonics, real-time spatial compound imaging, adaptive real-time image processing, panoramic and three-dimensional imaging, and real-time reformatting, have consolidated the role of US in the current clinical practice[33]. For hepatic imaging and in particular for diagnosis of primary liver lesions, though, the (fundamental) limitations of ultrasound remain. These include operator-dependency with low reproducibility, lack of overview of the anatomy, lack of (technical) ability to change the intrinsic tissue contrast. Contrast agents facilitate the characterization of solitary known liver lesions as has been described by several authors before[26,36,37]. A limitation of this examination however, is that surveying the entire liver after contrast administration is not possible, which is virtually always an important aspect of a liver study. Multiple liver lesions may be present, including multiple lesions of different benign and malignant histologies. These limitations result in low sensitivity and specificity of US for liver abnormalities. In many centers, the clinical and surgical decision making does not take place based on the US of the liver alone[33].

Computed Tomography

At CT, HCA without complications are likely to be isodense with the surrounding liver on unenhanced CT, and become visible in the arterial phase with a homogenous blush of contrast enhancement, and then fade to isodensity on the portal or delayed phase (Fig. 5a and b). Typically, on unenhanced CT scans hepatic adenomas are usually well circumscribed lesions that are predominantly isodense or slightly hyperdense if uncomplicated and relatively small (< 5 cm). Larger and more complicated HCAs may display a variety of density patterns, including a low attenuation if they

Figure 5: 31-year old female with typical HCA within a fatty liver. (a) Axial unenhanced CT (unenh CT) shows no lesion. (b) Axial enhanced CT shows HCA with a homogenous blush in the arterial (ART) phase (arrow), fading to isodensity in the portal (POR) phase. (c) Axial in- (IP) and opposed-phase (OP) T1-weighted gradient-echo shows no lesion on IP whereas a hyperintense lesion (arrow) appears on the OP due to decreased signal in the fatty liver. (d) Axial fat-suppressed single-shot black-blood T2-weighted echo planar imaging (BBEPI) shows the lesion (arrow) with faintly higher signal than the liver. Spleen (*). (e) Axial gadolinium-enhanced T1-weighted gradient-echo image in the arterial phase (ART) shows a homogenous blush of HCA (solid arrow). Note the intense enhancement of the aorta (open arrow) and the spleen (*). (f) Axial gradient-echo image in the delayed phase (DEL) shows no washout of contrast (i.e. homogenous enhancement) and the lesion is slightly more enhanced than the liver (arrow). Spleen (*). The findings at MR imaging are more specific for HCA than on CT.

contain fat, relatively high density if hemorrhagic, or fluid density if necrotic. In cases of recent hemorrhage, HCA is often obscured by the hematoma which appears heterogeneous with predominantly high attenuation values. In HCAs, calcification is present in 5-15 % of cases[10]. On CT scans obtained after IV contrast injection, hepatic adenomas usually show early homogeneous enhancement during the arterial dominance phase. On portal venous phase and delayed CT scans hepatic adenomas exhibit attenuation nearly identical to that of normal liver parenchyma[27,32]. In one study, all 44 adenomas (100%) showed homogenous enhancement in the arterial phase[27]. In another study, 22 of 27 (81%) HCAs showed enhancement in the arterial phase at CT. In the portal phase at CT, a minority (39%) of the lesions may be more enhanced than the surrounding liver, whereas in the delayed phase very few lesions (6%) may still be enhanced more than the liver[27]. As homogenous enhancement in the arterial phase plays an important role for diagnosis, proper timing strategy to obtain this phase may be crucial at CT.

The broad availability of CT as well as the recent development and implementation of the faster multirow detector machines, make this modality an excellent tool for detection and characterization of focal liver lesions. Current CT scanners can obtain simultaneous multiple acquisitions per each gantry rotation. With the current multidetector CT, fast data acquisition over a large anatomic area (entire body with isometric voxels) is possible in less than 30 seconds. The isometric nature of the data facilitates high quality reconstructions of mainly the vascular and bony structures in any desirable anatomic orientation[33]. The shorter scan times also allow the capture of distinct phases, including the unenhanced phase, the arterial phase, the portal phase, and the venous phase. These phases provide important information concerning the enhancement patterns and hence the possibility of characterization of focal liver lesions. In clinical practice though, the number of phases that are usually acquired with CT are limited and often kept to a minimum, mainly due to concerns about radiation hazard. The issue of radiation is even more important in relatively young and otherwise healthy patients with an incidental liver lesion, such as HCA, that needs characterization or follow-up. One fundamental limitation of CT remains the lack of the ability to alter the intrinsic soft tissue contrast, which is useful to assess diffuse and focal liver abnormalities. Evaluation of liver abnormalities at CT is based on two basic parameters: attenuation differences and differential enhancement.

Magnetic Resonance Imaging

At MR imaging, these HCAs often have the following characteristics: a) almost isointense or slightly hyperintense to the surrounding liver on T1-weighted in-phase gradient-echo images (indicating the hepatocellular nature of the lesions), b) compared to in-phase images, they may become relatively hyperintense to the liver (due to decreased signal of the fatty liver) or hypointense as well as heterogeneous to the liver (due to decreased signal within the fatty lesion) on the T1-weighted opposed-phase images, c) slightly hyperintense or hypointense on fat-suppressed T2-weighted images (depending mainly on whether HCA is surrounded by fatty liver or the lesion itself contains abundant fat or fibrosis, respectively), d) faint homogenous enhancement (blush) in the arterial phase, and e) isointense in the delayed phase without washout or capsular enhancement (Fig. 5c-f and Fig. 6). In one study of 51 pathology-proven lesions[30], HCA has the following characteristics: on T1-weighted spin-echo images, 30 of 51 (59%) were hyperintense, 17 of 51 (33%) isointense, and 4 of 51 (8%) hypointense to the liver; and on T2-weighted spin-echo images, 24 of 51 (47%) were hyperintense, 20 of 51 (39%) isointense, 2 of 51 (4%) hypointense to the liver. In two studies from 1994 and 1995, up to 87% of HCA showed homogenous enhancement on the gadolinium-enhanced gradient-echo images in the arterial phase[30,31]. In one study of 31 lesions, 26% showed fatty infiltration and 39% signs of hemorrhage at pathologic analysis[31]. MR imaging was able to detect fat in 63% and hemorrhage in 83% of the cases[31]. These data were mainly based on T1-weighted spin-echo sequence without fat-suppression. Chemical shift imaging, which is more sensitive for fatty infiltration, was not applied. A complete or partial pseudocapsule – comprised of compressed surrounding liver tissue or vessels - presenting as a rim

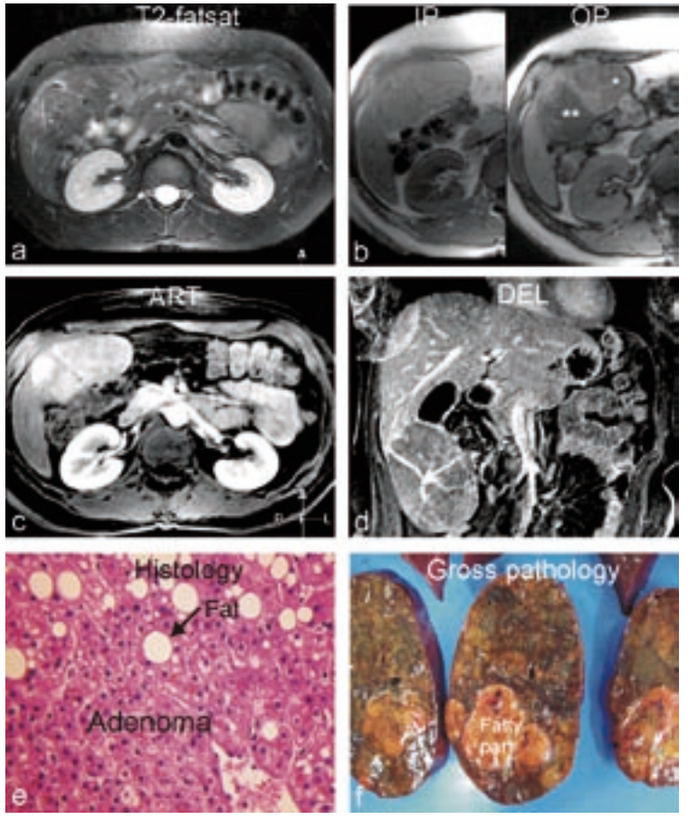

Figure 6: 41-year old female with a fatty HCA. (a) Axial fat-suppressed T2-weighted TSE image: adenoma is predominantly isointense to the liver. (b) Axial in- (IP) and opposed-phase (OP) T1-weighted gradient-echo: large parts of the adenoma shows decrease in signal on opposed-phase due to more (**) or less (*) fatty infiltration. (c) Axial arterial phase (ART) gadolinium-enhanced three-dimensional gradient-echo: adenoma shows moderately intense and homogeneous enhancement. (d) Coronal delayed phase (DEL) gradient-echo with high spatial resolution shows the adenoma as an exophytic lesion with a large intra-tumoral vessel. (e) Photomicrograph (H&E, original magnification 200x) shows typical mono-nuclear appearance of the hepatocytes with fatty infiltration. (f) Photograph of the resected specimen confirms that large parts of the tumor contain fat and appear yellowish (fatty part). Note the striking MR-pathology correlation.

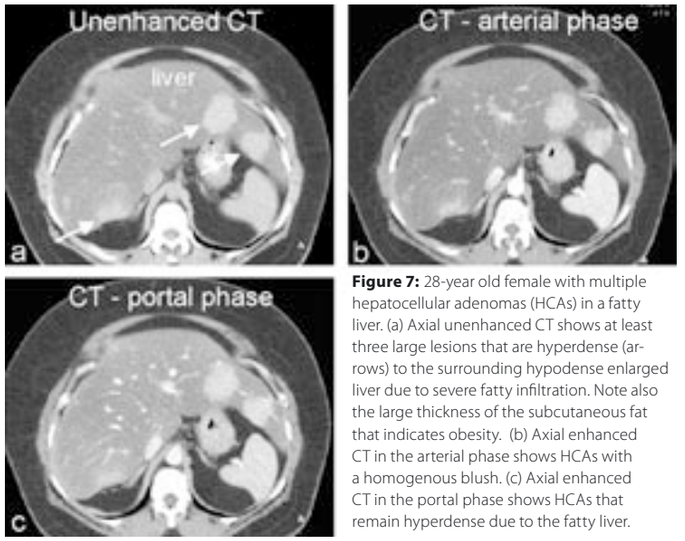

Figure 7: 28-year old female with multiple hepatocellular adenomas (HCAs) in a fatty liver. (a) Axial unenhanced CT shows at least three large lesions that are hyperdense (arrows) to the surrounding hypodense enlarged liver due to severe fatty infiltration. Note also the large thickness of the subcutaneous fat that indicates obesity. (b) Axial enhanced CT in the arterial phase shows HCAs with a homogenous blush. (c) Axial enhanced CT in the portal phase shows HCAs that remain hyperdense due to the fatty liver.

of low signal intensity at T1-weighted images and a high signal intensity at T2-weighted images, may be seen in some cases. In contrast, the true fibrous tumor capsule of HCC has a low signal intensity on both T1- and T2-weighted sequences[13].

The current state-of-the-art MR imaging provides a more comprehensive and accurate work-up of focal and diffuse liver disease[33,34]. This is based on the unique properties of MR imaging that comprise a combination of high intrinsic soft tissue contrast of the liver and liver lesions, various distinctly different tissue characteristics at imaging and high sensitivity for the

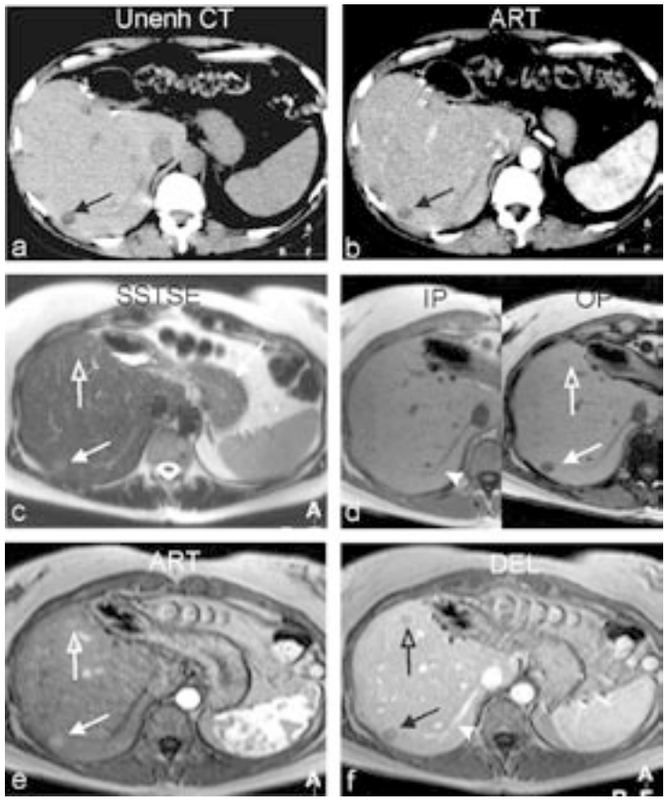

Figure 8: 39-year old female with small hepatocellular adenomas (HCAs) who underwent resection for a large HCA in the left liver: CT versus MR imaging. (a) Axial unenhanced computed tomography (unenh CT) shows lesion one lesion (arrow) that is hypodense to the liver. Probably due to partial volume effects, the density (Hounsefield value) was greater than zero, which fail to show fatty content of the lesion. (b) Axial enhanced CT in the arterial (ART) phase shows HCA with little or no enhancement. Based on these findings, CT was inconclusive about the nature of the lesions. (c) Axial T2-weighted SSTSE (SSTSE) shows a slightly hyperintense lesion (solid arrow) and a more faintly hyperintense small lesion (open arrow). (d) Axial in- (IP) and opposed-phase (OP) T1-weighted gradient-echo shows the larger lesion with more (solid arrow) and less (open arrow) loss in signal on OP based on the differences in fatty content. Note a prominent liver vein coming from the area of the lesion (arrowhead). (e) Axial gadolinium-enhanced T1-weighted gradient-echo image in the arterial phase (ART) shows a homogenous blush of the larger (solid arrow) and the smaller (open arrow) lesion. (f) Axial gradient-echo image in the delayed phase (DEL) shows washout of contrast (i.e. lesions become less enhanced than the liver). No capsular enhancement is visible. Based on CT findings as well as MRI findings on T2-weighted sequence and the enhancement pattern, hypervascular metastases cannot be excluded. Although, the findings on the chemical shift imaging (IP and OP) exclude this possibility and the lesions can safely be characterized as small fat-containing hepatocellular adenomas. Note a prominent liver vein coming from the area of the lesion (arrowhead).

Figure 9: 29-year old female with multiple adenomas in a fatty liver. (a) Axial SSTSE shows a lesion (arrow) that is slightly lower in signal intensity compared to the surrounding liver due to the higher signal of the fatty liver. Fat-suppressed turbo spin-echo (TSE-fatsat) shows the lesion (arrow) that is slightly hyperintense to the liver due to the fat suppression pulse. (b) Axial in- (IP) and opposed-phase (OP) T1-weighted gradient-echo: the liver shows marked decrease in signal due to fatty infiltration. The adenomas (arrows) remain unchanged in signal and hence appear bright. (c) Axial gadolinium-enhanced arterial phase (ART) gradient-echo: the larger adenoma shows moderately intense and homogeneous enhancement (arrow). The smaller lesion is not well visible.

standard part of their work-up of liver diseases. So unlike CT, many centers have been routinely employing a dynamic multi-phasic (often three or more phases) gadolinium-enhanced imaging protocol as the standard MR imaging investigation in patients with suspected liver disease for more than a decade[38-41]. Dynamic gadolinium-enhanced imaging is considered essential in detection and characterization of liver lesions. Therefore, for most body MR radiologists, the enhancement patterns of various focal liver lesions (as well as their signal intensity characteristics on T2- and T1-weighted sequences) are well known for many years.

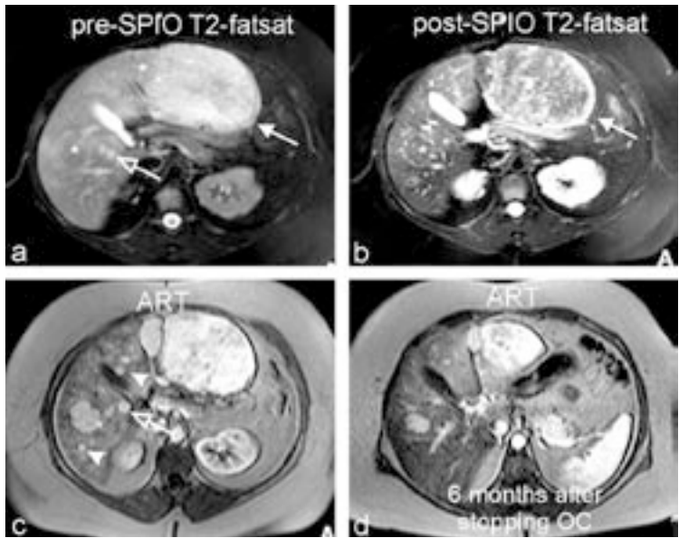

Figure 10: 43-year old female with multiple hepatocellular adenomas: MR imaging before and 6 months after withdrawal of oral contraceptives (OC). a) Axial fat-suppressed T2-weighted turbo spin-echo (pre-SPIO T2-fatsat) shows at least two lesions with high signal intensity: a large (solid arrow) and a small lesion (open arrow). In addition, two areas with low signal intensity (*) are visible in an abnormally bright liver. (b) Axial fat-suppressed T2-weighted turbo spin-echo after uptake of super-paramagnetic iron-oxide (post-SPIO T2-fatsat) into Kupffer cells shows signal loss with somewhat heterogeneous appearance of the largest lesion (solid arrow). This reflects variable distribution of Kupffer cells across this lesion. In addition, smaller lesions (*) show a more homogenous decrease in signal. The presence of Kupffer cells proves that the lesions are of hepatocellular origin, and hence excludes multiple metastases. (c) Axial gadolinium-enhanced gradient-echo in the arterial phase shows intense homogenous enhancement of all lesions, including the smaller lesion that was visible on T2 (open arrow) and additional lesions not visible on T2 (solid arrowheads). (d) Axial gadolinium-enhanced gradient-echo in the arterial phase (ART) (6 months after withdrawal of OC) shows decrease in size and intensity of enhancement of all lesions and confirms the diagnosis of OC-dependent multiple adenomas.

presence or absence of contrast-uptake and enhancement patterns using either non-specific or liver-specific contrast media. Because MR imaging lacks the hazards of ionizing radiation, most centers perform a multi-phasic gadolinium-enhanced examination as a

Multiple adenomas

Multiple HCAs are often surrounded by a fatty liver with altered shape and size of the segments of the liver. At US, such lesions will most likely be hypoechoic due to the increased echogenicity of the fatty liver,

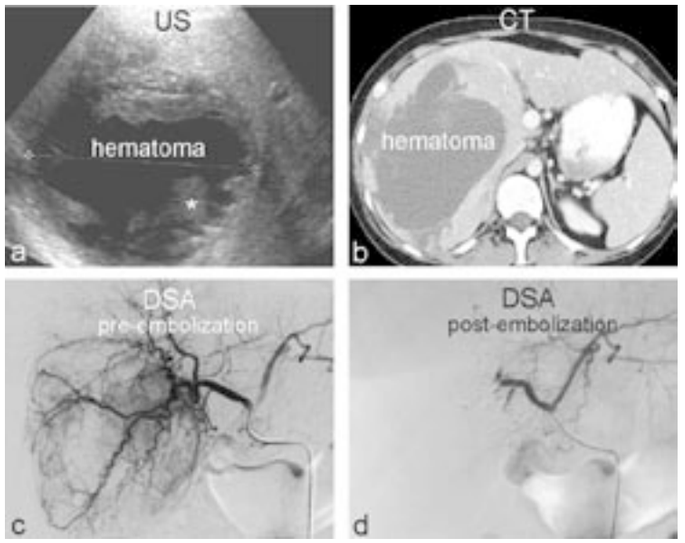

Figure 11: 24-year old female with ruptured adenoma: US, CT, and DSA. (a) US shows a large fluid collection without a distinct solid lesion or cause of the abnormality. Debris within the collection (*) as well as the acute history suggest a large hematoma. (b) Axial CT in the portal phase confirms the findings of US. No distinct solid lesion is visible. (c) Selective digital subtraction angiography (DSA) prior to embolization shows hypertrophic right hepatic artery with typical numerous tortuous (corkscrew) arteries and several areas with blush suggesting multiple adenomas around the hematoma. (d) DSA after embolization (with gelatin sponge particles and after placement of a coil) shows no evidence of adenomas.

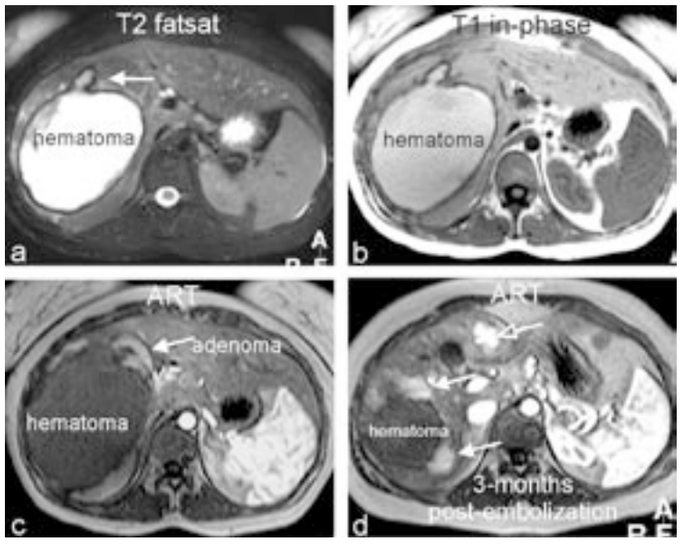

Figure 12: 24-year old female with ruptured adenoma (same patient as in Fig. 11): MR imaging before and after embolization. (a) Fat-suppressed T2-weighted turbo spin-echo (T2 fatsat) shows a large fluid collection with a stalk-like extension (arrow). (b) Axial in-phase T1-weighted gradient-echo (T1 in-phase) shows the fluid collection with high signal; the signal intensity is compatible with a large hematoma (high signal is caused by methemoglobin). (c) Axial gadolinium-enhanced T1-weighted gradient-echo in the arterial phase (ART) shows homogeneous enhancement around the stalk-like extension indicating the location of the ruptured adenoma. (d) Axial gadolinium-enhanced T1-weighted gradient-echo in the arterial phase (ART) (3-months after embolization) shows residual or recurrent adenomas surrounding the hematoma that has decreased in size (solid arrows). Note also an additional adenoma in the left side of the liver (open arrow).

and therefore may mimic a wide variety of lesions, including liver metastases. At CT, multiple HCAs may appear hyperdense on the unenhanced as well as enhanced scans because of the low density of the fatty liver. In such cases, the enhancement of the lesions may be difficult to appreciate (Fig. 7). Multiple HCAs may also be found in non-fatty livers. If these lesions are relatively small, and their fatty content cannot be detected with certainty, they may mimic hypovascular liver metastases particularly at CT (Fig. 8a-b). At MR imaging, very small liver lesions within fatty or non-fatty liver can be characterized with much higher accuracy because of the high intrinsic soft tissue contrast based on the T2 characteristics and chemical shift imaging, and the ability to visualize enhancement patterns on the routine gadolinium-enhanced dynamic imaging, (Figs. 8c-f and 9). It should be pointed out here that the signal intensity of HCA on non-fat-suppressed T2-weighted MR imaging can be high if the lesions contain abundant fat. Conversely, on similar sequences the signal intensity of HCA may be lower than the liver if the liver is steatotic (see Figs. 8 and 9). Whereas, on fat-suppressed T2-weighted sequences, the signal intensity may increase from lower to higher than the liver depending on the amount of liver steatosis (see Fig. 9). The use of super-paramagnetic iron-oxide (SPIO) contrast media for MR imaging as well as follow-up with imaging after stopping the oral contraceptives are additional possibilities to confirm the primary and benign nature of the lesions (Fig. 10). Specific contrast media such as SPIO are targeted at the Kupffer cells.

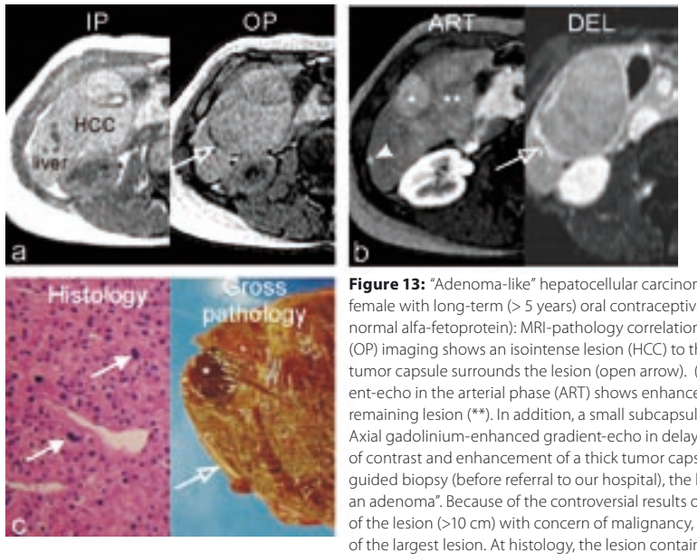

Figure 13: "Adenoma-like" hepatocellular carcinoma (HCC) in a healthy 30-years-old female with long-term (> 5 years) oral contraceptive use (negative viral serology and normal alfa-fetoprotein): MRI-pathology correlation. (a) Axial in- (IP) and opposed-phase (OP) imaging shows an isointense lesion (HCC) to the liver. On OP a low signal intensity tumor capsule surrounds the lesion (open arrow). (b) Axial gadolinium-enhanced gradient-echo in the arterial phase (ART) shows enhancement of a nodule (*) as well as the remaining lesion (**). In addition, a small subcapsular lesion is also enhanced (arrowhead). Axial gadolinium-enhanced gradient-echo in delayed phase (DEL) shows some washout of contrast and enhancement of a thick tumor capsule (open arrow). (c) At ultrasound-guided biopsy (before referral to our hospital), the lesion was characterized as "most likely an adenoma". Because of the controversial results of imaging, biopsy, and the large size of the lesion (>10 cm) with concern of malignancy, a surgical resection was performed of the largest lesion. At histology, the lesion contained hepatocyte-like cells of variable size. The nuclei were variable in size as well. Proliferative activity was low (solid arrow). The presence and the distribution of vessels varied. The exact nature of the lesion was difficult to determine. At gross pathology, tumor was composed of several confluent nodules (*), and the entire lesion was completely surrounded by a thick fibrous capsule (open arrow). To determine the exact nature of the lesion, the pathology material was sent to three authoritative pathologists in Europe: two of them characterized the lesion as "well-differentiated HCC with low malignant potential" and according to the third it was an "adenoma". Based on MR imaging and our own pathologic analysis, we considered the lesion as HCC, which might have originated from an adenoma. The smaller lesion could not be found at surgery and did not change on several follow-up MR imaging exams.

These contrast media can be used to demonstrate the hepatocellular origin of the lesions. The Kupffer cells show uptake of SPIO and this lowers the signal intensity of the lesions as well as the surrounding liver on T2- and T2*-weighted images (see Fig. 10a-b). In our experience, dynamic gadolinium-enhanced MR imaging in the arterial phase is more sensitive and specific than T2-weighted sequences after SPIO-uptake (see Fig. 10).

Large (complicated) adenomas

Larger HCAs as well as HCAs complicated with hemorrhage and malignant degeneration may appear heterogeneous on all imaging modalities. The heterogeneity of the lesions may be caused by several factors, including 1) the presence of hemorrhage, 2) the presence of necrosis or fibrosis, and 3) pre-malignant (LCD) or malignant (HCC) changes. Large hematomas, which have non-specific appearance on US and CT but can easily be recognized as typical bright fluid collections on T1-weighted MR images, can compress the surrounding liver tissue and conceal the underlying HCA as the cause of bleeding. After resolution of the hematoma or embolization of the tumor vessels, the HCAs may become evident (Fig. 11 and 12). "Adenoma-like" HCC may be discovered at imaging in female patients with long-term OC-use (Fig. 13). Such lesions may cause difficulty in making the correct diagnosis at US, US-guided biopsy, CT, preoperatively. And even after resection of the tumor, it may be difficult to distinguish between HCA and HCC at histopathology because of overlapping features. In this context, the ability of the state-of-the-art MR imaging for tissue characterization in vivo and distinction between HCA and HCC is unparalleled[33].

DIFFERENTIAL DIAGNOSIS

A number of lesions form the differential diagnosis for HCA. These include FNH, HCC in a non-cirrhotic liver, fatty or hemorrhagic HCC, focal steatosis, angiomyolipoma, and hypervascular metastases.

Most FNHs have distinct pathologic and imaging features and cause little to no difficulty in distinguishing from HCAs[42]. Particularly, classical FNH is composed of small nodules of normal hepatocytes surrounded by a network of capillaries and septa[42]. Larger septa and the central scar form a spoke-wheel configuration that is a typical feature of FNH. The signal intensity of FNHs on T1- and T2-weighted sequences may overlap with

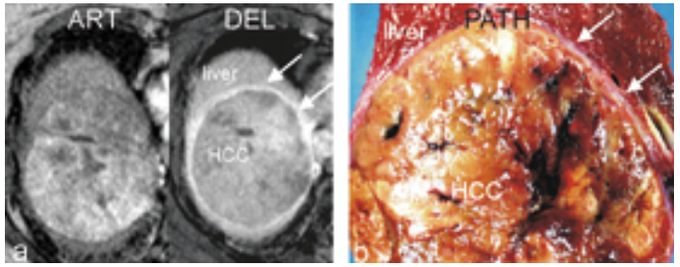

Figure 14: 70-year old female with hepatocellular carcinoma (HCC) in a non-cirrhotic liver: MRI-pathology correlation. (a) Axial gadolinium-enhanced gradient-echo in the arterial phase (ART) shows somewhat heterogeneous enhancement of the lesion. Axial gadolinium-enhanced gradient-echo in delayed phase (DEL) shows enhancement of a thick tumor capsule (solid arrows). (b) At gross pathology (PATH), the lesion was encapsulated by a thick fibrous capsule (solid arrows) and the liver was clearly non-cirrhotic, which confirmed the findings at MR imaging.

HCAs. However, FNHs less commonly exhibit high signal intensity on T1, less frequently show signs of fatty infiltration on chemical shift imaging, and show more intense homogenous enhancement in the arterial phase than most HCAs[42]. FNH with atypical features, such as small lesions, lack of a distinct central scar or septa, multiple lesions with minimal fatty content, may be difficult to distinguish from other entities, including HCAs. In this context, teleangiectatic "FNH" or "adenomas" may also cause difficulty in diagnosis[43].

Most HCC's in non-cirrhotic livers are typically large lesions with often a large heterogeneous central scar, a tumor capsule with or without satellite nodules, heterogeneous signal intensity, and heterogeneous enhancement with washout of contrast[13]. Some HCC in non-cirrhotic liver, especially with almost homogenous enhancement, fatty infiltration, and hemorrhage may cause diagnostic difficulties, particularly on CT (Figs. 14 and 15).

Focal steatosis may mimic focal lesions on US and CT[33]. This entity does not form a challenge on the state-of-the-art MR imaging. Typically, there will be loss of signal on the opposed-phase images, whereas on all other sequences, including on gadolinium-enhanced images these lesions will behave as normal liver tissue.

Angiomyolipoma in the liver is a rare entity and almost always will occur in conjunction with angiomyolipomas in the kidneys. Hypervascular metastases may form a differential diagnosis in patients with incidental findings of multiple hypervascular liver lesions with unknown underlying primary malignancy. At MR imaging, the signal intensity as well as the enhancement patterns of these lesions differs from HCAs[33,34]. In challenging cases, SPIO may be used to show the primary nature of the lesion[41].

Conclusion

In conclusion, this paper describes the most recent concepts and pertinent findings of hepatocellular adenomas at clinical presentation, gross pathology and histology including hepatocellular adenoma-liver cell dysplasia-carcinoma sequence, and imaging findings at ultrasound, computed tomography and state-of-the-art MR imaging. MR imaging provides the most comprehensive and non-invasive imaging work-up of patients with suspected hepatocellular adenomas.

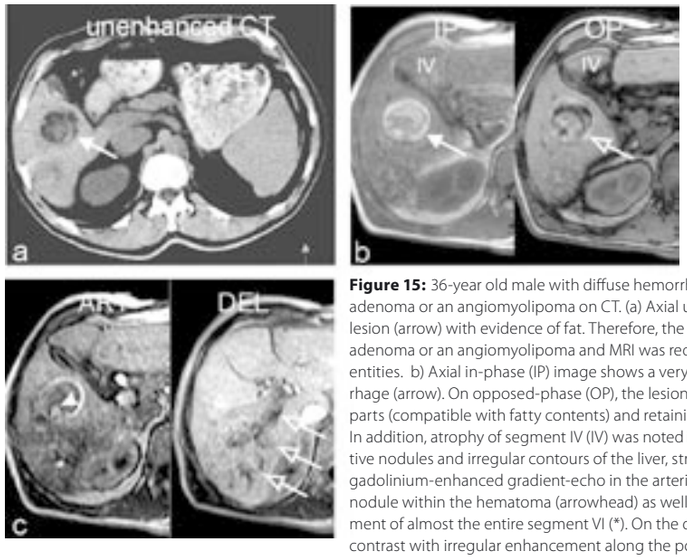

Figure 15: 36-year old male with diffuse hemorrhagic and fatty HCC mimicking an adenoma or an angiomyolipoma on CT. (a) Axial unenhanced CT shows a low density lesion (arrow) with evidence of fat. Therefore, the lesion was characterized as either an adenoma or an angiomyolipoma and MRI was requested to confirm one of these two entities. b) Axial in-phase (IP) image shows a very bright lesion compatible with hemorrhage (arrow). On opposed-phase (OP), the lesion shows strong loss of signal in some parts (compatible with fatty contents) and retaining the rim of high signal (open arrow). In addition, atrophy of segment IV (IV) was noted in combination with several regenerative nodules and irregular contours of the liver, strongly suggesting cirrhosis. (c) Axial gadolinium-enhanced gradient-echo in the arterial image (ART) shows an enhancing nodule within the hematoma (arrowhead) as well as diffuse heterogeneous enhancement of almost the entire segment VI (*). On the delayed phase (DEL), washout of contrast with irregular enhancement along the portal vein (open arrows) is visible. These findings are compatible with a diffuse HCC with portal invasion and a hemorrhage. Prospectively, at CT the signs for cirrhosis were not appreciated and therefore HCC was not considered as a possibility. In retrospect, portal vein thrombosis was also present on CT.

REFERENCES

1. Baum JK, Bookstein JJ, Holtz F, Klein EW. Possible association between benign hepatomas and oral contraceptives. Lancet 1973; 2:926-929.
2. Edmondson H. Tumors of the liver and intrahepatic bile ducts. In: Pathology WDAFIo, ed. Atlas of Tumor Pathology. Washington DC, 1958.
3. Edmondson HA, Henderson B, Benton B. Liver-cell adenomas associated with use of oral contraceptives. N Engl J Med 1976; 294:470-472.
4. Rooks JB, Ory HW, Ishak KG, et al. Epidemiology of hepatocellular adenoma. The role of oral contraceptive use. Jama 1979; 242:644-648.
5. Lindgren A, Olsson R. Liver damage from low-dose oral contraceptives. J Intern Med 1993; 234:287-292.
6. Mamada Y, Onda M, Tajiri T, et al. Liver cell adenoma in a 26-year-old man. J Nippon Med Sch 2001; 68:516-519.
7. Psatha EA, Semelka RC, Armao D, Woosley JT, Firat Z, Schneider G. Hepatocellular adenomas in men: MRI findings in four patients. J Magn Reson Imaging 2005; 22:258-264.
8. Terkivatan T, de Wilt JH, de Man RA, et al. Indications and long-term outcome of treatment for benign hepatic tumors: a critical appraisal. Arch Surg 2001; 136:1033-1038.
9. International Working Party. Terminology of nodular hepatocellular lesions. Hepatology 1995; 22:983-993.
10. Anthony P. Tumors and tumor-like lesions of the liver and biliary tract: aetiology, epidemiology and pathology. In: MacSween RNM BA, Portmann BC, ed. Pathology of the liver: Churchill Livingstone, 2002; 711-775.
11. Goodman ZD, Mikel UV, Lubbers PR, Ros PR, Langloss JM, Ishak KG. Kupffer cells in hepatocellular adenomas. Am J Surg Pathol 1987; 11:191-196.
12. Prasad SR, Wang H, Rosas H, et al. Fat-containing lesions of the liver: radiologic-pathologic correlation. Radiographics 2005; 25:321-331.
13. Hussain SM, Semelka RC, Mitchell DG. MR imaging of hepatocellular carcinoma. Magn Reson Imaging Clin N Am 2002; 10:31-52, v.
14. Lepreux S, Laurent C, Blanc JF, et al. The identification of small nodules in liver adenomatosis. J Hepatol 2003; 39:77-85.
15. Flejou JF, Barge J, Menu Y, et al. Liver adenomatosis. An entity distinct from liver adenoma? Gastroenterology 1985; 89:1132-1138.
16. Paradis V, Benzekri A, Dargere D, et al. Telangiectatic focal nodular hyperplasia: a variant of hepatocellular adenoma. Gastroenterology 2004; 126:1323-1329.
17. Bioulac-Sage P, Rebouissou S, Sa Cunha A, et al. Clinical, morphologic, and molecular features defining so-called telangiectatic focal nodular hyperplasias of the liver. Gastroenterology 2005; 128:1211-1218.
18. Gordon SC, Reddy KR, Livingstone AS, Jeffers LJ, Schiff ER. Resolution of a contraceptive-steroid-induced hepatic adenoma with subsequent evolution into hepatocellular carcinoma. Ann Intern Med 1986; 105:547-549.
19. Gyorffy EJ, Bredfeldt JE, Black WC. Transformation of hepatic cell adenoma to hepatocellular carcinoma due to oral contraceptive use. Ann Intern Med 1989; 110:489-490.
20. Tao LC. Oral contraceptive-associated liver cell adenoma and hepatocellular carcinoma. Cytomorphology and mechanism of malignant transformation. Cancer 1991; 68:341-347.
21. Ferrell LD. Hepatocellular carcinoma arising in a focus of multilobular adenoma. A case report. Am J Surg Pathol 1993; 17:525-529.
22. Foster JH, Berman MM. The malignant transformation of liver cell adenomas. Arch Surg 1994; 129:712-717.
23. Hussain SM, Zondervan PE, IJzermans JN, Schalm SW, de Man RA, Krestin GP. Benign versus malignant hepatic nodules: MR imaging findings with pathologic correlation. Radiographics 2002; 22:1023-1036; discussion 1037-1029.
24. Welch TJ, Sheedy PF, 2nd, Johnson CM, et al. Focal nodular hyperplasia and hepatic adenoma: comparison of angiography, CT, US, and scintigraphy. Radiology 1985; 156:593-595.
25. Numata K, Tanaka K, Mitsui K, Morimoto M, Inoue S, Yonezawa H. Flow characteristics of hepatic tumors at color Doppler sonography: correlation with arteriographic findings. AJR Am J Roentgenol 1993; 160:515-521.
26. Bryant TH, Blomley MJ, Albrecht T, et al. Improved characterization of liver lesions with liver-phase uptake of liver-specific microbubbles: prospective multicenter study. Radiology 2004; 232:799-809.
27. Ichikawa T, Federle MP, Grazioli L, Nalesnik M. Hepatocellular adenoma: multiphasic CT and histopathologic findings in 25 patients. Radiology 2000; 214:861-868.
28. Grazioli L, Federle MP, Ichikawa T, Balzano E, Nalesnik M, Madariaga J. Liver adenomatosis: clinical, pathologic, and imaging findings in 15 patients. Radiology 2000; 216:395-402.
29. Paulson EK, McClellan JS, Washington K, Spritzer

hepatocellular adenoma REVIEW OF IMAGING FINDINGS

CE, Meyers WC, Baker ME. Hepatic adenoma: MR characteristics and correlation with pathologic findings. AJR Am J Roentgenol 1994; 163:113-116.
30. Arrive L, Flejou JF, Vilgrain V, et al. Hepatic adenoma: MR findings in 51 pathology-proven lesions. Radiology 1994; 193:507-512.
31. Chung KY, Mayo-Smith WW, Saini S, Rahmouni A, Golli M, Mathieu D. Hepatocellular adenoma: MR imaging features with pathologic correlation. AJR Am J Roentgenol 1995; 165:303-308.
32. Mathieu D, Bruneton JN, Drouillard J, Pointreau CC, Vasile N. Hepatic adenomas and focal nodular hyperplasia: dynamic CT study. Radiology 1986; 160:53-58.
33. Hussain SM, Semelka RC. Hepatic imaging: comparison of modalities. Radiol Clin North Am 2005; 43:929-947, ix.
34. Hussain SM, Semelka RC. Liver masses. Magn Reson Imaging Clin N Am 2005; 13:255-275.
35. Bartolozzi C, Lencioni R, Paolicchi A, Moretti M, Armillotta N, Pinto F. Differentiation of hepatocellular adenoma and focal nodular hyperplasia of the liver: comparison of power Doppler imaging and conventional color Doppler sonography. Eur Radiol 1997; 7:1410-1415
36. Bartolotta TV, Midiri M, Quaia E, et al. Benign focal liver lesions: spectrum of findings on SonoVue-enhanced pulse-inversion ultrasonography. Eur Radiol 2005; 15:1643-1649.
37. Klein D, Jenett M, Gassel HJ, Sandstede J, Hahn D. Quantitative dynamic contrast-enhanced sonography of hepatic tumors. Eur Radiol 2004; 14:1082-1091.
38. Mahfouz AE, Hamm B, Taupitz M, Wolf KJ. Hypervascular liver lesions: differentiation of focal nodular hyperplasia from malignant tumors with dynamic gadolinium-enhanced MR imaging. Radiology 1993; 186:133-138.
39. McFarland EG, Mayo-Smith WW, Saini S, Hahn PF, Goldberg MA, Lee MJ. Hepatic hemangiomas and malignant tumors: improved differentiation with heavily T2-weighted conventional spin-echo MR imaging. Radiology 1994; 193:43-47.
40. Mitchell DG, Saini S, Weinreb J, et al. Hepatic metastases and cavernous hemangiomas: distinction with standard- and triple-dose gadoteridol-enhanced MR imaging. Radiology 1994; 193:49-57.
41. Semelka RC, Martin DR, Balci C, Lance T. Focal liver lesions: comparison of dual-phase CT and multisequence multiplanar MR imaging including dynamic gadolinium enhancement. J Magn Reson Imaging 2001; 13:397-401.
42. Hussain SM, Terkivatan T, Zondervan PE, et al. Focal nodular hyperplasia: findings at state-of-the-art MR imaging, US, CT, and pathologic analysis. Radiographics 2004; 24:3-17; discussion 18-19.
43. Attal P, Vilgrain V, Brancatelli G, et al. Telangiectatic focal nodular hyperplasia: US, CT, and MR imaging findings with pathologic correlation in 13 cases. Radiology 2003; 228:465-472.

chapter3.2 hepatocellular adenoma and the surrounding liver

Hepatocellular adenoma and the surrounding liver: A SPECTRUM OF CHARACTERISTIC FINDINGS

at state-of-the-art MR imaging, with pathologic correlation

ABSTRACT

Purpose: To evaluate the spectrum of imaging findings of both hepatocellular adenoma (HCA) and the surrounding liver at state-of-the-art MR imaging.

Materials and Methods: MR images of 13 patients (all female, mean age 39 years (range 21-52)) with pathology-proven HCA (n=51) were retrospectively assessed for morphologic features of liver and lesions. Signal intensity (SI) was determined with calculation of contrast-to-noise ratios (CNR). Quantitative analysis with percentage enhancement in arterial, portal and delayed phases of dynamic multiphasic contrast-enhanced imaging was calculated. Histology sections were retrieved for analysis.

Results: The mean lesion size was 2.45 cm (range 0.8-11 cm). Lesion SI was predominantly hyperintense on fat-suppressed T2-weighted sequences and isointense on in-phase T1-weighted GRE, with drop in SI on opposed-phase T1-weighted GRE indicating intratumoral fatty infiltration in >70%. Percentages of enhancement in liver and lesion respectively was 37, 107 and 95%; and 120, 151 and 133% (p<0.001). The liver showed abnormal segmental shape and size (100%), with steatosis (77%). Transient arterial patchy heterogeneous enhancement was observed in a diffuse or segmental distribution within the liver (92%). Parenchymal MRI findings correlated with histopathology findings that comprised large portal tracts, inflammatory infiltration and subtle fibrosis.

Conclusion: The results of our study indicate that in patients with HCA, both lesions as well as the surrounding liver parenchyma show similar soft tissue and vascular abnormalities.

Indra C. van den Bos, MD[1], Shahid M. Hussain, MD, PhD[1*], Pieter E. Zondervan, MD[2], Jan N. IJzermans, MD, PhD[3], Robert A. de Man, MD, PhD[4]

Departments of [1]Radiology, [2]Pathology, [3]Surgery and [4]Gastroenterology and Hepatology, Erasmus MC, University Medical Center Rotterdam, The Netherlands; [*]Department of Radiology, University of Nebraska Medical Center, Omaha, NE, USA

Submitted

INTRODUCTION

Hepatocellular adenoma (HCA) is rare[1], but the incidence has increased since the introduction of oral contraception (OC)[2]. Detection is important, not only because of associated risk of potentially life-threatening hemorrhage, but also because malignant transformation may occur[3,4]. Therefore, although the growth pattern is relatively benign, the International Working Party classified HCA as neoplastic[5].

Most frequently, HCA occurs in young women, strongly associated with use of OC. Also, HCA has been reported in use of anabolic steroids or in glycogen storage disease[1]. As has been described by Flejou and colleagues (1984), hepatic adenomatosis (more than ten adenomas, no association with use of OC) may represent a different entity from isolated adenoma[6]. However, no pathologic differentiation can be found between isolated adenoma and adenomas in case of presumed hepatic adenomatosis[7] and therefore, presumably, both entities are representations of the same ongoing disease process[8].

At imaging, HCA may have a heterogeneous appearance, which causes difficulty for diagnosis using ultrasound (US) or computed tomography (CT). At US, echogenicity of focal liver lesions varies considerably, and fewer lesions are detected compared to CT and magnetic resonance (MR) imaging[9]. Although current multislice CT scanners are promising for analysis of dynamic enhancement patterns[10], often, MR imaging is performed additionally for further characterization. The unique ability of MR imaging to detect intrinsic cellular characteristics combined with dynamic contrast-enhanced imaging renders it a superior technique for diagnosis of focal liver lesions[1]. Especially in work-up of focal liver lesions in young fertile women, MR imaging should be considered as primary tool for detection and characterization to avoid radiation exposure[11].

The spectrum of imaging features of HCA lesions has been described before. In one study, enhancement patterns were evaluated at multiphasic helical CT[10]. Several studies addressed the MR imaging findings[12-14], including enhancement patterns after specific hepatobiliary and non-specific contrast administration[15-17]. In one study, imaging and pathologic findings in liver adenomatosis were described[18].

To our knowledge, none of the previous imaging studies have described the spectrum of HCA findings in relation to findings within the surrounding liver parenchyma. We hypothesized that tissue changes in both liver parenchyma and HCA might be interrelated, due to similar effects of the causative agent (most frequently OC). Therefore, careful analysis of size, morphology and signal intensity of liver parenchyma in case of HCA could possibly provide further understanding in characterization and classification of these lesions. In this study, we combined the spectrum of imaging findings of pathology-proven HCA with morphology and characteristics of the liver parenchyma, at modern MR imaging. To the best of our knowledge, this has not been reported before.

The purpose of our study therefore, was to evaluate the spectrum of imaging findings of both hepatocellular adenoma (HCA) and the surrounding liver at state-of-the-art MR imaging.

MATERIALS AND METHODS

Patients

The study was performed in a large university referral hospital for hepatobiliary diseases. Permission of the institutional review board (IRB) was not required given the retrospective nature of the study. The hospital archive and pathology registration were searched for patients with pathology-proven HCA that underwent MR imaging in January 2000 – December 2005. A total of fourteen patients were identified, all female, with a mean age of 39 years (range 21-52 years) (Table 1). One patient was diagnosed with teleangiectatic adenoma and was excluded, since recent literature suggests this is a different entity[19,20]. A total of 53 lesions were identified, with a mean size of 2.45 cm (range 0.8-11 cm).

MR imaging protocol

All MR examinations were performed on a 1.5T unit (Philips Medical Systems, Best, The Netherlands or General Electrics, Signa, Milwaukee, Wisconsin, USA; using identical scan protocols). A four-channel body-array coil with capability of parallel imaging was used. Scan sequences included single-shot fast spin-echo (repetition-time msec/ echo-time msec 832/90-120; flip-angle 90º), fat-suppressed T2-weighted fast spin-echo (FSE) (3000/80, flip-angle 90º), diffusion T2-weighted black-blood echo-planar imaging (BBEPI) (shortest/60, flip-angle 90º) and 2D or 3D T1-weighted in- and opposed-phase gradient-echo sequences (shortest/4.6 and 2.3 respectively, flip-angle 80º). After intravenous administration of a gadolinium-chelate (28 ml; Magnevist [gadopentetate dimeglumine], Schering, Berlin, Germany) at 3 ml/sec using a power injector, dynamic imaging with either 2D T1-weighted gradient-echo (GRE) (Philips) or 3D T1-weighted fat-suppressed GRE (General Electrics) sequences in at least 4 phases (precontrast, arterial, portal and delayed phases) was performed. In each patient, a timing bolus technique using 2ml of the same contrast agent followed by 15ml saline was used to accurately capture the arterial phase. The high injection rate of 3 ml/sec was used to compensate for some signal loss due to implementation of parallel imaging. The portal phase was acquired approximately at 45 seconds, and the delayed phase at least 120 seconds after the acquisition of the arterial phase. A slice thickness of 7mm was used in most sequences, except the T1-weighted fat-suppressed GRE sequence, in which 4mm slices were acquired.

Table 1: Patient characteristics.

Mean age		39 (range 21-52)
Use of oral contraception		10/13
Storage disease		1/13
Amount of lesions	1	2/13 (15.4)
	1-10	7/13 (53.8)
	>10	4/13 (30.8)*
Surgical resection		9/13
Percutaneous biopsy		4/13

Data are the number of patients. Data in parenthesis are percentages.
* Of these four patients, only one patient did not use oral contraception.

Image analysis

All MR imaging exams were transferred to a picture archiving and communication system (PACS) viewing station. Evaluation was performed of each single lesion. Assessment of the lesions was based on qualitative and quantitative parameters. Analysis of all lesions was performed by two radiologists with experience in hepatobiliary imaging in consensus. All evaluations were categorized and documented using standardized data sheets.

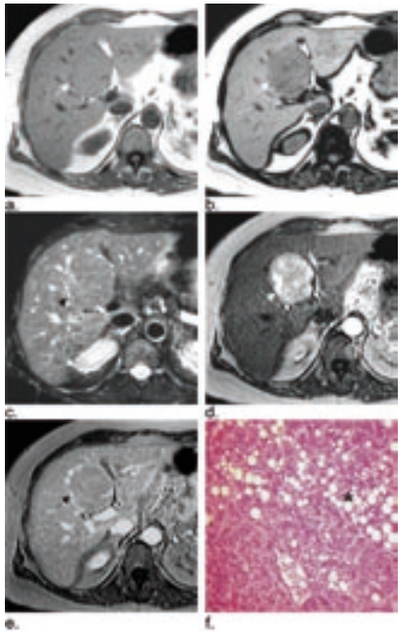

Figure 1: MR imaging findings of classic hepatocellular adenoma. (a) Transverse in-phase T1-weighted gradient-echo shows isointensity of the lesion (arrow). (b) Transverse opposed-phase T1-weighted gradient-echo shows marked decrease in signal intensity of the lesion, indicating marked fatty infiltration (arrow). (c) Transverse fat-suppressed T2-weighted fast spin-echo shows isointensity of the lesion (arrow). (d) Transverse arterial phase gadolinium-enhanced T1-weighted gradient-echo shows intense homogeneous enhancement of the lesion (arrow). (e) Transverse delayed phase gadolinium-enhanced T1-weighted gradient-echo shows the lesion has become isointense with the surrounding liver (arrow). (f) Photomicrograph (hematoxylin and eosin (HE) stain, original magnification x100) shows accumulation of fat within the lesion (*).

Qualitative assessment

Qualitative assessment of the following characteristics was performed: 1) visual assessment of liver size with segmental distribution (according to hepatic segment numbering system of Couinaud) categorized according to enlargement of right or left liver lobe or total enlargement; 2) signs of steatosis or cirrhosis (including undulating liver surface, hypertrophy of segment 1, atrophy of segment 4, enlargement of the peri-portal spaces and/or signs of portal hypertension such as splenomegaly or presence of collaterals); 3) total amount and localization of lesions; 4) presence of pseudo-capsule (defined as thin capsule composed of compressed vessels, slightly hyperintense on T2-weighted and slightly hypointense on T1-weighted sequences), true capsule (thicker, low signal intensity on both T1-weighted and T2-weighted sequences), intratumoral fat or hemorrhage; 5) signal intensity; 6) enhancement patterns at dynamic gadolinium-enhanced imaging.

Quantitative analysis

For quantitative analysis purposes, signal intensity measurements were performed using operator-defined regions-of-interest (ROI). For lesions, the largest possible ROI was selected that excluded hemorrhagic areas. For adjacent liver, ROI excluding vessels and artefacts was used. The lesion-to-liver contrast-to-noise ratio (CNR) was calculated as difference in signal intensity (SI) between lesion and liver scaled to standard deviation (SD) of background noise [$(SI_{lesion}-SI_{liver})/SD_{noise}$]. In dynamic gadolinium-enhanced imaging, ROI measurements were performed identically in arterial, portal and delayed phases. Definition of arterial phase consisted of enhancement of hepatic artery and aorta, slight enhancement of portal vein, no enhancement of hepatic veins and (almost) no enhancement of liver parenchyma. Percentages of contrast enhancement were calculated as follows: [$(SI_{enhanced} - SI_{unenhanced}) / SI_{unenhanced}$] x 100. Because of artefacts in the lesion area, the following lesions were excluded: 1 lesion for fat-suppressed T2-weighted FSE and 2 lesions for T2-weighted BBEPI. Because of technical problems with data acquisition, 3 other lesions were excluded in T2-weighted BBEPI.

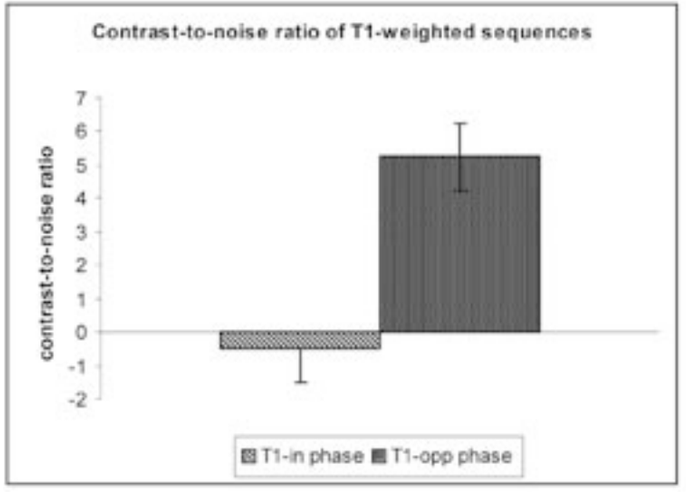

Figure 2: Contrast-to-noise ratio (CNR) of in-phase T1-weighted gradient-echo (T1 in-phase) and opposed-phase T1-weighted gradient-echo (T1 opp-phase), showing a statistically significant increase ($p<0.001$).

Pathologic analysis of the surrounding liver

Histopathology sections of selected study patients were retrieved and reviewed for abnormalities in adjacent liver parenchyma by an experienced hepatobiliary pathologist. Histology material was available in 10 patients. Qualitative analysis of the following characteristics was performed: 1) fatty infiltration; 2) aspect and size of vessels; 3) presence of inflammatory cells; 4) presence and thickness of liver plates; 5) variation in size of hepatocytes; 6) aspect of cytoplasm and size of nucleus versus cytoplasm; 7) presence of fibrosis (scaled according to the Metavir classification (F0=no fibrosis; F1=portal fibrosis without septa; F2=portal fibrosis with septa; F3=septal fibrosis without cirrhosis; and F4=cirrhosis); 8) presence of hemorrhagic components.

Table 2: Signal intensity of hepatocellular adenoma compared to the surrounding liver parenchyma.

	T1-in phase (n=53)	T1-op phase (n=53)	SSFE (n=53)	T2FSE fatsat (n=52)	BBEPI (n=48)
Markedly hyperintense	1 (2)	17 (33.3)	0	10 (19.6)	28 (54.9)
Slightly hyperintense	1 (2)	16 (31.4)	21 (41.2)	32 (62.5)	13 (25.5)
Isointense	42 (82.4)	13 (25.5)	27 (52.9)	6 (11.8)	2 (3.9)
Slightly hypointense	6 (11.8)	2 (3.9)	2 (3.9)	1 (2)	1 (2)
Markedly hypointense	1 (2)	3 (5.9)	1 (2)	1 (2)	2 (3.9)
Not performed	-	-	-	1 (2)	5 (9.8)

In-phase T1-weighted gradient-echo (T1-in phase), opposed-phase T1-weighted gradient-echo (T1-opp phase), single-shot T2-weighted fast spin-echo (SSFSE), fat-suppressed T2-weighted fast spin-echo (T2-FSE), diffusion-weighted black-blood echo-planar imaging (BBEPI).
N: number of included patients. Data are the number of lesions. Data in parenthesis are percentage of lesions classified in these categories.

RESULTS

Lesion analysis

Imaging findings of hepatocellular adenoma (HCA) that were most frequently observed included: 1) isointensity with surrounding liver on conventional T1- and single-shot T2-weighted sequences; 2) decrease in signal intensity of the lesion on opposed-phase T1-weighted GRE, indicating intratumoral fat; 3) hyperintensity on fat-suppressed T2-weighted FSE; 4) homogeneous enhancement on arterial phase gadolinium-enhanced imaging and 5) fading to isointensity with surrounding liver in delayed phase imaging (Fig. 1). Detailed findings are described below.

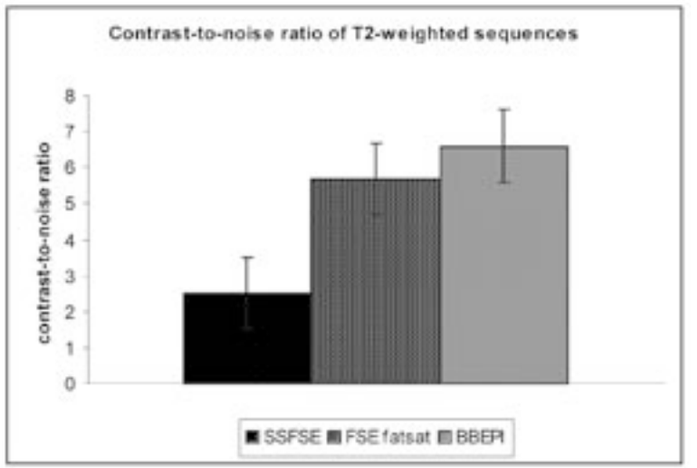

Figure 3: Contrast-to-noise ratio (CNR) of T2-weighted sequences, showing an increase in CNR of single-shot T2-weighted fast spin-echo (SSFSE) to fat-suppressed T2-weighted fast spin-echo (T2-FSE) to diffusion-weighted black-blood echo-planar imaging (BBEPI). (SSFSE from FSE fatsat and BBEPI $p<0.0001$ and BBEPI from FSE fatsat $p<0.05$).

Statistical analysis

Statistical parameters (mean, median, standard deviation and range) were calculated using the Statistical Package for Social Sciences (SPSS) program. The unit of measure was number of lesions, rather than number of patients. Significance levels were determined by the Wilcoxon signed rank test, since some data did not have a fully symmetric distribution. A p-value of less than 0.05 was considered statistically significant.

Signal intensity of HCA

Qualitative imaging findings are described in detail in Table 2. On T1-weighted imaging, most lesions appeared isointense to the liver on in-phase T1-weighted GRE (82.4%). On opposed-phase T1-weighted GRE, within the majority lesions (78%), areas of decreased signal intensity were observed indicating intratumoral fat. On the other hand, signal intensity of the overall lesion compared to the liver was predominantly hy-

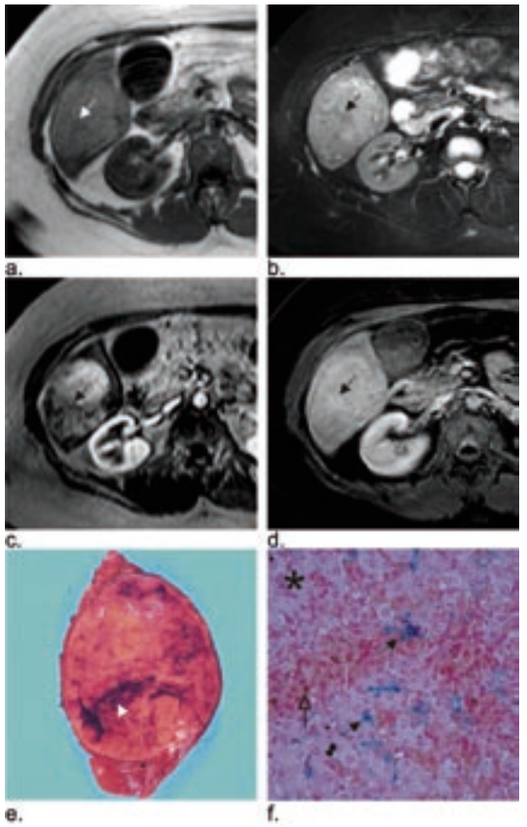

Figure 4: Large hepatocellular adenoma, with central fibrous tissue. (a) Transverse in-phase T1-weighted gradient-echo shows slight hyperintensity of a large adenoma, with an amorphous area of lower signal intensity in the center (arrow). (b) Transverse fat-suppressed T2-weighted fast spin-echo shows slight hyperintensity of the lesion, with slight hypointensity of the centrally oriented structure (arrow). (c) Transverse arterial phase gadolinium-enhanced T1-weighted gradient-echo shows heterogeneous enhancement of the lesion. The central area does not enhance and remains low in signal intensity (arrow). (d) Transverse delayed phase gadolinium-enhanced fat-suppressed three-dimensional T1-weighted gradient-echo shows near isointensity of the lesion compared to the liver, with slightly increased enhancement of the central structure (arrow). (e) Macroscopic image of the resected adenoma confirms a central amorphous area, with signs of fibrosis and recent hemorrhage (arrow). (f) Photomicrograph (iron staining, original magnification x200) shows enhancement of iron-containing macrophages (blue, arrow) and deposition of erythrocytes indicating more recent hemorrhage (open arrow).

perintense (64.7%) due to liver steatosis (Table 2). On fat-suppressed T2-weighted FSE, most lesions (82.1%) were slightly to markedly hyperintense (Table 2).

The quantitative measurements confirmed these data. CNR was calculated: for T1-weighted sequences: in-phase T1-weighted GRE -0.5 and opposed-phase T1-weighted GRE 5.24 ($p<0.0001$) (Fig. 2). For T2-weighted sequences CNR was: single-shot T2-weighted FSE (SSFSE) 2.51, fat-suppressed T2-weighted FSE (FSE fatsat) 5.68 and diffusion-weighted BBEPI 6.6 (Fig. 3). These values were significantly different (SSFSE from FSE fatsat and BBEPI $p<0.0001$ and BBEPI from FSE fatsat $p<0.05$)).

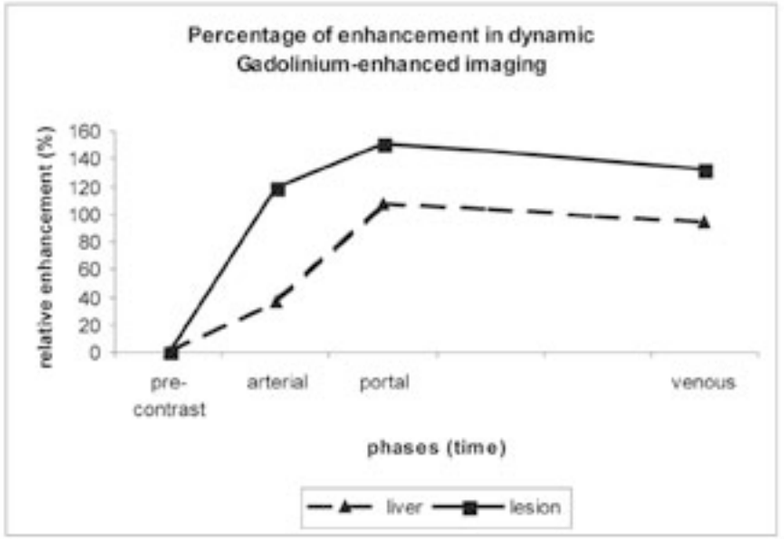

Figure 5: Percentage increase of enhancement of liver parenchyma and the lesion in arterial, portal and venous phases ($p<0.001$).

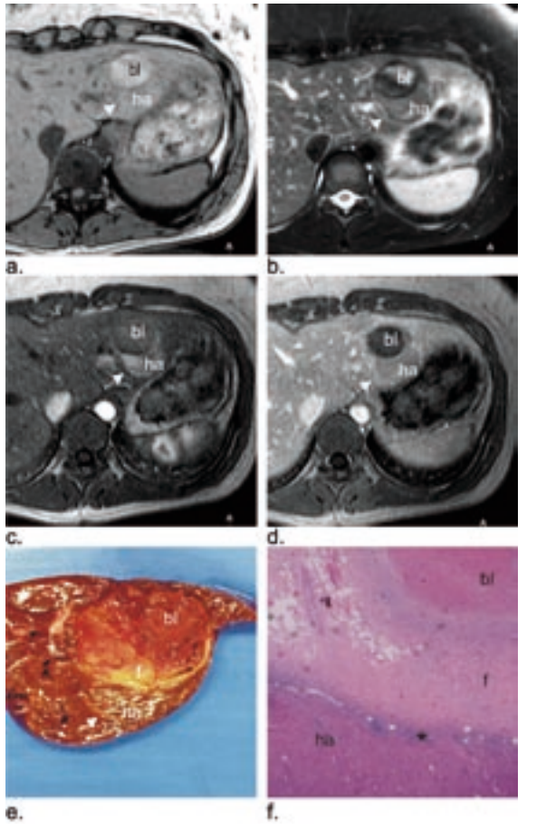

Figure 6: Hepatocellular adenoma with recent hemorrhage and a thin pseudocapsule. (a) Transverse in-phase T1-weighted gradient-echo shows a round area with high signal intensity in the left liver lobe (bl), with an adjacent moon-shaped hepatocellular adenoma (ha) which has isointense signal intensity. The HA is surrounded by a thin, hypointense pseudocapsule (arrow). (b) Transverse fat-suppressed T2-weighted fast spin-echo shows heterogeneous signal intensity of this area (bl), consisting of a layered area of low signal intensity, an area of higher signal intensity, surrounded by a hypointense rim; consistent with an hemorrhage of older and more recent date. The hepatocellular adenoma (ha) has a slightly hyperintense pseudocapsule (arrow). (c) Transverse arterial phase gadolinium-enhanced T1-weighted gradient-echo shows the hepatocellular adenoma enhances early in the arterial phase (arrow). (d) Transverse delayed phase gadolinium-enhanced T1-weighted gradient-echo shows the adenoma (ha) has become near isointense with the surrounding liver, with delayed enhancement of the pseudocapsule (arrow). (e) Macroscopic evaluation of the resected adenoma, shows a large lesion, consisting of blood (bl) surrounded by a rim of fibrosis (f), and a moon-shaped adenoma (ha) which is surrounded by a thin pseudocapsule (arrow), confirming the MR findings. (f) Photomicrograph (hematoxylin and eosin (HE) stain, original magnification x100) shows a transition of a focus of hepatocellular adenoma (ha) into an area of fibrosis (f) and blood (bl), surrounded by an inflammatory infiltrate (*).

Dynamic multiphasic gadolinium-enhanced imaging of HCA

Quantification of enhancement patterns by means of ROI measurements showed percentage increase of enhancement in liver parenchyma in arterial, portal and venous phases respectively of 37, 107 and 95%; in the lesion this was 120, 151 and 133 % ($p<0.0001$) (Fig. 5). This illustrates that HCA shows immediate, intense enhancement in the arterial phase after contrast administration, but behaves like the surrounding liver tissue in delayed phase imaging.

Secondary characteristics of HCA

A thin pseudocapsule was observed in 15 of 51 lesions (29.4%), with mildly higher signal intensity at T2-weighted images, isointense to slightly lower signal intensity at T1-weighted images and enhancing in delayed phases after gadolinium (Fig. 6). Intratumoral fat was was observed in 40 of 51 lesions (78.4%), diffusely present in 3 lesions (5.9%), heterogeneous in 3 lesions (5.9%) and focal in 34 lesions (66.7%). Hemorrhage associated with the lesion was observed in 6 of 51 lesions (11.8%). This was diffusely present in 1 lesion (2%) and focal in 5 lesions (9.8%). In 1 lesion, the hemorrhage extended beyond the lesion, but remained intrahepatic (Fig. 6).

Liver analysis

Most frequently observed findings at MR imaging and pathological analysis of the liver include: 1) moderate to marked fatty infiltration of the entire liver with MR-pathology correlation; 2) inhomogeneous arterial enhancement of the liver; 3) changes in segmental shape and size and 4) vessel malformation, inflammatory infiltration and subtle periportal fibrotic changes at histology (Fig. 7, 8 and 9). Detailed findings are described below.

Liver morphology at MR imaging

Visual assessment of size and shape of the liver was performed in 10 patients. The remaining 3 patients either underwent partial hepatic surgery previously (n=2) or had diffuse hepatic abnormalities because of storage disease (n=1). In all 10 patients, abnormal segmental size and shape was observed. In 6 of 10 patients, an enlarged left liver lobe was observed, in which the liver partially encircled the spleen in some cases (Fig 7a, b). In 3 of 10 patients, an abnormal size of the right liver lobe was present (Fig 7c, d). The aspect of the liver in these cases, with fatty infiltration, enlargement of Couinaud's segment 6 and 7, in combination with enlargement of segments 5 and 8 made co-existence of a Riedel's lobe less likely. In one pa-

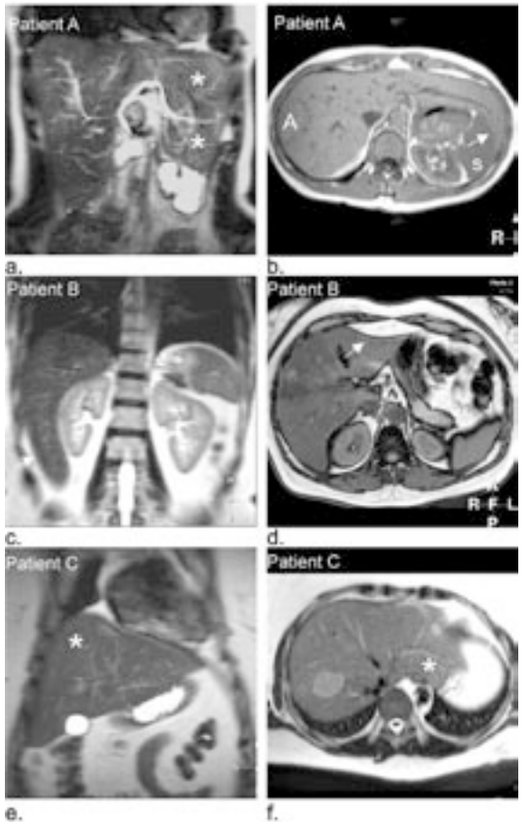

Figure 7: Abnormalities in segmental size and shape in three patients with hepatocellular adenoma. (a) Patient A; Coronal single-shot T2-weighted fast spin-echo shows an abnormally shaped and enlarged left liver lobe (*). (b) Patient A; Transverse in-phase T1-weighted gradient-echo shows a large left liver lobe, which extends beyond the spleen (s) and even partially encircles it (arrow). Note the adenoma (a), which is isointense to slightly hypointense to the surrounding liver. (c) Patient B; Coronal single-shot T2-weighted fast spin-echo shows an enlarged right liver lobe, which extends well beyond the right kidney (arrow). (d) Patient B; Transverse opposed-phase T1-weighted gradient-echo shows concavity of the left liver lobe, located in Couinaud's segment 3 (arrow). Note an inhomogeneous low signal intensity of the liver, indicating steatosis (in-phase T1-weighted gradient-echo not shown). (e) Patient C; Coronal single-shot T2-weighted fast spin-echo shows an entirely enlarged liver, with abnormal shape and dominant Couinaud's segment 8 (right liver lobe). (f) Patient C; Transverse single-shot T2-weighted fast spin-echo shows a slight bulging of the left liver lobe (*). Note the hyperintense adenoma in the right liver lobe.

tient, total liver enlargement was observed (Fig 7e, f). Whilst some segments showed enlargement, at the same time, other segment seemed atrophic, even with an empty gallbladder fossa at times. Assessment of size was performed only visually because the small group size would potentially result in unreliable data measurements. No signs of cirrhosis were present.

Signal intensity and dynamic gadolinium-enhanced imaging of the liver

Liver steatosis was observed in 10 of 13 patients (77%), graded as marked in 4 of 13 patients (30.8%) and focal in 6 patients (46.2%) (Fig. 8). In the arterial phase of dynamic gadolinium-enhanced imaging, abnormal enhancement of the liver parenchyma was observed in 12 of 13 patients (92.3%), which consisted of transient, diffuse or segmental, patchy, heterogeneous enhancement of the liver parenchyma (Fig 9). The enhancement became homogeneous in the portal and delayed phase in all patients. The inhomogeneous arterial enhancement is most likely explained by a combination of fatty infiltration and vascular malformation with shunting.

MR-histopathology correlation of the liver parenchyma

MR imaging findings of the liver parenchyma were confirmed at histopathology, which showed extensive steatosis of the hepatic stroma in 2 of 10 patients (20%) and moderate steatosis in 7 of 10 patients (70%). Vascular anatomy could be assessed in 9 patients, 8 of whom (89%) showed abnormally wide portal veins with periportal vessel formation. An inflammatory infiltrate was observed in 9 of 10 patients, consisting of lymphocytes and scattered macrophages (Fig 8). Arrangement of hepatocytes in layered plates was organized in 6 of 10 patients and mildly chaotic in 2 of 10 patients. Size of the hepatocytes was enlarged in 2 of 10 patients, mainly due to presence of extensive large vacuolar fatty infiltration in those cases. The size of nuclei and cytoplasm was mildly disturbed in one patient, who also had extensive fatty infiltration. Fibrosis could be assessed in 9 patients, and was scaled as F0 in 5 patients, F1 in 3 patients and F2 in one patient.

DISCUSSION

The results of our study show that in patients with hepatocellular adenomas (HCA), both lesions as well as the surrounding liver parenchyma show similar soft tissue and vascular abnormalities. Specific results of our study indicate that in patients with HCA, the lesions show the following characteristics: 1) accumulation of fat is present in >70% of HCA; 2) signal intensity of HCA is predominantly hyperintense on T2-weighted fat-suppressed sequences with high CNR, facilitating the detection of multiple lesions; 3) enhancement of HCA is early and intense in the arterial phase with

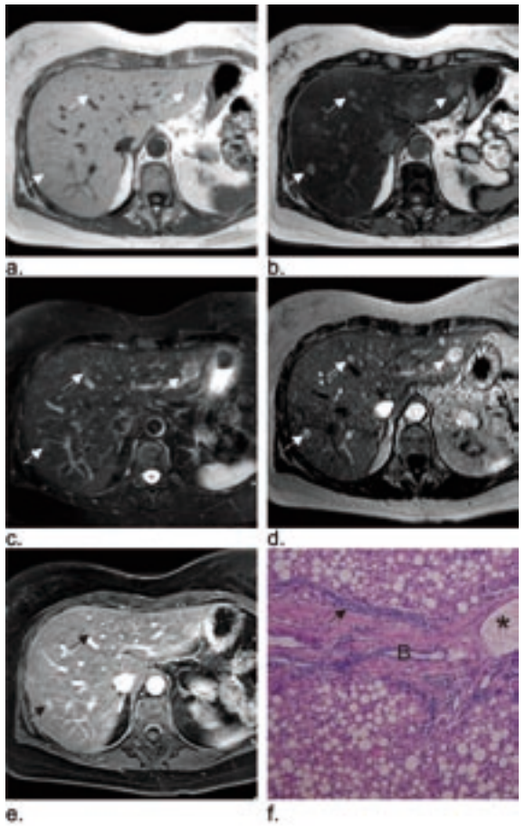

Figure 8: Liver abnormalities in hepatocellular adenoma. (a) Transverse in-phase T1-weighted gradient-echo shows isointensity of the lesions. (b) Transverse opposed-phase T1-weighted gradient-echo shows marked decrease in signal intensity of the entire liver parenchyma, indicating extensive steatosis. Note a hyperintense signal intensity of three lesions compared to the surrounding liver (arrows). (c) Transverse fat-suppressed T2-weighted fast spin-echo shows faint hyperintensity of the lesions (arrows). (d) Transverse arterial phase gadolinium-enhanced T1-weighted gradient-echo shows intense homogeneous enhancement of the lesions (arrows). (e) Transverse delayed phase gadolinium-enhanced three-dimensional T1-weighted gradient-echo shows the lesions remain slightly hyperintense compared to the liver (arrows) (f) Photomicrograph (hematoxylin and eosin (HE) stain, original magnification x100) shows extensive fatty infiltration within the hepatocytes, inflammatory infiltration (arrow) around the vessels consisting of small-cell lymphocytes and scattered macrophages. Note a large periportal vessel (*), aligned next to a bile duct (B).

fading to near isointensity in delayed phase imaging. The surrounding liver parenchyma shows co-existing abnormalities, including 1) changed segmental distribution; 2) steatosis and 3) inhomogeneous arterial enhancement. These findings confirm our hypothesis that an interrelation exists between the tissue changes in both lesions and liver parenchyma in patients with HCA.

These findings are clinically relevant. In our study, intratumoral fat was observed in >70% of HCA, in correspondence with a recent study in which accumulation of fat was described in 35-77%[20]. In contrast, fatty components are observed in only a minority of FNH[20]. On T2-weighted sequences, including single-shot T2-weighted FSE, fat-suppressed T2-weighted FSE and diffusion-weighted BBEPI, the lesions appeared increasingly hyperintense. The difference in liver-to-lesion contrast of fat-suppressed T2-weighted FSE and BBEPI compared to single-shot T2-weighted FSE most likely resulted from the fat suppression technique with fewer refocusing pulses. Also, in comparing single-shot FSE, fat-suppressed FSE and BBEPI, magnetic transfer of contrast (MTC) effects decrease, which result in improved detection of lesions with increased signal intensity compared to the liver, since MTC effects lower the liver-to-lesions contrast due to saturation of macromolecules[21]. In considering the observed enhancement pattern of HCA, early homogeneous enhancement was observed in the arte-

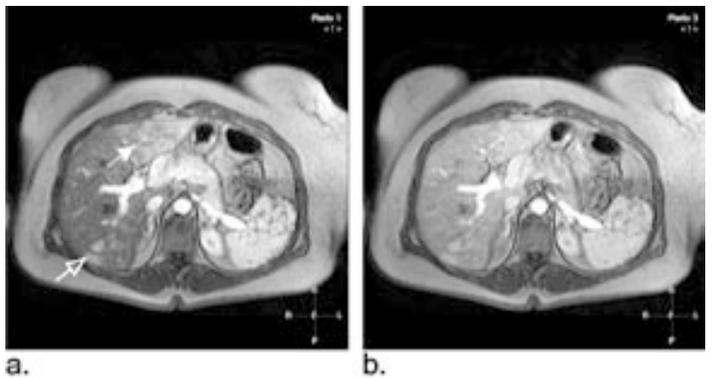

Figure 9: Patchy arterial enhancement of the liver in case of hepatocellular adenoma (the same patient as figure 7). (a) Transverse arterial phase gadolinium-enhanced T1-weighted gradient-echo shows patchy enhancement of the liver (left liver lobe, arrow). Note two intensely enhancing lesions in the right liver lobe (open arrow). (b) Transverse delayed phase gadolinium-enhanced T1-weighted gradient-echo shows the patchy enhancement has become near isointense.

rial phase with fading to isointensity in the delayed phase. Other primary liver lesions such as focal nodular hyperplasia (FNH) and hepatocellular carcinoma (HCC) show quite different enhancement patterns. FNH enhances more intensely in the arterial phase, with delayed enhancement of central scar and septa. Large (>5 cm) HCC shows heterogeneous enhancement, with delayed phase washout and capsule enhancement. Hemangioma, enhances in a peripheral nodular way, to become and remain isointense with the liver in delayed phase imaging[1]. Distinction of HCA from FNH in case of multiple primary liver lesions in (young) female patients is important, since diagnosis of HCA has direct therapeutic consequences. Oral contraceptives should be stopped and, more importantly, pregnancy may be contraindicated in case of multiple or larger lesions. In some cases, partial liver resection or even liver transplantation is considered[22]. Considering the reported liver abnormalities, previously, the assessment of abnormalities in liver architecture has mainly served for evaluation purposes in liver cirrhosis. A multitude of abnormalities have been described in cirrhosis, including altered volume ratios of right-, left and caudate liver lobe[23] representing both atrophic and hypertrophic reactions, resulting from changes in perfusion pattern. In our study, morphologic changes with abnormal segmental shape and size were observed in all patients, although pathological analysis showed only slight fibrotic changes in a few cases. Also, areas of patchy enhancement in the arterial phase were observed, most likely related to vascular alterations and inflammatory infiltration at histology, which has also been described in acute or chronic hepatitis[24,25]. These findings suggest diffuse alterations in the liver as part of the ongoing disease process in case of HCA, most likely related to oral contraception use, coexistence of overweight, pre-existing liver steatosis and genetic risk factors; but this is yet to be defined.

There are several limitations to our study, including 1) relatively small amount of included patients, 2) creation of an inclusion bias in considering only pathology-proven HCA; 3) the retrospective study design and 4) absence of a control group of normal liver parenchyma of matched patients that did not use OC for the analyses of histology sections. In our opinion, the small amount of included patients results directly from the ability of MR imaging to differentiate and characterize focal liver lesions in a highly accurate way. Although percutaneous needle biopsy is still considered the golden standard, in many centers, diagnostic confidence in MR imaging diagnosis has improved at such rate that histological proof is not routinely obtained in all cases. Only larger HA (>5 cm), or lesions with signs suspect for HCC at imaging will need surgical resection or at least percutaneous biopsy. Even though the analysis of liver sections in case of HCA is limited, we think the results of this study warrants further evaluation of the exact extent and underlying pathogenesis of the abnormalities in hepatic stroma in case of HCA. This may include further prospective studies with more extensive pathologic evaluation of the liver, combined with data after intake of oral contraceptives have been stopped.

In conclusion, our findings indicate that in patients with HCA, abnormalities are observed in both lesions and liver; 1) HCA shows intratumoral fat in >70%, hyperintense signal intensity on T2-weighted fat-suppressed sequences and early arterial enhancement; 2) the surrounding liver parenchyma shows changed segmental distribution; steatosis and inhomogeneous patchy arterial enhancement. These results indicate that in patients with HCA, both lesions as well as surrounding liver parenchyma show similar soft tissue and vascular abnormalities.

REFERENCES

1. Hussain SM, Semelka RC. Liver masses. Magn Reson Imaging Clin N Am 2005; 13:255-275.
2. Rooks JB, Ory HW, Ishak KG, et al. Epidemiology of hepatocellular adenoma. The role of oral contraceptive use. Jama 1979; 242:644-648.
3. Tao LC. Are oral contraceptive-associated liver cell adenomas premalignant? Acta Cytol 1992; 36:338-344.
4. Grazioli L, Federle MP, Brancatelli G, Ichikawa T, Olivetti L, Blachar A. Hepatic adenomas: imaging and pathologic findings. Radiographics 2001; 21:877-892; discussion 892-874.
5. International Working Party. Terminology of nodular hepatocellular lesions. Hepatology 1995; 22:983-993.
6. Flejou JF, Barge J, Menu Y, et al. Liver adenomatosis. An entity distinct from liver adenoma? Gastroenterology 1985; 89:1132-1138.
7. Anthony PP. Tumors and tumor-like lesions of the liver and biliary tract: aetiology, epidemiology and pathology. In: MacSween RNM BA, Portmann BC, ed. Pathology of the liver: Churchill Livingstone, 2002; 711-775.
8. Hussain SM, Semelka RC. Hepatic imaging: comparison of modalities. Radiol Clin North Am 2005; 43:929-947, ix.
9. Ichikawa T, Federle MP, Grazioli L, Nalesnik M. Hepatocellular adenoma: multiphasic CT and histopathologic findings in 25 patients. Radiology 2000; 214:861-868.
10. Semelka RC. Radiation Risk From CT Scans: A Call for Patient-Focused Imaging. Medscape Radiology 2005; 6(1).
11. Chung KY, Mayo-Smith WW, Saini S, Rahmouni A, Golli M, Mathieu D. Hepatocellular adenoma: MR imaging features with pathologic correlation. AJR Am J Roentgenol 1995; 165:303-308.
12. Arrive L, Flejou JF, Vilgrain V, et al. Hepatic adenoma: MR findings in 51 pathology-proven lesions. Radiology 1994; 193:507-512.
13. Paulson EK, McClellan JS, Washington K, Spritzer CE, Meyers WC, Baker ME. Hepatic adenoma: MR characteristics and correlation with pathologic findings. AJR Am J Roentgenol 1994; 163:113-116.
14. Grazioli L, Morana G, Kirchin MA, Schneider G. Accurate differentiation of focal nodular hyperplasia from hepatic adenoma at gadobenate dimeglumine-enhanced MR imaging: prospective study. Radiology 2005; 236:166-177.
15. Scharitzer M, Schima W, Schober E, et al. Characterization of hepatocellular tumors: value of mangafodipir-enhanced magnetic resonance imaging. J Comput Assist Tomogr 2005; 29:181-190.
16. Psatha EA, Semelka RC, Armao D, Woosley JT, Firat Z, Schneider G. Hepatocellular adenomas in men: MRI findings in four patients. J Magn Reson Imaging 2005; 22:258-264.
17. Grazioli L, Federle MP, Ichikawa T, Balzano E, Nalesnik M, Madariaga J. Liver adenomatosis: clinical, pathologic, and imaging findings in 15 patients. Radiology 2000; 216:395-402.
18. Bioulac-Sage P, Rebouissou S, Sa Cunha A, et al. Clinical, morphologic, and molecular features defining so-called telangiectatic focal nodular hyperplasias of the liver. Gastroenterology 2005; 128:1211-1218.
19. Hussain SM, van den Bos IC, Dwarkasing RS, Kuiper JW, den Hollander J. Hepatocellular adenoma: findings at state-of-the-art magnetic resonance imaging, ultrasound, computed tomography and pathologic analysis. Eur Radiol 2006 Sep; 16(9): 1873-86.
20. Prasad SR, Wang H, Rosas H, et al. Fat-containing lesions of the liver: radiologic-pathologic correlation. Radiographics 2005; 25:321-331.
21. Hussain SM, De Becker J, Hop WC, Dwarkasing S, Wielopolski PA. Can a single-shot black-blood T2-weighted spin-echo echo-planar imaging sequence with sensitivity encoding replace the respiratory-triggered turbo spin-echo sequence for the liver? An optimization and feasibility study. J Magn Reson Imaging 2005; 21:219-229.
22. Terkivatan T, de Wilt JH, de Man RA, et al. Indications and long-term outcome of treatment for benign hepatic tumors: a critical appraisal. Arch Surg 2001; 136:1033-1038.
23. Ito K, Mitchell DG, Hann HW, et al. Progressive viral-induced cirrhosis: serial MR imaging findings and clinical correlation. Radiology 1998; 207:729--735.
24. Martin DR, Seibert D, Yang M, Salman K, Frick MP. Reversible heterogeneous arterial phase liver perfusion associated with transient acute hepatitis: findings on gadolinium-enhanced MRI. J Magn Reson Imaging 2004; 20:838-842.
25. Semelka RC, Chung JJ, Hussain SM, Marcos HB, Woosley JT. Chronic hepatitis: correlation of early patchy and late linear enhancement patterns on gadolinium-enhanced MR images with histopathology initial experience. J Magn Reson Imaging 2001; 13:385-391.

chapter4
MR IMAGING OF HEPATO-CELLULAR CARCINOMA

chapter4.1
step-wise carcinogenesis of hepatocellular carcinoma

Step-wise carcinogenesis of HEPATOCELLULAR CARCINOMA

in the cirrhotic liver:
demonstration on serial MR imaging

ABSTRACT

Purpose: To demonstrate imaging findings of step-wise carcinogenesis of hepatocellular carcinoma (HCC) in cirrhosis at serial state-of-the-art MR imaging exams.

Material and Methods: In a retrospective search of the hospital archives, three patients were identified in which developing HCC was observed in serial MR examinations, with histopathology or alpha-foetoprotein (AFP) correlation. Image findings were assessed for signal intensity of the lesions at multiple sequences, including dynamic gadolinium-enhanced imaging.

Results: Initial findings in patient A showed a small nodule with fatty infiltration, which developed in HCC in follow-up MR imaging, comprised of low-grade dysplastic nodule (DN), high-grade DN and eventually classic HCC. In patient B, increased signal intensity on T2-weighted images in a single DN among numerous regenerative nodules was the only initial sign. Follow-up MR imaging showed further increase in signal intensity and increased neovascularity, which suggested focal HCC in a high-grade DN. Patient C demonstrated gradually increasing neovascularity as only initial sign, with development of classic HCC over time.

Conclusion: MR imaging provides insight in various pathways of step-wise carcinogenesis of developing hepatocellular carcinoma in cirrhosis. This may further explain the genetic heterogeneity, and may facilitate early detection and better selection of patients for follow-up.

Indra C. van den Bos, MD[1], Shahid M. Hussain, MD, PhD[1,2], Türkan Terkivatan, MD, PhD[3], Pieter E. Zondervan, MD[4], Robert A. de Man, MD, PhD[5]

Departments of [1]Radiology, [3]Surgery, [4]Pathology and [5]Gastroenterology and Hepatology, Erasmus MC, University Medical Center Rotterdam, The Netherlands; [2]Department of Radiology, University of Nebraska Medical Center, Omaha, NE, USA

Journal of Magnetic Resonance Imaging, 2006 Nov; 24(5): 1071-80.

INTRODUCTION

In cirrhotic livers, HCC typically develops in a step-wise fashion, which has been described by Sakamoto and colleagues in 1991[1]. According to their findings, the step-wise carcinogenesis of HCC is based on increasing cellularity and size of the liver lesion. In 1995, an International Working Party of Gastroenterology proposed a terminology in which dysplastic features of the hepatic nodule is expressed[2]. The currently accepted nomenclature in step-wise carcinogenesis of HCC is regenerative nodule (RN) – low grade dysplastic nodule (DN I)) – high grade dysplastic nodule (DN II) – small HCC – large HCC (see Fig. 1)[3].

Early detection of HCC in patients with cirrhosis is important in improving patient outcome and decision making in therapeutic strategies. Observation of the patient, regular blood serum analysis of liver function and tumor antigens such as alpha-fetoprotein (AFP) and follow-up imaging examinations are indicated for correct and timely decision-making[4]. Although AFP is not specific for HCC, and can give false-positive results in hepatitis, fibrosis, and cirrhosis[5], it is useful in monitoring the disease process in combination with imaging results. Currently, treatment of HCC includes liver transplantation, segmental liver resection, percutaneous minimal invasive therapies, such as radiofrequency ablation (RFA), stereotactic radiation therapy[6], transarterial (chemo)-embolization procedures and gene or immune therapies[7].

Accurate detection of small HCC in cirrhosis and distinction from other hepatocellular nodules may be challenging using ultrasound and CT[8]. Although helical multi-phasic CT is promising for evaluation of neo-vasculature in patients with clinically suspect disease[9,10], it may create diagnostic dilemmas due to presence of hemodynamic changes because of portal hypertension and extensive structural abnormalities[11]. For early detection of HCC, MR imaging is potentially more promising[8,12].

State-of-the-art MR allows better visualization of intrinsic contrast characteristics of liver tissue[13]. Adequate information can be provided on both accumulations of fat on chemical-shift imaging and iron on T2*-weighted sequences. Current high spatial and temporal resolution of fat-suppressed three-dimensional T1-weighted sequences with thin sections allows superior dynamic contrast-enhanced scanning which enables detection of neovascularity in an early stage[14], without radiation exposure. Tissue specific contrast agents, such as super-paramagnetic iron-oxide particles (SPIO), are specifically targeted at Kupffer cells and should mainly serve to determine the primary versus secondary nature of a liver lesion non-invasively[15,16]. In addition, diffusion information and spectroscopy may facilitate diagnostics in the future[17]. These characteristics make MR imaging an ideal imaging modality for detection and differentiation of focal liver lesions.

Several studies have described the characteristics of different cirrhotic nodules at MR imaging. In one study, published by Sadek and colleagues in 1995, it was demonstrated that lesions with a nodule-within-a-nodule appearance on T2-weighted images have potential for rapid growth[18]. To our knowledge however, serial state-of-the-art MR imaging findings of developing HCC have not been demonstrated in detail before.

The purpose of this paper therefore was to evaluate and illustrate the imaging findings of step-wise carcinogenesis of hepatocellular carcinoma in cirrhosis at sequential state-of-the-art MR imaging.

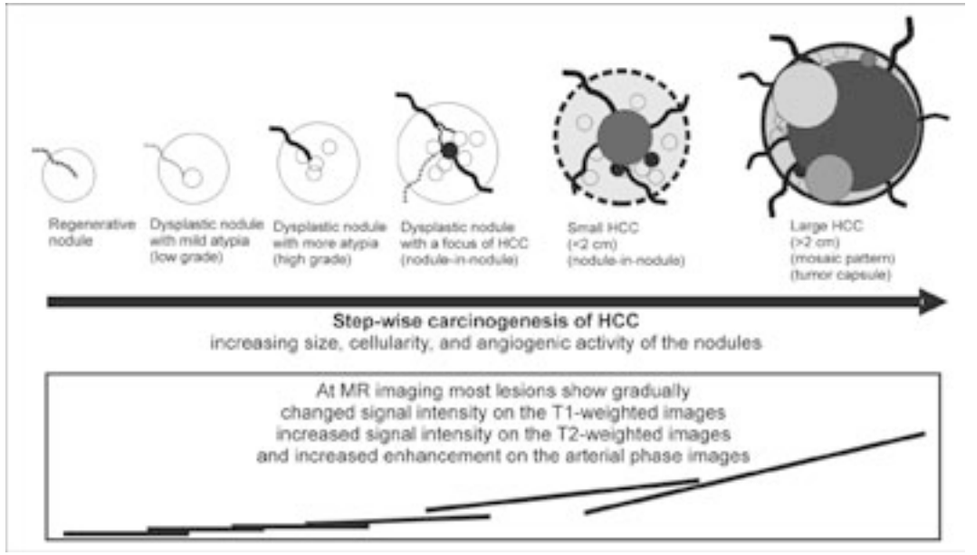

Figure 1: In the step-wise transition of RN-DN-HCC, increase in size, increasing cellularity and increasing neovascularity surrounding the nodules are observed. Enhancement patterns on dynamic gadolinium-enhanced images show increasing arterial enhancement, which may overlap with previous or next stages in the carcinogenesis.

MATERIALS AND METHODS

MR imaging reports of all patients who had undergone MR imaging of the liver between January 2000 and December 2004 were reviewed to identify patients with sequential exams in the setting of cirrhosis or fibrosis. MR imaging data were cross-referenced with pathology and laboratory reports from the same period. Patients were included if: 1) they had undergone sequential MR imaging examinations; 2) they had evidence of a suspected lesion or area within pathology-proven cirrhotic or fibrotic liver that showed changes over time; and 3) MRI findings could be correlated to either AFP or pathology findings.

Only three patients from a total of 320 patients fulfilled the inclusion criteria. These patients were all male with a range in age of 42 to 59 years (mean 52 years). A total of 19 (10, 5, 4 respectively) MR examinations were performed in a mean period of 24 months (range 14-33).

All examinations were performed at 1.5T (Philips Medical Systems, Best, The Netherlands or General Electrics, Signa, Milwaukee, Wis; with identical scan protocols) using a body-array coil. The standard MR imaging protocol in our institution includes single-shot fast spin-echo (repetition-time msec/ echo-time msec 832/90-120; flip-angle 90°), fat-suppressed T2-weighted fast spin-echo (3000/80, flip-angle 90°), and T1-weighted in- and opposed-phase gradient-echo

(shortest/4.6 and 2.3 respectively, flip-angle 80º) sequences. Dynamic contrast-enhanced exams were performed either with two-dimensional T1-weighted gradient-echo (126/shortest, flip angle 90º) or three-dimensional T1-weighted fat-suppressed gradient-echo (shortest/shortest, flip angle 15º), in at least 4 phases using 0.1 mmol/kg of non-liver specific gadolinium-chelate (Magnevist [gadopentetate-dimeglumine], Schering, Berlin, Germany). The MR imaging exams were transported digitally using a picture archiving and communication system to a viewing station. Analysis of the liver lesions was performed by two radiologists in consensus for the following items: 1) detection of focal liver lesions, 2) signal intensity at various T1- and T2-weighted sequences, 3) characterization of enhancement patterns at dynamic gadolinium-enhanced imaging, and 4) description of morphology of both liver and lesion in combination with growth pattern of the lesion.

RESULTS

Patient A

A 54-year old man with chronic hepatitis C infection since 1974 and long-term alcoholism was referred to our department for follow-up MR imaging. At physical examination no abnormalities were observed. Pathological evaluation of a percutaneous needle biopsy in 2000 showed liver fibrosis without septa (Metavir F3[19]). Ultrasound imaging revealed a small (5 mm) hypoechogenic nodule in the left liver lobe, which was subsequently evaluated with CT. This confirmed a small hypodense nodule without any enhancement in the arterial and portovenous phases after contrast administration. For further characterization and evaluation, the patient was referred for MR imaging. In the following section, the findings at various follow-up MR imaging exams will be described and correlated to the AFP level (see Fig. 2).

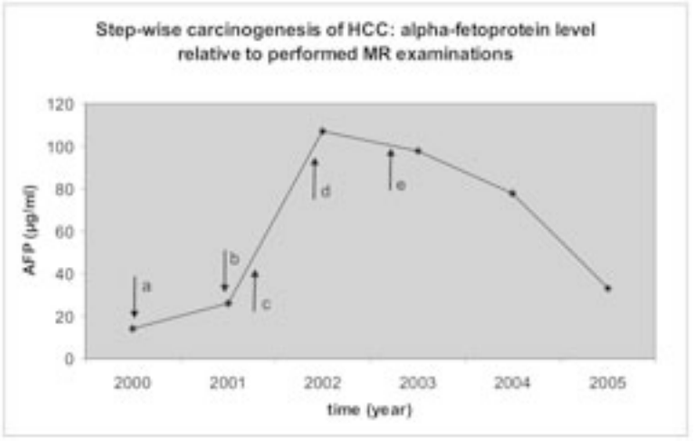

Figure 2: Alpha-fetoprotein (AFP) level (range < 7 µg/ml) relative to performed MRI exams in patient A; (a) initial MRI (see Fig. 3); (b) MRI at 12 months after initial exam (see Fig. 4); (c) MRI at 15 months after initial exam (Fig. 5); (d) MRI at 25 months after initial exam (Fig. 6); (e) radiofrequency ablation (RFA).

Initial MR imaging findings: On in-phase T1-weighted gradient-echo (GRE) (see Fig. 3a), no lesions were detected, whereas on opposed-phase GRE (see Fig. 3b), a small area of 7 mm in diameter was visible with decreased signal intensity compared to the surrounding liver, indicating a fat-containing area, most likely within a nodule. Fat-suppressed T2-weighted fast spin-echo (FSE) showed no abnormalities (see Fig. 3c). In the arterial phase of gadolinium-enhanced T1-weighted gradient-echo (GRE) (see Fig. 3d), slightly less intense enhancement was noted, most likely due to a combination of less enhancement and focal accumulation of fat. These findings were interpreted as a local area with fat infiltration or a RN/DN I with fatty infiltration. Follow-up MRI imaging was recommended in 6 months. AFP was 14 µg/ml (normal range < 7 µg/ml) (see Fig. 2). Because of poor patient compliance, the follow-up MR imaging was performed only after one year.

MR imaging findings at 12 months after the initial exam: on in-phase T1-weighted GRE still no nodule was visible (not shown). Opposed-phase T1-weighted GRE (see Fig. 4a) showed an increase in size (10 mm). Fat-suppressed T2-weighted FSE now demonstrated a subtle hyperintensity in the area (see Fig. 4b). In arterial phase gadolinium-enhanced T1-weighted GRE, the nodule was now isointense with the liver, possibly because of increasing enhancement of the lesion (see Fig. 4c). In the delayed phase of the same sequence, the nodule was slightly hypointense (see Fig. 4d), most likely due to a combination of local accumulation of fat and some washout. Serum AFP was about twice as high at 26µg/ml (see Fig. 2). The lesion was classified as possible DN II without clear evidence of HCC.

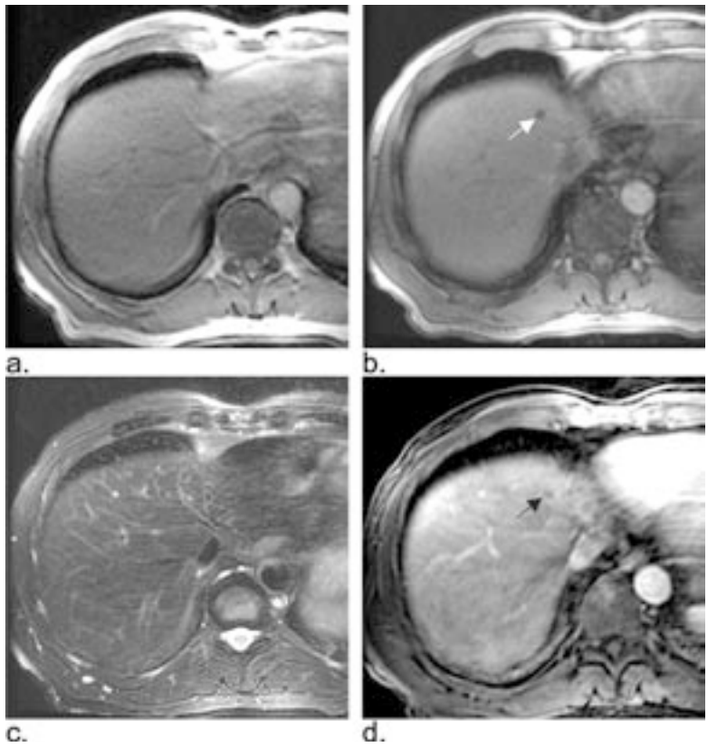

Figure 3: Initial MR examination in patient A, a 54-year old man with hepatitis C – related liver fibrosis. (a) In-phase T1-weighted gradient-echo shows no lesion (b) Transverse opposed-phase T1-weighted gradient-echo shows a small area with decreased signal (arrow), most likely within a regenerative or low-dysplastic nodule. (c) Transverse fat-suppressed T2-weighted fast spin-echo shows no abnormalities. (d) Transverse arterial phase gadolinium-enhanced fat-suppressed three-dimensional T1-weighted gradient-echo shows slight hypointensity (arrow), most likely due to a combination of less enhancement and effect of the fat suppression pulse.

MR imaging findings at 15 months after the initial exam: the nodule had increased in size to 15 mm, and now showed a clear hypointense signal intensity on both in-phase and opposed-phase T1-weighted GRE (see Fig. 5a), and subtle hyperintensity on fat-suppressed T2-weighted FSE (see Fig. 5b). At gadolinium-enhanced imaging, intense arterial phase enhancement was noted in a small nodule within the lesion (see Fig. 5c) (nodule-within-a-nodule), with washout in the delayed phase (see Fig. 5d). This was compatible with DN II, now with a focus of HCC. Serum AFP had risen to 39 µg/ml (see Fig. 2). Meanwhile, the patient showed poor compliance with the advice to reduce alcohol intake, regular visits to our outpatient clinic and regular follow-up MR imaging. Therefore, follow-up MRI imaging was only performed after 9 months.

MR imaging findings at 25 months after the initial exam: the lesion had tripled in size (3 cm). Signal intensity was low on in-phase T1-weighted GRE (see Fig. 6a), and markedly hyperintense on fat-suppressed T2-weighted FSE (see Fig. 6b). gadolinium-enhanced imaging showed intense, homogeneous enhancement in the arterial phase with washout and capsule enhancement in the delayed phase (see Fig. 6c-d), compatible with a large (>2 cm) HCC. Serum AFP had risen to 107 µg/ml (see Fig. 2).

Based on the presence of a single lesion and preserved liver functions, the liver tumor board of the hospital recommended partial liver resection to our patient who refused to undergo surgical treatment for his condition. Alternatively, to achieve local control of the disease and to prevent local dissemination, ultrasound guided radiofrequency ablation therapy was applied. Serum AFP lowered to 33µg/ml (see Fig. 2). Currently, follow-up MR examinations are performed every 3 months.

Patient B

A 59-year old man with chronic hepatitis B infection since 1981 and pathology-proven cirrhosis (Metavir F4) since 1992 showed slightly increased liver transaminases as well as AFP (10-15 µg/ml). These values, though, had been stable since several years. Routine follow-up ultrasound examinations were performed every 6 to 12 months since 1987, which showed a macro-nodular, inhomogeneous liver. The first MR imaging was performed in November 2000 because of complaints of pain in the right upper abdomen.

Initial MR imaging findings (not shown): an impressive macro-nodular liver parenchyma was observed with multiple nodular structures. Subcapsular in the left liver lobe, a larger nodule was observed with slightly higher signal intensity at T2-weighted images compared to the surrounding nodules, which was considered a possible DN. Apart from this lesion, over time, several other areas showed subtle changes in

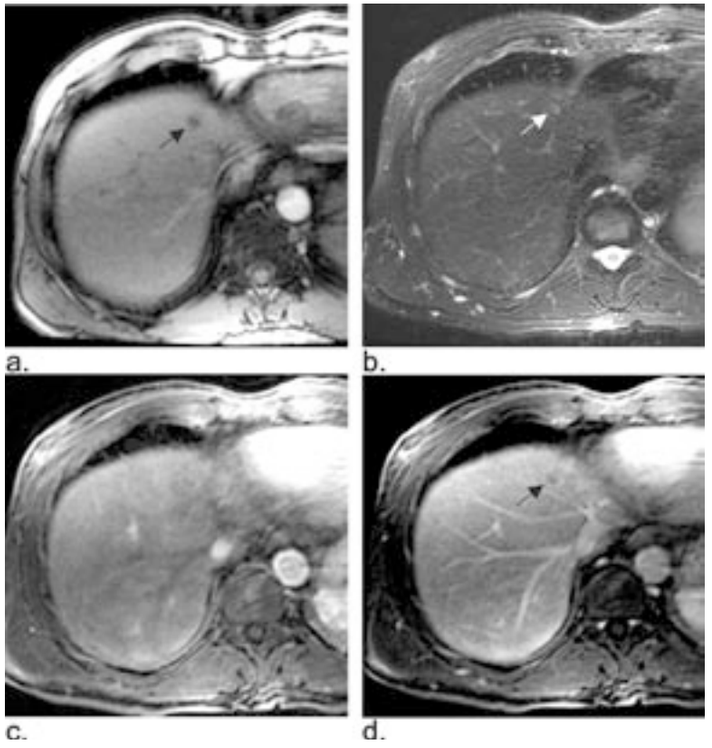

Figure 4: MR imaging findings at 12 months after initial exam in patient A. (a) Transverse opposed-phase T1-weighted gradient-echo shows increase in size of the nodule (arrow). (b) Transverse fat-suppressed T2-weighted fast spin-echo shows a subtle increase in signal intensity (arrow). (c) Transverse arterial phase gadolinium-enhanced fat-suppressed three-dimensional T1-weighted gradient-echo shows near isointensity of the nodule, indicating increasing arterial enhancement. (d) Transverse delayed phase gadolinium-enhanced fat-suppressed three-dimensional T1-weighted gradient-echo shows the nodule appears hypointense compared to the liver (arrow), probably due to a combination of some washout and fatty content.

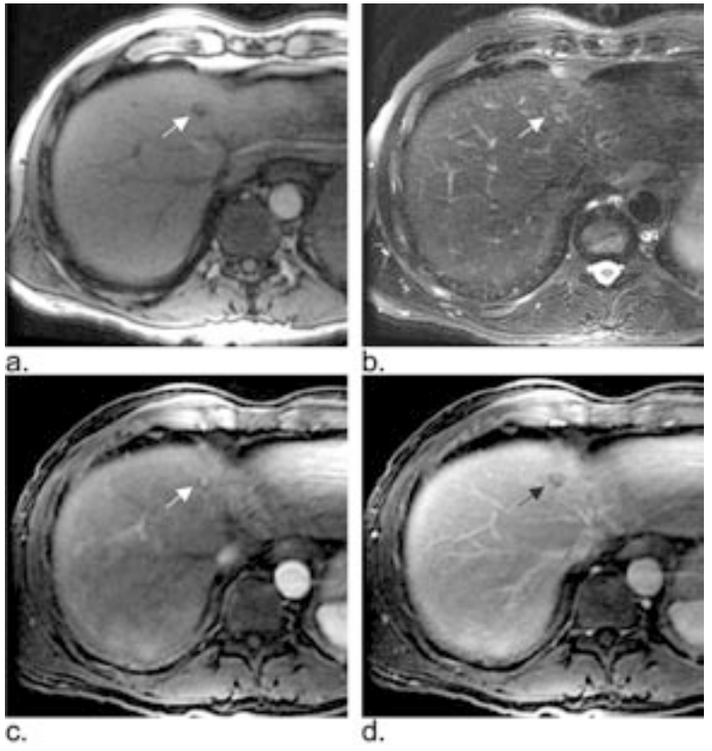

Figure 5: MR imaging findings at 15 months after the initial exam in patient A. (a) Transverse opposed-phase T1-weighted gradient-echo shows the nodule has further increased in size (arrow). (b) Transverse fat-suppressed T2-weighted fast spin-echo shows a larger area with subtle increase in signal intensity (arrow). (c) Transverse arterial phase gadolinium-enhanced fat-suppressed three-dimensional T1-weighted gradient-echo shows a smaller enhancing nodule (arrow) within the larger nodule (nodule-within-a-nodule appearance). (d) Transverse delayed phase gadolinium-enhanced fat-suppressed three-dimensional T1-weighted gradient-echo shows the nodule becomes much more hypointense, due to clear washout of contrast material (arrow).

signal intensity of the nodules over time, which was interpreted as multiple RN with high risk of dysplastic transformation, for which short-term follow-up examinations were advised and performed. Mainly based on the MR imaging findings and expected high risk of malignant transformation, the liver tumor board decided on admission to the national liver-transplant waiting list.

The last MR examination, performed 2 months prior to liver transplantation, showed the above described multiple nodular structures, slightly hyperintense on opposed-phase T1-weighted GRE (see Fig. 7a) and slightly hypointense on T2-weighted imaging (see Fig. 7b). The dominant, subcapsular nodule now showed a heterogeneous high signal intensity in fat-suppressed T2-weighted FSE (see Fig. 7b), which had increased slightly compared to the previous exam (not shown). At gadolinium-enhanced arterial phase imaging, subtle nodular enhancement was now observed in the periphery of the lesion (see Fig. 7c) whilst the remainder of the nodule enhanced in a fashion similar to the other nodules, although better visible in the delayed phase (see Fig. 7d).
Because of this new finding, this DN was now classified as possibly having a small focus of HCC. After liver transplantation, macroscopic examination of the explant liver specimen confirmed the diffusely macronodular liver parenchyma, with the dominant nodule subcapsular in left liver lobe (see Fig. 7e). Photomicrograph (original magnification x100) showed a transition of almost normal appearing hepatocytes into a focus of HCC, in which crowding of small nuclei and small cell dysplasia in combination with more than three-cells thick plates and very small vessels was observed (see Fig 7f).

Patient C

A 42-year old man with a chronic hepatitis B infection since 1985 and pathology-proven cirrhosis (Metavir F4) in 1997 was referred to our department for diagnostic imaging. Clinical examination showed no abnormalities. Liver function was normal; AFP was 44 µg/ml and stable at this level since 3 years. Initial routine ultrasound examination showed a small inhomogeneous liver with irregular borders. Detection of lesions was technically unreliable, for which patient was referred for MR imaging in 2003.

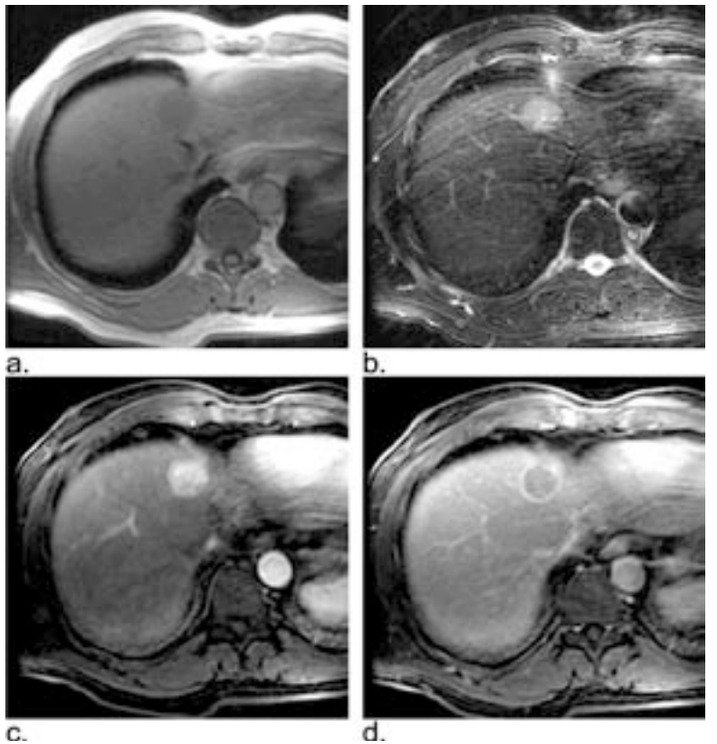

Figure 6: MR imaging findings at 25 months after the initial exam in patient A. (a) Transverse in-phase T1-weighted gradient-echo shows the nodule has tripled in size (3 cm). (b) Transverse fat-suppressed T2-weighted fast spin-echo shows a clear, markedly high signal intensity. (c) Transverse arterial phase gadolinium-enhanced fat-suppressed three-dimensional T1-weighted gradient-echo shows clear intense enhancement of the entire lesion. (d) Transverse delayed phase gadolinium-enhanced fat-suppressed three-dimensional T1-weighted gradient-echo shows washout of contrast material and capsule-enhancement. The combination of the findings is compatible with a classic hepatocellular carcinoma.

Initial MR imaging findings: both T1-weighted and T2-weighted images (see Fig. 8a) did not show any distinct nodules. Dynamic imaging in the arterial phase revealed a small area (7 mm) with increased arterial enhancement (see Fig. 8b). In delayed phase

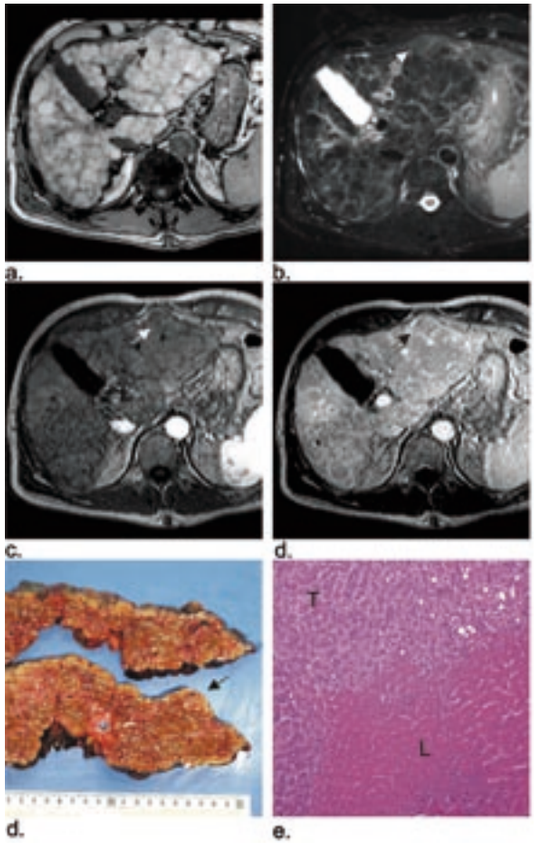

Figure 7: MR imaging findings in patient B, a 59-year old man with hepatitis B – related liver cirrhosis. (a) Transverse opposed-phase T1-weighted gradient-echo shows a frankly macronodular liver with multiple nodular structures. In the left lobe, a slightly larger and eccentric subcapsular nodule is present, with slightly lower signal intensity (arrow). (b) Transverse fat-suppressed T2-weighted fast spin-echo shows subtle hyperintensity within the dominant nodule (arrow). (c) Transverse arterial phase gadolinium-enhanced two-dimensional T1-weighted gradient-echo shows a subtle focus of enhancement within the nodule (arrow). (d) Transverse delayed phase gadolinium-enhanced two-dimensional T1-weighted gradient-echo shows that the nodule is surrounded by prominent septal enhancement (arrow). (e) Explant liver specimen with cross sections at two levels shows impressive macronodular cirrhosis, with the dominant nodule subcapsular in the left liver lobe (arrow) confirming the MRI findings. (f) Photomicrograph (hematoxylin and eosin (HE) stain, original magnification x100) shows a detailed view from an area within the dominant nodule with clear transition between almost normal appearing hepatocytes (L) into a focus of hepatocellular carcinoma (T), which is characterized by 1) crowding of small nuclei; 2) small cell dysplasia in combination with more than three-cells thick plates and 3) very small vessels.

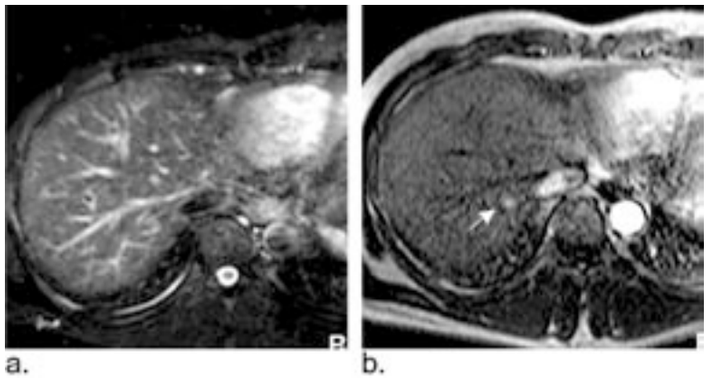

Figure 8: MR imaging findings in patient C, a 42-year old man with hepatitis B – related liver cirrhosis. (a) Transverse fat-suppressed T2-weighted fast spin-echo shows no abnormalities. (b Transverse arterial phase gadolinium-enhanced two-dimensional T1-weighted gradient-echo shows a small, early enhancing area in the right liver lobe (arrow).

imaging, no washout of contrast medium was visible. This small enhancing area, in the absence of other findings such as high signal intensity in T2-weighted images or washout was interpreted as a possible vascular shunt, or an early enhancing lesion. Follow-up MR was recommended to exclude the possibility of a developing small HCC.

MR imaging at 3 months after the initial exam: the enhancing area had increased in size (14 mm), and now showed a nodular configuration. Signal intensity was low on opposed-phase T1-weighted GRE (see Fig. 9a) and high on fat-suppressed T2-weighted FSE (see Fig. 9b). Dynamic gadolinium-enhanced T1-weighted GRE showed an intense arterial enhancement (see Fig. 9c) and subtle washout in the delayed phase (see Fig. 9d), suspicious for a small HCC. AFP was stable at 44 µg/ml. Based on these MR imaging findings, long-standing liver disease and clinical condition, the patient was placed on the national waiting list for liver transplantation.

MR imaging at 9 months after the initial exam: the lesion had doubled in size (9 to 23 mm), with identical signal intensity on T1- and T2-weighted images. In arterial phase gadolinium-enhanced T1-weighted GRE an intense enhancement was observed in the arterial phase (see Fig. 10a), with washout in the delayed phase. In addition, a second lesion was observed in the left liver lobe, with similar characteristics and strong, homogenous enhancement in the arterial phase of dynamic imaging (see Fig. 10b), suspicious for a second localization of HCC. AFP had risen to 56 µg/ml.

MR imaging at 13 months after the initial exam: both lesions had further increased in size (not shown). Because of a rapidly growing HCC and taking a waiting-list for liver transplantation into consideration, patient underwent a living-related liver-transplantation 4 months after the last MR examination, at which both lesions were proved to be a HCC. Macroscopic evaluation of the cirrhotic liver confirmed the two lesions, which had both increased in size. (see Fig 10c). Microscopic evaluation confirmed the diagnosis of HCC (see Fig. 10d). Specific endothelial staining (CD34) showed striking vascularity within the tumor (see Fig 10e).

DISCUSSION

This paper describes detailed imaging findings of developing hepatocellular carcinoma in cirrhosis at sequential MR imaging in three patients. State-of-the-art MR imaging displayed a spectrum of findings in the initial detection of developing HCC, including

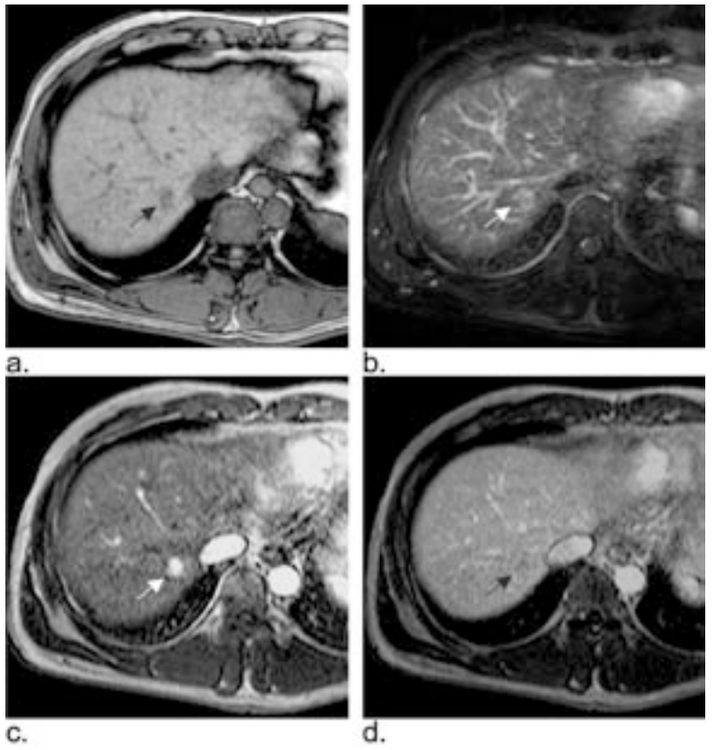

Figure 9: MR imaging findings at 3 months after the initial exam in patient C. (a) Transverse opposed-phase T1-weighted gradient-echo shows a hypointense nodule (arrow). (b) Transverse fat-suppressed T2-weighted fast spin-echo shows subtle increase in signal intensity (arrow). (c) Transverse arterial phase gadolinium-enhanced two-dimensional T1-weighted gradient-echo shows intense, increased enhancement of the nodule (arrow). (d) Transverse portal phase gadolinium-enhanced two-dimensional T1-weighted gradient-echo shows subtle washout of contrast material in at least a part of the nodule (arrow).

1) localized fatty infiltration within a developing dysplastic nodule that gradually evolved into HCC in combination with a slowly increasing AFP; 2) development of a focus of pathology-proven HCC with high signal intensity at T2-weighted imaging in a dysplastic nodule; 3) prominent neovasculature as the initial sign of developing, fast growing HCC, confirmed pathologically after liver explantation.

These findings provide evidence in support of the proposed step-wise carcinogenesis in HCC in vivo. Such findings are clinically significant and can be used for early detection of HCC, which may allow improved patient selection for close follow-up MR imaging. Also, the heterogeneity of MR imaging findings suggests that development of HCC may consist of a number of different genetic pathways, eventually leading to the

same entity. For better understanding of the various MR imaging findings and the possible explanation, this will be discussed in more detail.
In patient A, HCC developed in a period of 25 months. Initially, focal fatty infiltration was observed. In follow-up MR imaging, this nodule slowly increased in size, accompanied by changing signal intensity at T2-weighted imaging, which showed a discrete focus of hyperintensity (nodule-within-a-nodule appearance[20]). This change in signal intensity presumably indicated increased amount of fluid, but the exact nature remains unknown. In a later stage, developing neovascularity surrounding the lesion was detected, with a small focus of intense enhancement in a small area inside the nodule in the arterial phase of dynamic gadolinium-enhanced imaging. Basically, the poor patient compliance allowed detailed MR documentation of step-wise development of HCC, from RN through DN into full-blown HCC. MR imaging findings correlated with steadily increasing AFP. In patient B, development of focal HCC in a DN is illustrated, which showed focal high signal intensity within a nodule, with subtle nodular enhancement in the arterial phase of gadolinium-enhanced imaging. In this patient, liver transplantation was offered at an early stage, because of imaging findings of extensive macronodular changes of the liver parenchyma and expected high risk of malignant transformation. In patient C, HCC presented itself as prominent neovasculature as an initial finding, without any clear nodular changes in the area. In a period of 13 months, a large HCC had rapidly developed in this area, and, in addition a second lesion with identical characteristics had developed in the contralateral liver lobe. Both lesions were proved to be a HCC after pathological examination of the explanted liver.

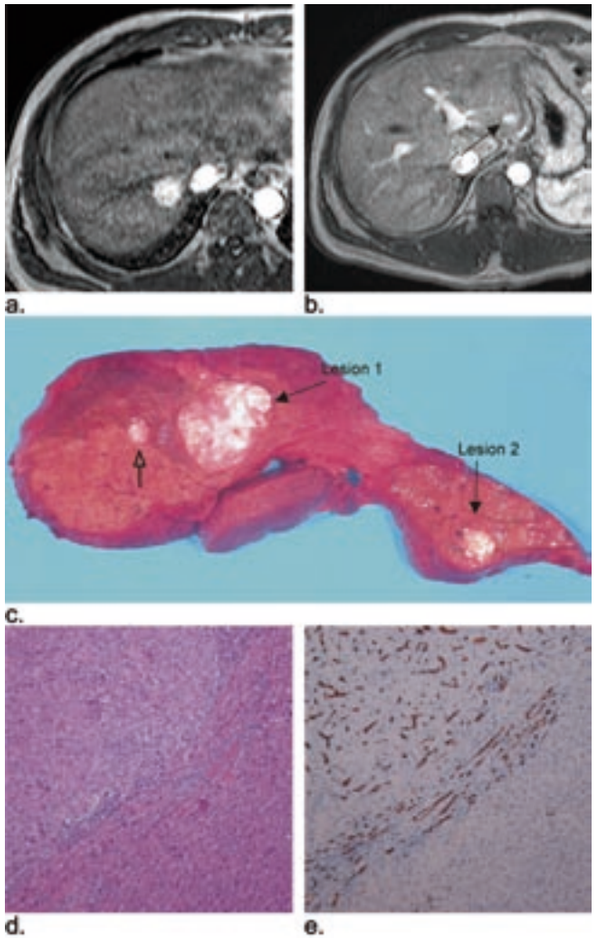

Figure 10: MR imaging findings at 9 months after the initial exam in patient C. (a) Transverse arterial phase gadolinium-enhanced two-dimensional T1-weighted gradient-echo shows further increased intense homogenous enhancement of the entire lesion which has doubled in size as well. (b) Transverse arterial phase gadolinium-enhanced two-dimensional T1-weighted gradient-echo shows that in addition, a second nodule has appeared (arrow) with striking similarity in appearance and enhancement (other sequences not shown). (c) Explant liver specimen (8 months later) shows a cirrhotic liver and confirms the two lesions observed at MR imaging which have further increased in size. Note also a satellite nodule in approximity of the larger nodule (open arrow). (d) Photomicrograph (hematoxylin and eosin (HE) stain, original maginification x100) shows hepatocellular carcinoma within a cirrhotic liver. (e) Photomicrograph (stained with endothelial marker CD34, x100) shows numerous arterial vessels with stained endothelial linings indicating extensive neovascularity inside the tumor.

The findings of our study may have a number of implications in considering clinical management of cirrhosis and HCC. First, although the incidence of HCC has increased in recent years, potentially curative surgical therapy for HCC is still limited to only approximately 40% of patients with HCC[21]. This is partly caused by advanced cirrhotic liver disease, but also because of often advanced HCC at presentation[22]. Therefore, improvement in patient outcome seems feasible not only through improved and extended therapeutic options, but also in improved imaging analysis with early detection of developing HCC. Second, our findings suggest that MR imaging should be regarded as primary imaging tool in the work-up and follow-up of patients with liver cirrhosis at high risk for development of HCC. Currently, clinical surveillance for early detection of HCC is typically performed by follow-up clinical examinations, monitoring of serum liver functions and ultrasound examination every six months, as recommended by the European Association for the Study of the Liver (EASL, 2000)[4]. Ultrasound is considered an inexpensive and accessible modality, but the reported sensitivity and specificity for detection of focal lesions in the liver is low[8] and there is significant interobserver variability. Multi-detector (MD) CT is improving rapidly for detection purposes of especially larger (> 1cm) lesions[23-25] when compared to contrast-enhanced MR imaging. However, when analyzing comparative studies for CT and dynamic contrast-enhanced MR imaging using a non-liver specific contrast agent only, higher sensitivities are reported for MR imaging[12,23]. Understanding of the step-wise carcinogenesis in HCC at MR imaging and applying it at follow-up MR imaging every three to six months in identified high-risk patients, may aid in timely diagnosis of developing HCC and therapeutic measures in an early stage. Third, in analyzing the image characteristics of developing HCC in the three presented patients, we observed a difference in presentation of the malignancy which may possibly reflect the polygenic predisposition for carcinogenesis in cirrhosis which has been described by several authors[26-28]. This observation may warrant further study for correlation of MR imaging findings to the genetic changes found in HCC.
Previously, several studies have described the imaging features of step-wise carcinogenesis of HCC at MR imaging[16,29-34]. In 1995, Sadek and colleagues evaluated the imaging findings and growth rate of lesions that presented with a nodule-within-a-nodule appearance with high signal intensity on T2-weighted images[18]. More recently, Taouli and colleagues have described imaging findings and enhancement patterns of cirrhotic nodules and HCC in several patients[35]. Yeong and colleagues described imaging features of cirrhotic nodules, with emphasis on enhancement patterns of RN, DN and HCC respectively, which show a gradual change of normal, portovenous- to early arterial enhancement[32]. The findings on individual MRI exams in our study confirm the observations of these previous investigators. In addition to these studies, however, our study clearly demonstrates the serial changes in various cirrhotic nodules, which eventually lead to full blown HCC. To our knowledge, this is the first description of findings in developing HCC on serial state-of-the-art MR imaging.
Our study is limited by the small amount of presented patients. However, this also reflects the situation in the clinical practice, in which: 1) MRI is often not applied as the primary exam and follow-up is performed with various imaging modalities which do not provide reliable correlation; 2) at our hospital, early detected HCC lesions are often treated as soon as possible; 3) pathological analysis of lesions may sometimes not be possible due to location and size of the lesion; 4) detection of HCC at MR imaging in very early stages of development may be hampered by unfamiliarity with imaging features and characteristics of developing HCC. More studies are needed with a larger number of patients for better understanding and identification of additional characteristics of developing HCC at MR imaging.
In conclusion, state-of-the-art MR imaging provides insight in various pathways of step-wise carcinogenesis of developing hepatocellular carcinoma in cirrhosis, which may facilitate early detection, improve patient outcome, provide better identification of patients for follow-up and further explain the genetic heterogeneity of hepatocellular carcinoma.

REFERENCES

1. Sakamoto M, Hirohashi S, Shimosato Y. Early stages of multistep hepatocarcinogenesis: adenomatous hyperplasia and early hepatocellular carcinoma. Hum Pathol 1991; 22:172-178.
2. International Working Party. Terminology of nodular hepatocellular lesions. Hepatology 1995; 22:983-993.
3. Hussain SM, Semelka RC, Mitchell DG. MR imaging of hepatocellular carcinoma. Magn Reson Imaging Clin N Am 2002; 10:31-52, v.
4. Bruix J, Sherman M, Llovet JM, et al. Clinical management of hepatocellular carcinoma. Conclusions of the Barcelona-2000 EASL conference. European Association for the Study of the Liver. J Hepatol 2001; 35:421-430.
5. Trevisani F, D'Intino PE, Morselli-Labate AM, et al. Serum alpha-fetoprotein for diagnosis of hepatocellular carcinoma in patients with chronic liver disease: influence of HBsAg and anti-HCV status. J Hepatol 2001; 34:570-575.
6. Mendez AM, Hussain SM, Nowak PJCM. Stereotactic Radiotherapy for primary and metastatic liver tumors: preliminary results (abstract). Radiology 2004; S638.
7. Sangro B, Mazzollini G, Prieto J. Future therapies for hepatocellular carcinoma. Eur J Gastroenterol Hepatol 2005; 17:515-521.
8. Hussain SM, Semelka RC. Hepatic imaging: comparison of modalities. Radiol Clin North Am 2005; 43:929-947, ix.
9. Efremidis SC, Hytiroglou P. The multistep process of hepatocarcinogenesis in cirrhosis with imaging

correlation. Eur Radiol 2002; 12:753-764.
10. Peterson MS, Baron RL, Marsh JW, Jr., Oliver JH, 3rd, Confer SR, Hunt LE. Pretransplantation surveillance for possible hepatocellular carcinoma in patients with cirrhosis: epidemiology and CT-based tumor detection rate in 430 cases with surgical pathologic correlation. Radiology 2000; 217:743-749.
11. Iannaccone R, Laghi A, Catalano C, Rossi P, Passariello R. Focal liver lesions in the cirrhotic patient: multislice spiral CT evaluation. Radiol Med (Torino) 2004; 107:304-314; quiz 315-306.
12. Semelka RC, Martin DR, Balci C, Lance T. Focal liver lesions: comparison of dual-phase CT and multisequence multiplanar MR imaging including dynamic gadolinium enhancement. J Magn Reson Imaging 2001; 13:397-401.
13. Braga L, Guller U, Semelka RC. Modern hepatic imaging. Surg Clin North Am 2004; 84:375-400.
14. Martin DR, Semelka RC. Magnetic resonance imaging of the liver: review of techniques and approach to common diseases. Semin Ultrasound CT MR 2005; 26:116-131.
15. Ward J, Guthrie JA, Scott DJ, et al. Hepatocellular carcinoma in the cirrhotic liver: double-contrast MR imaging for diagnosis. Radiology 2000; 216:154-162.
16. Bhartia B, Ward J, Guthrie JA, Robinson PJ. Hepatocellular carcinoma in cirrhotic livers: double-contrast thin-section MR imaging with pathologic correlation of explanted tissue. AJR Am J Roent genol 2003; 180:577-584.
17. Hyslop WB, Balci NC, Semelka RC. Future Horizons in MR Imaging. Magn Reson Imaging Clin N Am 2005; 13:211-224.
18. Sadek AG, Mitchell DG, Siegelman ES, Outwater EK, Matteucci T, Hann HW. Early hepatocellular carcinoma that develops within macroregenerative nodules: growth rate depicted at serial MR imaging. Radiology 1995; 195:753-756.
19. Bedossa P, Poynard T. An algorithm for the grading of activity in chronic hepatitis C. The METAVIR Cooperative Study Group. Hepatology 1996; 24:289-293.
20. Mitchell DG, Rubin R, Siegelman ES, Burk DL, Jr., Rifkin MD. Hepatocellular carcinoma within siderotic regenerative nodules: appearance as a nodule within a nodule on MR images. Radiology 1991; 178:101-103.
21. Bosch FX, Ribes J, Cleries R, Diaz M. Epidemiology of hepatocellular carcinoma. Clin Liver Dis 2005; 9:191-211, v.
22. McCormack L, Petrowsky H, Clavien PA. Surgical therapy of hepatocellular carcinoma. Eur J Gastroenterol Hepatol 2005; 17:497-503.
23. Kim YK, Kim CS, Chung GH, et al. Comparison of gadobenate dimeglumine-enhanced dynamic MRI and 16-MDCT for the detection of hepatocellular carcinoma. AJR Am J Roentgenol 2006; 186:149-157.
24. Kim SH, Choi D, Lim JH, et al. Ferucarbotran-enhanced MRI versus triple-phase MDCT for the preoperative detection of hepatocellular carcinoma. AJR Am J Roentgenol 2005; 184:1069-1076.
25. Kim YK, Kwak HS, Kim CS, Chung GH, Han YM, Lee JM. Hepatocellular carcinoma in patients with chronic liver disease: comparison of SPIO-enhanced MR imaging and 16-detector row CT. Radiology 2006; 238:531-541.
26. van Dekken H, Verhoef C, Wink J, et al. Cell biological evaluation of liver cell carcinoma, dysplasia and adenoma by tissue micro-array analysis. Acta Histochem 2005; 107:161-171.
27. Feo F, De Miglio MR, Simile MM, et al. Hepatocellular carcinoma as a complex polygenic disease. Interpretive analysis of recent developments on genetic predisposition. Biochim Biophys Acta 2006 Apr; 1765(2):126-47
28. Kato N, Ji G, Wang Y, et al. Large-scale search of single nucleotide polymorphisms for hepatocellular carcinoma susceptibility genes in patients with hepatitis C. Hepatology 2005; 42:846-853.
29. Earls JP, Theise ND, Weinreb JC, et al. Dysplastic nodules and hepatocellular carcinoma: thin-section MR imaging of explanted cirrhotic livers with pathologic correlation. Radiology 1996; 201:207-214.
30. Hussain SM, Semelka RC. Liver masses. Magn Reson Imaging Clin N Am 2005; 13:255-275.
31. Ito K, Mitchell DG. Imaging diagnosis of cirrhosis and chronic hepatitis. Intervirology 2004; 47:134-143.
32. Jeong YY, Yim NY, Kang HK. Hepatocellular Carcinoma in the Cirrhotic Liver with Helical CT and MRI: Imaging Spectrum and Pitfalls of Cirrhosis-Related Nodules. AJR Am J Roentgenol 2005; 185:1024-1032.
33. Krinsky GA, Lee VS, Nguyen MT, et al. Siderotic nodules at MR imaging: regenerative or dysplastic? J Comput Assist Tomogr 2000; 24:773-776.
34. Shinmura R, Matsui O, Kobayashi S, et al. Cirrhotic Nodules: Association between MR Imaging Signal Intensity and Intranodular Blood Supply. Radiology 2005; 237:512-519.
35. Taouli B, Losada M, Holland A, Krinsky G. Magnetic resonance imaging of hepatocellular carcinoma. Gastroenterology 2004; 127:S144-152.

chapter4.2
hepatocellular carcinoma, relation between lesion size and imaging findings

MR imaging of hepatocellular carcinoma: RELATIONSHIP BETWEEN LESION SIZE AND IMAGING FINDINGS,

including signal intensity and dynamic enhancement patterns

ABSTRACT

Purpose: To assess the relationship between lesion size and MR imaging findings of pathology-proven hepatocellular carcinoma (HCC).

Materials and Methods: In a retrospective, single-center study, a cohort of 37 consecutive patients was identified between 1999-2005, that underwent both pre-operative MR imaging and surgical resection of HCC. A total of 47 lesions (mean size 6.85 cm (range 1-25 cm)) was assessed both qualitatively and quantitatively for signal intensity (SI), enhancement patterns and secondary morphologic features. Interobserver rating for the qualitative assessment, percentages of enhancement and contrast-to-noise-ratio (CNR) were determined. Lesions were assessed for combinations of T2-weighted signal, arterial and delayed phase enhancement patterns. Regression analysis was used to assess relations between MR imaging findings and tumor size.

Results: On fat-suppressed T2-weighted fast spin-echo, smaller lesions had significantly lower SI compared to larger lesions, which were more frequently hyperintense ($p<0.05$). In the arterial phase, smaller lesions showed significantly higher percentage enhancement compared to larger lesions ($p<0.05$). In the delayed phase, smaller lesions showed less pronounced washout (qualitative assessment, $p<0.05$). Heterogeneity of the lesions, including fatty infiltration, internal nodules or mosaic pattern, was observed significantly more frequently in larger lesions ($p<0.001$). The classic combination of high T2-weighted signal, strong arterial enhancement and delayed phase washout was present in 23/44 lesions (52%).

Conclusion: Smaller HCC often showed lower signal intensity on T2-weighted, more intense arterial enhancement, and less pronounced delayed washout compared to larger HCC. Therefore, small liver lesions in the setting of liver cirrhosis need to be evaluated with caution.

Indra C. van den Bos, MD[1], Shahid M. Hussain, MD, PhD[1,2], Roy S. Dwarkasing, MD[1], Wim C.J. Hop, Msc, PhD[3], Pieter E. Zondervan, MD[4], Robert A. de Man, MD, PhD[5], Jan N.M. IJzermans, MD, PhD[6], Craig W. Walker, MD[2], Gabriel P. Krestin, MD, PhD[1]

Departments of [1]Radiology, [3]Epidemiology and Biostatistics, [4]Pathologie, [5]Gastroenterology and Hepatology and [6]Surgery, Erasmus MC, University Medical Center Rotterdam, The Netherlands; [2]Department of Radiology, University of Nebraska Medical Center, Omaha, NE, USA

Journal of Magnetic Resonance Imaging, in press

INTRODUCTION

Hepatocellular carcinoma (HCC) is the most common primary hepatocellular malignancy[1]. The incidence is highest in patients with hepatitis B or C related cirrhosis and cirrhosis related to alcohol abuse, metabolic liver diseases and others[2-4]. In cirrhosis, HCC develops in a step-wise fashion[5]. In this sequence, a regenerative nodule (RN) develops in low grade dysplastic nodule (DN I)) – high grade dysplastic nodule (DN II) – small HCC – large HCC, respectively[6]. Although HCC in a non-cirrhotic liver develops in a de-novo fashion, histologically, it is indistinguishable from HCC occurring in cirrhosis[6].

In many centers, state-of-the-art MR imaging is regarded the modality of choice for diagnostic work-up of primary liver tumors[7,8]. Even though multiphasic multidetector computed tomography (CT) is an excellent modality for imaging of hepatic vasculature and assessment of neovasculature surrounding suspect liver nodules, characterization of especially smaller lesions remains challenging[9].

Current routinely used MR imaging protocols contain a combination of breath-hold T2-weighted sequences, chemical shift imaging, and multi-phasic gadolinium-enhanced T1-weighted imaging. This provides consistent and reproducible information on 1) intrinsic soft tissue contrast; 2) different intracellular components, including accumulation of iron and fat; and 3) enhancement patterns on dynamic gadolinium-enhanced imaging; which renders MR imaging a superior technique for detection and characterization of primary liver tumors[6,10].

During the recent years, faster MR imaging protocols have become available which have further improved confident diagnosis of focal liver lesions[1]. In such protocols, sequences have been developed which make use of multiple refocusing pulses and/or parallel imaging[11]. Application of multiple refocusing pulses however, may result in increased magnetic-transfer-contrast (MTC) effects, which may alter signal behavior of lesions and lower lesion-to-liver contrast. Particularly on (fast spin-echo (FSE)) T2-weighted sequences, which are important for characterization of cirrhotic nodules, malignant lesions may not present with the characteristic high signal intensity[11]. Parallel imaging techniques have enabled faster acquisition of T1-weighted dynamic contrast-enhanced images, with improved visualization of distinct enhancement phases and -patterns. This provided improved visualization of particularly smaller nodules.

Eventually, these sequences may have influenced the assessment of classical MR imaging findings in cirrhotic nodules. Classically, the MR imaging features of HCC included high signal intensity on (conventional) T2-weighted sequences[12,13], arterial enhancement, and washout with capsular enhancement in the delayed phase[6,13]. However, based on our own experience as well as observations of others[13], MR imaging features of especially smaller HCC may be more variable on currently used T2-weighted FSE and dynamic gadolinium-enhanced sequences.

To further evaluate these observations, we designed a single-center retrospective study to systematically assess MR imaging findings of histologically proven HCC, based on current MR imaging sequences. To the best of our knowledge, this has not been reported before.

The purpose of this study therefore, was to assess the relationship between lesion size and MR imaging findings of pathology-proven hepatocellular carcinoma.

MATERIALS & METHODS

Patient population

The institutional review board (IRB) granted permission for this retrospective cohort study, which was performed in a large university referral hospital for hepatobiliary diseases. The hospital archive system and pathology registration were searched for patients with pathology-proven HCC following surgical partial liver resection or liver transplantation; and preoperative MR imaging in January 1999 – December 2004. A total of 37 patients was identified, with 47 pathology-proven HCC. The patient group (Table 1) consisted of 11 female and 27 male patients, with a mean age of 50.8 years (range 23-76 years).

MR imaging technique

All MR examinations were performed on a 1.5T unit (Philips Medical Systems, Best, The Netherlands or General Electrics, Signa, Milwaukee, Wisconsin, USA; using identical scan protocols). A four-channel body-array coil with capability of parallel imaging was used. Scan sequences included single-shot fast spin-echo (SSFSE) (repetition-time (TR) msec/ echo-time (TE) msec 832/80; flip-angle 90º), respiratory-gated fat-suppressed T2-weighted fast spin-echo (FSE) (3000/80, flip-angle 90º), and T1-weighted in- and opposed-phase gradient-echo sequences (shortest/4.6 and 2.3 respectively, flip-angle 90º). After intravenous administration of a gadolinium-chelate (28 ml; Magnevist [gadopentetate dimeglumine], Schering, Berlin, Germany) at 3 ml/sec using a power injector, dynamic imaging with either 2D T1-weighted gradient-echo (GRE) (Philips) or 3D T1-weighted fat-suppressed GRE (General Electrics) sequences in at least 4 phases (precontrast, arterial, portal and delayed phases) was performed. In each patient, a timing bolus technique using 2ml of the same contrast agent followed by 15ml saline was used to accurately capture the arterial phase. The high injection rate was used to compensate for some signal loss due to implementation of parallel imaging. The portal phase was acquired approximately at 45 seconds, and the delayed phase at least 120 seconds after the acquisition of the arterial phase. A slice thickness of 7mm was used in most sequences, except the T1-weighted fat-suppressed GRE sequence, in which 4mm slices were acquired.

Table 1

Hepatitis B infection	14/37* (41%)
Hepatitis C infection	10/37** (27%)
Chronic alcohol abuse	1/37† (3%)
Biliary atresia	1/37 (3%)
Non-cirrhotic liver disease	11/37 (30%)

Underlying liver disease, expressed in number of patients compared to the total group (37 patients). Data in parenthesis are percentages. Multiple etiologies existed in 9 patients: *2 with co-existing hepatitis C, **6 with co-existing hepatitis B, and † 1 with chronic alcohol abuse.

Image analysis

All MR imaging exams were transferred to a picture archiving and communication system (PACS) viewing

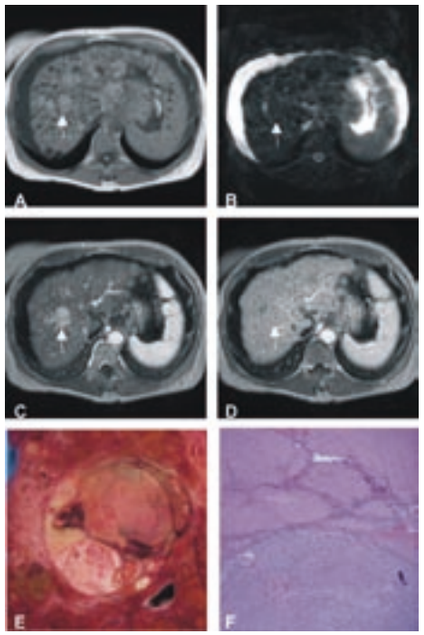

Figure 1: Extensive cirrhotic changes in 54-year female with chronic hepatitis B infection and a 2-cm HCC (arrows), with low T2-weighted signal, marked arterial enhancement and minimal washout (Type I enhancement). (a) In-phase T1-weighted GRE, showing the lesion in the right liver lobe, with slightly higher signal intensity (SI) compared to the surrounding liver, surrounded by a hypointense tumor capsule. Note multiple regenerative nodules within the entire liver. (b) Fat-suppressed T2-weighted FSE, showing isointensity of the lesion. (c) Arterial phase T1-weighted GRE, showing marked arterial enhancement of the lesion. (d) Delayed phase T1-weighted GRE, showing only slight hypointensity of the lesion, with enhancement of the tumor capsule. (e) Macroscopic correlation after liver explantation, illustrating multiple internal nodules within the lesion, and a surrounding fibrous tumor capsule. (f) Photomicrograph (hematoxylin and eosin (HE) stain, original magnification x10), showing a focus of HCC surrounded by multiple regenerative nodules.

station. Evaluation was performed on basis of of each single lesion. Assessment of the lesions was based on qualitative and quantitative parameters. Only lesions with a diameter >10mm were included to ensure reproducible measurement of data in the quantitative analysis. Primary lesions were assessed only, therefore, all satellite lesions in close proximity to the main tumor were excluded from the study. The four most important MR sequences for diagnosis were evaluated, including: 1) T1-weighted in-phase GRE, 2) fat-suppressed (fatsat) T2-weighted FSE, 3) arterial-phase – and 4) delayed phase after contrast administration. In three patients, fatsat T2-weighted FSE was not performed because of technical reasons. All MR images were qualitatively assessed by two readers with experience in hepatobiliary imaging (3 and 6 years respectively). These observers first evaluated the MR images independently, then a consensus reading was performed of all MR examinations. The quantitative assessment was performed by one reader. All evaluations were categorized and documented by using standardized data sheets.

Qualitative assessment

The qualitative assessment included the following characteristics of both liver and lesions: 1) signal intensity of the lesion compared to the liver, assessed visually (graded as: 1=markedly hypointense, 2=slightly hypointense, 3=isointense, 4=slightly hyperintense, 5=markedly hyperintense); 2) visual interpretation of enhancement at dynamic gadolinium-enhanced imaging, expressed as signal intensity of the lesion compared to the surrounding liver (graded as: 1=markedly lower, 2=slightly lower, 3=similar to liver, 4=slightly higher, 5=markedly higher); 3) presence of capsule; 4) fatty infiltration, hemorrhage or central scar within the lesion; 5) presence of heterogeneity within lesion, defined as multiple nodular structures or mosaic pattern with varying signal intensity.

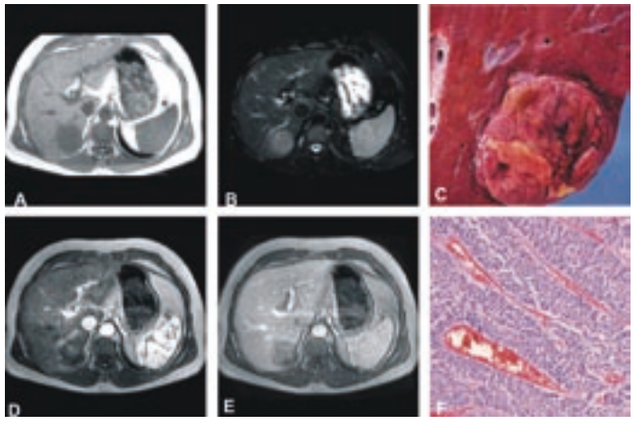

Figure 2: 52-year old male, with chronic hepatitis B infection, moderate fibrosis and 4-cm HCC, with high T2w signal, slight heterogeneous arterial enhancement and marked delayed washout (Type III enhancement). (a) In-phase T1-weighted GRE, showing hypointensity of the tumor in the right liver lobe. (b) Fat-suppressed T2-weighted FSE, showing heterogeneous hyperintensity of the lesion. (c) Macroscopic correlation after surgical resection of the tumor, illustrating multiple nodules within the lesion and a fibrous tumor capsule. (d) Arterial-phase T1-weighted GRE after gadolinium, showing minimal patchy arterial enhancement. (e) Delayed-phase T1-weighted GRE after gadolinium, showing hypointensity of the lesion accompanied by enhancement of a tumor capsule. (f) Photomicrograph (hematoxylin and eosin (HE) stain, original magnification x20, illustrating multiple vessels and chaotic organization of hepatocytes with dysplastic nuclei.

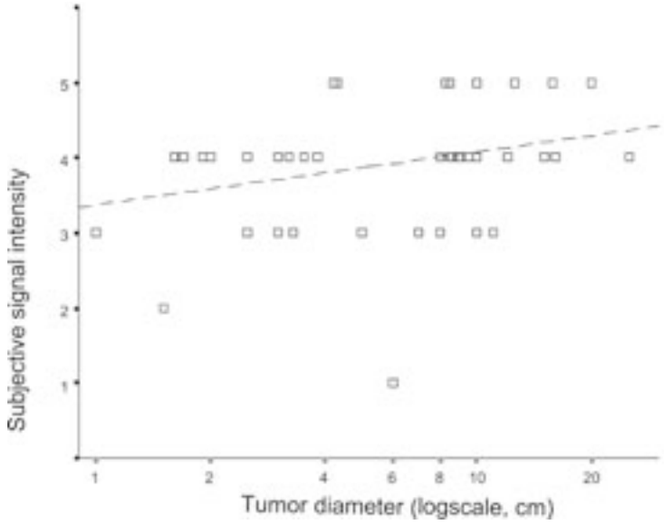

Figure 3: Subjective signal intensity of HCC on fat-suppressed T2w FSE, in relation to tumor size, showing a significant increase for larger lesions ($p<0.05$) (graded as: 1=markedly hypointense, 2=slightly hypointense, 3=isointense, 4=slightly hyperintense, 5=markedly hyperintense).

For an assessment of different combinations of T2-weighted signal intensity, arterial enhancement and delayed phase washout, four different types of enhancement were determined based on presence or absence of arterial phase enhancement and delayed phase washout, namely: I -strong arterial enhancement with minimal delayed phase washout; II - strong arterial enhancement with clear delayed phase washout; III - slight, heterogeneous arterial enhancement with clear delayed phase washout, and IV – slight, heterogeneous arterial enhancement with minimal delayed phase washout.

Quantitative assessment

The quantitative assessment included measurements of signal intensity, using operator-defined regions-of-interest (ROI). For the lesions, the largest possible ROI was selected that excluded areas of intra-tumoral fat or hemorrhage. For the liver adjacent to the tumor, a ROI that excluded vessels and artifacts was used. CNR was calculated as difference in signal intensity between lesion and liver, scaled to SD of background noise. In dynamic gadolinium-enhanced imaging, measurements using ROI were performed identically in arterial, portal and delayed phases. Definition of the arterial phase consisted of enhancement of hepatic artery and aorta; no enhancement of hepatic veins and (almost) no enhancement of the liver parenchyma. Percentages of contrast enhancement were calculated as follows: [(SIenhanced - SIunenhanced) / SIunenhanced] x 100 (SI=signal intensity). Correlation between tumor size and MR imaging findings was assessed for all itineraries described. Smaller lesions are considered <2 cm, whilst larger lesions are considered >2 cm, in consensus with the guidelines of the International Working Party for hepatocellular nodules[14].

Statistical analysis

Statistical parameters (mean, median, standard deviation and range) were calculated using the Statistical Package for Social Sciences (SPSS 11.0) program. To assess the interobserver agreement for the qualitative analysis, κ statistic for multiple observers was calculated. A κ value of less than 0.200 indicated positive but poor agreement; 0.210 - 0.400, fair agreement; 0.410 – 0.600, moderate agreement; 0.610 – 0.800, good agreement; and greater than 0.810, excellent agreement. Data were analyzed taking account of intra- and inter-patient differences, using mixed model ANOVA (SAS PROC MIXED; version 8.2, SAS Institute Inc., Cary, NC, USA). Tumor size was logarithmically transformed to reduce the influence of outlying observations. A p-value of less than 0.05 was considered statistically significant.

RESULTS

The mean size of all assessed lesions was 6.85 cm (range 1-25). The interobserver agreement for the qualitative assessment, expressed as κ score, was 0.68 (good) for in-phase T1-weighted GRE, 0.78 (good) for fat-suppressed T2-weighted FSE, 0.89 (excellent) for arterial phase T1-weighted GRE and 0.86 (excellent) for delayed phase T1-weighted GRE respectively. The consensus reading was used for the correlation between signal intensity and tumor size.

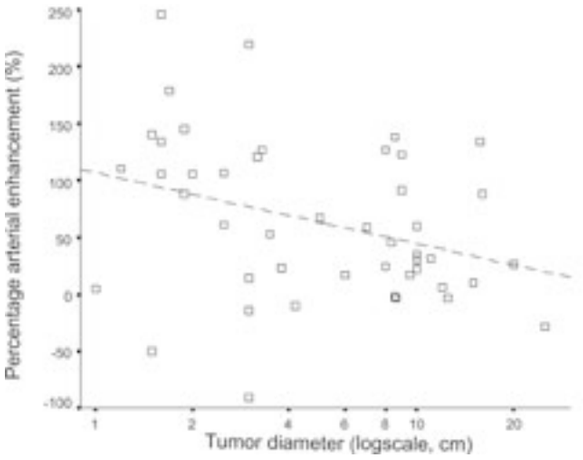

Figure 4: Arterial-phase percentage increased ehancement of HCC compared to the liver, showing a significantly higher percentage enhancement in smaller HCC (p<0.05).

Signal intensity

On in-phase T1-weighted GRE, the subjective, graded qualitative analysis showed no relation with tumor size; although a tendency for higher signal intensity was observed in smaller lesions (Fig. 1a). CNR did not vary significantly.

On fat-suppressed T2-weighted FSE (FS-FSE), the subjective, graded qualitative analysis showed a significantly lower signal intensity for smaller lesions (p<0.05) (see Fig. 1b, 2b, 3). CNR assessments showed a tendency for higher CNR in larger lesions, which did not reach statistical significance (p=0.10, in which for each doubling of the tumor, CNR increased 1.4 (95% CI –0.3 - +3.1)).

Dynamic enhancement

In the arterial phase, the subjective analysis showed a higher SI for small lesions, which approached statistical significance (p=0.052, in which for each doubling of the tumor size, the graded outcome increased 0.24, 95% CI 0.04 – 0.44) (Fig. 1c, 2c). The quantitative analysis showed a significantly higher percentage increased enhancement of HCC compared to the surrounding liver in smaller lesions (p<0.05) (Fig. 4).

In the delayed phase, the subjective analysis illustrated a significantly lower SI for larger lesions (p<0.05) (Fig. 1d, 2d, 4). The quantitative analysis showed a persistent increased percentage enhancement of HCC versus liver, which did not reach statistical significance.

Morphologic tumor characteristics

A capsule was present in 79% of HCC (37 of 47 lesions) for the assessments based on delayed phase imaging after gadolinium. On T1-weighted imaging, a hypointense capsule was observed in 25/37 lesions (68%); and on T2-weighted imaging this was observed in 21/36 lesions (58%). There was no correlation between presence or absence of a tumor capsule and tumor size. Fatty infiltration occurred significantly more often in larger HCC (p<0.001). Hemorrhage occurred in 6 cases, without clear association with size of the tumor. A central scar was observed in 3 patients with larger tumors, in 2 patients with cirrhosis (Fig. 5), and 1 patient with a non-cirrhotic liver. Heterogeneity within the tumor, with internal nodules was observed more significantly more often in larger lesions (p<0.001), in the assessment of fat-suppressed T2-weighted FSE.

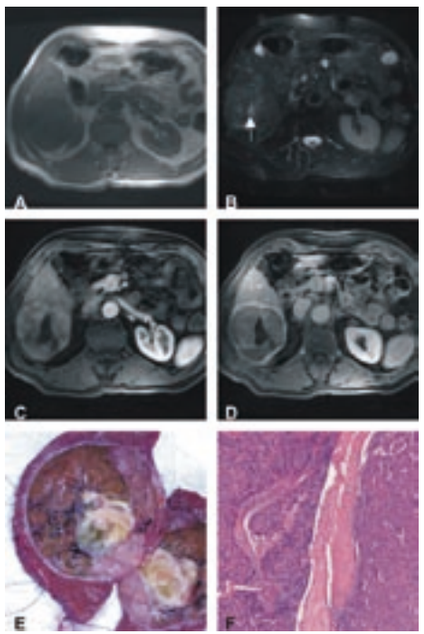

Figure 5: 74-year old male, with chronic hepatitis C infection, incomplete septal cirrhosis and a 9-cm HCC with a central scar, with low T2-weighted signal, marked arterial enhancement and marked delayed phase washout (type II enhancement). (a) In-phase T1-weighted GRE, showing hypointensity of the lesion. (b) Fat-suppressed T2-weighted FSE, showing only slight hyperintensity of the lesion compared to the surrounding liver, and with a slightly hyperintense central scar (arrow). (c) Arterial-phase fat-suppressed 3D T1-weighted GRE after gadolinium, showing classic heterogeneous arterial enhancement of the lesion, with sparing of the central scar. (d) Delayed-phase fat-suppressed 3D T1-weighted GRE after gadolinium, showing hypointensity of the lesion with delayed capsule enhancement. (e) Macroscopic correlation after surgical resection, illustrating multiple tumor nodules, central scar and a fibrous tumor capsule. (f) Photomicrograph (hematoxylin and eosin (HE) stain, original magnification x10) of the tumor, showing atypical hepatocytes with multiple nuclei, variation in size of the nuclei and multiple nuclei within one cell. Note fibrous scar tissue in the center.

Combined diagnostic imaging sequences

The classic combination of high T2-weighted signal intensity, arterial enhancement and delayed phase washout (type II enhancement) (Fig. 6) as determined in the qualitative assessment was observed in 23 of 44 lesions (52%). The remaining 21 lesions have different combinations of MR imaging findings, including presence or absence of high T2-weighted signal intensity, in combination with three types of enhancement (I, II and III) The comparison of these six groups shows a steady increase in tumor size (Fig. 7). Groups I, II an III with high T2-weighted signal occurred in 3/44 lesions (7%), 23/44 (53%), and 6/44 (14%) respectively. Groups I, II and III with low T2-weighted signal occurred in 7/44 (16%), 1/44 (2%) and 4/44 (9%), respectively.

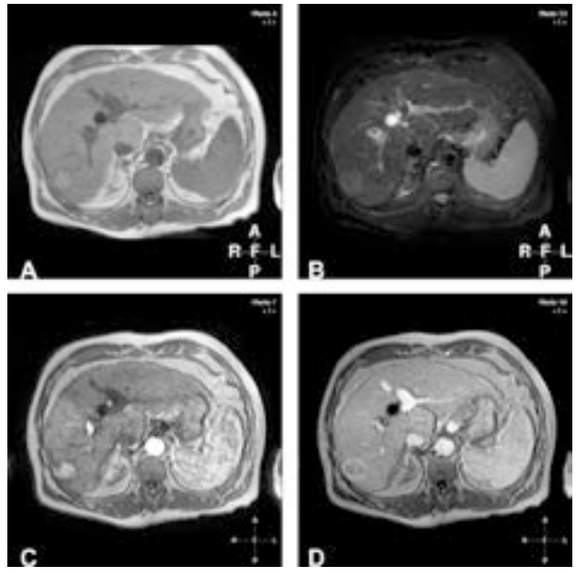

Figure 6: 69-year old male, with cirrhosis based on prolonged alcohol abuse, and a 4-cm large HCC in the right liver lobe, with classical appearance (high T2 signal, strong arterial enhancement and clear delayed washout (Type II enhancement). (a) in-phase T1-weighted GRE, showing slight hyperintensity of the lesion. (b) fat-suppressed T2-weighted FSE, showing slight hyperintensity of the lesion. (c) Arterial phase T1-weighted GRE, showing marked arterial enhancement of the lesion; (d) Delayed phase T1-weighted GRE, illustrating washout of contrast within the lesion, accompanied by capsular enhancement.

Figure 7: Different combinations of the three most important sequences (T2-weighted signal intensity, arterial enhancement and delayed phase washout), in relation to tumor size. Groups I, II and III (x-axis, enhancement patterns) represent the following: I – strong arterial enhancement with minimal delayed phase washout; II – strong arterial enhancement with marked delayed phase washout; and III – slight, heterogeneous arterial enhancement with marked delayed phase washout. Note that in these groups, tumor size increases from groups I to III.

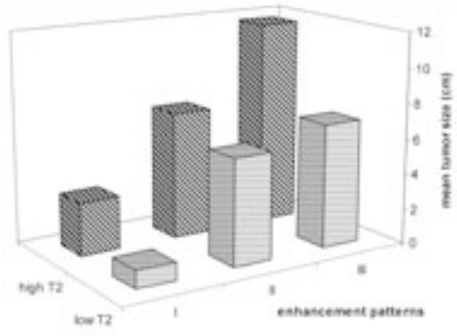

DISCUSSION

The results of this study indicate that a relationship exists between tumor size of hepatocellular carcinoma and MR imaging findings. The most important findings of our study include: 1) the classic combination of high T2-weighted signal, strong arterial enhancement and delayed washout is not present in all lesions; 2) smaller HCC have tendency for hypo- or isointensity on fat-suppressed T2-weighted sequences; 3) smaller HCC show more pronounced arterial enhancement compared to larger HCC; 4) smaller HCC show less pronounced washout in the delayed phase; 5) smaller lesions more frequently show an enhancing tumor capsule than previously reported in literature, based on enhancement in the delayed phase after contrast administration.

These findings are clinically relevant for a number of reasons. First, the classical combination of high signal intensity on T2-weighted sequences and arterial enhancement was not present in all evaluated patients on currently used state-of-the-art MR imaging. Isointensity or hypointensity of small HCC may pose diagnostic challenges. In case of a

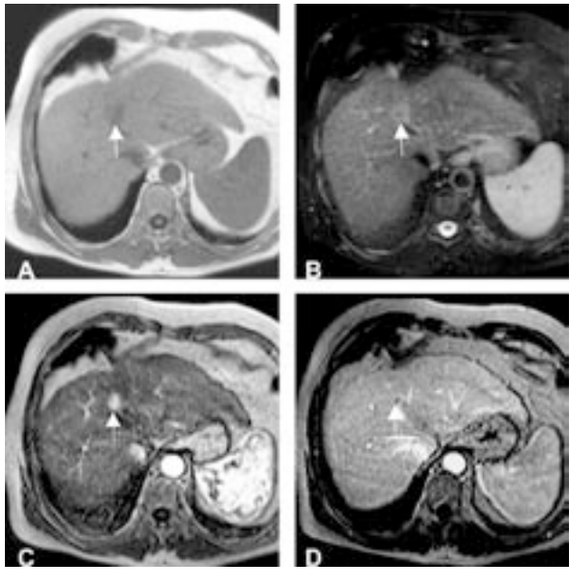

Figure 8: Small HCC in a 53-year old male patient with hepatitis B related cirrhosis and a 1.5-cm HCC in the left liver lobe (arrows), with nodule-within-nodule appearance that shows low T2-weighted signal, strong arterial enhancement and some delayed washout (Type II enhancement). (a) In-phase T1-weighted GRE, showing slight hypointensity of the lesion. (b) Fat-suppressed T2-weighted FSE, showing heterogeneous, slightly higher SI of the lesion compared to the liver. (c) Arterial phase T1-weighted GRE, showing marked arterial enhancement of the lesion. (d) Delayed phase T1-weighted GRE, illustrating some washout of contrast agent within the lesion without any capsular enhancement.

hyperenhancing area in cirrhosis, a wider differential diagnosis is considered, which may include vascular shunts, early enhancing lesions, pseudo-lesions, or others. In these cases, careful analysis of other phases in the dynamic examination is useful, since the delayed phase will show some degree of washout in the visual interpretation of signal intensity, accompanied by enhancement of a tumor capsule. If differential diagnosis remains unclear, short term follow-up examination is indicated (6 to 12 week follow-up) to evaluate changes or growth of the lesion.

The lower T2-weighted SI in smaller lesions as documented in our study likely results from the following: 1) smaller lesions have different cellular characteristics, including more cellularity with relatively smaller fluid component, and correlation between the degree of histological differentiation and tumor size; and 2) changes related to technical effects of the applied sequence, with a higher number of refocusing pulses in current echo-train FSE sequences which result in increased magnetic-transfer-contrast (MTC) effects[15,16].

According to the step-wise carcinogenesis, HCC changes in appearance in the course of the development. This is reflected as changing signal intensity and vascularity on MR imaging. A previous study showed different imaging findings in developing HCC, which may reflect different pathways or even different genetic backgrounds in the step-wise development of HCC[16]. This includes steadily increasing SI on T2-weighted sequences with gradually more neovascularity for most lesions. Based on the results of this study and prior observations, it is suggested that in most cases the increased signal on T2-weighted images lags behind the developing neovascularity of such lesions.

The increased arterial enhancement as observed in this study for smaller HCC is beneficial for early diagnosis of HCC. This relates directly to the technique applied for the dynamic imaging series, because adequate timing of the arterial phase is essential. Inaccurate timing may result in a lower percentage arterial enhancement, which may cause false-negative diagnostic results in especially smaller lesions. The more pronounced arterial enhancement in smaller lesions, as observed in this study, most likely corresponds to the step-wise carcinogenesis described before, in which most lesions show hypervascularity as an initial sign. Even though the exact relation and differential diagnosis from benign enhancing lesions remains complicated, even slight washout accompanied by capsule enhancement suggests HCC, as observed in this study. In cases in which no clear washout is observed in the delayed phase, observation of early enhancement warrants close follow-up for evaluation of potential growth[18].

The combination of MR imaging findings of smaller lesions in this study, including lower signal intensity (rendering the lesion iso- or even hypointense) on T2-weighted sequences and pronounced arterial enhancement underlines the importance of dynamic contrast-enhanced imaging in patients at risk for development of HCC. In this setting, T2-weighted imaging seems less important in the overall evaluation, which is in correspondence with a recent study which described the overall confidence levels for diagnosis of HCC, based on different combinations of T1-weighted, T2-weighted and dynamic contrast-enhanced imaging[19]. However, both in our experience as reported in literature as well, inclusion of T2-weighted sequences in a full MR imaging protocol is essential for both detection and characterization of focal liver lesions of both primary and secondary nature[20].

Finally, in the quantitative, ROI-based analysis of the signal intensity in the delayed phase after contrast administration did not follow the visually observed signal intensity which demonstrated more pronounced washout in larger lesions. This may be related to a combination of the following: 1) dual-input blood supply of the liver, based on inflow from both the hepatic artery and the portal vein, resulting in an overall higher signal intensity of the lesion compared to the liver; and 2) the ROI measurements which were performed included a measurement of the entire lesion that excluded areas of intra-tumoral fatty infiltration or hemorrhage, including therefore areas with different washout characteristics.

Previously, the imaging findings of HCC have been described by several authors who evaluated the imaging findings of smaller lesions as well[5,12,21-23]. Yamashita and colleagues evaluated the histological subtypes and differentiation degree of HCC in correlation with dynamics enhancement patterns, illustrating a correlation between degree and pattern of enhancement with tumor differentiation and internal architecture[24]. More recently, several studies addressed the imaging findings of HCC using liver specific contrast agents[25-27] In one study, the imaging findings of HCC were described in a multicenter study, to describe the most common imaging findings of these lesions[13]. In this study, a cut-off was described for 1.5-cm large lesions. In our report, no significant cut-off value was observed in the statistical analysis, most likely related to the fact that signal behavior of HCC changes only gradually as the tumor increases in size. In addition to this study, we evaluated the imaging findings of HCC with a wide range in diameter in a single-center study, specifically aiming at the evaluation of the spectrum of MR imaging findings in relation to the size of the lesion.

Our study is limited by the following factors. First, the retrospective nature of the study may have resulted in an inclusion bias of studied subjects. However, in our opinion, the retrospective study design would sufficiently answer the defined research question. In addition, the applied MR imaging protocol we routinely apply in our institution was kept relatively constant over the years; therefore this did not result in extensive variation in signal intensity or imaging findings. Second, the inclusion of both patients with and without cirrhotic liver disease was based on the fact that larger HCC in fact have comparable imaging findings compared to HCC occurring in non-cirrhotic liver. The fact that HCC in non-cirrhotic liver is discovered only when lesions are much larger most likely depends on the metabolic function of the underlying liver, which is preserved for a much longer time in non-cirrhosis compared to cirrhosis. The assumption that imaging findings are in fact similar in HCC occurring in absence or presence of cirrhosis was confirmed by our study results, which did not show any significant differences. Finally, the small sample size may have resulted in biased study results.

In conclusion, our study indicates that the imaging features of HCC on MR imaging are related to tumor size. Smaller lesions often showed lower SI on T2-weighted, more intense arterial enhancement, slight delayed washout whereas larger lesions were predominantly hyperintense on T2-weighted with less intense, heterogeneous arterial enhancement, and more pronounced delayed washout. Therefore, small liver lesions in the setting of liver cirrhosis need to be evaluated with caution.

REFERENCES

1. Hussain SM, Semelka RC. Liver masses. Magn Reson Imaging Clin N Am 2005; 13:255-275.
2. Fattovich G, Stroffolini T, Zagni I, Donato F. Hepatocellular carcinoma in cirrhosis: incidence and risk factors. Gastroenterology 2004; 127:S35-50.
3. El-Serag HB. Hepatocellular carcinoma: recent trends in the United States. Gastroenterology 2004; 127:S27-34.
4. El-Serag HB, Davila JA, Petersen NJ, McGlynn KA. The continuing increase in the incidence of hepatocellular carcinoma in the United States: an update. Ann Intern Med 2003; 139:817-823.
5. Sakamoto M, Hirohashi S, Shimosato Y. Early stages of multistep hepatocarcinogenesis: adenomatous hyperplasia and early hepatocellular carcinoma. Hum Pathol 1991; 22:172-178.
6. Hussain SM, Semelka RC, Mitchell DG. MR imaging of hepatocellular carcinoma. Magn Reson Imaging Clin N Am 2002; 10:31-52, v.
7. Semelka RC, Martin DR, Balci C, Lance T. Focal liver lesions: comparison of dual-phase CT and multisequence multiplanar MR imaging including dynamic gadolinium enhancement. J Magn Reson Imaging 2001; 13:397-401.
8. Hussain SM, Semelka RC. Hepatic imaging: comparison of modalities. Radiol Clin North Am 2005; 43:929-947, ix.
9. Iannaccone R, Laghi A, Catalano C, Rossi P, Passariello R. Focal liver lesions in the cirrhotic patient: multislice spiral CT evaluation. Radiol Med (Torino) 2004; 107:304-314; quiz 315-306.
10. Shinmura R, Matsui O, Kobayashi S, et al. Cirrhotic Nodules: Association between MR Imaging Signal Intensity and Intranodular Blood Supply. Radiology 2005; 237:512-519.
11. Hussain SM, De Becker J, Hop WC, Dwarkasing S, Wielopolski PA. Can a single-shot black-blood T2--weighted spin-echo echo-planar imaging sequence with sensitivity encoding replace the respiratory-triggered turbo spin-echo sequence for

hepatocellular carcinomaLESION SIZE AND MR IMAGING FINDINGS

the liver? An optimization and feasibility study. J Magn Reson Imaging 2005; 21:219-229.
12. Matsui O, Kadoya M, Kameyama T, et al. Adenomatous hyperplastic nodules in the cirrhotic liver: differentiation from hepatocellular carcinoma with MR imaging. Radiology 1989; 173:123-126.
13. Kelekis NL, Semelka RC, Worawattanakul S, et al. Hepatocellular carcinoma in North America: a multiinstitutional study of appearance on T1-weighted, T2-weighted, and serial gadolinium-enhanced gradient-echo images. AJR Am J Roentgenol 1998; 170:1005-1013.
14. Ebara M, Fukuda H, Kojima Y, et al. Small hepatocellular carcinoma: relationship of signal intensity to pathologic findings and metal content of the tumor and surrounding hepatic parenchyma. Radiology 1999; 210:81-88.
15. Kadoya M, Matsui O, Takashima T, Nonomura A. Hepatocellular carcinoma: correlation of MR imaging and pathologic findings. Radiology 1992; 183:819-825.
16. Van den Bos IC, Hussain SM, Terkivatan T, Zondervan PE, De Man RA. Step-wise carcinogenesis of hepatocellular carcinoma in the cirrhotic liver: demonstration on serial MR imaging. JMRI 2006 Nov; 24(5): 1071-80.
17. Hyslop WB, Balci NC, Semelka RC. Future horizons in MR imaging. Magn Reson Imaging Clin N Am 2005; 13:211-224.
18. Jeong YY, Mitchell DG, Kamishima T. Small (<20 mm) enhancing hepatic nodules seen on arterial phase MR imaging of the cirrhotic liver: clinical implications. AJR Am J Roentgenol 2002; 178: 1327-1334.
19. Hecht EM, Holland AE, Israel GM, et al. Hepatocellular carcinoma in the cirrhotic liver: gadolinium-enhanced 3D T1-weighted MR imaging as a stand-alone sequence for diagnosis. Radiology 2006; 239:438-447.
20. Kondo H, Kanematsu M, Itoh K, et al. Does T2-weighted MR imaging improve preoperative detection of malignant hepatic tumors? Observer performance study in 49 surgically proven cases. Magn Reson Imaging 2005; 23:89-95.
21. Sadek AG, Mitchell DG, Siegelman ES, Outwater EK, Matteucci T, Hann HW. Early hepatocellular carcinoma that develops within macroregenerative nodules: growth rate depicted at serial MR imaging. Radiology 1995; 195:753-756.
22. Mitchell DG, Rubin R, Siegelman ES, Burk DL, Jr., Rifkin MD. Hepatocellular carcinoma within siderotic regenerative nodules: appearance as a nodule within a nodule on MR images. Radiology 1991; 178:101-103.
23. Tang Y, Yamashita Y, Arakawa A, et al. Detection of hepatocellular carcinoma arising in cirrhotic livers: comparison of gadolinium- and ferumoxides-enhanced MR imaging. Am J Roentgenol 1999; 172:1547-1554.
24. Yamashita Y, Fan ZM, Yamamoto H, et al. Spin-echo and dynamic gadolinium-enhanced FLASH MR imaging of hepatocellular carcinoma: correlation with pathologic findings. J Magn Reson Imaging 1994; 4:83-90.
25. Kim YK, Kwak HS, Kim CS, Chung GH, Han YM, Lee JM. Hepatocellular carcinoma in patients with chronic liver disease: comparison of SPIO-enhanced MR imaging and 16-detector row CT. Radiology 2006; 238:531-541.
26. Tanimoto A, Kuribayashi S. Application of super paramagnetic iron oxide to imaging of hepatocellular carcinoma. Eur J Radiol 2006; 58:200-216.
27. Kim YK, Kim CS, Chung GH, et al. Comparison of gadobenate dimeglumine-enhanced dynamic MRI and 16-MDCT for the detection of hepatocellular carcinoma. AJR Am J Roentgenol 2006; 186:149-157.

chapter4.3
hepatocellular carcinoma after Kasai porto-enterostomy

Hepatocellular carcinoma
COMPLICATING BILIARY ATRESIA

after Kasai porto-enterostomy

ABSTRACT

Kasai portoenterostomy (PE) increases the survival for children with biliary atresia and consequently postpones subsequential liver transplantation. However, all longterm survivors develop complications of biliary cirrhosis. We report a case of hepatocellular carcinoma (HCC) in a 19-year old male patient with biliary atresia and Kasai PE. The preoperative abdominal ultrasound and magnetic resonance (MR) imaging showed a large hepatic mass (diameter 10cm). The serum alpha-fetoprotein level was within normal range. Pathologic findings of the mass, after orthotopic liver transplantation, demonstrated a well-differentiated HCC ($T_1N_0M_0$). HCC is a rare complication of biliary atresia, but will intensively impair the survival. Therefore, clinicians should be alert to the development of HCC in this very young patient group. Repeated sequential MR imaging of the native liver in patients with Kasai PE is necessary to monitor possible malignant transformation of liver nodules that may potentially develop as a result of chronic cholestatic liver disease.

INTRODUCTION

In 1959, Kasai portoenterostomy (PE) for children with biliary atresia (BA) was introduced in clinical practice[1]. This operation increased the survival to a 20-year patient survival without liver transplantation of 23%[2]. Nevertheless, almost all patients develop features of end-stage liver disease and biliary cirrhosis[2]. Kasai PE is clearly not a curative treatment, but a bridge to liver transplantation. Although the indication for liver transplantation is clear, the timing depends on development of complications of biliary cirrhosis.

The purpose of this paper is 1) to describe the Kasai procedure; 2) to inform clinicians of the possibility of developing hepatocellular carcinoma at a relatively young age; and 3) to indicate the necessity for repeated sequential MR imaging to monitor possible malignant transformation of liver nodules in patients with Kasai PE.

Lieke Hol, MD[1], Indra C. van den Bos, MD[2], Shahid M. Hussain, MD, PhD[2,3], Pieter E. Zondervan, MD[4], Robert A. de Man, MD, PhD[1]

Departments of [1]Gastroenterology and Hepatology, [2]Radiology, and [4]Pathology, Erasmus MC, University Medical Center Rotterdam, The Netherlands; [3]Department of Radiology, University of Nebraska Medical Center, Omaha, NE, USA

Submitted

CASE REPORT

In 2000, a 19-year old Caucasian male was seen in the outpatient clinic of our hospital because of abdominal pain in the right upper quadrant. He underwent a successful Kasai procedure during his neonatal period for congenital biliary atresia type III and had recurrent episodes of jaundice, pale stools and dark urine without overt evidence of cholestasis during his teen ages.

Since 1990, the patient was known with a macronodular appearance of the liver on ultrasound (US). A dominant nodule, located caudally in the right liver lobe, was first visualized on US in 1991, with a diameter of 3.8cm. The exact nature of this lesion was unknown, and percutaneous biopsies performed in 1991 and 1993 of both liver and dominant nodule showed moderate to extensive fibrosis and chronic cholestasis, without malignant features. In a period of 9 years, the lesion steadily increased in size, including a diameter of 3.8cm in 1991; 5.2cm in 1992; and 6.5cm in 1996. For further characterization of the lesion, magnetic resonance (MR) imaging of the liver was performed in 2000, which showed an atrophic cirrhotic macronodular liver with multiple regeneration nodules. The dominant nodule in the right liver lobe had a diameter of 9.5cm. There were some areas of high signal intensity on both the T1- and T2-weigthed sequences, which did not enhance after contrast-administration, suspect for hemorrhage. After contrast administration, no arterial enhancement was detected in the nodules nor clear washout in the delayed phase. Taking these characteristics into account, the differential diagnosis of the lesion was dysplastic or degenerative nodule; or hepatocellular adenoma (HCA), without clear evidence for hepatocellular carcinoma (HCC). The laboratory findings showed a serum alpha-fetoprotein within the normal range.

In 2003 the patient was re-admitted to our hospital with a similar episode of abdominal pain in the right upper quadrant. Additionally, he had pale stools, dark urine, pruritis and a low-grade fever. Physical examination showed a jaundiced skin and sclerae with scratch lesions on his extremities. The abdominal examination revealed non-tender hepatomegaly and splenomegaly. The laboratory results showed a serum bilirubin of 346 µmol/L (normal range 0-16 µmol/L), alkaline phosphatase 446 IU/l (normal range 40–120 IU/l), albumin 39 g/L (normal range 35-50 g/L), International Normalized Ratio (INR) 1.1. The virology failed to demonstrate a hepatitis B or C infection (HBsAg, anti-HBc and anti-HCV all negative) An ultrasound of the liver failed to demonstrate overt biliary obstruction, but did show that the above described dominant nodule had further increased in size. A MR imaging was advised and performed (Fig. 1). This confirmed the now 10cm large lesion . In comparison with the previous MR examination, the lesion now clearly showed areas with decreased signal intensity on the opposed-phase T1-weighted gradient-echo (GRE) sequence compared to the in-phase GRE, indicating intratumoral fatty infiltration (Fig. 1 b, c). There were a few areas of high signal intensity on the T1-weighted and low signal intensity on the T2-weighted sequence (Fig 1a), indicating hemorrhage of older date. After contrast administration, the dynamic series revealed enhancement of the tumor in the arterial phase (Fig 1e): followed by hypointensity compared to the liver in the delayed phase indicating washout (Fig. 1f). In addition, there was delayed enhancement of a fibrous tumor capsule (Fig. 1f). These findings were suspect for HCC given the combination of intratumoral fat, hemorrhage, washout and capsule enhancement. Taking the extensive cirrhotic changes of the liver into account, hepatocellular adenoma (HCA) seemed unlikely. Additional biochemic examination revealed an AFP of 1 µg/l (normal range < 20 µg/l). Percutaneous liver biopsy of the lesion was performed, which showed disturbance of the architecture and irregular fibrosis without portal fields or bile ducts. The hepatocytes were uniform with irregular arrangement, vacuolar steatosis, cholestasis and minimal loss of reticulin; and were organized in cell plates of maximum one or

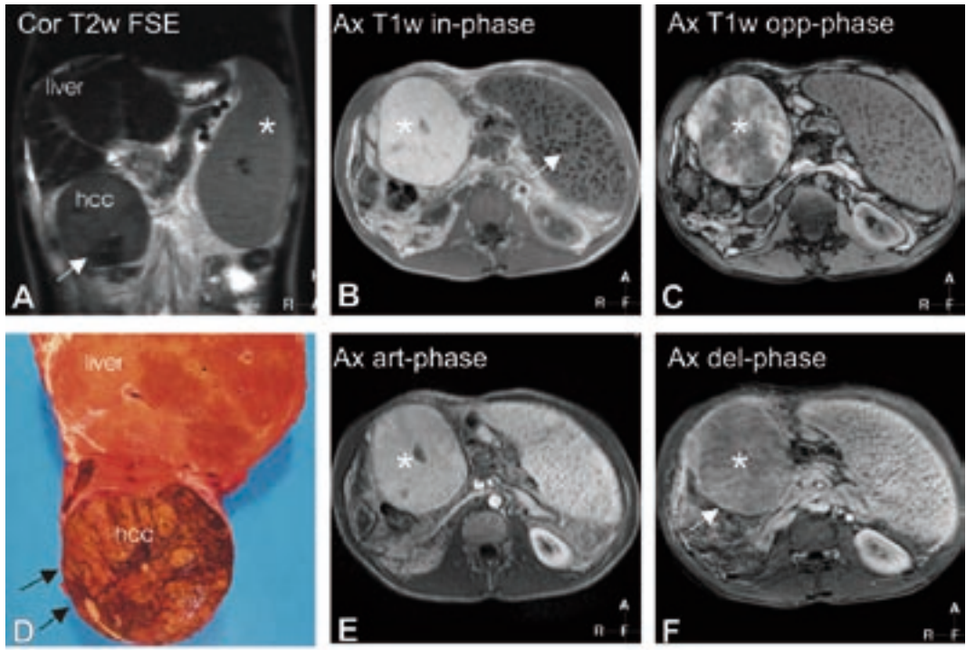

Figure 1: MR examination performed in 2003, with characteristic findings for hepatocellular carcinoma (HCC). (a) Coronal single-shot T2-weighted fast spin-echo (Cor T2-weighted FSE), showing an atrophic cirrhotic liver, splenomegaly (*) and an HCC, located caudally to the right liver lobe. Note an area of decreased signal intensity within the tumor (arrow) indicating hemorrhage of older date; (b) axial in-phase T1-weighted gradient-echo (GRE) (Ax T1-weighted in-phase), showing multiple gamna gandy bodies in the spleen (arrow) and a high signal intensity of the tumor (*); (c) axial opposed-phase T1-weighted GRE (Ax T1-weighted opp-phase), illustrating patchy areas of decreased signal intensity (*) compared to the in-phase sequence which illustrates diffuse intratumoral fatty infiltration; (d) macroscopic correlation after liver explantation, illustrating a cirrhotic atrophic liver and HCC with multiple internal nodules. Note the surrounding fibrous tumor capsule (arrows); (e) axial arterial phase T1-weighted GRE (Ax art-phase) after contrast shows enhancement of the entire lesion (*); (f) axial delayed phase T1-weighted GRE (Ax del phase) after contrast shows washout of contrast rendering the tumor hypointense, and delayed enhancement of a tumor capsule.

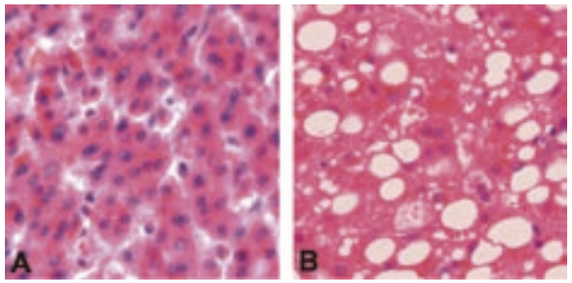

Figure 2: (a) Photomicrograph of the biopsy specimen in 2003 (original magnification x 400 H-E stain) shows a hepatocellular adenoma. The specimen demonstrates: (i) disturbance of the architecture and irregular fibrosis without portal fields or bile ducts; (ii) uniform hepatocytes with irregular arrangement, vacuolar steatosis, cholestasis and minimal loss of reticulin. (iii) hepatocyte arrangement of one or two cells in width. (b) Photomicrograph of a biopsy specimen after liver explantation in 2006 (original magnification x400 H-E stain) shows a well-differentiated HCC.

two cells in width. This resulted in a histologic conclusion of HCA (Fig 2a). Because pathology is regarded the gold standard for analysis of hepatocellular tumor, and considering the absence of clinical signs, the diagnosis was set to HCA beyond the opposing results of the MR imaging. However, it was decided to perform regular follow-up MR examinations to evaluate changes of the lesion, and to refer this patient to our liver transplant clinic because of recurrent and increasingly frequent episodes of cholestasis. Follow-up MR examination performed in July 2004 revealed a stable tumor size, but the combination of imaging finding was still highly suspect for HCC despite the absence of growth or any changes in tumor behavior. In January 2005 he underwent an orthotopic liver transplantation (OLT) with Roux Y reconstruction. The examination of the native liver showed entirely disturbed anatomy with a tumor of 10 cm diameter located caudally to the liver (Fig. 1d). Histologic examination demonstrated incomplete septal cirrhosis, and a well-differentiated hepatocellular carcinoma without vascular invasion nor lymph node involvement ($T_1N_0M_0$) (Fig 2b). Currently, the patient is in a good condition, without any evidence of tumor recurrence.

Table 1: Survival after a Kasai procedure for biliary cirrhosis

AUTHOR	STUDY PERIOD	no pts	5yr (%)	10yr (%)	20yr (%)
Houwen 1989	1977-1987	71	47	-	-
Karrer 1990	1976-1989	670	48	30	-
Chardot 1999	1986-1996	440	32	27	-
Nio 2003	1989-1994	735	60	53	-
Hung 2006	1976-2000	141	35	31	-
Lykavieris 2005	1968-1983	271	40	32	23

DISCUSSION

Four decades of Kasai surgery increased the survival of patients with biliary atresia to respectively 32-60% at 5 year, 27-53% at 10 years and a 23% at 20 years (Table 1)[2-7]. The survival benefit of the Kasai procedure can delay the subsequent liver transplantation, since primary liver transplantation in very young patients has a high morbidity and mortality rate. The backside of postponing a liver transplantation is an increased complication rate in the long-time survivor group with a native liver[2]. This emphasizes the importance of accurate timing for a liver transplantation.

HCC as complication of biliary atresia after Kasai PE is rare. The patient presented in this report developed a very slow growing tumor (over 14 years) with an extremely benign growth pattern, confirmed to be a well-differentiated HCC after liver explantation. The prevalence of HCC in explanted livers of patients transplanted for biliary atresia is 0.73-2.44% (three patients with a HCC in 316 pediatric transplantations)[8,9]. Eight cases of HCC after Kasai PE have been described in literature (Table 2). The described cases were diagnosed with HCC at a very young age (4 to 12 years old)[8-12]. The late delayed presentation of this patient may be due to the extremely benign growth pattern of the HCC that he developed.

Young patients that develop HCC in this group have a poor overall 2 and 5 year survival of 28%[13]. Complete tumor resection is the only curative option with an overall disease free survival of 57%[13] compared to a 5 year survival rate of 0% for unresectable tumors[14,15]. All reported patients had end-stage liver disease at the time of diagnosis, which made a partial resection of the tumor impossible. Therefore, liver transplantation was the only viable option. The short time survival (18-60 months) after liver transplantation was 86% (6 of 7 pts)[8-12]. This is comparable to the 4 and 5-year survival rate of all pediatric patients who underwent a liver transplantation for HCC (72 and 63%, respectively)[16,17].

Diagnostic delay is common in this patient group. This is demonstrated by this case and 3 of the 8 described cases in which HCC was also diagnosed after liver explantation[8-12]. This diagnostic delay impairs the post-transplantation prognosis[13], since lymph node involvement and tumor size are independent risk factors for recurrence of HCC after transplantation[13,18]. More crucial are distant metastatic disease or macroscopic vascular involvement, which are exclusion criteria for liver transplantation[16,17,19]. This underlines, that early detection of (pre-) malignant hepatic lesions in this young patient group is of paramount importance. Especially, since living related liver transplantation makes a more timely transplantation possible. Clinical examination of these patients is insufficient since the clinical presentation of a HCC is non-specific: abdominal swelling, dull abdominal pain, progressive weight loss and fatigue[13,17]. In addition, serum AFP as a screenings tool lacks specificity since 8-18% of the pediatric patients with a HCC have a serum AFP within a normal range[13,19].

Pathology is the golden standard for diagnosis of hepatocellular tumors. However, as demonstrated by this patient, sampling errors can occur due to the step-wise development of HCC, which may give rise to distinct regions of either dysplastic or truly malignant features within in one tumor. Also, distinction between well-differentiated HCC and HCA may be complicated. Furthermore, the invasive character of percutaneous liver biopsy is associated with a relatively high complication rate, especially in young children.

Currently, MR imaging is regarded the modality of choice for the work-up for patients with focal liver lesions[20]. The ability to detect intrinsic tissue characteristics on T1- and T2-weighted sequences in combination with dynamic contrast-enhanced imaging renders it a superior imaging modality for detection and characterization of focal liver lesions[21]. More importantly, MR imaging compared to computed tomography (CT) acquires its data without radiation exposure, which is important for especially this young patient group, since routine follow-up multiphasic CT examinations result in high radiation dosages[22]. MR imaging of patients with Kasai PE should be performed frequently to monitor eventually malignant transformation of liver nodules as seen in this patient. This step-wise process of carcinogenesis in post-Kasai livers can be very subtle[23]. In addition, the surveillance with MR imaging should start at an early age, since a HCC presents on an early age in this patient group[8-12].

In conclusion, Kasai PE increased the life expectations of patients with biliary atresia. The development of HCC in this patient population is rare, but will intensively impair the survival. Therefore, clinicians should be alert to the development of HCC in this very young patient group. Follow-up MR imaging of the native liver is important in order to monitor and evaluate development of focal liver lesions in patients with a Kasai PE.

Table 2: Cases of hepatocellular carcinoma associated with biliary atresia

Author	Age (yr) at diagnosis	diagnosis	stage	Survival after LT	Outcome
Van Wyk (1972)	12	Liver transplantation	NA	10 wk	LT: †, Long metastasis
	4	Liver transplantation	NA	18 mo	LT: alive, no recurrence
Esquivel (1994)	11	Liver transplantation	II	44 mo	LT: alive, no recurrence
Kohno (1995)	4	Incidental	I	-	No LT: †
Superina (1996)	12	Incidental	II	36 mo	LT: alive, no recurrence
Tatekawa (2001)	8	Incidental	Iva	60 mo	LT: alive, no recurrence
	5	Incidental	II	33 mo	LT: alive, no recurrence
Hol (2006)	23	Incidental	I	17 mo	LT: alive, no recurrence

†: died. Stage I-IV: TNM classification for HCC
Abbreviations: LT: Liver transplantation; NA: not available; wk: week; mo: month; yr: year.

REFERENCES

1. Kasai M. Surgical treatment of biliary atresia. J pediatr Surg 1968; 3:665-75.
2. Lykavieris P, Chardot C, Sokhn M, Gauthier F, Valayer J, Bernard O. Outcome in adulthood of biliary atresia: a study of 63 patients who survived for over 20 years with their native liver. Hepatology 2005 Feb; 41(2):366-71.
3. Chardot C, Carton M, Spire-Bendelac N, Le PC, Golmard JL, Auvert B. Prognosis of biliary atresia in the era of liver transplantation: French national study from 1986 to 1996. Hepatology 1999 Sep; 30(3):606-11.
4. Houwen RH, Zwierstra RP, Severijnen RS, Bouquet J, Madern G, Vos A, et al. Prognosis of extrahepatic biliary atresia. Arch Dis Child 1989 Feb; 64(2): 214-8.
5. Hung PY, Chen CC, Chen WJ, Lai HS, Hsu WM, Lee PH, et al. Long-term prognosis of patients with bi-

liary atresia: a 25 year summary. J Pediatr Gastroenterol Nutr 2006 Feb; 42(2):190-5.
6. Karrer FM, Lilly JR, Stewart BA, Hall RJ. Biliary atresia registry, 1976 to 1989. J Pediatr Surg 1990 Oct; 25(10):1076-80.
7. Nio M, Ohi R, Miyano T, Saeki M, Shiraki K, Tanaka K. Five- and 10-year survival rates after surgery for biliary atresia: a report from the Japanese Biliary Atresia Registry. J Pediatr Surg 2003 Jul; 38(7): 997-1000.
8. Esquivel CO, Gutierrez C, Cox KL, Garcia-Kennedy R, Berquist W, Concepcion W. Hepatocellular carcinoma and liver cell dysplasia in children with chronic liver disease. J Pediatr Surg 1994 Nov; 29(11): 1465-9.
9. Tatekawa Y, Asonuma K, Uemoto S, Inomata Y, Tanaka K. Liver transplantation for biliary atresia associated with malignant hepatic tumors. J Pediatr Surg 2001 Mar; 36(3):436-9.
10. Kohno M, Kitatani H, Wada H, Kajimoto T, Matuno H, Tanino M, et al. Hepatocellular carcinoma complicating biliary cirrhosis caused by biliary atresia: report of a case. J Pediatr Surg 1995 Dec; 30(12): 1713-6.
11. Superina R, Bilik R. Results of liver transplantation in children with unresectable liver tumors. J Pediatr Surg 1996 Jun; 31(6):835-9.
12. Van WJ, Halgrimson CG, Giles G, Lilly J, Martineau G, Starzl TE. Liver transplantation in biliary atresia with concomitant hepatoma. S Afr Med J 1972 Jun 24; 46(26):885-9.
13. Czauderna P, Mackinlay G, Perilongo G, Brown J, Shafford E, Aronson D, et al. Hepatocellular carcinoma in children: results of the first prospective study of the International Society of Pediatric Oncology group. J Clin Oncol 2002 Jun 15; 20(12): 2798-804.
14. Katzenstein HM, Krailo MD, Malogolowkin MH, Ortega JA, Liu-Mares W, Douglass EC, et al. Hepatocellular carcinoma in children and adolescents: results from the Pediatric Oncology Group and the Children's Cancer Group intergroup study. J Clin Oncol 2002 Jun 15; 20(12):2789-97.
15. Yu SB, Kim HY, Eo H, Won JK, Jung SE, Park KW, et al. Clinical characteristics and prognosis of pediatric hepatocellular carcinoma. World J Surg 2006 Jan; 30(1):43-50.
16. Austin MT, Leys CM, Feurer ID, Lovvorn HN, III, O'Neill JA, Jr., Pinson CW, et al. Liver transplantation for childhood hepatic malignancy: a review of the United Network for Organ Sharing (UNOS) database. J Pediatr Surg 2006 Jan; 41(1):182-6.
17. Reyes JD, Carr B, Dvorchik I, Kocoshis S, Jaffe R, Gerber D, et al. Liver transplantation and chemotherapy for hepatoblastoma and hepatocellular cancer in childhood and adolescence. J Pediatr 2000 Jun; 136(6):795-804.
18. Chen JC, Chen CC, Chen WJ, Lai HS, Hung WT, Lee PH. Hepatocellular carcinoma in children: clinical review and comparison with adult cases. J Pediatr Surg 1998 Sep; 33(9):1350-4.
19. Arikan C, Kilic M, Nart D, Ozgenc F, Ozkan T, Tokat Y, et al. Hepatocellular carcinoma in children and effect of living-donor liver transplantation on outcome. Pediatr Transplant 2006 Feb; 10(1):42-7.
20. Cohen MB, Kader HH, Lambers D, Heubi JE. Complications of percutaneous liver biopsy in children. Gastroenterology 1992 Feb; 102(2):629-32.
21. Hussain SM, Semelka RC. Hepatic imaging: comparison of modalities. Radiol Clin North Am 2005 Sep; 3(5):929-47, ix.
22. Hussain SM, Semelka RC, Mitchell DG. MR imaging of hepatocellular carcinoma. Magn Reson Imaging Clin N Am 2002 Feb; 10(1):31-52, v.
23. Martin DR, Semelka RC. Health effects of ionising radiation from diagnostic CT. Lancet 2006 May 27; 367(9524):1712-4.
24. Hussain SM, Zondervan PE, IJzermans JN, Schalm SW, de Man RA, Krestin GP. Benign versus malignant hepatic nodules: MR imaging findings with pathologic correlation. Radiographics 2002 Sep; 22(5):1023-36.
25. Hussain SM, van den Bos IC, Dwarkasing RS, Kuiper JW, den Hollander JW. Hepatocellular adenoma: findings at state-of-the-art magnetic resonance imaging, ultrasound, computed tomography and pathologic analysis. Eur Radiol 2006 Sep; 16(9):1873-86.

chapter4.4
hepatoid adenocarcinoma as mimicker of hepatocellular carcinoma

Hepatoid adenocarcinoma OF THE GALL-BLADDER:

a mimicker of hepatocellular carcinoma

ABSTRACT

We present a case with a large gallbladder tumor in a patient with no known liver disease and elevated alpha-fetoprotein (AFP), in which differential diagnosis with hepatocellular carcinoma (HCC) in a non-cirrhotic liver was particularly difficult given the combination of the size of the tumor, solitary nature, elevated AFP, and striking resemblance with HCC at histology. In presenting this patient, we would like to emphasize the role of MR imaging as a problem-solving tool for analysis of rare tumors of non-hepatocellular origin, including hepatoid adenocarcinoma of the gallbladder.

INTRODUCTION

Hepatoid adenocarcinoma (HAC) is a rare variant of extrahepatic adenocarcinoma, consisting of foci of both adenomatous and hepatocellular differentiation which behave like hepatocellular carcinoma (HCC) in morphology and functionality[1]. It occurs in a multitude of organs, most frequently in the stomach[2,3], but it has been reported to occur rarely in other areas as well, including the lung[4], kidney[5], female reproductive tract[6,7], pancreas[8] and gallbladder[1,9]. Typically, an elevated level of serum alpha-fetoprotein (AFP) is detected, although normal levels have also been described[2,3]. We report a patient with a large tumor in the gallbladder detected at magnetic resonance (MR) imaging, combined with an elevated serum AFP. Differential diagnosis with HCC in a non-cirrhotic liver was particularly difficult given the combination of the size of the tumor with invasion of the surrounding liver, solitary nature, elevated AFP, and striking resemblance with HCC at histology.

Indra C. van den Bos, MD[1], Shahid M. Hussain, MD, PhD[1,4], Roy S. Dwarkasing, MD[1], Hans Stoop, Msc[2], Pieter E. Zondervan, MD[2], Gabriel P. Krestin, MD, PhD[1], Robert A. de Man, MD, PhD[3]

Departments of [1]Radiology, [2]Pathology, and [3]Gastroenterology and Hepatology, Erasmus MC, University Medical Center Rotterdam, The Netherlands; [4]Department of Radiology, University of Nebraska Medical Center, Omaha, NE, USA

British Journal of Radiology, in press.

CASE REPORT

A 55-year old woman was referred to our hospital for evaluation of a hepatic mass. The lesion was discovered at ultrasound (US) performed in another clinic for work-up of right upper quadrant abdominal pain. Previous history was unremarkable. At physical examination, no abnormalities were noted. Routine laboratory investigations were performed, showing slightly elevated liver enzymes and an abnormally elevated AFP (511 µg/ml, normal value below 20 µg/ml). Hepatitis B and C serology tests were negative. Magnetic resonance (MR) imaging was performed for further characterization of the lesion, which confirmed the presence of a well-demarcated tumor adjacent to the gallbladder, with longest diameter of 7 cm (Fig. 1). The liver showed a normal size and morphology, without signs of cirrhosis.

MR imaging findings

On T1-weighted gradient-echo (GRE) images, the lesion was hypointense to the surrounding liver parenchyma (Fig. 1a). The tumor was located in the gallbladder fossa, with a slightly bilobar shape and with narrowing of the gallbladder lumen. Fat-suppressed T2-weighted fast spin-echo (FSE) images showed hyperintensity of the lesion, without evidence for internal nodules or internal heterogeneity (Fig. 1b). Specifically, the signal intensity was higher in the periphery of the lesion, with slightly lower values in the center suggestive for central fibrosis. After intravenous administration of a non-liver specific gadolinium chelate (Magnevist [gadopentetate dimeglumine], Schering, Berlin, Germany), the lesion enhanced predominantly in the periphery (Fig. 1c). Dynamic gadolinium-enhanced images revealed peripheral enhancement in the arterial phase, slowly progressing centripetally (Fig. 1c-d). In the delayed phase, no clear washout of contrast material was seen. No tumor capsule could be detected. In addition, 3 small lesions with diameter < 1 cm were observed in proximity of the tumor, with identical signal intensity at fat-suppressed T2-weighted imaging and after contrast-administration. These alterations were suspect for metastases or satellite lesions. For further characterization of the tumor, additional imaging using a liver-specific contrast medium was performed, using superparamagnetic iron-oxide particles (SPIO) contrast agent (Resovist, Schering AG, Berlin, Germany). After uptake of SPIO fat-suppressed T2-weighted FSE showed no evident decrease of signal intensity within the lesion, indicating that it was not a primary tumor with abundant amount of Kupffer cells. This finding virtually excluded the possibility of a well-differentiated HCC, hepatocellular adenoma, and focal nodular hyperplasia. The findings of the MR imaging examination posed a diagnostic dilemma: the combination of signal intensity, morphology of the tumor, close proximity to the gallbladder, and enhancement pattern was strongly suggestive for a cholangiocarcinoma or another type of malignant lesion, which originated from the gallbladder. However, the elevated serum AFP, solitary nature, large size, non-cirrhotic liver suggested a hepatocellular carcinoma as the most likely possibility. Therefore, the final differential diagnosis consisted of hepatoid adenocarcinoma (HAC) of the gallbladder, cholangiocarcinoma and HCC. Particularly, we considered HAC the most likely diagnosis because this entity does show hepatoid differentiation and can present with a liver tumor and elevated AFP[1].

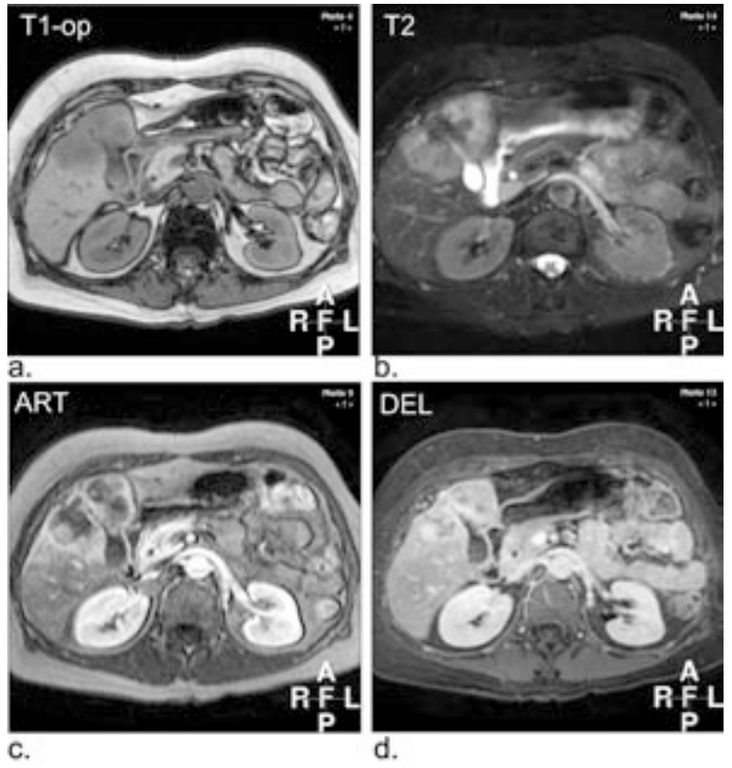

Figure 1: (a) Axial opposed-phase T1-weighted gradient-echo (GRE) (T1-op) shows hypointensity of the lesion compared to the surrounding liver, and shows the lesion originates in the fundus of the gallbladder. (b) Axial fat-suppressed T2-weighted fast spin-echo (T2) shows faint hyperintensity of the lesion. (c) Axial arterial phase gadolinium-enhanced T1-weighted GRE (ART) shows patchy, predominantly peripheral enhancement of the lesion. Note the intense enhancement of the aorta (open arrow) and the spleen. (d) Axial 3D delayed phase fat-suppressed T1-weighted GRE (DEL) shows the lesion retains the contrast material with a patchy distribution.

Histology

Subsequently, ultrasound-guided percutaneous liver biopsy was performed. At microscopic evaluation, a combination of hepatocyte-like- and adeno-structures was observed, embedded in a fibrous tissue matrix (Fig. 2a). Some trabecular formations were present. Immunohistochemical analysis showed positivity for cytokeratin CK7 and CK19 in all areas, while CK20 was negative. These findings on itself supported the general diagnosis of a carcinoma. Also, CD10 positivity was observed which indicated sporadic canalicular differentiation (see Fig 2b-c). Staining with AFP showed cytoplasm positivity (Fig. 2d). CD56 staining showed slight positivity in the cell membrane in some more solid areas. These findings provided evidence for hepatocellular differentiation of the tumor, suggesting HCC, or rather combined HCC with cholangiocarcinoma (CC). However, the combination of immunohistochemical results with positivity for CD10, the canalicular formation of some cells in combination with high serum AFP and the location of the tumor were atypical for diagnosis of either HCC or HCC-CC. Therefore, the most likely histological diagnosis was hepatoid adenocarcinoma.

Even though the location of the tumor was problematic for successful resection, it was decided to perform exploratory hepatic surgery to assess resectability. At surgery however, liver metastases were detected, confirming the MR findings of suspected metastases in proximity of the tumor.

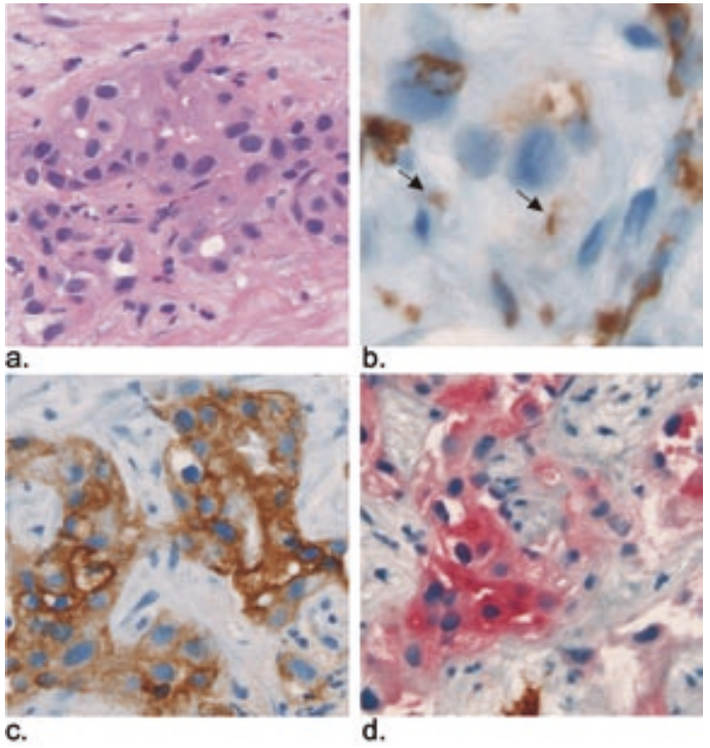

Figure 2: (a) Photomicrograph (hematoxylin and eosin (HE) stain, original magnification x200) shows a detailed view of the tumor with solid areas and adeno structures. (b) Photomicrograph (stained with endothelial marker CD 10, x400) shows positivity (arrows) indicating canalicular differentiation of areas within the tumor. (c) Photomicrograph (stained with cytokeratin CK 7, x200) shows abundant positive staining, indicating epithelial differentiation. (d) Photomicrograph (stained with AFP, x200) shows widespread positivity, and hence a hepatocellular origin of the tumor.

Currently, patient is undergoing palliative chemotherapy and is in reasonable condition.

DISCUSSION

Hepatoid adenocarcinoma (HAC) is a rare form of adenocarcinoma with hepatoid differentiation of the tumor cells. In this report, a case is described with a large gallbladder tumor in combination with high AFP, in which the signal intensity on T2-weighted images showed predominantly high signal intensity in the periphery of the lesion, with hypointensity in the center of the lesion without clear heterogeneity. The enhancement pattern on dynamic gadolinium-enhanced images showed slow peripheral enhancement with centripetal progression over time, without washout or capsule enhancement. Given the combination of tumor morphology and location, signal intensity, contrast enhancement and high AFP in absence of cirrhosis, HAC of the gallbladder was the most likely diagnosis. HCC in a non-cirrhotic liver was less likely these tumors are usually very large at presentation, with striking heterogeneity and capsule formation[12,13]. These findings are clinically relevant since HCC, combined HCC-CC with peripheral location or HAC all have a different therapeutic approach, especially in a non-cirrhotic liver. As in our patient, in case of localization of the tumor within the gallbladder wall, differentiation with HCC or combined hepatocellular carcinoma – cholangiocarcinoma (HCC-CC) is challenging. Additional immunohistochemistry is often helpful for tumor characterization[1,3,9,11]. In our patient, diffuse positivity with CK7 and CK19 was observed, which suggested presence of an adenocarcinoma. Also, CD10 was sporadically positive, indicating canalicular differentiation and thus hepatocellular origin. This was also supported by a positive AFP, although some rare cases of AFP negative HAC in the gallbladder have been described[9]. The combination of positivity for CD10, the canalicular formation of some cells in combination with high serum AFP and the location of the tumor supported hepatoid adenocarcinoma as the most likely diagnosis. As has been described by Sakamoto and colleagues before[11], HCC or combined HCC-CC invading the gallbladder is the main differential diagnosis of gallbladder HAC. In these cases, considering the clinical presentation may be helpful, since for example HCC occurring in a non-cirrhotic liver is typically very large, with striking heterogeneity and capsule formation.

The present case demonstrates the value of state-of-the-art MR imaging for lesion characterization. The unique ability to detect intrinsic cellular characteristics combined with dynamic contrast-enhanced imaging render MR imaging superior for detection and characterisation of focal liver lesions[12]. MR imaging findings of HCC in non-cirrhotic liver tissue are well known[12,13]. Typically, a solitary, large tumor is observed with striking heterogeneity, inhomogeneous enhancement, capsule formation and often a central scar[10,13]. HCC in a cirrhotic liver however, has quite different imaging characteristics, including hyperintense signal intensity on T2-weighted images, intense arterial enhancement with washout in delayed phase contrast-enhanced imaging and delayed enhancement of a tumor capsule[10]. Typical imaging findings of cholangiocarcinoma include hypointensity on T1-weighted images, hyperintensity on T2-weighted images with central hypointensity and peripheral enhancement, with centripetal progression on delayed phase images[14]. Imaging findings of primary gallbladder carcinoma are different, with eccentric tumor formation in 76%, liver invasion in 91% and marked heterogeneity and inhomogeneous enhancement after contrast administration[15]. As demonstrated in our case, the combination of imaging findings before and after contrast administration did not quite fit the diagnosis of HCC, cholangiocarcinoma nor primary gallbladder carcinoma. Given the combination of tumor morphology and location, signal intensity, contrast enhancement and high AFP in absence of cirrhosis, HAC of the gallbladder was the most likely diagnosis at MR imaging, confirmed by histo-immunochemical analysis of the tumor.

In presenting this patient, we would like to emphasize the role of MR imaging as a problem-solving tool for analysis of rare tumors of non-hepatocellular origin, including hepatoid adenocarcinoma of the gallbladder.

REFERENCES

1. Sakamoto K, Monobe Y, Kouno M, Moriya T, Sasano H. Hepatoid adenocarcinoma of the gall–bladder: Case report and review of the literature. Pathol Int 2004; 54:52-56.
2. Ishikura H, Kishimoto T, Andachi H, Kakuta Y, Yoshiki T. Gastrointestinal hepatoid adenocarcinoma: venous permeation and mimicry of hepatocellular carcinoma, a report of four cases. Histopathology 1997; 31:47-54.
3. Terracciano LM, Glatz K, Mhawech P, et al. Hepatoid adenocarcinoma with liver metastasis mimicking hepatocellular carcinoma: an immunohistochemical and molecular study of eight cases. Am J Surg Pathol 2003; 27:1302-1312.
4. Arnould L, Drouot F, Fargeot P, et al. Hepatoid adenocarcinoma of the lung: report of a case of an unusual alpha-fetoprotein-producing lung tumor. Am J Surg Pathol 1997; 21:1113-1118.
5. Ishikura H, Ishiguro T, Enatsu C, et al. Hepatoid adenocarcinoma of the renal pelvis producing alpha-fetoprotein of hepatic type and bile pigment. Cancer 1991; 67:3051-3056.
6. Shintaku M, Kariya M, Shime H, Ishikura H. Adenocarcinoma of the uterine cervix with choriocarcinomatous and hepatoid differentiation: report of a case. Int J Gynecol Pathol 2000; 19:174-178.
7. Matsuta M, Ishikura H, Murakami K, Kagabu T, Nishiya I. Hepatoid carcinoma of the ovary: a case report. Int J Gynecol Pathol 1991; 10:302-310.
8. Yano T, Ishikura H, Wada T, et al. Hepatoid adenocarcinoma of the pancreas. Histopathology 1999; 35:90-92.
9. Nakashima H, Nagafuchi K, Satoh H, et al. Hepatoid adenocarcinoma of the gallbladder. J Hepatobiliary Pancreat Surg 2000; 7:226-230.
10. Sakamoto K, Kimura N, Tokumura H, Ogasawara T, Moriya T, Sasano H. Hepatoid adenocarcinoma of the gallbladder. Histopathology 2005; 47:649-651.
11. Hussain SM, Semelka RC. Hepatic imaging: comparison of modalities. Radiol Clin North Am 2005; 43:929-947, ix.
12. Winston CB, Schwartz LH, Fong Y, Blumgart LH, Panicek DM. Hepatocellular carcinoma: MR imaging findings in cirrhotic livers and noncirrhotic livers. Radiology 1999; 210:75-79.
13. Hussain SM, Semelka RC, Mitchell DG. MR imaging of hepatocellular carcinoma. Magn Reson Imaging Clin N Am 2002; 10:31-52, v.
14. Manfredi R, Barbaro B, Masselli G, Vecchioli A, Marano P. Magnetic resonance imaging of cholangiocarcinoma. Semin Liver Dis 2004; 24:155-164.
15. Schwartz LH, Black J, Fong Y, et al. Gallbladder carcinoma: findings at MR imaging with MR cholangiopancreatography. J Comput Assist Tomogr 2002; 26:405-410.

chapter5

MR IMAGING AT HIGH MAGNETIC FIELD STRENGTH

chapter5.1
application of variable-rate selective excitation (VERSE) RF pulses

Extending slice coverage for breath-hold FAT-SUPPRESSED T2-WEIGHTED FAST SPIN-ECHO OF THE LIVER AT 3.0T:

application of variable-rate selective excitation (VERSE) RF pulses

ABSTRACT

Purpose: To determine the benefits of variable-rate-selective excitation (VERSE) RF pulses for increased slice coverage in breath-hold fat-suppressed T2-weighted fast spin-echo (FS-T2-weighted-FSE) liver imaging at 3.0T.

Material and Methods: Twelve healthy volunteers were imaged at 3.0T, using FS-T2-weighted-FSE. Slice coverage and specific absorption rate (SAR) levels were monitored for VERSE- and standard-RF, respectively. breath-hold time was 25 sec; slice thickness 3.5 mm. Maximum coverage was assessed for interactive variation of repetition time (TR), bandwidth (BW) and echo-train length (ETL). Image quality was assessed qualitatively and quantitatively.

Results: Total slice coverage was always higher using VERSE-RF, but varied depending on the selected parameters. For BW ≥62.5 KHz, slice coverage using VERSE increased between 38% (TR=8200 msec) and 58% (TR=2500 msec). Maximum coverage was obtained for TR=5000 msec, ETL=12 and BW ≥62.5 KHz; with a mean of 31.8 slices for VERSE and 22.5 slices for standard-RF, respectively (p<0.005, 41% increased coverage). SAR was lower for VERSE-RF using BW <41.67 KHz (p<0.05), and equal to standard-RF for higher BW. Image quality was best for TR ≤5000 msec (p<0.05). Fat-suppression was more homogeneous for lower ETL (p<0.05). Blood suppression was best for TR ≤5000 msec (p<0.05).

Conclusion: VERSE RF pulses can be applied for thin-slice breath-hold fat-suppressed T2-weighted liver imaging at 3.0T, with significantly improved slice coverage.

Indra C. van den Bos, MD[1], Shahid M. Hussain, MD, PhD[1,2], Gabriel P. Krestin, MD, PhD[1], Piotr A. Wielopolski, PhD[1]

Departments of [1]Radiology, Erasmus MC, University Medical Center Rotterdam, The Netherlands; [2]Department of Radiology, University of Nebraska Medical Center, Omaha, NE, USA

Submitted

INTRODUCTION

Annually, magnetic resonance (MR) imaging of the liver is routinely performed in thousands of patients worldwide, as part of clinical imaging work-up in case of suspected or proven focal liver lesions[1]. The unique ability of MR imaging to detect intrinsic cellular characteristics combined with dynamic contrast-enhanced imaging renders it a superior technique for detection and characterization of liver lesions compared to other imaging modalities such as computed tomography (CT) or ultrasound (US), without radiation exposure[2,3].

At 1.5T, routine state-of-the-art imaging consists of T1-weighted sequences with in- and opposed-phase (chemical shift) imaging; single-shot T2-weighted fast spin echo (FSE) sequences; fat-suppressed T2-weighted sequences and dynamic multiphasic gadolinium-enhanced imaging[4]. Fat-suppressed T2-weighted sequences are essential for detection of liver nodules, including metastases[5,6].

The introduction of 3.0T MRI systems with the development of coils with capability of parallel imaging has provided a number of potential advantages for hepatobiliary MR imaging[7,8]. With about double the signal-to-noise ratio (SNR) of a 1.5T system, 3.0T MR systems can substantially improve image quality and image acquisition speed, and can potentially deliver √2 improvement in resolution in the same acquisition time of a comparable study at 1.5T; or ½ slice thickness with identical coverage; or 4-fold speed up in scanning time for identical resolution settings[9]. Even though T1, and to a lesser degree also T2 relaxation times change with magnetic field strength, understanding of these changes and consequent adjustment of applied imaging protocols can help to improve image quality at 3.0T[10-12].

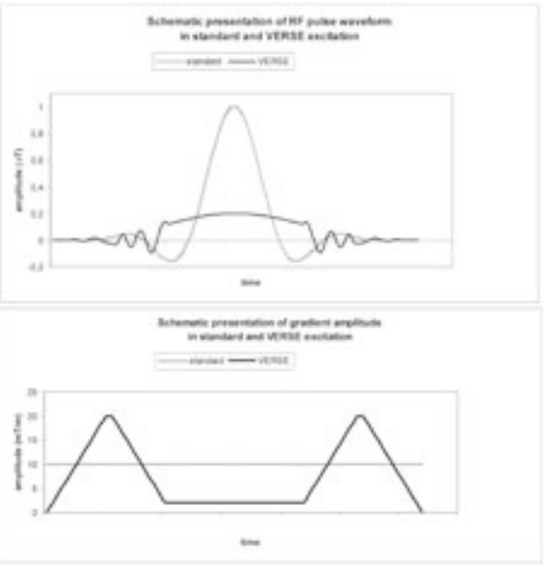

Figure 1: Schematic presentation of radio-frequency (RF) waveform in standard en variable-rate selective excitation (VERSE).
(a) RF pulse waveform in standard and VERSE excitation. Note that the standard RF pulse is stronger towards the center of the wav, whilst the RF amplitude for VERSE excitation is increased and acceleration towards the edges of the pulse. (b) Accompanying gradient waveform, which is constant during the entire excitation for standard excitation. Note the waveform has changed in VERSE excitation, with increased amplitude toward the edges of the pulse.

However, the implementation of T2-weighted-, and particularly FSE sequences at 3.0T has been challenging. Such sequences are RF intensive due to application of multiple refocusing RF pulses. This translates into higher specific absorption rates (SAR), which are quadrupled at 3.0T[12]. Higher SAR values diminish the anatomic coverage and can lengthen the exam times considerably. In addition, B_1 inhomogeneities and dielectric resonances may create intensity modulations including focal shading or local decrease in signal intensity, which are more pronounced at higher field strength[13]. This may degrade image quality even in well-shimmed imaging volumes and may result in insufficient or heterogeneous fat suppression. .

One way of getting around B1-inhomogeneities is to apply adiabatic fast passage (AFP) RF pulses during excitation and refocusing. These RF pulses have been implemented in current FSE readout modules at 3.0T[7,14]. Nonetheless, AFP RF pulses are longer and necessitate higher power to overcome the inhomogeneous B1 excitation that otherwise would occur with normal RF pulses. Therefore, application of AFP RF pulses can increase SAR and hence result in lower anatomic coverage per TR with longer exam times at 3.0T.

In addition, variable-rate selective excitation (VERSE) radiofrequency (RF) pulses have been proposed and re-introduced to reduce SAR at 3.0T[15-19]. In essence, a VERSE-RF pulse is non-adiabatic, and is designed and played during an amplitude-modulated gradient waveform rather than during a constant gradient. By reshaping the gradient waveform, the gradient amplitude is lower during the main lobe and higher at the edges of the RF pulse. This reduces SAR while keeping the same excitation time and essentially the same spatial excitation profile (Fig. 1)(16). In addition, the VERSE designed pulses are less sensitive to B1-inhomogeneity[20].

To our knowledge, none of the previous publications have reported the application of VERSE-RF pulses in T2-weighted FSE sequences as a mean to increase slice coverage and to obtain improved image quality by using combined partial Fourier and parallel imaging for liver imaging at 3.0T.

The purpose of this paper was therefore, to determine the benefits of variable-rate selective excitation (VERSE) RF pulses for extending slice coverage in breath-hold fat-suppressed T2-weighted fast spin-echo (FS-T2-weighted-FSE) liver MR imaging at 3.0 T.

MATERIALS AND METHODS

This study was approved by the local ethics committee as part of an ongoing sequence optimization project. Twelve healthy volunteers (7 male, 5 female) were imaged on a 3.0T MR scanner (General Electric Healthcare, Signa Eclipse, Milwaukee, Wisconsin, USA) under software release 12X (Excite HD), using a body coil as signal transmitter and an 8-channel phased-array coil for signal reception. The MR system has high performance gradients (40 mT/m, 266 msec rise time to peak maximum) and parallel imaging acceleration factor of 2.00 for two-dimensional (2D) imaging. The operating mode was set to first level dB/dt and first level SAR limits (according to the FDA guidelines: SAR threshold for normal and first-level controlled modes are 2 and 4 W/kg respectively)[21]. Informed consent was signed by all participants after a brief interview to check for contraindications and explanation of the procedure.

MR imaging sequence

Imaging was performed with a breath-hold fat-suppressed T2-weighted fast spin-echo (FS-T2-weighted-FSE) sequence using VERSE and standard RF (sRF) pulses, respectively. The goal was to acquire full anatomic coverage of the liver in a maximum of 2 breath-hold acquisitions of 25 seconds each. Thin slices (3.5 mm, no interslice gap) were prescribed to obtain better through-plane resolution for improved multiplanar sections in all orientations. To assess image quality and slice coverage, an interactive variation of repetition time (TR) (8200, 5000, 3100 and 2500 msec), read bandwidth (BW) (125, 83.33, 62.50, 41.67, 30.83 and 20.83 KHz), echo-train length (ETL) (32, 16, 12 and 8 respectively) was performed using both VERSE and sRF pulses. The echo time (TE) was kept constant at 80 msec. Imaging matrix was set to 320 x 288; field of view (FOV) 320-400 x 240-300 cm^2 (to fit the anatomy); rectangular FOV of 75%; frequency direction left-to-right; standard fat suppression pulse; partial Fourier (1/2 NEX); and parallel imaging acceleration factor (ASSET, Array Spatial Sensitivity Encoding Technique) of 2.00, resulting in a final voxel size of 1.0-1.25 x 0.83-1.0 x 3.5 mm^3. The shim was adjusted once at the beginning of the measurements and kept constant for all the iterations performed.

Image analysis

On scans collected with VERSE-RF and sRF pulses, the maximum number of slices obtained within one 25-second breath-hold was registered. SAR parameters (mean and maximum levels) were recorded for each scan. The following items were evaluated qualitatively (subjectively): 1) overall image quality; 2) delineation of the liver (i.e. how well the liver contours could be identified); 3) tissue blurring from T2 decay during the FSE train; 4) fat-suppression homogeneity and 5) blood signal inside the hepatic vessels. These items were rated on a 1-5 scale (1 = unacceptable, 2 = poor, 3 = fair, 4 = good and 5 = excellent). For quantitative measurements, region-of-interest (ROI) of approximately 100 mm^2 were placed in liver, subcutaneous fat (where the largest variation in signal was observed with changes in ETL) and spleen. Care was taken to exclude vessels or biliary structures. For quantitative analyses of SNR of liver, signal intensity (SI) measurements close to the anterior coils of the array coil were compared to SI of central liver parenchyma. SNR was calculated as mean signal intensity scaled to background noise. ROI measurements were performed in the ventral subcutaneous fat (close to the anterior coils) and in the dorsal subcutaneous fat for analysis of the homogeneity and quality of the fat-suppression. In addition, to compare the SNR of measurements using the VERSE and the normal RF pulses, the optimally selected VERSE sequence parameters were compared to the corresponding one using normal RF pulses, with ROI evaluations performed in liver, kidney, spleen and muscle in identical locations. For analysis of the liver-to-spleen (which can be used for an indication for liver-to-lesion contrast) contrast-to-noise ratio (CNR), ROI measurements were performed both in spleen and liver at approximately 5 cm from the posterior coil array. CNR was calculated as difference in signal intensity between lesion and liver scaled to standard deviation of background noise of the liver SI sample.

Statistical analysis

Statistical parameters (mean, median, standard deviation, and range) were calculated using the Statistical Package for Social Sciences (SPSS) program. Significance levels were determined by a Wilcoxon signed rank test analysis. A p-value of less than 0.05 was considered statistically significant.

RESULTS

Slice coverage

For the set 25 sec breath-hold period, the use of VERSE-RF provided a 38 – 58% increase in slice coverage over sRF, for the different measurement parameters evaluated (TR, ETL and BW). With measurements using VERSE-RF, marked increase in slice coverage was noted with increasing BW, whilst for sRF, total slice coverage remained relatively stable (Fig. 2). A maximum mean of 31.8 slices was obtained for measurements using VERSE-RF, with TR=5000 msec, TE=80 msec, ETL=12 and BW≥ 62.5 KHz. For the same parameters, but using sRF, the mean number of slices was 22.5 (difference of 9.3 slices, p=0.003) (Fig. 2). Better slice efficiency was obtained for measurements with shorter TRs. In this regard, the best performance for measurements using VERSE-RF in comparison to sRF was obtained with TR=2500 msec, TE=80 msec, ETL=8 and BW ≥ 62.5 KHz (Fig. 2).

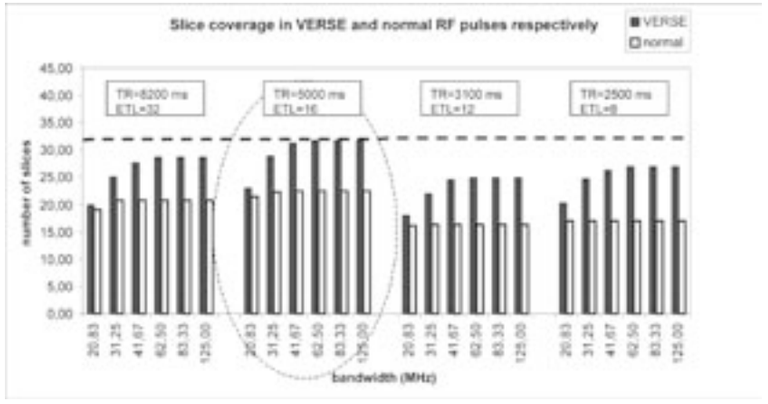

Figure 2: Slice coverage in VERSE and normal RF pulses respectively. The maximum amount of slices can be obtained using a combination of repetition time (TR) of 5000 msec and echo train length (ETL) of 16 respectively, for bandwidth (BW) > 62.5 KHz. For this set of parameters, a mean total of 31.8 slices can be achieved, compared to 22.5 slices for sequences obtained with the same parameters and the application of a standard RF pulse (p=0.003).

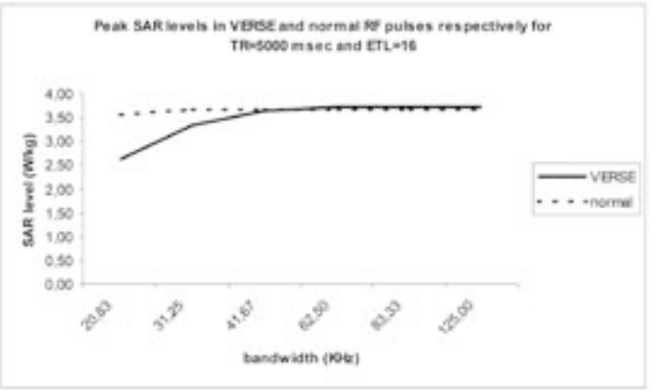

Figure 3: Peak SAR levels in VERSE and normal RF pulses respectively, for TR=5000 msec and ETL=16. Note that peak SAR levels in VERSE RF pulse sequences were lower for bandwidth <41.67 kHz.

Specific absorption rate

The sequence program keeps SAR levels constant for all measurement parameter combinations so that the slice coverage is obtained within a set TR. For settings using lower BW (<41.67 KHz), lower SAR figures were obtained using VERSE-RF compared to sRF (Fig. 3). For the lowest BW (20.83 kHz), the difference between VERSE-RF and sRF approached significance (p=0.07). The SAR levels were similar for both RF pulses for BW >41.67 KHz, showing a slow but steady increase towards the FDA limit and settling asymptotically to a mean value around 1.8/ 3.7 W/kg ((mean / peak SAR levels). The average mean/peak SAR levels were 1.73/ 3.47 W/kg and 1.83/ 3.65 W/kg for VERSE-RF and sRF, respectively.

IMAGE QUALITY

Qualitative assessment

VERSE-RF pulses

The qualitative evaluation was performed for the following TR/ETL combinations, assessed for BW=62.5KHz, including A) 8200/ 32; B) 5000/ 16; C) 3100/ 12; and D) 2500/8 (see Table 1).

Overall image quality for the four above setting was assessed on a 1-5 scale: A) 2.9 (range 2-3); B) 4.0 (range 3-5); C) 4.2 (range 4-5) and D) 4.4 (range 4-5) respectively. These differences were statistically significant (A compared to B, C and D respectively, p<0.05). This shows that images obtained with TR/ETL = 8200/32 were of inferior overall quality (Fig. 4).

The delineation of the liver was assessed as: A) 3.0 (range 3-3); B) 4.0 (range 3-5); C) 4.4 (range 4-5) and D) 4.3 (range 4-5). These differences were statistically significant (A compared to B, C and D respectively; and B compared to C, p<0.05). This shows that delineation of the liver is significantly better for sequences obtained with lower TR and ETL, with best image quality for TR/ETL=3100/12 and TR/ETL=2500/8, respectively (Fig. 4). In addition, images obtained with BW>62.5 KHz resulted in significantly lower SNR, which was detrimental to delineate liver borders.

The mean score for tissue sharpness related to blurring was assessed as: A) 3.0 (range 2-4); B) 3.7 (range 3-4); C) 3.9 (range 3-4) and D) 4.0 (range 3-5). These differences were statistically significant (A compared to B, C and D respectively, p<0.05). This shows that images obtained with TR/ETL=8200/32 have significantly increased blurring in the phase encoding direction with any BW selected (Fig. 4). Conversely, images acquired at lower BW (e.g. ≤ 31.25 KHz) demonstrate blurring with ETL ≥12. It is regarded that all images collected with acquisitions windows over 150 msec during the FSE readout show increased blurring from T2 decay. This is related to faster T2 signal decay for longer T2 species compared to shorter species, an effect which is more pronounced for sequences obtained with longer ETL. Since longer ETL values allow more time for signal decay, this results in increased image blurring.

The quality and homogeneity of the fat-suppression was assessed as: A) 2.5 (range 2-3); B) 3.9 (range 3-4); C) 4.1 (range 4-5) and D) 4.4 (range 4-5). These differences were statistically significant (A compared to B, C and D respectively; and B compared to C, p<0.05). This confirms that images obtained with lower ETL values have better and more homogeneous fat-suppression (Fig. 4).

Table 1

	Repetition time / echo train length			
	8000 / 32	**5000 / 16**	**3100 / 12**	**2500 / 8**
Overall image quality	2.9 (2.0-3.0)	4.0 (3.0-5.0)	4.2 (4.0-5.0)	4.4 (4.0-5.0)
Liver delineation	3.0 (3.0-3.0)	4.0 (3.0-5.0)	4.4 (4.0-5.0)	4.3 (4.0-5.0)
Tissue blurring	3.0 (2.0-4.0)	3.7 (3.0-4.0)	3.9 (3.0-4.0)	4.0 (3.0-5.0)
Suppression fat signal	2.5 (2.0-3.0)	3.9 (3.0-4.0)	4.1 (4.0-5.0)	4.4 (4.0-5.0)
Suppression blood signal	3.4 (3.0-4.0)	4.0 (4.0-4.0)	4.0 (4.0-4.0)	4.0 (4.0-4.0)

Qualitative assessment of image quality in VERSE, assessed on a 1-5 scale.

The quality of blood signal suppression in vessels was assessed as: A) 3.4 (range 3-4); B) 4.0 (range 4-4); C) 4.0 (range 4-4) and D) 4.0 (range 4-4). These differences were statistically significant (A compared to B, C and D respectively ($p<0.05$). Sequences obtained with TR/ETL=8200/32 showed more remnant blood signal. The optimized sequence using TR/ETL=5000/16 showed homogeneous, good suppression of the signal from inflowing blood (Fig. 4).

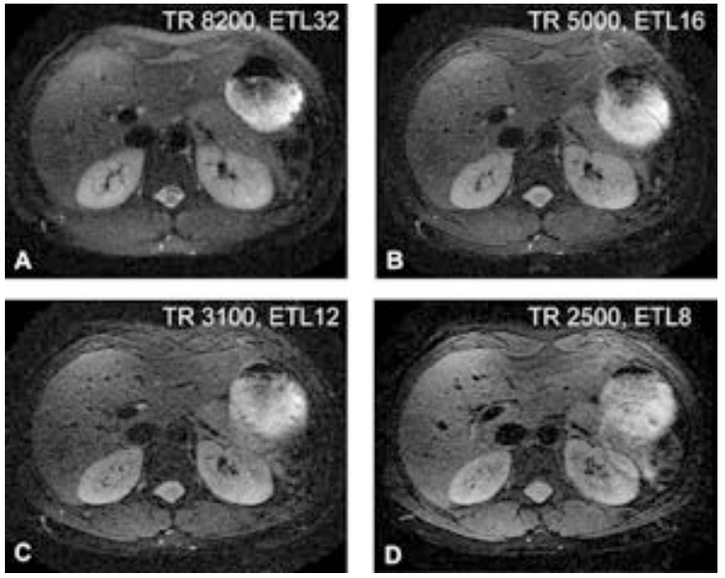

Figure 4: Variation in repetition time (TR) and echo train length (ETL) for VERSE sequences, with fixed bandwidth (BW) of 62.5 KHz and TE=80 msec. Note that in image (a), more blurring and more inhomogeneous fat-suppression is noted compared to the other images.

VERSE compared to standard-RF pulses

The image quality of the VERSE-RF sequence with optimal coverage (TR=5000msec, ETL=16, and BW=62.5KHz) was compared to the sequence obtained with standard-RF pulses, illustrating comparable subjective image quality, and better suppression of the blood signal on images obtained with VERSE-RF ($p=0.008$) (Table 2, Fig. 5).

Quantitative measurements

VERSE-RF pulses

The mean SNR of liver was significantly higher close to the anterior section of the cardiac array coil, when compared to mean SNR of central liver parenchyma (Fig. 7) ($p<0.05$). Although SNR varied significantly over the entire liver, the lowest SNR recorded was considered good enough to delineate structures with the selected BW of 62.5 KHz and 3.5 mm slices. SNR increased for images obtained with TR/ETL=2500/8, related to automatic system adjustment of TE, with lowering to 50 msec. For scans obtained with decreasing ETL, significant decrease in mean SI of subcutaneous fat was observed. This confirmed the quantitative measurement data (Fig. 8).

The CNR measurements between liver and spleen decreased with lower TR, providing values of 5.66 / 4.44 / 3.77 / 2.26 for TR 8000 / 5000 / 3100 / 2500, respectively ($p<0.05$). This illustrates that maximum CNR is obtained for measurements with longer TR.

VERSE compared to standard-RF pulses

The SNR and CNR of the VERSE sequence with optimal coverage (TR=5000 msec, ETL=16, and BW=62.5 KHz) was compared to the data obtained in the standard-RF sequence obtained with identical parameters (Fig. 5). This showed a range of slightly decreased signal intensity of VERSE-RF compared to normal RF of 0.8 - 10.5% for liver, spleen, kidney and muscle respectively (Table 3).

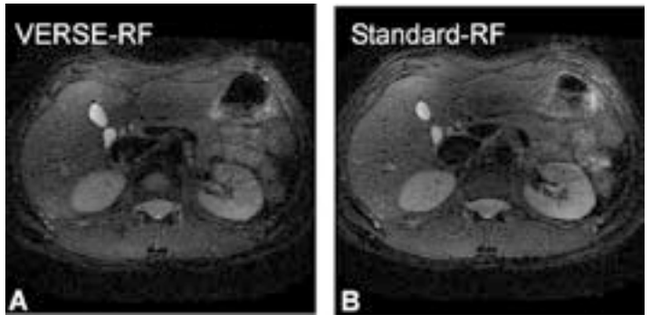

Figure 5: Comparison of image quality in VERSE versus standard-RF, for TR=5000 msec, ETL=16, and BW=62.5 KHz (slice thickness 3.5mm, no interslice gab), illustrating that the visual image quality is comparable.

DISCUSSION

In this study, we evaluated the application of SAR-reduced VERSE-RF pulses as a means for providing increased slice coverage for liver imaging at 3.0T. A FS-T2W-FSE sequence was selected for performance comparison of VERSE-RF and sRF pulses respectively, because of proven benefits of similar sequences for lesion detection at 1.5T.

The most important findings of our study include: 1) fat-suppressed T2-weighted imaging of the liver at 3.0T can be improved and facilitated by the application of VERSE-RF pulses; 2) the use of VERSE-RF pulses provides a 38 – 58% increase in slice coverage for breath-hold fat-suppressed T2-weighted imaging of the liver at 3.0T; 3) the potential for large volume coverage using VERSE permits thin-slice volumetric imaging, showing better suppression of the blood signal, which, in turn, facilitates the detection of smaller liver lesions.

These findings are clinically relevant for a number of reasons. First, imaging restrictions for abdominal imaging at 3.0T associated with higher SAR deposition can be relieved by use of VERSE-RF. SAR scales proportional to square the static magnetic field strength B_0, which implies that sequences using sRF will produce fourfold SAR increase at 3.0T[8]. RF intensive sequences such as breath-hold FS-T2-weighted-FSE scans used had severe limitations at 3.0T in prior software implementations in which SAR levels dramatically limited the amount of refocusing pulses per unit time[8,12]. This provided poor slice coverage performance per breath-hold that translated into prolonged scan durations for full anatomic liver coverage.

Secondly, state-of-the-art MR imaging protocols typically include FS-T2-weighted-FSE sequences, which many centers consider as an essential part of

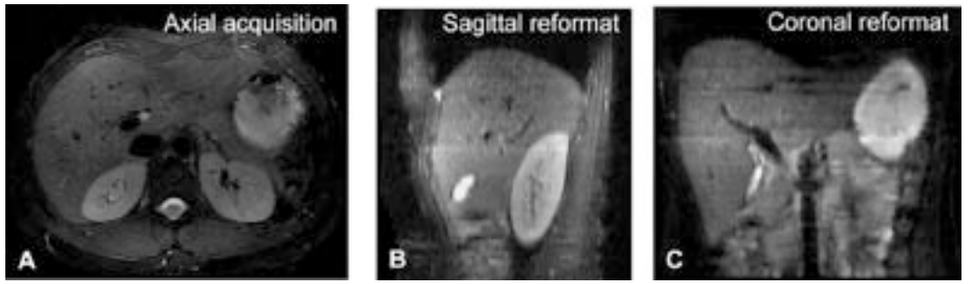

Figure 6: Multiplanar reformatting capabilities for volumetric fat-suppressed T2-weighted FSE with VERSE (TR=5000 msec, ETL=12, BW=62.5 KHz). (a) Axial image acquired with slice thickness 3.5mm, allowing for multiplanar reformatting capabilities; (b) sagittal reconstruction and (c) coronal reconstruction. Note the clear and homogeneous suppression of the blood signal.

Table 2

	VERSE-RF	**standard-RF**
Overall image quality	4.0 (3.0-5.0)	3.7 (3.0-4.0)
Liver delineation	4.0 (3.0-5.0)	3.6 (3.0-4.0)
Tissue blurring	3.7 (3.0-4.0)	3.4 (3.0-4.0)
Suppression fat signal	3.9 (3.0-4.0)	3.7 (3.0-4.0)
Suppression blood signal	4.0 (4.0-4.0)	3.4 (3.0-4.0)

Comparison of qualitative image quality for VERSE-RF compared to standard-RF, for TR=5000 msec, ETL=16, and BW=62.5 KHz (slice thickness 3.5mm, no interslice gab), using a 1-5 scale

Table 3

	VERSE-RF	standard-RF	percentage decrease SNR in VERSE-RF (%)
SNR liver	5.04	5.57	10.5
SNR spleen	7.03	7.14	1.16
SNR kidney	8.33	8.85	6.21
SNR muscle	5.74	5.78	0.79

Table 3: Comparison of SNR, for VERSE-RF compared to standard-RF, for TR=5000 msec, ETL=16, and BW=62.5 KHz (slice thickness 3.5mm, no interslice gab).

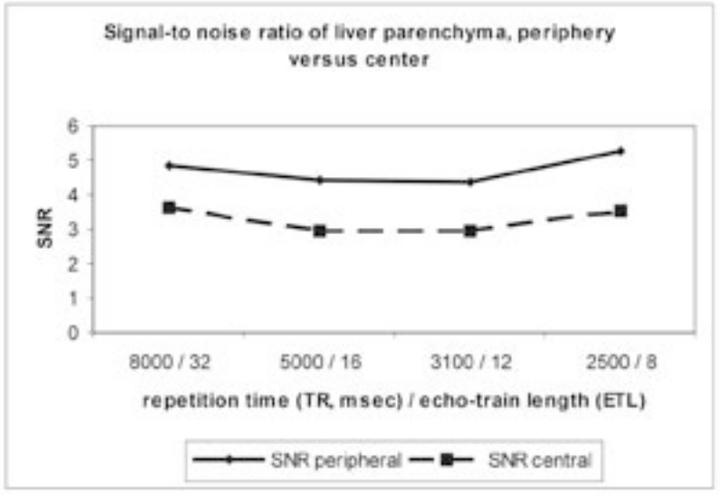

Figure 7: Signal-to-noise ratio (SNR) of the liver close to the anterior coils of the receiving coil (liver periphery) compared to SNR of the central part of the liver, showing a statistically significant difference ($p<0.05$).

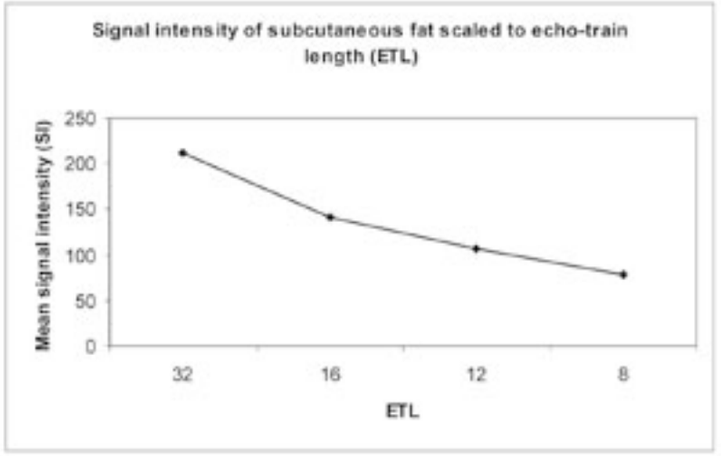

Figure 8: Mean signal intensity of subcutaneous fat, plotted versus echo-train length (ETL), showing a significant decrease in signal intensity.

MRI protocol for detection and characterization of focal liver lesions[2]. The translation of already optimized protocols at 1.5T to the 3.0T domain with equal or improved performance was important and proved challenging in our experience. The results of this study indicate that FS-T2-weighted-FSE obtained with VERSE-RF can provide a good alternative for T2-weighted imaging at 3.0T. The combination of parallel imaging, partial-Fourier, VERSE-RF and higher SNR proved a natural choice to overcome imaging restrictions at 3.0T, including limitations imposed by a short breath-hold period; the necessity to lengthen TR to improve slice coverage; and increased SAR levels. Without partial Fourier and parallel imaging combined, the 25 sec breath-hold scan would be a scan of approximately 1 min 15 sec (for all TR/ETL/BW combinations). In this study we did not evaluate (nor noted particularly in our comparisons) if the increased number of RF excitations per unit time possible with VERSE-RF would change contrast significantly (e.g. spleen-to-liver contrast) in comparison to sRF from magnetization transfer contrast (MTC) effects. In essence, if MTC effects are related directly to SAR levels and not the number of RF pulses played, measurements performed with both RF excitation pulses only differed in number of slices acquired and not in SAR levels recorded for the same settings. Therefore, we assume that MTC effects are similar.

Third, it is well recognized that fat-suppression is difficult using FSE readout modules because of j-coupling effects that enhance fat signal. This effect is more noticeable with larger ETL values (e.g., as observed in long TE, plain or fat suppressed single shot FSE scans). It is well documented that elimination of fat provides an increased dynamic range for effective lesions detection. Also, fat-suppression helps to reduce anterior-posterior ghosting when patients are not able breath-hold adequately, arising from high fat signal due to its proximity to the coil placed over chest and upper abdomen. Another advantage of fat-suppression is improved SNR and resolution, by optimizing signal reception gain and elimination of quantification errors at the edges of k-space. In our study, fat-suppression improved for lower ETL selections, since lowering the number of RF refocusing pulses reduces j-coupling effects. Likewise, shorter ETL, specifically with larger BW readouts, reduces the module duration which promotes a more frequent fat-suppression pulse application with further reduction in fat signal.

Fourth, the larger volume coverage that is possible using VERSE-RF can be used for thin-slice volumetric liver imaging at 3.0T. The acquisition of thin slices results in better suppression of blood signal, facilitating detection of smaller liver lesions. Alternatively, the slice thickness can be increased to further improve anatomic coverage and SNR.

Our study has a number of limitations. The most important limitation is the use of only volunteers as test subjects, without inclusion of patients with focal liver disease. However, to address slice efficiency for VERSE RF pulses in FSE scans, in our opinion, evaluating a group of healthy volunteers would sufficiently answer our research question. Additionally, the selection of sequence parameters was wide, but limited and based on assumptions made from our own experiences as well as based on current literature. Our decision to aim at varying TR and ETL rather than varying TE was based on the fact that the T2 relaxation time of tissues at 3.0T are similar to 1.5T but T1 relaxation times are prolonged and longer TR (in conjunction with partial Fourier and parallel imaging) can be effectively prescribed to compensate. Also, longer TR requires larger ETL values (or, alternatively, reduced matrix size) in order to keep the breath-hold limited to 25 seconds.

To our knowledge, none of previous reports have described the potential of VERSE-RF to increase slice coverage for SAR-intensive MR imaging sequences. In some review articles, the limitations of T2-weighted imaging at 3.0T have been discussed, including decreased T2 signal differences between tissues[8-10] and prolonged scan times related to SAR limits[7]. More recently, Busse and colleagues have described a technique to generate a sequence of reduced and varying refocusing flip angles that can provide a lower SAR. In this set-up, SNR is maintained at but T2 contrast is managed differently through the use of T2-magnetization preparation schemes[22]. Several other studies have compared imaging findings for abdominal diseases at 1.5T and 3.0T[23-25]. These reports conclude that imaging at 3.0T is feasible and promising, although some problems related to signal homogeneity, artifacts and SNR optimization remain to be solved. The present study shows that improvements can be made for liver imaging at 3.0T, making use of imaging potential at higher magnetic field strength and providing solutions for known restrictions. Currently, the described optimized FS-T2-weighted-FSE VERSE-RF sequence is being evaluated at 3.0T, in patients with liver disease.

In conclusion, the results of our study indicate that VERSE-RF can be applied for thin-slice breath-hold fat-suppressed T2-weighted liver imaging at 3.0T, with significantly improved slice coverage compared to sequences obtained with normal RF pulses. These preliminary findings are important for all centers that have the intention to apply 3.0T MR systems for body imaging.

REFERENCES

1. Hussain SM, Semelka RC. Liver masses. Magn Reson Imaging Clin N Am 2005; 13:255-275.
2. Hussain SM, Semelka RC. Hepatic imaging: comparison of modalities. Radiol Clin North Am 2005; 43:929-947, ix.
3. Martin DR, Semelka RC. Health effects of ionising radiation from diagnostic CT. Lancet 2006; 367:1712-1714.
4. Semelka RC, Martin DR, Balci NC. Magnetic resonanceimagingoftheliver:howIdoit.JGastroenterol Hepatol 2006; 21:632-637.
5. Kondo H, Kanematsu M, Itoh K, et al. Does T2-weighted MR imaging improve preoperative detection of malignant hepatic tumors? Observer performance study in 49 surgically proven cases. Magn Reson Imaging 2005; 23:89-95.
6. Hussain SM, De Becker J, Hop WC, Dwarkasing S, Wielopolski PA. Can a single-shot black-blood T2-weighted spin-echo echo-planar imaging sequence with sensitivity encoding replace the respiratory-triggered turbo spin-echo sequence for the liver? An optimization and feasibility study. J Magn Reson Imaging 2005; 21:219-229.
7. Hussain SM, Wielopolski PA, Martin DR. Abdominal Magnetic Resonance Imaging at 3.0 T: Problem or a Promise for the Future? Top Magn Reson Ima-

ging 2005; 16:325-335.
8. Merkle EM, Dale BM, Paulson EK. Abdominal MR Imaging at 3T. Magn Reson Imaging Clin N Am 2006; 14:17-26.
9. MartinDR,FrielHT,DanradR,DeBeckerJ,HussainSM. Approach to abdominal imaging at 1.5 Tesla and optimization at 3 Tesla. Magn Reson Imaging Clin N Am 2005; 13:241-254, v-vi.
10. de Bazelaire CM, Duhamel GD, Rofsky NM, Alsop DC. MR imaging relaxation times of abdominal and pelvic tissues measured in vivo at 3.0 T: preliminary results. Radiology 2004; 230:652-659.
11. Stanisz GJ, Odrobina EE, Pun J, et al. T1, T2 relaxation and magnetization transfer in tissue at 3T. Magn Reson Med 2005; 54:507-512.
12. Schick F. Whole-body MRI at high field: technical limits and clinical potential. Eur Radiol 2005; 15:946-959.
13. Greenman RL, Shirosky JE, Mulkern RV, Rofsky NM. Double inversion black-blood fast spin-echo imaging of the human heart: a comparison between 1.5T and 3.0T. J Magn Reson Imaging 2003; 17:648-655.
14. Nezafat R, Stuber M, Ouwerkerk R, Gharib AM, Desai MY, Pettigrew RI. B1-insensitive T2 preparation for improved coronary magnetic resonance angiography at 3 T. Magn Reson Med 2006; 55:858-864.
15. Conolly S, Glover G, Nishimura D, Macovski A. A reduced power selective adiabatic spin-echo pulse sequence. Magn Reson Med 1991; 18:28-38.
16. Hargreaves BA, Cunningham CH, Nishimura DG, Conolly SM. Variable-rate selective excitation for rapid MRI sequences. Magn Reson Med 2004; 52:590-597.
17. Shen J, Chen Z, Yang J. New FOCI pulses with reduced radiofrequency power requirements. J Magn Reson Imaging 2004; 20:531-537.
18. Busse RF. Reducing SAR in real-time SSFSE imaging with variable-flip hard refocusing RF pulses. Proceedings of the 9th Annual Meeting of ISMRM, Glasgow, Scotland 2001:1790.
19. Busse RF, Li X. Body imaging at 3T: lower SAR yields improved coverage with VERSE and modulated angle refocusing trains. Proceedings of the 11th Annual Meeting of ISMRM, Toronto, Canada 2003; 2003:206.
20. Rosenfeld D, Panfil SL, Zur Y. Design of selective adiabatic inversion pulses using the adiabatic condition. J Magn Reson 1997; 129:115-124.
21. Brix G, Seebass M, Hellwig G, Griebel J. Estimation of heat transfer and temperature rise in partial-body regions during MR procedures: an analytical approach with respect to safety considerations. Magn Reson Imaging 2002; 20:65-76.
22. Busse RF, Hariharan H, Vu A, Brittain JH. Fast spin echo sequences with very long echo trains: de sign of variable refocusing flip angle schedules and generation of clinical T2 contrast. Magn Reson Med 2006; 55:1030-1037.
23. Edelman RR, Salanitri G, Brand R, et al. Magnetic resonance imaging of the pancreas at 3.0 tesla: qualitative and quantitative comparison with 1.5 tesla. Invest Radiol 2006; 41:175-180.
24. O'Regan DP, Fitzgerald J, Allsop J, et al. A comparison of MR cholangiopancreatography at 1.5 and 3.0 Tesla. Br J Radiol 2005; 78:894-898.
25. Chang JM, Lee JM, Lee MW, et al. Superparamagnetic iron oxide-enhanced liver magnetic resonance imaging: comparison of 1.5 T and 3.0 T imaging for detection of focal malignant liver lesions. Invest Radiol 2006; 41:168-174.

chapter5.2
diffusion-induced black-blood echo-planar imaging (BBEPI)

Liver imaging at 3.0T: diffusion-induced black-blood echo-planar imaging (BBEPI) WITH LARGE ANATOMIC VOLUMETRIC COVERAGE

as an alternative for specific absorption rate (SAR) - intensive echo-train spin-echo sequences

ABSTRACT

We evaluated breath-hold diffusion-induced black-blood echo-planar-imaging (BBEPI) as potential alternative for SAR-intensive spin-echo sequences, in particular the fast spin-echo (FSE) sequences, at 3.0T. Fourteen healthy volunteers (7 male, 7 female; mean age 32.6 years (range +/- 6.8 years)) were imaged after institutional review board approval and informed consent were obtained. Imaging parameters were adjusted to obtain isotropic liver coverage in one breath-hold (max 25 seconds). BBEPI with short and long TE (25 and 80 msec respectively) were evaluated and compared to breath-hold fat-suppressed T2-weighted fast spin-echo (FS-T2-weighted-FSE) by two radiologists in consensus, providing: 1) comparable diagnostic image quality, including liver delineation, blurring and geometric distorsions; 2) improved suppression of fat- and blood-signal and 3) higher CNR and SNR. In 6 of 14 volunteers, the images were obtained both on 1.5T and 3.0T, showing higher SNR and CNR for BBEPI on 3.0T. In conclusion, BBEPI can be used for ultrafast, low SAR, thin-slice morphologic imaging of the entire liver in a single breath-hold at 3.0T.

Indra C. van den Bos, MD[1], Shahid M. Hussain, MD, PhD[1,2], Gabriel P. Krestin, MD, PhD[1], Piotr A. Wielopolski, PhD[1]

Departments of [1]Radiology, Erasmus MC, University Medical Center Rotterdam, The Netherlands; [2]Department of Radiology, University of Nebraska Medical Center, Omaha, NE, USA

Submitted

INTRODUCTION

Magnetic resonance (MR) imaging is considered to be an imaging modality with high accuracy for diagnostic work-up of patients with suspected or proven focal liver lesions[1]. Typically, the routine MR imaging protocol for diagnostic work-up of liver diseases consists of T1-weighted gradient-echo (GRE) sequences before- and after injection of gadolinium; and various echo-train fast spin-echo (FSE) sequences, with- and without fat-suppression. Particularly, multi-shot echo-train FSE sequences are important for lesion detection[2,3].

Currently, the transition of imaging protocols from 1.5T to 3.0T is being evaluated by several authors[4-8]. The introduction of 3.0T MR imaging systems and coil development with capability of parallel imaging has shown to be promising for improved hepatobiliary imaging[5,9]. The combination of higher signal-to-noise ratio (SNR) compared to 1.5T (theoretically 2x higher), high performance gradient-systems and advanced software platforms allow a number of potential advantages[4]. Consequently, 3.0T systems can deliver $\sqrt{2}$ improved spatial resolution, ½ slice thickness with identical coverage; or 4-fold speed up in scanning time for identical resolution settings[9]. Nonetheless, the 4-fold higher specific absorption rate (SAR) as compared to 1.5T, T1-lengthening and slight shortening of T2-relaxation times necessitate a revision of the imaging parameters for optimal imaging sequences, to provide better image quality and performance at 3.0T. In addition, the theoretically doubled SNR on 3.0T is usually lowered by a combination of several factors, including B_1 inhomogeneities, lengthening of T1-relaxation times and higher readout bandwidths[10,11]. These factors limit the introduction of routine clinical imaging of the abdomen on 3.0T.

T1-weighted GRE sequences at 3.0T have taken full advantage of increased SNR, translating into fat-suppressed thin-section three-dimensional imaging with high in-plane resolution and good imaging quality[9]. However, T2-weighted FSE sequences at 3.0T are challenging for several reasons. First, fourfold higher energy (higher B_1) radio-frequency (RF) pulses are needed for proton excitation, which result in increased RF heating and SAR levels[12]. Higher SAR values limit the efficiency for all sequences based on FSE-readouts and steady-state free precession, resulting in lower number of slices per TR. This diminishes anatomic coverage and necessitates multiple breath-hold periods for anatomic liver coverage, with considerably longer exam times at 3.0T to obtain comparable diagnostic information as routinely acquired at 1.5T. Second, B_1-field inhomogeneities and dielectric resonances are more pronounced at higher field strength, resulting in intensity modulations (focal shading or local decrease in signal intensity). Implementation of alternative T2-weighted sequences with lower RF energy deposition and less B_1-inhomogeneities may circumvent many of these issues. One of these sequences may be based on echo-planar imaging (EPI).

EPI has been evaluated as potential ultrafast imaging method for evaluation of abdominal diseases[13,4], and can be applied for both morphologic imaging and more functional-oriented imaging, including apparent-diffusion coefficient (ADC) mapping[13-15]. It has been advocated as promising imaging sequence at 1.5T[13,16], because it is fast, provides consistent image quality and provides higher contrast-to-noise ratio (CNR) for lesions[14,17].

To our knowledge, none of the previous studies have reported the implementation of a diffusion-induced, black-blood echo-planar imaging at 3.0T with thin-sections for volumetric coverage of the entire liver within a single breath-hold.

The purpose of this paper was to evaluate breath-hold diffusion-weighted black-blood echo-planar-imaging (BBEPI) with short and long echo time as potential alternative for specific absorption rate (SAR) intensive echo-train spin-echo sequences for liver imaging at 3.0T.

MATERIALS AND METHODS

Subjects and imaging systems

Fourteen healthy volunteers with no previous history of liver problems nor recent heavy alcohol consumption (7 male, 7 female; mean age 32.6 years (+/- 6.8 years)) were imaged on a General Electric 3.0T MRI (General Electric Healthcare, Signa Eclipse, Milwaukee, Wisconsin, USA), using the whole-body coil for RF excitation, and an 8-channel phased-array cardiac coil for signal reception. The system was equipped with high performance gradients (40 mT/m, 266 msec rise time to peak maximum) and the option of using parallel imaging (ASSET, array spatial sensitivity encoding technique) with a maximum acceleration factor of 2.00 for two-dimensional (2D) imaging. A subset of 6 volunteers was imaged at a General Electric 1.5T MRI (General Electric Healthcare, Signa CV/i, Milwaukee, Wisconsin, USA) unit for signal-to-noise (SNR) and contrast-to-noise ratio (CNR) comparisons using identical gradient hardware specifications and identical imaging parameters. Informed consent was signed by all participants after a brief interview to check for contraindications and explanation of the procedure. The study followed approval by the institutional review board, as part of an ongoing sequence optimization project.

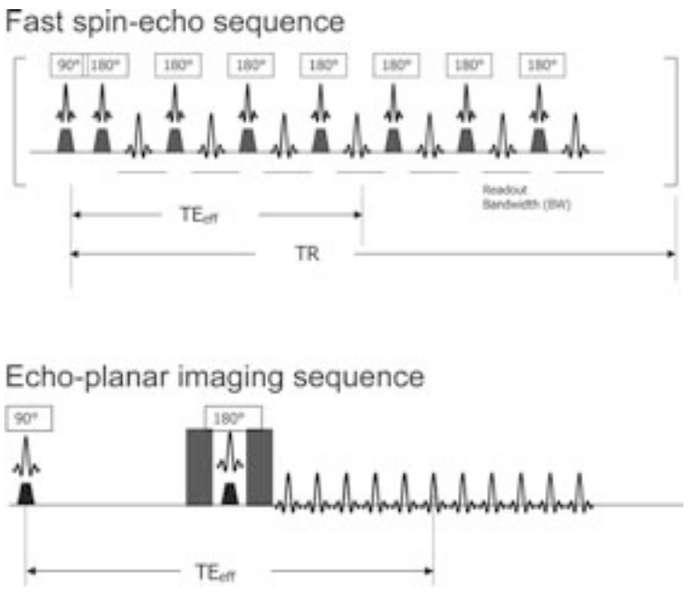

Figure 1: Schematic presentation of fast spin-echo (FSE) and echo-planar imaging (EPI) sequences, illustrating multiple 180° pulses after the initial 90° degree pulse in FSE module, while in EPI, there is only one single 180° pulses after the initial 90° degree pulse. This results in decreased magnetic-transfer contrast effects, facilitating the detection of focal liver lesions.

MR imaging sequence

Diffusion-induced black-blood echo-planar imaging (BBEPI) (Fig. 1) providing a trace diffusion-induced image (addition of three independent scans with diffusion sensitizing gradients in x, y and z, respectively) was chosen for volumetric liver imaging. The sequence was selected from an existing pulse sequence program on the system: pulse sequence family EPI, DW-EPI, 2D imaging mode. A 25-second breath-hold at end-expiration was considered for evaluation. The following imaging parameters were varied interactively to obtain full liver coverage in an optimization setting: slice thickness (2, 3 and 4 mm), ASSET acceleration factor (none, 2) and diffusion b-value (10, 20, 40, 50, 100, 250 and 500 s/mm^2). Matrix size was set to 160x192 (frequency and phase-encoding directions); field of view (FOV) 520 x 260 cm^2, rectangular FOV of 50% and number of excitations (NEX) of one. The resulting voxel size was 3.00x2.70x(1.60-4.00)mm^3. A standard fat-suppression pulse was used. Repetition time (TR) was kept constant at 6300msec. Echo time (TE) was internally adjusted by the sequence program, but could be varied using an "optimize TE" setting (resulting in TE variation of 20-35msec, depending on b-value setting). For low-TE setting (< 35msec), full liver coverage with 2.0-mm slice thickness was obtained. The high-TE setting (80msec) slice thickness of 4.0-mm was chosen to obtain identical coverage, since this resulted in 40% reduced slice coverage. To evaluate the extent of geometrical distortions and signal loss around air-tissue interface regions (e.g., vascular structures), three matrix sizes were collected: 64 x 192, 160 x 192 and 192x192. The optimized sequences were prescribed with parameters as described in Table 1.

Table 1

	short-TE-BBEPI	long-TE-BBEPI	FS-T2-weighted-FSE
Slice thickness	2.0 mm	4.0 mm	3.5 mm
Matrix size	160 x 192	160 x 192	320 x 288
Field-of-view	520 x 260 cm^2	520 x 260 cm^2	400 x 300 cm^2
Voxel size	3.1 x 2.6 x 2.0 mm^3	3.1 x 2.6 x 4.0 mm^3	1.25 x 1.0 x 3.5 mm^3
Echo time (TE)	25 msec	80 msec	80 msec
Repetition time (TR)	6300 msec	6300 msec	5000 msec
b-value (x, y, z)	10 s/mm^2	10 s/mm^2	-
Number of excitations (NEX)	1	1	1/2
Acceleration factor (ASSET)	2.00	2.00	2.00

Selected optimized parameters for short-TE diffusion-induced black-blood echo-planar imaging (BBEPI), long-TE-BBEPI, and fat-suppressed T2-weighted fast spin-echo (FS-T2-weighted-FSE); with the objective to reach full anatomic liver coverage (25-cm max) within one breath-hold period (25 sec).

Fat-suppressed T2-weighted fast spin-echo (FS-T2-weighted-FSE) (Fig. 1) was performed in a 25-second breath-hold period, using the following parameters: TR 5000msec, TE 80msec, echo-train-length (ETL) 12, read-out bandwidth 62.5 KHz, imaging matrix 320x288, field of view (FOV) 320-400 x 240-300cm2 (to fit the anatomy); rectangular FOV of 75%; frequency direction left-to-right; standard fat suppression pulse; partial Fourier (1/2 NEX); and acceleration factor (ASSET) 2.00, resulting in a final voxel size of 1.0-1.25x0.83-1.0x3.5mm^3.

Image analysis

Image quality was assessed both qualitatively (subjectively) and quantitatively on the optimized short-TE- and long-TE-BBEPI sequences. For the qualitative assessment, the following items were evaluated by two authors in consensus (IB, SH; 3 and 11 years experience in interpretation of abdominal MR respectively): 1) overall image quality; 2) delineation of the liver (e.g. how well the liver can be distinguished from the surrounding tissues); 3) tissue blurring; 4) fat-suppression homogeneity; 5) suppression of the blood signal inside the hepatic vessels; and 6) geometric distortion at air-tissue interfaces, using the FSE sequence as the reference standard. These items were rated using a 1–5 scale (1=unacceptable, 2=poor, 3=fair, 4=good and 5=excellent). For quantitative measurements, operator-defined regions-of-interest (ROI) of approximately 100 mm2 were placed in liver and spleen for measurement of mean signal intensity (SI), all performed by one of the authors (IB). Care was taken to exclude vessels or biliary structures. For analysis of the liver-to-spleen CNR (which can be used for an indication for liver-to-lesion contrast), ROI measurements were performed in both spleen and liver at approximately 5 cm from the posterior coil array. The SI was normalized to the standard deviation (SD) of background noise of the liver SI sample, and expressed as SNR. CNR was calculated as difference in SI between lesion and liver scaled to SD of background noise.

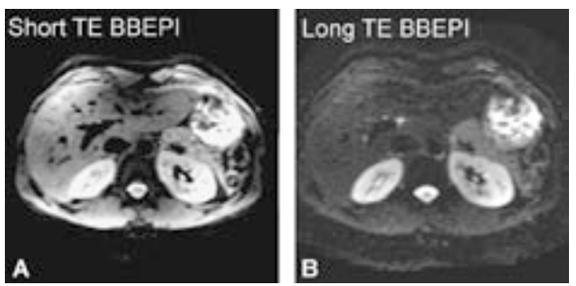

Figure 2: Optimal BBEPI settings in a healthy volunteer (a) Axial short-echotime black-blood EPI scan (short-TE-BBEPI) (TE=25 msec, TR=6300 msec and b=10 s/mm2); (b) Axial long-echotime black-blood EPI scan (long-TE-BBEPI) (TE=80 msec, TR=6300 msec and b=10 s/mm2).

Statistical analysis

Statistical parameters (mean, median, standard deviation, and range) were calculated using the Statistical Package for Social Sciences (SPSS, version 12.0.1) program. Significance levels of the data obtained in the qualitative and quantitative assessements were determined by a non-parametric Wilcoxon's signed rank test analysis. A p-value of less than 0.05 was considered the limit for statistical significance.

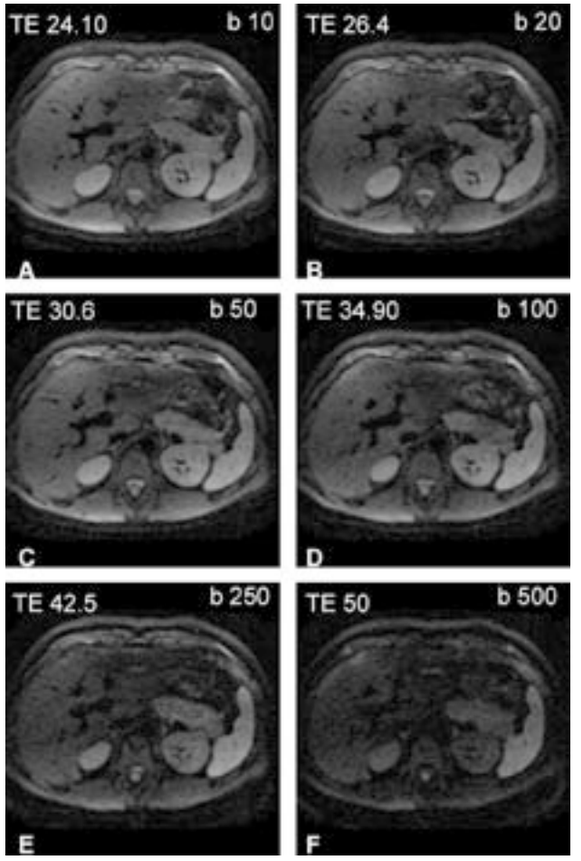

Figure 3: Variation in diffusion factor (b-factor) for short-TE-BBEPI in the same volunteer (TR=6300 msec). (a) b=10 s/mm^2, TE=24.1 msec; (b) b=20 s/mm^2, TE=26.4 msec; (c) b=50 s/mm^2, TE=30.6 msec; (d) b=100 s/mm^2, TE=34 msec; (e) b=250 s/mm^2, TE=42 msec; (f) b=500 s/mm^2, TE=50 msec. SNR decreases with increasing b-factor as a result of resulting longer TE necessary to accommodate the requested b-factor value. With increasing b-value, signal dephasing in regions with motion is more prominent, mainly from bowel motion and cardiac pulsation.

RESULTS

The optimized short-TE- and long-TE-BBEPI provided 1) comparable image quality, liver delineation and blurring; 2) improved suppression of fat- and blood-signal and 3) higher CNR and SNR compared to FS-T2-weighted-FSE. Geometrical distortions in BBEPI were acceptable. Comparison of the data for BBEPI on 1.5T versus 3.0T showed comparable, or even improved SNR and CNR for both short-TE and long-TE-BBEPI. The results are described in more detail below.

Sequence and parameter optimization

The selected short-TE- and long-TE-BBEPI sequences (Fig. 2) were optimized for maximum slice coverage, resulting in imaging parameters as provided in Table 1. The optimization process involved the following steps:

1) Slice coverage: within the set 25 second breath-hold, complete anatomic thin-slice liver coverage was possible using short-TE-BBEPI (2 mm slices). Slice thickness was doubled (4 mm) for long-TE-BBPEPI to increase SNR and to keep total liver coverage similar to short-TE-BBEPI, because the selection of longer TE resulted in an approximate 40% reduced slice coverage.

2) b-value: slice efficiency and image quality (sensitivity to bulk motion) were dependent on the selected b-value (Fig 3). Increased b-values resulted in lower slice efficiency, but with more consistent blood suppression, especially in the region of the inferior caval vein. Higher b-values increased the sensitivity to bulk motion, demonstrating better suppression of slow-flowing blood but with appearance of darker

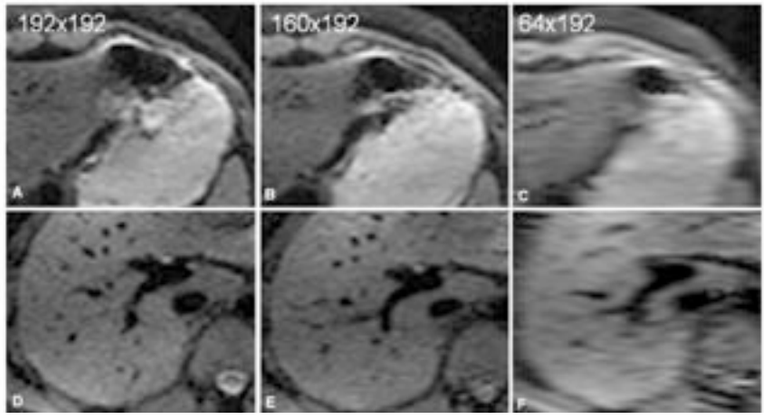

Figure 4: Effect of matrix size in signal loss, geometrical distortions and resolution: short-TE-BBEPI (TE=25 msec, TR=6300 msec and b=10 s/mm2). (a) matrix size of 192 x 192; (b) 160 x 192 and (c) 64x192, using 2 mm slice thickness. On the upper row the effect of decreasing frequency points (left-right direction) is shown, illustrating increased geometrical distortions and signal loss in regions of increased magnetic susceptibility for higher frequency encoding points (a and d), with approximately a three-fold inter-echo spacing as compared to (c and f).

regions around the heart and bowel, especially with thin imaging sections (2.0 mm). Because SNR and CNR between liver and vascular structures decreased with longer TE, a b=10 s/mm^2 was taken as optimal, even though some remnant blood signal was sometimes observed in peripheral intrahepatic veins when thicker slices were selected.

3) Matrix size: variations in the number of frequency encoding points used demonstrated increased geometrical distortions for higher frequency encoding points, as well as increased signal loss (Fig. 4). As previous experience demonstrated optimal image quality for measurements with fewer frequency points than phase-encoding steps[14], the optimal imaging matrix was set to 160x192.

Table 2

	short-TE-BBEPI	long-TE-BBEPI	FS-T2-weighted-FSE
Overall image quality	3.6 (3 - 4)	3.2 (3 – 4)	3.7 (3 – 4)
Liver delineation	3.9 (3 – 4)	3.0 (3 – 3	3.6 (3 – 4)
Tissue blurring	3.2 (3 – 4)	3.0 (3 – 3)	3.4 (3 – 4)
Suppression fat signal	4.4 (4 – 5)	4.2 (4 - 5)	3.7 (3 - 4)
Suppression blood signal	4.9 (4 – 5)	4.4 (3 – 5)	3.4 (3 – 4)
Geometrical distorsions	3.4 (3 - 4)	3.2 (3 - 4)	5.0 (5 - 5)

Qualitative analysis of short-TE diffusion-induced black-blood echo-planar imaging (BBEPI), long-TE-BBEPI and fat-suppressed T2-weighted fast spin-echo (FS-T2-weighted-FSE) (rated using a 1–5 scale (1=unacceptable, 2=poor, 3=fair, 4=good and 5=excellent)).

Image quality

Qualitative assessment

The subjective analysis was performed for the two optimized EPI sequences (short-TE- and long-TE-BBEPI) and FS-T2-weighted-FSE (Table 2).

Overall image quality was 3.6 (range 3-4) in short-TE-BBEPI, 3.2 (range 3-4) in long-TE-BBEPI and 3.7 (3-4) in FS-T2-weighted-FSE. These results were not significantly different, showing that image quality in BBEPI is comparable to FSE sequences.

The delineation of the liver was assessed as 3.9 (range 3-4) in short-TE-BBEPI, 3.0 (range 3-3) in long-TE-BBEPI and 3.6 (range 3-4) in FS-T2-weighted-FSE. This was not significantly different, showing comparable delineation for the optimized BBEPI sequence compared to the FSE sequence. Blurring was assessed as 3.2 (range 3-4) in short-TE-BBEPI, 3.0 (range 3-3) in long-TE-BBEPI and 3.4 (range 3-4) in FS-T2-weighted-FSE. Although there was slightly increased blurring in the BBEPI sequences, this was not significantly different.

Table 3

	short-TE-BBEPI	long-TE-BBEPI	FS-T2-weighted-FSE
SNR liver	11.5 (5.2 – 19.8)	4.04 (2 – 8.4)	5.6 (4 – 6.7)
SNR spleen	13.8 (8.7 - 25.6)	11.4 (8.8 – 18)	9.9 (6 – 16.7)
CNR liver-spleen	7.8 (1.1 – 12)	15 (10.9 – 24.2)	4.8 (2.2 – 9.6)

Qualitative analysis of signal-to-noise ratios (SNR) for liver and spleen on 3.0T, and contrast-to-noise ratio (CNR) for short-TE diffusion-induced black-blood echo-planar imaging (BBEPI), long-TE-BBEPI and fat-suppressed T2-weighted fast spin-echo (FS-T2-weighted-FSE), illustrating that CNR is always lowest in FS-T2-weighted-FSE, compared to the BBEPI sequences (p=0.03 compared to long-TE-BBEPI and p=0.06 for short-TE-BBEPI). CNR is highest in long-TE-BBEPI (15, compared to 7.8 and 4.8 in short-TE-BBEPI and FS-T2-weighted-FSE) (p<0.05). SNR was highest in short-TE-BBEPI for both liver and spleen (p<0.05). Values represent means (range).

Table 4

short-TE-BBEPI	3.0T 2 mm	1.5T 2 mm	1.5T 4 mm
SNR liver	11.5 (5.2 – 19.8)	5.6 (3.8 – 7.6)	10 (4.3 – 15.2)
SNR spleen	13.8 (8.7 - 25.6)	9.9 (8.1 – 12)	10.6 (9.7 – 12.5)
CNR	7.8 (1.1 – 12)	4.9 (3.1 – 7.4)	7.2 (4.2 – 8.8)

Comparison of SNR on short-TE diffusion-induced black-blood echo-planar imaging (BBEPI),for images acquired at 1.5T versus 3.0T show that different slice thickness acquired at 1.5T results in increasing SNR for thicker slices, but SNR is still lower compared to 3.0T images (see Table 3). Even with double the slice thickness on 1.5T, (4 mm compared to 2 mm at 3.0T), SNR is lower.

The quality of the fat-suppression was assessed as 4.4 (range 4-5) in short-TE-BBEPI, 4.2 (range 3-5) in long-TE-BBEPI and 3.7 (3-4) in FS-T2-weighted-FSE. Fat-suppression was more homogeneous in BBEPI, illustrating improved fat-suppression compared to FSE sequences (p<0.05).

The suppression of the blood signal inside the hepatic vessels was assessed as 4.9 (range 4-5) in short-TE-BBEPI, 4.4 (range 4-5) in long-TE-BBEPI and 3.4 (range 3-4) in FS-T2-weighted-FSE (p<0.05). This shows improved suppression of the signal resulting from inflowing blood in sequences obtained with BBEPI.

The extent of geometric distortions at air-tissue interfaces was assessed as 3.4 (3-4) in short-TE-BBEPI, 3.2 (3-4) in long-TE-BBEPI and 5 (5-5) in FS-T2-weighted-FSE. This shows that geometric distortions are significantly lower in FSE (p<0.05), but the extent of distortions is acceptable for BBEPI (mean score of 3 means fair image quality) (Fig. 5).

Quantitative assessment

For the quantitative assessment, SNR of liver and spleen, and CNR were calculated (Table 3).

These results show that in all cases, SNR and CNR is lowest in FS-T2-weighted-FSE, compared to the BBEPI sequences (p=0.03 compared to long-TE-BBEPI and p=0.06 for short-TE-BBEPI) (Fig. 6, 7). SNR was highest in short-TE-BBEPI for both liver and spleen, statistically significant for liver (p<0.05). (see Fig. 6, 7 for illustrations). CNR was highest in long-TE-BBEPI (15, compared to 7.8 and 4.8 in short-TE-BBEPI and FS-T2-weighted-FSE) (p< 0.05). This shows that BBEPI is likely to be superior to FS-T2-weighted-FSE for lesion detection.

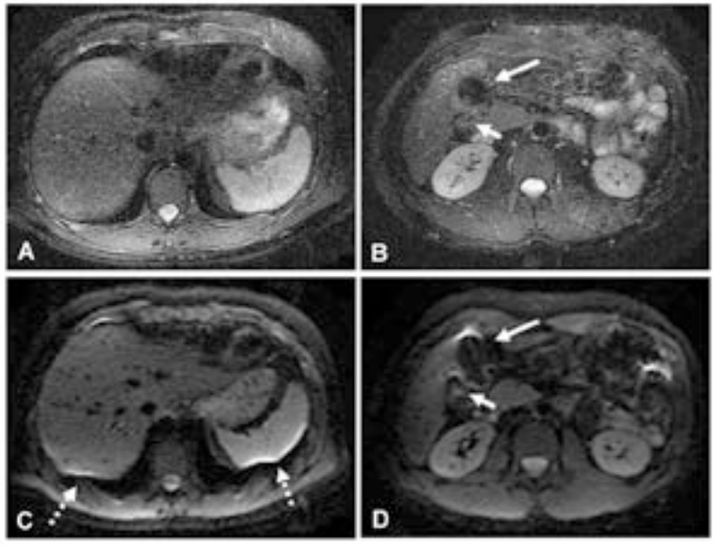

Figure 5: Geometrical distortions comparison between FSE and EPI scans. (a,b) Axial breath-hold 3.5 mm T2-weighted fat-suppressed FSE (TE=80 msec, TR=5000 msec); (c,d) Corresponding axial 2 mm thick section short-TE-BBEPI (TE=25 msec, TR=6300 msec and b=10 s/mm2), showing locations where geometric distortions occur. The solid arrows point at air close to the liver from the small bowel inducing in the short-TE-BBEPI scan geometrical distortions and signal loss. In this particular volunteer, the geometrical distortions close to the liver-lung interface (dotted arrows) were the largest among all volunteers evaluated.

Comparison 3.0T and 1.5T

Overall image quality of BBEPI sequences at 3.0T was improved due to increased SNR compared to 1.5T (Fig. 8). The comparison of SNR at short-TE-BBEPI for images acquired at 1.5T versus 3.0T shows that different slice thickness acquired at 1.5T results in increasing SNR for thicker slices, but SNR is lower compared to 3.0T (Table 4, Fig. 8). When comparing CNR for both

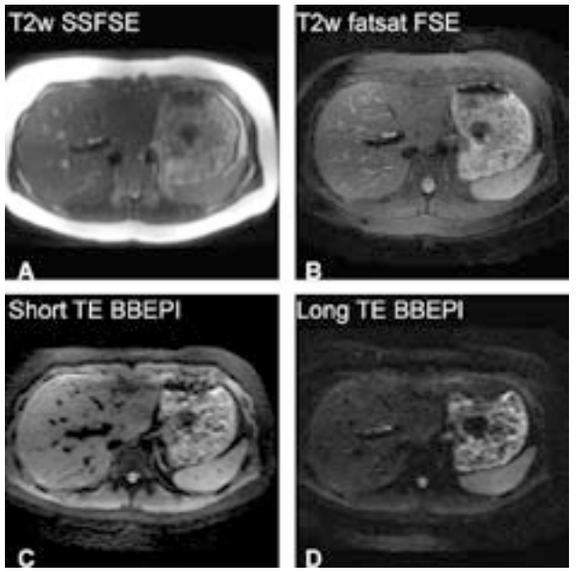

Figure 6: Image quality of FSE and BBEPI sequences in the same volunteer. (a) Breath-hold 3.5 mm thick section T2-weighted single-shot FSE (TE=80 msec, TR=infinity), showing high signal of the subcutaneous fat; (b) Breath-hold 3.5 mm thick section T2-weighted fat-suppressed FSE (TE=80 msec, TR=5000 msec); (c) 2 mm thick section short-TE-BBEPI, showing improved suppression of fat and blood signals ; (d) 4 mm thick section long-TE-BBEPI, showing marked decrease in signal intensity of the liver, but maintained signal of the spleen indicating good CNR.

short-TE-BBEPI and long-TE-BBEPI, values are higher for 3.0T compared to 1.5T imaging, although this did not reach statistical significance (Fig. 9). This suggests that lesion detection on BBEPI at 3.0T will at least be comparable or perhaps even better than at 1.5T.

DISCUSSION

In this study, we evaluated the application of black-blood echo-planar imaging (BBEPI) at 3.0T as an alternative for SAR-intensive T2-weighted echo-train spin-echo sequences. Our results indicate that: 1) thin-section volumetric imaging of the entire liver can be acquired in a single breath-hold, providing good overall image quality, acceptable anatomic distortion and diagnostic SNR and CNR; 2) the optimized BBEPI sequence shows high SNR and CNR on 3.0T compared to 1.5T; 3) near-isotropic data obtained in short-TE-BBEPI allows multi-planar reformats with completely darkened hepatic vessels; 4) our findings favor the implementation of combined short-TE- and long-TE-BBEPI as a part of a comprehensive protocol for routine liver imaging at 3.0T. BBEPI, in combination with other (gadolinium-enhanced) T1- and T2-weighted sequences, may facilitate improved detection and characterization of liver lesions at 3.0T.

The results of our study are clinically relevant for a number of reasons. First, the optimized short-TE- and long-TE-BBEPI sequence provides an alternative for more SAR-intensive FS-T2-weighted-FSE sequences. Routinely, T2-weighted sequences for liver imaging are acquired using FSE sequences, which are RF-intensive due to multiple refocusing RF-pulses (Fig. 1). At 3.0T compared to 1.5T, radio-frequency (RF) pulses with fourfold higher energy (higher B_1) are needed to excite the protons, resulting in more RF heating and a fourfold higher SAR at 3.0T[9,12]. Total anatomic coverage within a single breath-hold diminishes, resulting in several breath-hold sessions to cover the entire liver. Since T2-weighted fat-suppression sequences are essential for diagnostic liver imaging, development of low SAR T2-weighted protocols is important for improvement of liver imaging at higher magnetic field strength, including 3.0T or higher strength, including 7.0T.

Second, BBEPI may provide a solution for increased B_1-inhomogeneity, dielectric resonances and problematic fat-suppression using FS-T2-weighted-FSE sequences on 3.0T. B_1-inhomogeneity results from eddy currents, which act against the applied external RF-pulses. Since RF wavelength is reduced at 3.0T due to higher operational frequency of 128 MHz (compared to 64 MHz at 1.5T), conductivity increases, which results in stronger eddy currents. B_1-inhomogeneities, in combination with the nature of the fat-suppression and refocusing pulses in echo-train spin-echo sequences, may also be responsible for relatively poorer fat-suppression quality. Fat-suppression is essential for diagnostic T2-weighted imaging of the liver, as it is utilized to improve the dynamic range of the acquisition, which translates into an easier reading when bright lesions are found against a darkened surrounding[3,14]. Therefore, improved fat-suppression is important, for which the optimized BBEPI may provide an alternative.

Third, in many centers diffusion-weighted EPI with relatively short TE is routinely applied in the liver to obtain ADC maps that can potentially help to improve differentiation between benign and malignant liver lesions[15]. The results of our study show that such short-TE EPI sequence can also be utilized as black-blood sequence with the application of a low b-value in three orthogonal directions, with an inherent high SNR and CNR for morphologic imaging of the liver[14,18]. BBEPI images collected with good suppression of blood can therefore augment the sensitivity for visualization of smaller liver lesions. Even though current EPI parameters are limited by a relatively low in-plane resolution, the detection of focal liver lesions at MR imaging mainly depends on contrast resolution and less on the in-plane spatial resolution. Therefore, the combination of inherent high contrast resolution, the absence of magnetic transfer contrast (MTC) effects (hence with higher liver-to-lesion contrast than echo-train spin-echo sequences) and dark vessels allow for optimal detection of even very small liver lesions, including high fluid-content lesions such as cysts and hemangiomas, as well as solid liver lesions such as liver metastases.

Finally, the possibility to collect isotropic datasets with black-blood contrast can be of interest for detection of intravascular thrombi in the portal and hepatic veins, as an adjunct to gadolinium-enhanced T1-weighted

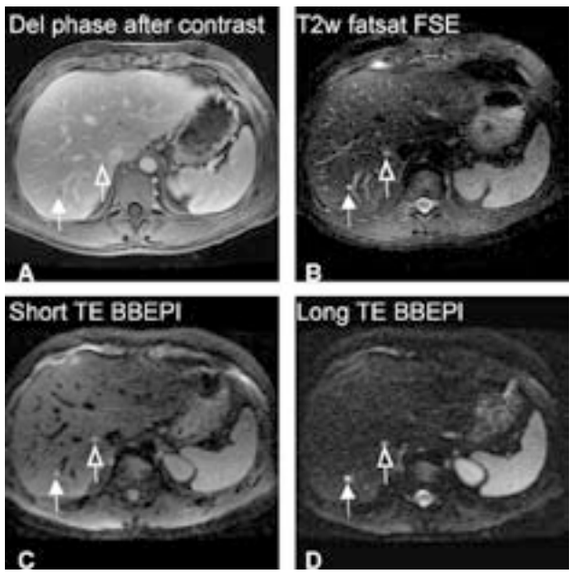

Figure 7: Image quality in a healthy volunteer with small liver hemangioma as an incidental finding. (a) Delayed-phase contrast-enhanced multiphasic 3D fat-suppressed T1-weighted gradient-echo (1.5T) (TE=shortest, TR=shortest), which was performed in a routine follow-up clinical MR imaging after the incidental finding in the sequence optimization study, showing peripheral nodular enhancement, slowly increasing over time (other phases not shown) and filling in towards the center, as is characteristic for hemangioma (arrow and open arrow); (b) 3.0T T2-weighted fat-suppressed fast spin-echo (FSE) (TE=80 msec, TR=5000 msec), showing the two hyperintense lesions (arrows); (c) Axial 3.0T short-TE-BBEPI (TE=25 msec, TR=6300 msec and b=10 s/mm^2), showing improved suppression of the fat- and blood-signal, with improved conspicuity of the two lesions (arrows); (d) Axial 3.0T long-TE-BBEPI (TE=80 msec, TR=6300 msec and b=10 s/mm2), showing marked darkening of the liver, but with high SNR and CNR of the two lesions (arrows).

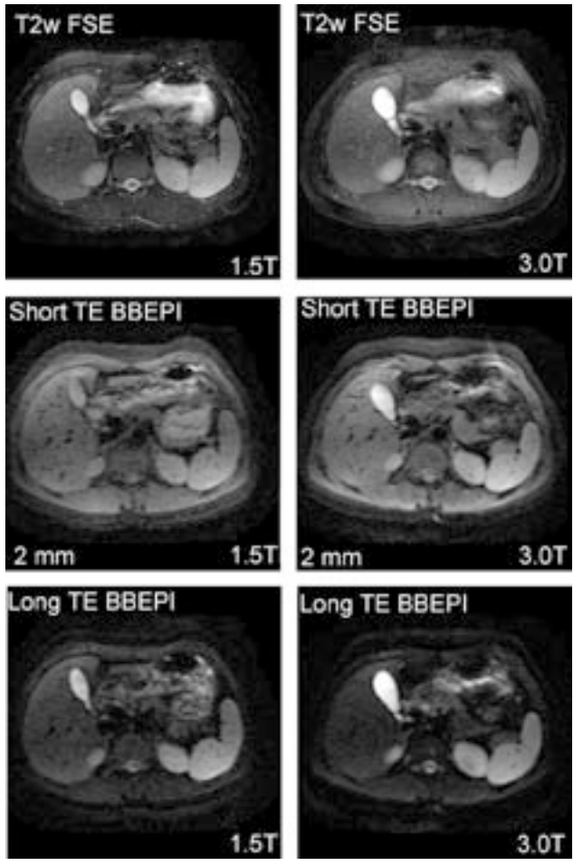

Figure 8: Image quality of FS-T2-weighted-FSE (TE=80 msec, TR=5000 msec), short-TE-BBEPI (TE=25 msec, TR=6300 msec and b=10 s/mm^2)and long-TE-BBEPI (TE=80 msec, TR=6300 msec and b=10 s/mm^2)on 1.5T and 3.0T in the same volunteer as in Fig 7.Note comparable, or even slightly better image quality of 2-mm thick short-TE-BBEPI on 3.0T compared to 1.5T, and comparable image quality of 4-mm thick long-TE-BBEPI on 3.0T compared to 1.5T. The long-TE-BBEPI images show lower signal intensity of the liver parenchyma compared to 1.5T, explaining the higher CNR values on 3.0T.

images, for improved diagnostic confidence. Such findings may potentially have an impact on clinical decision making in patients with known or suspected hepatocellular carcinomas. In addition, patients with suspected or known Budd-Chiari syndrome may benefit from liver MR imaging protocols that include BBEPI sequences. Apart from hepatic imaging, the optimized BBEPI sequence may have potential applications in other anatomic areas as well.

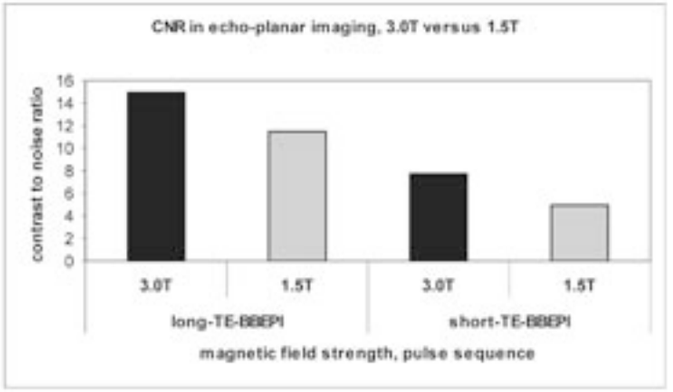

Figure 9: Contrast-to-noise ratio of EPI, on 3.0T versus 1.5T. Note the lower CNR for both long-TE-BBEPI and short-TE-BBEPI.

Our study indicates that the selection of a long-TE-BBEPI improves CNR at the cost of thicker slices, whilst lower TE values provide a lower CNR but higher SNR to provide isotropic voxel imaging (~8mm^3). The combination of these two acquisitions can prove useful for a simplified, highly sensitive liver protocol at higher magnetic field strengths. In this case, the implementation of a dual-echo BBEPI to acquire both contrasts simultaneously would result in a further decrease in total scan duration.

To our knowledge, none of the previous reports have evaluated the application of black-blood echo-planar imaging (BBEPI) at 3.0T as an alternative for SAR-intensive T2-weighted echo-train spin-echo sequences. Previously, other alternatives have been proposed to address problems related to high SAR values associated with T2-weighted FSE sequences, including RF-pulses with reduced flip angle, hyper-echo mechanism, "transition between pseudo–steady-states" (TRAPS) and specialized RF-pulses[19-22]. Hyperechoes are based on a spin refocusing strategy that maintains the benefits of FSE by employing echoes of echoes, preserving SNR as in conventional FSE sequences but with dramatically reduced SAR[19,20]. In TRAPS, high flip-angles are only used for data encoding for the central part of k-space, which results in a considerable reduction in RF power[20]. Specialized RF pulses including variable-rate-selective excitation (VERSE) have been proposed to reduce SAR as well, based on an amplitude-modulated gradient waveform which reshapes the RF excitation to reduce SAR while keeping the same spatial excitation profile[22]. Our study shows that an EPI-based sequence can be optimized on a clinical 3.0T system without additional requirements, which provides thin-slice volumetric anatomic coverage of the entire liver within a single breath-hold; better fat-suppression; lower SAR with increased coverage in the z-axis; higher SNR and low MTC effects. Our study is limitated by the fact that only volunteers were used as test subjects and that no patients were included. The aim of this study however, was merely to evaluate the potential of BBEPI for morphologic imaging at 3.0T, to evaluate image quality including fat-suppression and anatomic coverage compared to fat-suppressed T2-weighted FSE sequences, for which, in our opinion, evaluating a group of healthy volunteers would sufficiently answer our research question. Also, the comparison between 1.5T and 3.0T was limited to a few volunteers only, using a cardiac-array coil for reception with slightly different sizes, which may have influenced the outcome. However, this was merely included to illustrate the capacity of BBEPI to provide comparable image quality on 3.0T. Currently, the described optimized BBEPI sequence is being evaluated in patients with liver disease.

Figure 10: Multiplanar reformatting capability in short-TE-BBEPI. (a) Axial short-TE-BBEPI. (b) Coronal reconstruction, using the minimum-intensity projection module (14 mm thick slices). Note the excellent suppression of the blood signal. (c) Reconstruction in the sagittal plane (14 mm thick slices).

In conclusion, the results of our study indicate that 1) thin-section volumetric imaging of the entire liver can be acquired in a single breath-hold, providing good overall image quality, acceptable anatomic distortion and diagnostic SNR and CNR; 2) the optimized BBEPI sequence shows high SNR and CNR on 3.0T compared to 1.5T; 3) near-isotropic data obtained in short-TE-BBEPI allows multi-planar reformats with completely darkened hepatic vessels; 4) our findings favor the implementation of combined short-TE- and long-TE-BBEPI as a part of a comprehensive protocol for routine liver imaging at 3.0T. BBEPI, in combination with other (gadolinium-enhanced) T1- and T2-weighted sequences, may facilitate improved detection and characterization of liver lesions at 3.0T.

REFERENCES

1. Semelka RC, Martin DR, Balci NC. Focal lesions in normal liver. J Gastroenterol Hepatol 2005; 20: 1478-1487.
2. Semelka RC, Martin DR, Balci NC. Magnetic resonance imaging of the liver: how I do it. J Gastroenterol Hepatol 2006; 21:632-637.
3. Kondo H, Kanematsu M, Itoh K, et al. Does T2-weighted MR imaging improve preoperative detection of malignant hepatic tumors? Observer performance study in 49 surgically proven cases. Magn Reson Imaging 2005; 23:89-95.
4. Martin DR, Friel HT, Danrad R, De Becker J, Hussain SM. Approach to abdominal imaging at 1.5 Tesla and optimization at 3 Tesla. Magn Reson Imaging Clin N Am 2005; 13:241-254, v-vi.
5. Merkle EM, Dale BM, Paulson EK. Abdominal MR imaging at 3T. Magn Reson Imaging Clin N Am 2006; 14:17-26.
6. O'Regan DP, Fitzgerald J, Allsop J, et al. A comparison of MR cholangiopancreatography at 1.5 and 3.0 Tesla. Br J Radiol 2005; 78:894-898.
7. Edelman RR, Salanitri G, Brand R, et al. Magnetic resonance imaging of the pancreas at 3.0 tesla: qualitative and quantitative comparison with 1.5 tesla. Invest Radiol 2006; 41:175-180.
8. von Falkenhausen MM, Lutterbey G, Morakkabati-Spitz N, et al. High-Field-Strength MR imaging of the liver at 3.0 T: intraindividual comparative xtudy with MR imaging at 1.5 T. Radiology 2006; 241(1): 156-66.
9. Hussain SM, Wielopolski PA, Martin DR. Abdominal magnetic resonance imaging at 3.0 T: problem or a promise for the future? Top Magn Reson Imaging 2005; 16:325-335.
10. de Bazelaire CM, Duhamel GD, Rofsky NM, Alsop DC. MR imaging relaxation times of abdominal and pelvic tissues measured in vivo at 3.0 T: preliminary results. Radiology 2004; 230:652-659.
11. Stanisz GJ, Odrobina EE, Pun J, et al. T1, T2 relaxation and magnetization transfer in tissue at 3T. Magn Reson Med 2005; 54:507-512.
12. Schick F. Whole-body MRI at high field: technical limits and clinical potential. Eur Radiol 2005; 15:946-959.
13. Muller MF, Edelman RR. Echo planar imaging of the abdomen. Top Magn Reson Imaging 1995; 7:112-119.
14. Hussain SM, De Becker J, Hop WC, Dwarkasing S, Wielopolski PA. Can a single-shot black-blood T2-weighted spin-echo echo-planar imaging sequence with sensitivity encoding replace the respiratory-triggered turbo spin-echo sequence for the liver? An optimization and feasibility study. J Magn Reson Imaging 2005; 21:219-229.
15. Taouli B, Vilgrain V, Dumont E, Daire JL, Fan B, Menu Y. Evaluation of liver diffusion isotropy and characterization of focal hepatic lesions with two single-shot echo-planar MR imaging sequences: prospective study in 66 patients. Radiology 2003; 226:71-78.
16. Wielopolski PA SF, Stehling MK. Echo-planar imaging pulse sequences. In: Schmitt F SM, Turner R., ed. Echo-planar imaging: theory, technique and application. Berlin: Springer-Verlag, 1998; 65-141.
17. Namimoto T, Yamashita Y, Sumi S, Tang Y, Takahashi M. Focal liver masses: characterization with diffusion-weighted echo-planar MR imaging. Radiology 1997; 204:739-744.
18. Nasu K, Kuroki Y, Nawano S, et al. Hepatic metastases: diffusion-weighted sensitivity-encoding versus SPIO-enhanced MR imaging. Radiology 2006; 239:122-130.
19. Hennig J, Scheffler K. Hyperechoes. Magn Reson Med 2001; 46:6-12.
20. Hennig J, Weigel M, Scheffler K. Multiecho sequences with variable refocusing flip angles: optimization of signal behavior using smooth transitions between pseudo steady states (TRAPS). Magn Reson Med 2003; 49:527-535.
21. Frank LR, Wong EC, Liu TT, Buxton RB. Increased diffusion sensitivity with hyperechos. Magn Reson Med 2003; 49:1098-1105.
22. Hargreaves BA, Cunningham CH, Nishimura DG, Conolly SM. Variable-rate selective excitation for rapid MRI sequences. Magn Reson Med 2004; 52:590-597.

chapter6
POSTPROCESSING

chapter6
postprocessing of dynamic gadolinium-enhanced MRI

Postprocessing of dynamic gadolinium-enhanced MRI exams of the liver:
EXPLANATION AND POTENTIAL CLINICAL APPLICATIONS

for color-coded qualitative and quantitative analysis

ABSTRACT

The purpose of this article is to explain and illustrate the current status and potential applications of automated and color-coded post-processing techniques for analysis of dynamic multiphasic gadolinium-enhanced MR imaging of the liver. Post-processing of these images on dedicated workstations allows generation of time-intensity curves (TIC) as well as color-coded images, which provides useful information on (neo)-angiogenesis within a liver lesion, if necessary combined with information on enhancement patterns of surrounding liver parenchyma. Analysis of TIC and color-coded images, which are based on pharmacokinetic modeling, provides an easy to interpret schematic presentation of tumor behavior, providing additional characteristics for adequate differential diagnosis. Inclusion of TIC and color-coded images as part of the routine abdominal MR imaging work-up protocol may help to further improve the specificity of MR imaging findings and may facilitate the diagnostic work-up of disease for detection, staging, and monitoring of anti-tumor therapy.

*†Liang Wang, MD; *Indra C. van den Bos, MD; *†††Shahid M. Hussain, MD, PhD; *Peter M. Pattynama, MD, PhD; *Mika W. Vogel, MSc, PhD; *Gabriel P. Krestin, MD, PhD

*Department of Radiology, Erasmus MC, University Medical Center Rotterdam, The Netherlands; and †††Department of Radiology, University of Nebraska Medical Center, Omaha, NE, USA
† Present address: Department of Radiology, Memorial Sloan-Kettering Cancer Center, New York, USA.

Accepted for publication in Acta Radiologica.

INTRODUCTION

In the analysis of liver diseases, dynamic multiphasic gadolinium-enhanced magnetic resonance (MR) imaging is routinely used as part of the imaging protocol, since it provides information on a multitude of parameters, including information on tumor angiogenesis related to tumor growth, tumor grade, metastatic potential and anti-tumor therapy response[1,2]. Since hepatic perfusion regarding blood flow per tissue unit is essential for analysis and differential diagnosis of either focal or diffuse liver abnormalities, quantification of these parameters may facilitate improved evaluation of hepatic diseases[3].

Analysis of hepatic enhancement is more complex compared to other abdominal organs such as kidneys, pancreas or spleen, because the blood inflow of the liver is made up by two components, which include inflow from both the hepatic artery and the portal vein[4,5]. These two vessels provide blood to the liver in two different time settings, which are related to each other in the analysis of arrival, distribution and excretion of contrast media. Additionally, the analysis of data may potentially be influenced by different flow curves, which include a typical arterial enhancement curve (diastolic and systolic peaks) for the hepatic artery, and a continuous positive venous inflow curve for the portal vein[6].

In previous studies, several imaging methods for non-invasive quantification of hepatic hemodynamics have been proposed[3]. Ultrasound can be applied for quantification by means of Doppler ultrasonography or contrast-enhanced ultrasonography[7-9]. However, the main limitation of ultrasound examinations is that it is operator dependent, hence with low reproducibility, and has low sensitivity[10]. Computed tomography (CT) has been proposed and evaluated for quantification of enhancement patterns[11]. With the introduction of modern multislice multidetector CT scanners, even more robust data can be obtained, allowing for a multitude of post-processing techniques, but this remains yet to be defined[12]. MR imaging is increasingly being used for analysis of liver diseases. The unique ability of MR imaging to detect intrinsic tissue components, in combination with capability of multiphasic dynamic imaging after gadolinium administration renders it a superior technique for both the detection and characterization of focal liver lesions, without radiation exposure[10]. In addition, in the future, the combination of diffusion-weighted imaging of the liver, MR-elastography and perfusion imaging may provide additional tools to assess the liver function, enabling a combination of both morphologic and metabolic imaging in a one-step imaging protocol[13]. MR imaging has been proposed as well for quantification of hepatic perfusion and biliary excretion[14,15], using different types of contrast agents including T1-shortening agents, T2-shortening agents and macromolecular agents[16].

The purpose of this review article is to explain and illustrate the current status and potential applications of automated and color-coded post-processing techniques for analysis of dynamic multiphasic gadolinium-enhanced MR imaging of the liver using state-of-the-art MR imaging exams.

MR imaging technique for dynamic multiphasic imaging

Breath-hold T1-weighted contrast-enhanced dynamic magnetic resonance imaging of the liver can be performed on any modern MR imaging unit, with a magnetic field strength >1.0 Tesla (T). Because the introduction of parallel imaging has facilitated fast acquisition of sequences, with increased possibilities for dynamic contrast-enhanced imaging of the abdomen, this will be discussed shortly.

Parallel MR imaging (pMRI) is based on a method to undersample K-space in order to reduce total scan time. Currently, pMRI is routinely available on all commercial MR scanners, including sensitivity-encoded imaging (SENSE), array spatial sensitivity encoding technique (ASSET), simultaneous acquisition of spatial harmonics (SMASH) and others[17,18]. The undersampling of the k-space data, with some loss of the signal-to-noise ratio (SNR), results in considerably increased temporal resolution which is essential for a better TIC fit. Currently, pMRI is still being improved, and new methods are being published on a regular basis[19-21].

For dynamic contrast-enhanced imaging, scan protocols are tailored for the desired measurements. The choice of sequence and parameters therefore, will depend on anatomic coverage, acquisition times, susceptibility to artifacts resulting from magnetic field inhomogeneities and need for quantification[22].

For dynamic multiphasic imaging, 2D/3D T1-weighted sequences (gradient-echo (GRE), saturation recovery / inversion recovery snapshot sequences, or echo-planar sequences) can be performed after administration of an intravenous bolus of 0.1 mmol/kg of a non-liver-specific gadolinium-chelate such as gadolinium-DTPA (Magnevist, Schering AG, Berlin, Germany) or gadolinium-DTPA-BMA (Omniscan, GE Healthcare, Oslo, Norway). To correct additionally for the loss in SNR by the use of pMRI, the total dosage may be slightly increased for compensation. Routinely, an injection rate of 3ml/s is used by means of a power injector, followed by a bolus of saline (15 or 20ml total). The higher injection rate compensates for the SNR loss due to the pMRI application.

Dynamic imaging of the liver entails imaging in at least four different vascular phases that may be extended depending on performance of the system. The phases that should be included are: 1) precontrast phase, 2) arterial phase, 3) portal (or equilibrium) phase and 4) delayed (or venous) phase). To accurately capture the arterial phase, a timing bolus technique can be applied, using 2ml of the same contrast agent with inject rate 3ml/sec bolus followed by 15ml saline. The timing bolus technique and adjustment of the total amount of contrast according to the body weight will compensate for differences in cardiac output and distribution volume. The portal phase is usually acquired at 45 seconds after the arterial phase, and the delayed phase at least 120 seconds after acquisition of the arterial phase[23-25]. The sequence should be adjusted to obtain full anatomic coverage of the liver in each scanned phase within a maximum of one breath-hold period (<25 sec). Routinely, a slice thickness of 6-8 mm is used for 2D GRE sequences, which can be thinner (3 or 4mm) in 3D GRE sequences. Ideally, a time-resolved gadolinium-enhanced sequence should be applied to have more data points on the TIC. In the abdomen, however, due to the breath-holding requirements it is not always possible yet to have continuous scanning in order to obtain multiple scans within each vascular phase. Therefore, most body MRI centers acquire at least four distinct phases.

With the introduction of higher-field-strength magnets (3.0T), improved dynamic imaging of the abdomen became feasible through inherently increased SNR (theoretically in the order of 2), high performance gradient-systems and advanced software platforms. This has enabled increased spatial resolution, scanning with thinner slices or accelerated scanning times, which is particularly useful for angiographic MR imaging[26,27].

Contrast agents for dynamic multiphasic imaging

Dynamic multiphasic contrast-enhanced MR imaging may be performed with low- or high-molecular-weight agents, non-liver-specific gadolinium chelates or liver-specific gadolinium-chelates. After injection into the intravascular compartment, non-liver-specific gadolinium-chelates such as Magnevist ([gadopentetate dimeglumine], Schering, Berlin, Germany)

Figure 1: Basic time-intensity curve

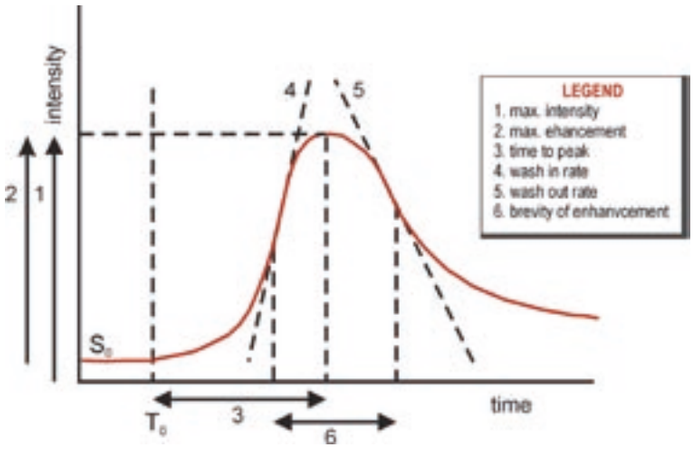

and similar low molecular-weight agents are rapidly diluted in the circulating plasma volume. They rapidly leak out of this space into the extra-vascular (or extracellular) space (interstitium) and then equilibrate between the intravascular and interstitial spaces. Only 1–2% at most of an administered dose enters cells[28]. The non-liver-specific gadolinium chelates that are most frequently used in humans are extracellular agents. In these contrast agents, tissue enhancement depends on arterial input function, kinetic of distribution of blood into the capillary bed, leakage across the capillary walls, and volume of the interstitial space. However, they have inherent disadvantages in estimating blood volume and capillary permeability exclusive of the brain due to the high rate of their vascular extraction, even in normal vessels.

Macromolecular contrast agents, also called blood pool agents, have been developed, such as gadopentetate dimeglumine–labeled albumin[29]. Blood pool contrast agents have advantages for both spatial resolution and SNR at vascular imaging. However, the availability as well as the direct clinical applicability of blood pool agents is limited, due to the slow glomerular filtration rate (GFR) and weak and reversible protein-binding.

The development of liver-specific gadolinium chelates has increased the accuracy of MR for identification and characterization of focal liver lesions[30]. Liver-specific gadolinium-chelates including gadobenate dimeglumine (gadolinium-BOPTA) and gadolinium-ethoxybenzyl-diethylene-triaminepentaacetic acid (gadolinium-EOB-DTPA) with a first phase of extracellular distribution give both dynamic (morphologic) and late phase (functional) information useful for lesion characterization[30]. They combine the properties of a conventional extracellular gadolinium-chelate with those of an agent targeted specifically at the liver and behave in a manner analogous to conventional gadolinium-chelates during the dynamic phase of contrast enhancement[31] In the delayed phase it improves the impact of MRI for the detection of liver lesions[30]. Some liver-specific contrast agents such as mangafodipir (Teslascan, Mn-DPDP, Amersham, GE Health Care) or superparamagnetic iron-oxide particles (SPIO) have no dynamic imaging capability. The possibility of sequential administration of gadolinium-chelates and Teslascan in a single visit to obtain both dynamic and late imaging was proposed[32]. However, such combinations are highly undesirable because of the high cost; complex combined T1-shortening effects of two agents, and recently described potential neurotoxic side effects (Parkinson-like progressive extrapyramidal disorder)[33].

Figure 2: Typical time-intensity curves (TIC)

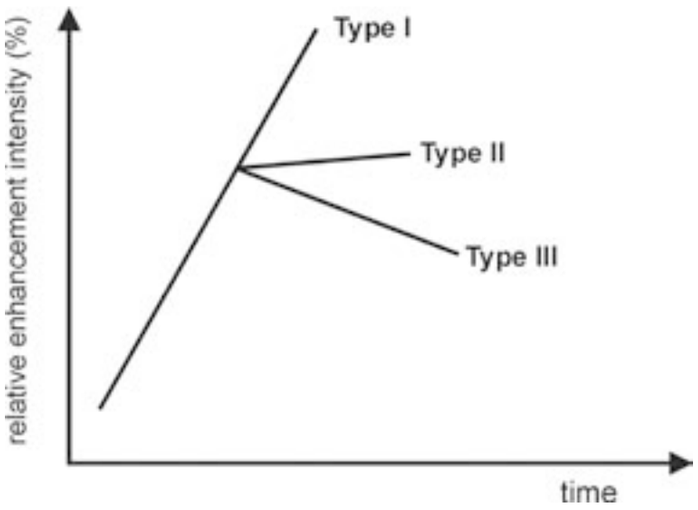

Post-processing hardware and software

Currently, several vendors provide software packages to facilitate the post-processing of gadolinium-enhanced dynamic MRI data on a workstation. For example, Easy Vision (Philips), which runs the Quantitative Analysis package; and 2) Advantage Windows (GE), which supports the Functool package. The Easy Vision package provides the display of a reference image, a subtraction imaging, and nine functional images: relative enhancement, maximum enhancement, maximum relative enhancement, wash-in rate, washout rate, brevity-of-enhancement, area-under-curve, time-to-peak, T0. Advantage Windows can display a subtraction imaging, and seven functional images: mean time to enhance, time to maximum enhancement, positive enhancement integral, negative enhancement integral, signal enhancement ratio, maximum slope of increase, and maximum slope of decrease in enhancement. Both software packages allow the display of the time-intensity curves and statistics of region-of-interest (ROI), either as a graph or a table format.

Time intensity curves and derived parameters

The software package analyses these data over time, to provide a plotted corrected graph which illustrates the step-wise changes in enhancement over time in different vascular phases after contrast administration[34]. The pharmaco-kinetic time intensity curves (TIC) model provides a number of different parameters that can be used to characterize specific tumor enhancement patterns. These parameters can be used to obtain data on microvessel density, flow through the vessels, vascular resistance, capillary wall permeability, composition of the extracellular space, and venous outflow. Currently the two most widely applied models for analyzing dynamic MRI gadolinium-DTPA data are shutter-speed model proposed by Charles S. Springer Jr. and Tofts model proposed by Paul S. Tofts[35,36].

The color-coded images are based on qualitative pixel-wise display of various quantitative modeling parameters, which can be derived from the quantitative data of the TIC at each pixel. This method provides an automatic conversion of kinetic contrast information into easy to interpret color-scaled images, which provides a quick overview of degree and heterogeneity of enhancement within the tissue.

The generation of TIC is based on signal intensity measurements obtained by defining region-of-interest (ROI) areas on the color-coded images, which are placed by the operator. To correct for minimal differences in signal intensity in images acquired before and after injection of the contrast agent, measurements for TIC generation are based on subtracted images only. Subtracting the analyzed contrast-enhanced image with the precontrast image, acquired at the same level, creates these subtractions. This is performed automatically by the software program. It is important to note that semi-automated interpretation of dynamic examination may suffer from respiratory motion, which may potentially cause a varying position of the liver in the z-axis over time. In our experience, this is most frequently encountered in sub-cm focal lesions located under the diaphragm.

An example of a baseline TIC illustrates that a number of parameters can be derived, including specific enhancement patterns such as maximum intensity, maximum enhancement, time to peak, wash-in- and washout rate, and brevity of enhancement (Fig. 1). In literature[37], a number of typically shaped TIC have been described (Fig. 2). Type I (steady enhancement) curve shows continuously increasing signal intensity within the lesion, which is considered a benign feature. Type II enhancement curve shows a steep increase in signal intensity in the first phases after contrast administration, which becomes less steep in the more delayed phases, sometimes with plateau formation. This type of curve is considered to be an indicator of viable tumor with stable microcirculation. Type III enhancement curve shows steep arterial enhancement, with loss of signal intensity in the delayed phases, rendering the curve to a negative slope, which is interpreted as washout of contrast within the tumor. This is considered a strong indicator of malignancy, proliferating edge of tumor or vessels.

TIC is determined by contrast agent in the intravascular and extravascular compartments. During the first pass, the contrast agent is predominantly intravascular and contrast enhancement reflects perfusion and blood volume. Delayed enhancement is determined by the passage of contrast agent into and out of the extravascular space, as determined by rate constants ktrans and kep.

Definitions of parameters derived from TIC or multicompartment pharmacokinetic modeling:

1. T_0: Time of arrival of contrast inflow, which determines the arrival moment of the contrast agent at the tissue.
2. S_0: Intensity before arrival of contrast inflow.
3. Maximum intensity: absolute peak value of curve.
4. Maximum enhancement: difference between peak value and S0.
5. Time to peak (uptake speed): time between T0 and time of peak intensity.
6. Wash in rate: maximum slope between T0 and time of peak intensity, which determines the maximum rate of contrast agent uptake during

the acquisition and can adequately estimate the degree of early strong enhancement of tumor tissue..

7. Washout rate: absolute value of maximum slope between time of peak intensity and last measurement point, which determines the maximum rate of contrast agent outflow during the acquisition.
8. Brevity of enhancement: time between wash in and washout.
9. Relative enhancement: percentage of signal intensity increases between the post-contrast and the pre-contrast signal intensities respectively. Relative enhancement reflects the plasma volume and is highly correlated with microvessel density
10. Maximum relative enhancement: percentage of signal intensity increase between the maximum post-contrast and the pre-contrast signal intensities.
11. Area under curve: sum (integral) of the area underneath the time intensity curve.
12. Volume transfer constant (ktrans): the constant determines the passage of contrast agent into the extravascular compartment from the intra vascular compartments. ktran approximates to endothelial permeability surface area product (kfp)
13. Rate constant (kep): the constant determines the passage of contrast agent out of the extravascular compartment to the intravascular compartments. kep is highly influenced by the vessel permeability and is highly correlated with microvessel density[38] and relative blood volume (rBV)[39,40].
14. Extracellular extravascular space (Ve): the constant determines leakage volume of fractional interstitial space. Ve is the volume of extravascular extracellular space per unit volume of tissue[38].

Time intensity curves and color-coded imaging of focal and diffuse liver lesions

Benign liver lesions

According to the currently used nomenclature for hepatocellular focal liver lesions, two types of liver lesions exist: regenerative and neoplastic or dysplastic lesions[41]. Regenerative lesions include regenerative nodules, segmental or lobar hyperplasia, and focal nodular hyperplasia. Neoplastic or dysplastic lesions include hepatocellular adenoma, dysplastic foci, dysplastic nodules, and hepatocellular carcinoma (HCC). Hepatocellular lesions with benign growth behavior are common, and include cysts, hemangiomas, focal nodular hyperplasia (FNH) and hepatocellular adenomas, although the latter one is referred to as neoplastic lesion because of rare reports of malignant transformation[23,42]. To illustrate the role of the subtraction images, and the time-intensity curves in various types of benign lesions, examples of hemangioma, hepatocellular adenoma, and FNH are provided below.

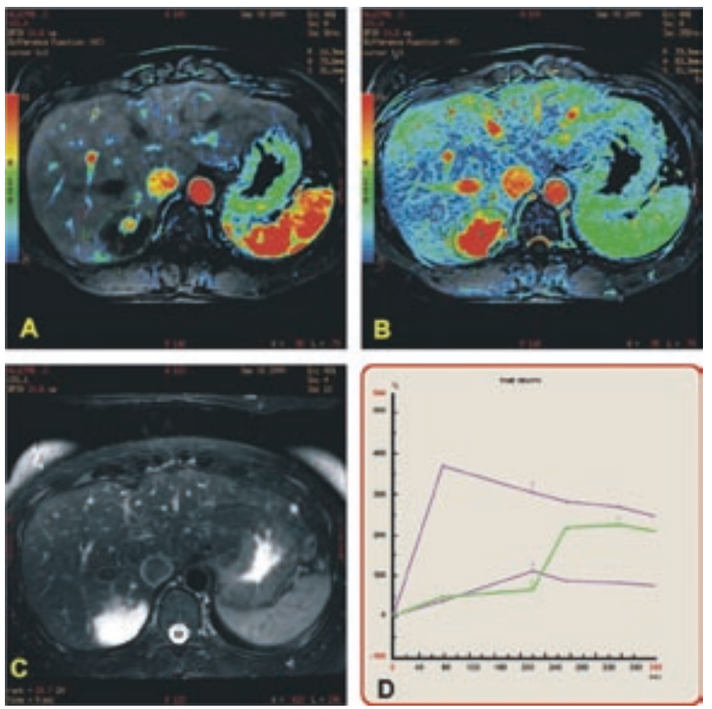

Figure 3: Hemangioma
40-year old female with a 48×35mm hemangioma in the right lobe of the liver. (a) (Color-coded parameter image from the arterial phase, calculated using relative enhancement) Nodular enhancement in the periphery of the lesion. (b) (Color-coded parameter image from the delayed phase, calculated using relative enhancement) Complete fill-in of the entire lesion. The lesion is entirely red. (c) (T2-weighted image, TR/TE= 1059/99.4 msec) High signal intensity, lobulated and well-circumscribed lesion typical for hemangioma. (d) The time-intensity curve from the ROI of the lesion (green curve) reflects the steady enhancement of hemangioma (atypical Type I curve). The time-intensity curve from the ROI of the blue curve (line 3) shows normal liver parenchyma enhancement, and line 2 represents the signal intensity within the aorta at the acquired vascular phase. Note: decremental value in color spectrum: red > orange > yellow > green > blue > indigo > violet.

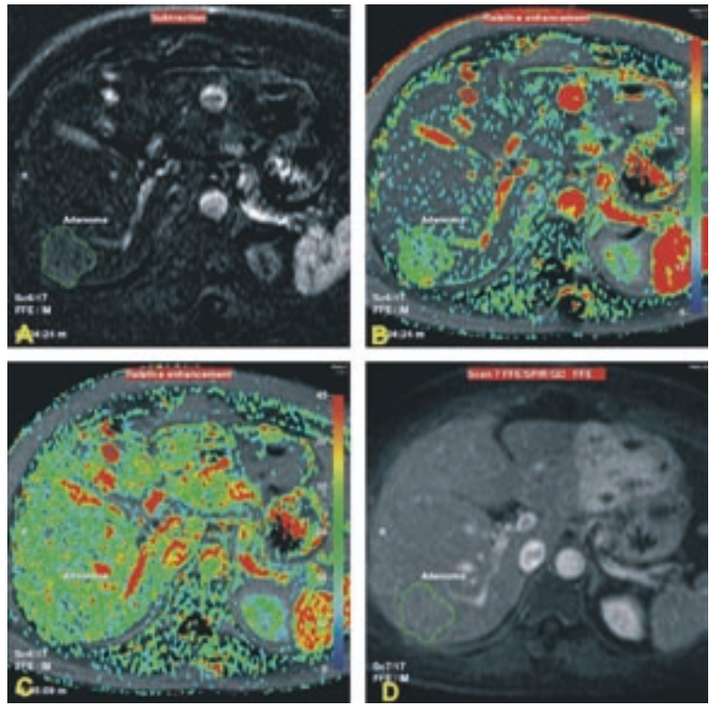

Figure 4: Hepatocellular adenoma
32-year old female with a hepatocellular adenoma in the right lobe of liver and a hemangioma in the left lobe of the liver. (a) (Subtraction image from the arterial phase) Hypervascular lesion. (b) (Color-coded parameter image from the arterial phase, calculated using relative enhancement) Homogeneous blush of the lesion. (c) (Color-coded parameter image from the portal phase, calculated using relative enhancement) Isointensity of the lesion with the surrounding liver. (d) (Delayed fat-suppressed T1-weighted image) Isointensity of the adenoma in the right lobe of the liver and homogeneously enhanced hemangioma in the left lobe of the liver. Note: decremental value in color spectrum: red > orange > yellow > green > blue > indigo > violet.

Hemangiomas are the most common hepatic neoplasms, with an incidence between 0.4-20%[43]. Hemangiomas are lesions with long T2 values, so they have high signal intensity on T2-weighted images. Also, they maintain their signal intensity on images with longer echo times that illustrates the lesion consists of multiple fluid-filled spaces. The vast majority of hemangiomas show a typical peripheral nodular enhancement pattern with complete fill-in of the entire lesion over time. This enhancement pattern is of a typical benign lesion with a Type I curve (Fig. 3).

Hepatocellular adenoma often occurs in young adult women and is associated with the used of birth oral contraceptives[42]. Hepatocellular adenomas vary in signal intensity on T1- and T2- weighted images. Characteristically, liver adenomas show a transient blush in the arterial phase of the dynamic gadolinium-enhanced images, and fade to isointensity on delayed images (Fig. 4).

Focal nodular hyperplasia (FNH) most commonly occurs in adult female patients, but can also occur in men[44]. FNH is not related to the use of oral contraceptives and is solitary in 2/3 of cases. FNH is mostly slightly hypointense on T1- and slightly hyperintense to the liver on T2-weighted images, and typically has a central scar which enhances in the delayed phase after gadolinium administration.[44,45]. Typically, FNH shows very intense homogeneous enhancement in the arterial phase, with fading to isointensity in the delayed phase. The central scar is enhanced on delayed images. Even though FNH is a benign liver lesion, typically, this type of lesion does not show a Type I, but rather a Type III enhancement curve. The exact reason for this is not clear, but it is important to notice that in the delayed phase, the enhancement curve of FNH remains higher than the liver, indicating absence of washout. The time-intensity curve for FNH is characterized as showing signs of "arterialization" (steep enhancement) in the first part of the curve and subsequently showing signs of "hepatization" (curve running slightly above but parallel to the curve of the liver), as was described in a recent study assessing the MR imaging findings of FNH (Fig. 5)[45].

Malignant liver lesions

Malignant liver lesions are common, and include primary liver lesions such as HCC, which develops in a step-wise fashion in patients with cirrhotic liver disease. In this sequence, dysplastic foci may develop into dysplastic nodules, and eventually in HCC. Metastatic liver disease is a major health problem, which occurs most commonly in patients with colorectal malignancies. To illustrate the role of the subtraction images, color-coded images, and the TIC in primary and secondary liver lesions, examples of HCC and liver metastasis are provided below.

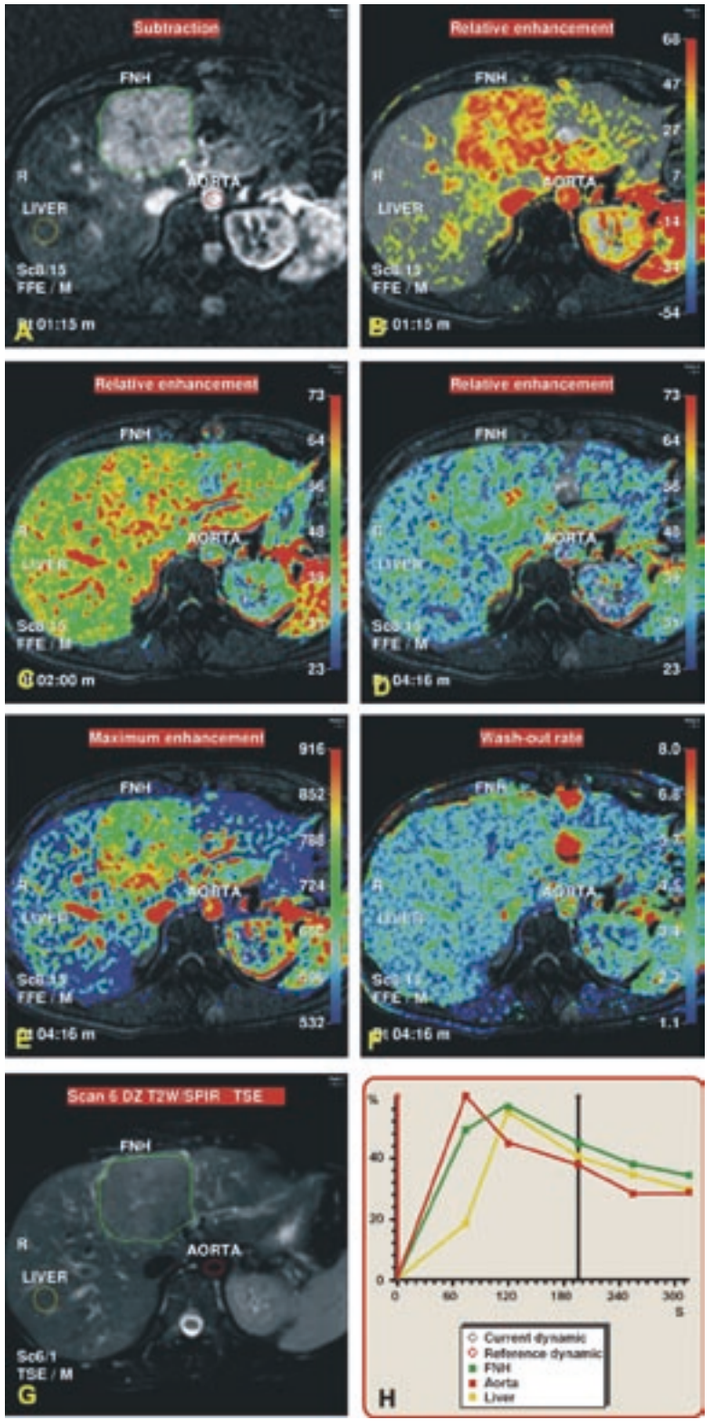

Figure 5: Focal nodular hyperplasia
32-year old female, with large focal nodular hyperplasia (FNH) in the left liver lobe. (a) (Subtraction image from the arterial phase) Intense homogeneous enhancement of the lesion. (b) (Color-coded parameter image from the arterial phase, calculated by using relative enhancement) Homogeneous intense enhancement of the lesion. (c) (Color-coded parameter image from the portal phase, calculated by using relative enhancement) The lesion is almost isointense to the liver. (d) (Color-coded parameter image from the delayed phase, calculated by using relative enhancement) Delayed enhancement of the central scar. (e) (Color-coded parameter image, calculated by using maximum enhancement) The absolute values of enhancement of the lesions are higher than the liver. (f) (Color-coded parameter image, calculated by using washout rate) This lesion has a similar washout rate as the surrounding liver. (g) (T2- weighted image (TR/TE=1500/80 msec) The lesion is only slightly hyperintense to the liver. (h) The time-intensity curve of the lesion (green curve) parallels the curve of the aorta in the arterial phase, indicating a very steep enhancement (Type III). In the delayed phases it parallels the curve of the liver, reflecting its benignity as well as its similarity to the normal liver tissue. Note: decremental value in color spectrum: red > orange > yellow > green > blue > indigo > violet.

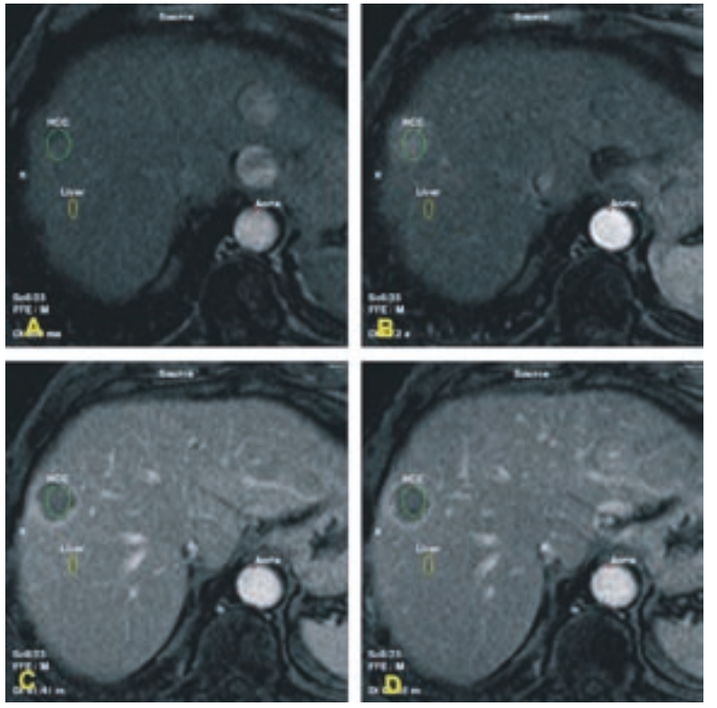

Figure 6: Hepatocellular carcinoma
62-year old male with hepatocellular carcinoma (HCC) in the right liver lobe. (a-d) Four images illustrating the typical four phases of dynamic gadolinium enhanced sequence, including the pre-contrast phase (a), arterial phase (b), portal phase (c), and delayed phase (d). Note that the HCC is intensely enhancing in the arterial phase and shows washout in the delayed phases with late enhancement of a ptumor capsule.

HCC is the most common primary malignancy of the liver and occurs most frequently in males[1]. HCC is solitary in 50%, multifocal in 40%, and diffuse in 10% of the cases. Often, HCC will show a moderately high signal on T2-weighted images. HCC typically shows intense enhancement of the tumor in the arterial phase (high wash-in rate) and looses much of its contrast in later phases (high washout rate). In later phases, most HCCs show enhancement of a tumor capsule. A combination of high signal intensity on T2-weighted images and the enhancement pattern described above, particularly in a patient with pre-existing hepatitis or cirrhosis, is considered diagnostic for HCC. HCCs demonstrate Type III enhancement curves, in which the delayed phase images show a lower signal intensity of the lesion compared to the lesion (washout) (Fig. 6-8). Fibrolamellar HCC is an uncommon variety of HCC, which often occurs, in young female patients[23]. At MR imaging, fibrolamellar HCC may show some overlap with FNH, including arterial enhancement and presence of a fibrous central scar. Important differences between FNH and fibrolamellar HCC include: 1) a more pronounced and homogeneous enhancement in the arterial phase for FNH, and heterogeneous, less pronounced arterial enhancement for fibrolamellar HCC; and 2) presence of washout in the delayed phase in fibrolamellar HCC and persistent higher signal intensity in the delayed phase after contrast administration in FNH. Time-intensity curves as well as the color-coded images may further facilitate the distinction between fibrolamellar HCC and FNH.

Liver metastases are the most common malignant tumors of the liver. Optimal evaluation with MR imaging includes detection as well as characterization. Characterization is important because patients with known primary malignancies commonly have small hepatic lesions that are benign cysts or hemangiomas. In addition, accurate assessment of the segmental extent of the metastatic disease may have a substantial impact on patient management. Liver metastases are generally low on T1-and moderately high on T2-weighted images. Small hypervascular metastases may show intense enhancement in the arterial phase. Most commonly, liver metastases show a peripheral irregular ring of enhancement. The color-coded images may provide more information concerning the vascularity of the lesions. The time-intensity curves of liver metastases most closely fit into the Type II enhancement curves. The enhancement pattern is similar to the surrounding liver in the arterial phase, but with different behavior in the later phases, including the portal and delayed phases. In these phases, the intensity of enhancement is routinely lower than the surrounding liver, resulting in a Type II enhancement curve which is located below the enhancement curve of the surrounding hepatic stroma (Fig. 9).

Diffuse liver lesions

Diffuse liver parenchymal abnormalities may include a wide variety of disease entities, such as hepatitis, cirrhosis, hemochromatosis, steatosis, and diffuse malig-

nancies[1,23]. Acute hepatitis may present with reversible heterogeneous patchy enhancement of the hepatic stroma in the arterial phase. In the portal and delayed phases, the abnormal enhancement pattern is occult. To illustrate the role of the subtraction images and the color-coded images in detection of diffuse liver parenchymal disease as well as monitoring of therapy, an example of acute hepatitis in a patient with primary sclerosing cholangitis before and after medical treatment with Prednisone is provided (Fig 10).

Discussion

Post-processing of dynamic gadolinium-enhanced MRI exams of the abdomen allows generation of the color-coded images and time-intensity curves[46]. The information may further improve the diagnostic capability of MRI at high temporal and spatial resolution. Unlike the original gadolinium-enhanced images, the color-coded images provide information concerning the intra-tumoral distribution of vessels (vascular density) as well as the nature of the vascular wall (intact or immature and leaky blood vessels). This may contribute to a better understanding of tumor enhancement patterns and angiogenesis, and hence may result in improved characterization of tumors. As described in literature[47], tumors do not grow beyond 2 mm^3 in size as a result of hypoxia unless angiogenesis, a process of the development of new capillaries derived from host tissues that allow tumors to grow exponentially.

The enhancement mechanisms behind dynamic gadolinium-enhanced MRI

Because of the unique dual blood supply of the liver (arterial and portal), hepatic lesions probably have different contrast kinetics as compared to lesions in other organs with only a single (arterial) blood supply. Therefore, the generated TICs of focal liver lesions should always be compared with the curves of the surrounding liver.

The mechanisms behind the differential contrast enhancement are thought to include differences in tumor perfusion and the levels of tumor capillary wall permeability and hydrostatic pressure. The growth of a tumor, and its associated angiogenesis, is often rapid and disordered, leading to: 1) a relatively high fraction of immature blood vessels; 2) abnormal basal membranes in the vessel wall with relative lack of pericytes or smooth muscle associations with endothelial cells which render the vessels more "leaky" or permeable (providing an access point for contrast agents); 3) tumor vessels are tortuous, vary in diameter, and tend toward excessive branching and shunt formation; 4) intermittent or unstable blood flow with acutely collapsing vessels; and 5) hydrostatic pressure differences between tumors and normal tissue, partly reduced or absent lymphatics which may influence contrast agent uptake.

Blood volume, blood flow, mean transit time and microvascular permeability–surface area product are all, in principle, quantifiable through analysis of dynamic

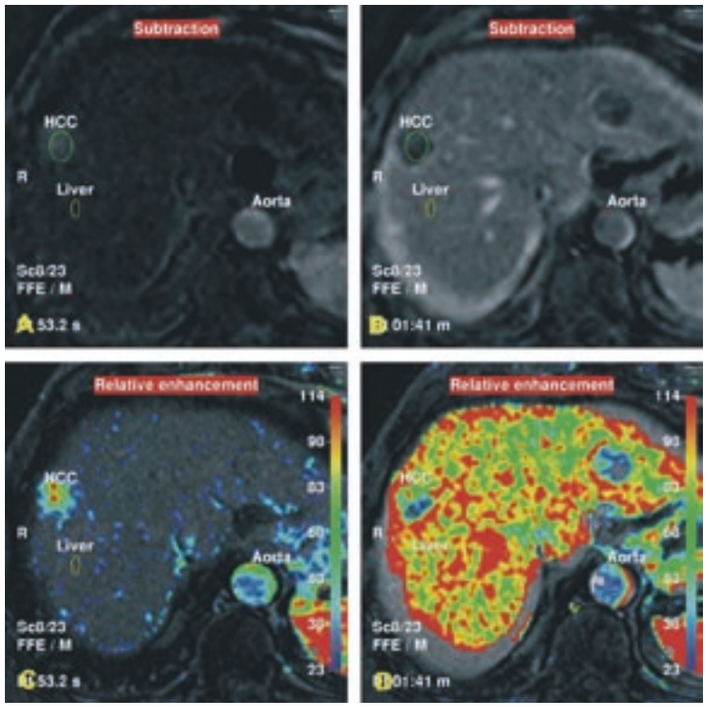

Figure 7: Hepatocellular carcinoma
The same patient as in Figure 6. (a-b) (Two subtraction images from the arterial and portal phases, respectively) Improved visualization of the HCC. (c-d) (Two color-coded parameter images from the arterial and portal phases, respectively, calculated by using relative enhancement) Heterogeneous enhancement of the lesion, i.e. the lesion is enhancing more intensely in the center than in the periphery (more red in the center) (c), and lost contrast in the center (sign of a high washout rate), with enhancing tumor capsule (more red in the periphery of the lesion) (d).

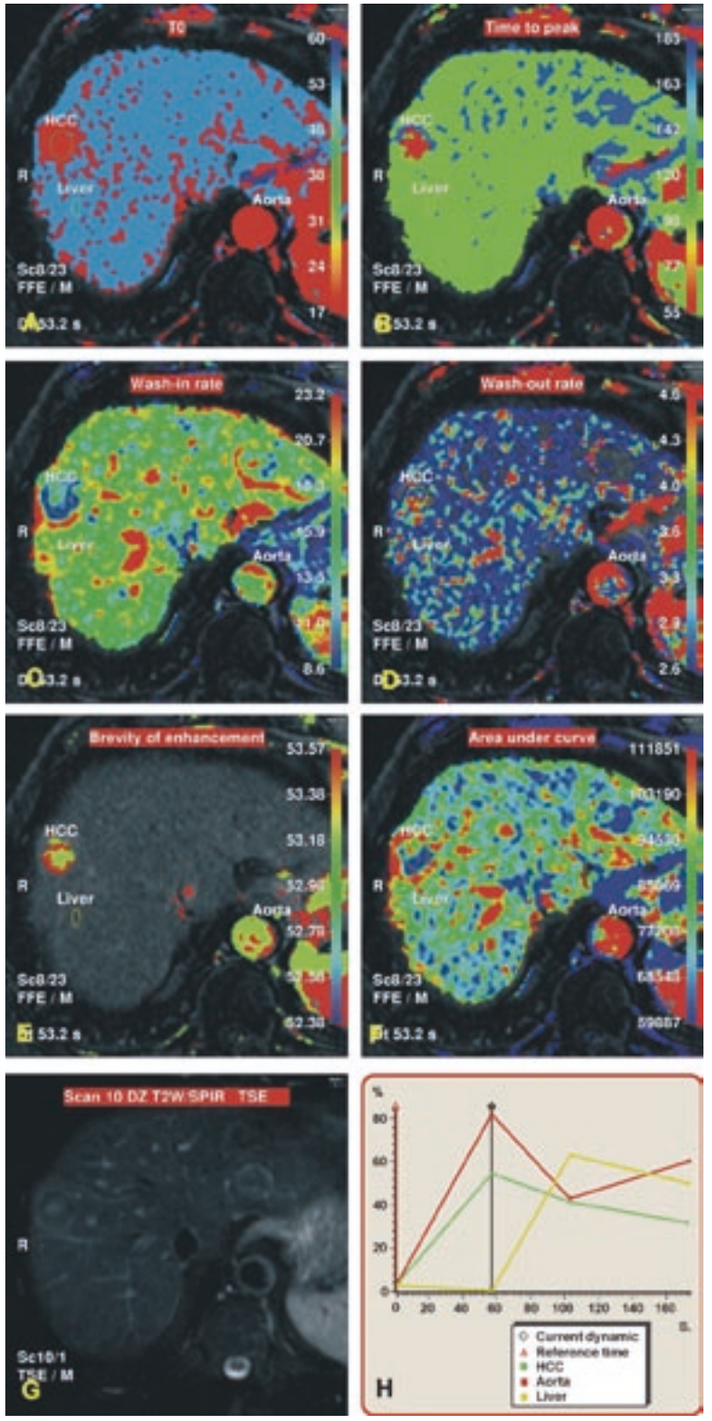

Figure 8: Hepatocellular carcinoma
The same patient as in Figures 6-7. This figure shows various parameters as color-coded images. (a) (Color-coded parameter image, calculated by using T0) The lesion has a shorter T0 (i.e. enhances earlier) than the surrounding liver. (b) (Color-coded parameter image, calculated by using time-to-peak (TTP)) The center of this lesion has a shorter TTP as compared to the tumor capsule. This indicates that the peak of contrast reaches the center of the lesion in an earlier phase. (c) (Color-coded parameter image, calculated by using wash-in rate) The center of this lesion has a lower wash-in rate as compared to the tumor capsule. (d) (Color-coded parameter imaging, calculated by using washout rate) The center of the lesion has a slightly higher washout rate than the surrounding liver. (e) (Color-coded parameter image, calculated by using brevity-of-enhancement) The time between the wash-in rate and washout rate is longer in the center of this lesion as compared to the surrounding liver. (f) (Color-coded parameter image, calculated by using area-under-curve) The tumor capsule of this lesion received a higher dosage of contrast agent than the center of the lesion. (g) (T2-weighted image (TR/TE=1500/80 msec) Slightly hyperintensity in the center as well as the tumor capsule of the lesion. (h) The time-intensity curve shows that the lesion (green curve) enhances more than the liver and less than aorta in the arterial phase, and loses contrast in the later phases (sign of washout). Please note that the curve, unlike the curve in the FNH (see Figure 5h), is not parallel to the curve of the liver in any phase. Note: decremental value in color spectrum: red > orange > yellow > green > blue > indigo > violet.

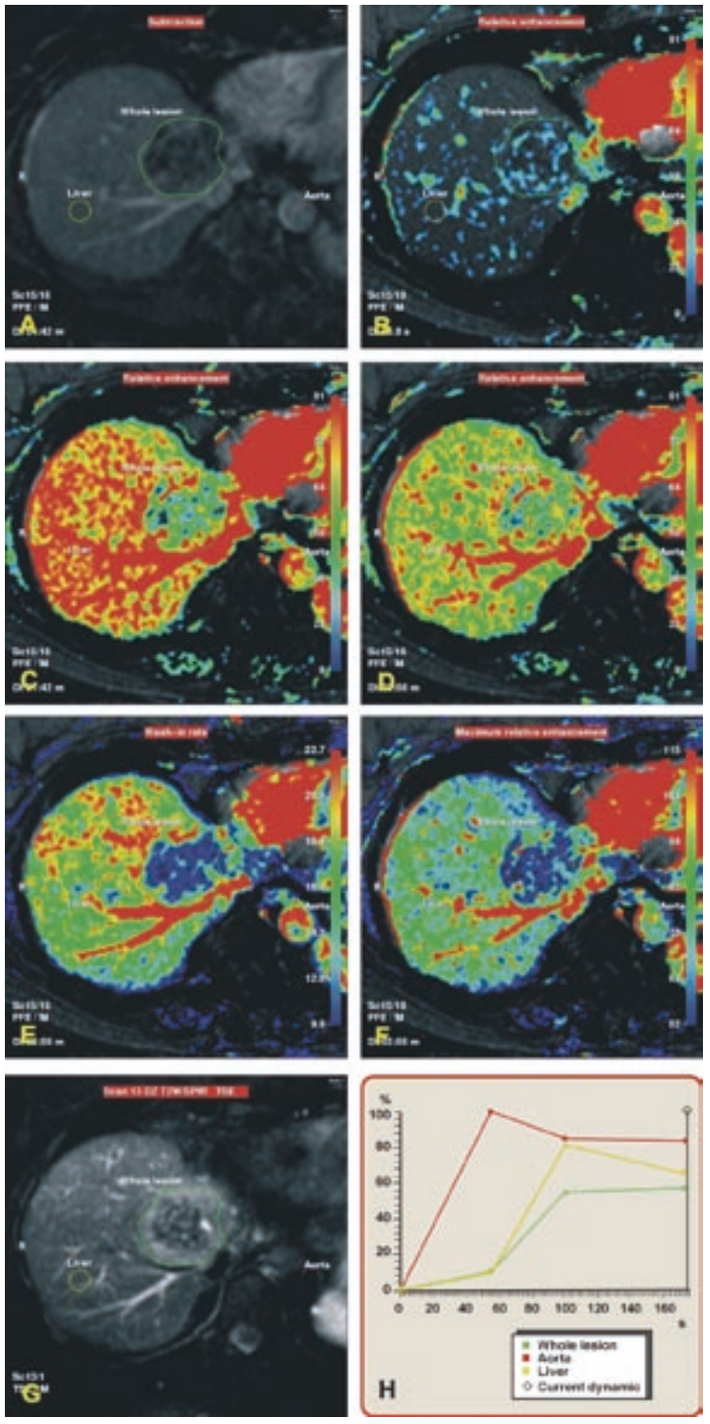

Figure 9: Liver metastasis
56-year old female with a large hepatic metastasis from sigmoid carcinoma. a) (Substraction image from the portal phase) Irregular ring enhancement of the lesion as well as a faint enhancement in the center of the lesion. b) (Color-coded parameter image from the arterial phase, calculated by using relative enhancement) Faint enhancement of the lesion. c) (Color-coded parameter image from the portal phase, calculated by using relative enhancement) Irregular ring of enhancement in the periphery of the lesion, whereas the more central parts of the lesion are enhanced less than the surrounding liver. d) (Color-coded parameter image from the delayed phase, calculated by using relative enhancement) The lesion has enhanced slightly more than in the previous phase, whereas the liver has lost some of its contrast. Therefore, the conspicuity of lesion has decreased. e) (Color-coded parameter image, calculated by using wash-in rate) The periphery of the lesion has a higher wash-in rate than the center of the lesion. f) (Color-coded parameter image, calculated by using the maximum relative enhancement) The central parts of the lesion enhance less than the surrounding liver. g) (T2-weighted image (TR/TE=1500/80 msec) The periphery of the lesion is slightly hyperintense to the liver. h) The time-intensity curve of the lesion (green curve) shows that the lesion is enhancing similar to the liver in the arterial phase. In the portal phase, there is the greatest difference in enhancement between the lesion and the surrounding liver. In the delayed phase, the lesion shows slight further increase in enhancement, whereas, the liver loss some contrast. Therefore, the conspicuity of the lesion decreases after the portal phase. Note: decremental value in color spectrum: red > orange > yellow > green > blue > indigo > violet.

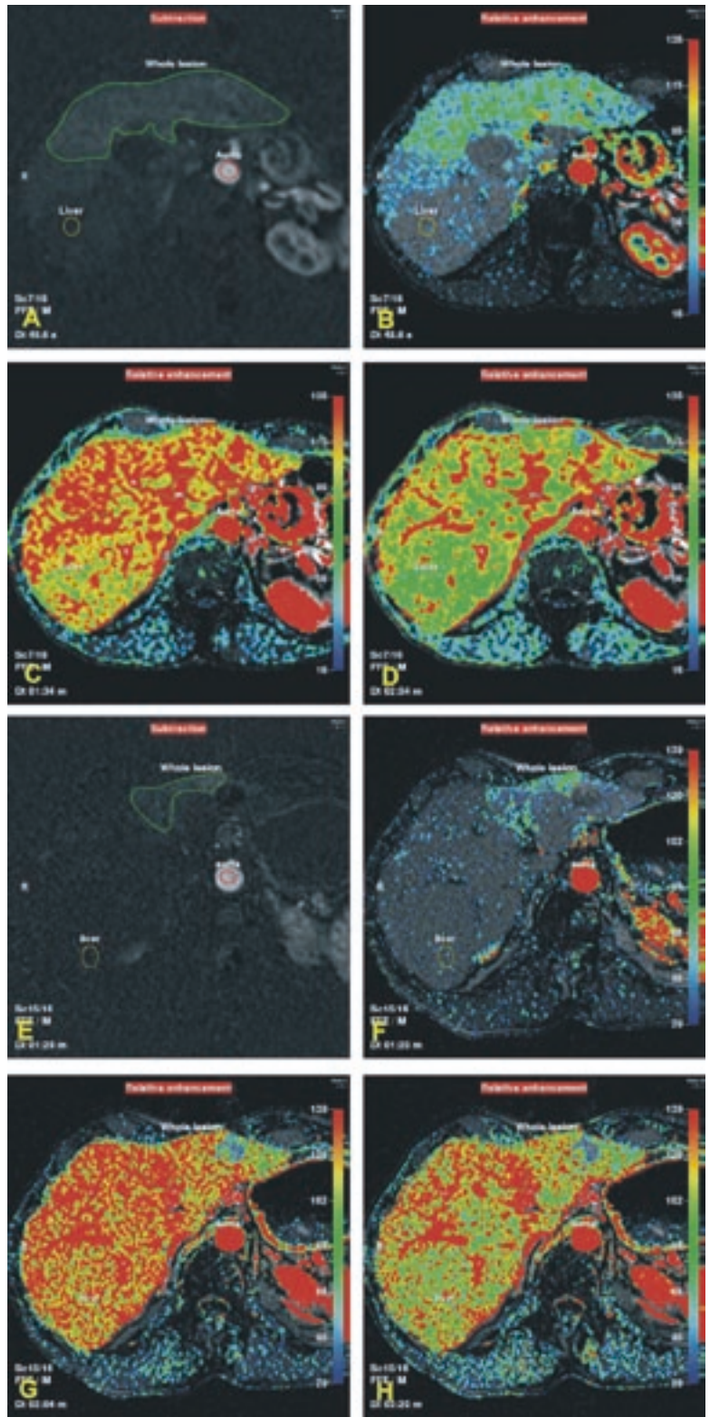

Figure 10: Diffuse parenchymal liver disease
Diffuse liver disease, before and after medical treatment. 59 year old male with primary sclerosing cholangitis with an acute hepatitis in the left and part of the right liver. Images A-D were performed prior to medical treatment, while images E-H were performed after a three-month treatment with Prednison. (a) (Subtraction image from the arterial phase) Abnormally increased enhancement of the liver parenchyma in the left and part of the right liver. (b) (Color-coded parameter image from the arterial phase, calculated by using relative enhancement) The heterogeneous increased enhancement of the liver. (c) (Color-coded parameter image from the portal phase, calculated by using relative enhancement) The abnormalities are less well depicted in this phase. (d) (Color-coded parameter image from the delayed phase, calculated by using relative enhancement) No abnormalities at all. (e) (Subtraction image from the arterial phase, after treatment) Substantially less abnormal enhancement of the liver parenchyma. (f) (color-coded parameter image from the arterial phase, after treatment, calculated by using relative enhancement) Decreased heterogeneous increased enhancement of the liver. (g and h) (Two color-coded parameter images from the portal and delayed phases calculated by using relative enhancement) The abnormalities have become occult. Note: decremental value in color spectrum: red > orange > yellow > green > blue > indigo > violet.

gadolinium-enhanced MRI by using pharmaco-kinetic models[36]. Tumor regions with dense neovasculature may enhance more rapidly compared to other regions. The position of these regions is related to the distribution of viable blood supply within the tumor. In necrotic or cystic regions, vascular density can be extremely low, whereas in highly active regions, the vascular density can be high.

Dynamic contrast-enhanced MR imaging proposed as an in-vivo marker of angiogenesis

Due to its high quality and reproducible measurements, dynamic contrast-enhanced MR imaging is being proposed as an in-vivo marker of angiogenesis[22,48] with the advantage over the "gold standard" of direct histologic quantification of angiogenesis with discrepancy between "true" functional and histologic microvessel density: 20% to 85% of microvessels are perfused at any given time depending on the microenvironment[22,39]. Dynamic contrast-enhanced MR imaging may help define the pharmacological response and dose of vascular endothelial growth factor (VEGF)-mediated angiogenesis inhibitors, such as PTK787/ZK 222584, an orally active inhibitor of VFGF receptor tyrosine kinases, for further clinical development in patients with advanced colorectal cancer[49].

Functional CT versus dynamic contrast-enhanced MRI

Functional CT using multidetector row, as with dynamic contrast-enhanced MRI, has also been proposed for evaluation of tumor vascularity. Both techniques are easily incorporated into routine examinations and provide reliable quantitative perfusion data, although for both imaging modalities, there remains a lack of consensus regarding optimal acquisition technique, type of analysis method, and surrogate measurement to use[22]. There are differences between the two imaging modalities in acquisition techniques, mathematical analysis, measurement parameters, and propensity to artifacts[22]. The benefit of functional CT is the direct linear relationship between CT attenuation value and contrast agent concentration. The functional CT analysis technique includes deconvolution, distributed parameter model. Unfortunately, the risks of contrast agent reactions and potential biologic hazards from radiation exposure to the patients (especially oncologic patients that undergo repeated scans to monitor therapy response) are associated with functional CT. The radiation burden associated with a functional CT acquisition protocol is determined by the number of images in the sequence and the tube current (mAs) used for each image. Dynamic contrast-enhanced MRI does not involve the use of ionizing radiation, which is a particular advantage for serial examinations to monitor treatment response. The choice between functional CT and dynamic contrast-enhanced MRI depends on machine availability, doctor expertise, tumor location, desired parameters, and the requirement of decreased radiation burden[22].

The benefits of the color-coded images and time-intensity curves

Color-coded images can provide information concerning focal as well as diffuse disease processes. This reduces the risk of creating ROIs containing more than one tissue type, and makes further ROI analysis more accurate. In addition, the color-coded images combine both the enhancement pharmaco-kinetics of tissues and morphology, and visualize the enhancement changes over time.

The generation of TIC by placing ROIs has two benefits over functional images: 1) sampling only a limited number of pixels at once increases the signal-to-noise ratio; and 2) small spatial misregistration between points only introduces small errors. However, there are also some drawbacks. The time-intensity curves are insensitive to regional variation in the parameter being examined, small foci of high or low signal intensity may be missed as they are averaged out within an ROI, and diffuse disease may be difficult to analyze. Patient motion might lead to faulty time-signal intensity curves at each pixel, and hence to faulty functional images.

The parameters derived from the time-intensity curves, which is the basis of the color-coded images have contributions from MR imaging protocols. Therefore, it may be difficult to compare the results of studies from different institutions. Application of pharmaco-kinetic modeling has the potential to standardize these results[22].

In conclusion, the generation of color-coded images and time-intensity curves based on dynamic multiphasic gadolinium-enhanced MR imaging data sets provides new opportunities for research. Moreover, it facilitates the diagnostic work-up of hepatic disease for the detection, staging, therapeutic monitoring; and development of anti-tumor drugs.

REFERENCES

1. Hussain SM, Semelka RC. Liver masses. Magn Reson Imaging Clin N Am 2005; 13:255-275.
2. Mendez Romero A, Wunderink W, Hussain SM, et al. Stereotactic body radiation therapy for primary and metastatic liver tumors: A single institution phase i-ii study. Acta Oncol 2006; 45:831-837.
3. Materne R, Smith AM, Peeters F, et al. Assessment of hepatic perfusion parameters with dynamic MRI. Magn Reson Med 2002; 47:135-142.
4. Becker GA, Muller-Schauenburg W, Spilker ME, Machulla HJ, Piert M. A priori identifiability of a one-compartment model with two input functions for liver blood flow measurements. Phys Med Biol 2005; 50:1393-1404.
5. Materne R, Van Beers BE, Smith AM, et al. Non-invasive quantification of liver perfusion with dynamic computed tomography and a dual-input one-compartmental model. Clin Sci (Lond) 2000; 99:517-525.
6. Cosar S, Oktar SO, Cosar B, Yucel C, Ozdemir H. Doppler and gray-scale ultrasound evaluation of morphological and hemodynamic changes in liver vascualture in alcoholic patients. Eur J Radiol 2005; 54:393-399.
7. Li J, Dong BW, Yu XL, Li CF. Gray scale contrast enhancement and quantification in different positions of rabbit liver. J Ultrasound Med 2006; 25:7-14.
8. Renault G, Tranquart F, Perlbarg V, Bleuzen A, Herment A, Frouin F. A posteriori respiratory gating in contrast ultrasound for assessment of hepatic perfusion. Phys Med Biol 2005; 50: 4465-4480.
9. Krix M, Plathow C, Kiessling F, et al. Quantification of perfusion of liver tissue and metastases using a multivessel model for replenishment kinetics of ultrasound contrast agents. Ultrasound Med Biol 2004; 30:1355-1363.
10. Hussain SM, Semelka RC. Hepatic imaging: comparison of modalities. Radiol Clin North Am 2005; 43:929-947, ix.
11. Bader TR, Herneth AM, Blaicher W, et al. Hepatic perfusion after liver transplantation: noninvasive measurement with dynamic single-section CT. Radiology 1998; 209:129-134.
12. Pandharipande PV, Krinsky GA, Rusinek H, Lee VS. Perfusion imaging of the liver: current challenges and future goals. Radiology 2005; 234:661-673.
13. Hyslop WB, Balci NC, Semelka RC. Future horizons in MR imaging. Magn Reson Imaging Clin N Am 2005; 13:211-224.
14. Planchamp C, Pastor CM, Balant L, Becker CD, Terrier F, Gex-Fabry M. Quantification of Gadolinium-BOPTA uptake and biliary e cretion from dynamic magnetic resonance imaging in rat livers: model validation with 153 gadolinium-BOPTA. Invest Radiol 2005; 40:705-714.
15. Schwickert HC, Roberts TP, Shames DM, et al. Quantification of liver blood volume: comparison of ultra short TI inversion recovery echo planar imaging (ULSTIR-EPI), with dynamic 3D-gradient recalled echo imaging. Magn Reson Med 1995; 34:845-852.
16. Wang YX, Hussain SM, Krestin GP. Superparamagnetic iron oxide contrast agents: physicochemical characteristics and applications in MR imaging. Eur Radiol 2001; 11:2319-2331.
17. Pruessmann KP, Weiger M, Scheidegger MB, Boesiger P. SENSE: sensitivity encoding for fast MRI. Magn Reson Med 1999; 42:952-962.
18. Sodickson DK, Manning WJ. Simultaneous acquisition of spatial harmonics (SMASH): fast imaging with radiofrequency coil arrays. Magn Reson Med 1997; 38:591-603.
19. Wiesinger F, Van de Moortele PF, Adriany G, De Zanche N, Ugurbil K, Pruessmann KP. Potential and feasibility of parallel MRI at high field. NMR Biomed 2006; 19:368-378.
20. Weiger M, Boesiger P, Hilfiker PR, Weishaupt D, Pruessmann KP. Sensitivity encoding as a means of enhancing the SNR efficiency in steady-state MRI. Magn Reson Med 2005; 53:177-185.
21. Heidemann RM, Griswold MA, Seiberlich N, et al. Direct parallel image reconstructions for spiral trajectories using GRAPPA. Magn Reson Med 2006; 56:317-326.
22. Goh V, Padhani AR. Imaging tumor angiogenesis: functional assessment using MDCT or MRI? Abdom Imaging 2006; 31:194-199.
23. Hussain SM, Semelka RC, Mitchell DG. MR imaging of hepatocellular carcinoma. Magn Reson Imaging Clin N Am 2002; 10:31-52, v.
24. Grazioli L, Morana G, Kirchin MA, Schneider G. Accurate differentiation of focal nodular hyperplasia from hepatic adenoma at gadobenate dimeglumine-enhanced MR imaging: prospective study. Radiology 2005; 236:166-177.
25. Kim SK, Lim JH, Lee WJ, et al. Detection of hepatocellular carcinoma: comparison of dynamic three-phase computed tomography images and four-phase computed tomography images using multidetector row helical computed tomography. J Comput Assist Tomogr 2002; 26:691-698.
26. Hussain SM, Wielopolski PA, Martin DR. Abdominal magnetic resonance imaging at 3.0 T: problem or a promise for the future? Top Magn Reson Imaging 2005; 16:325-335.
27. Michaely HJ, Dietrich O, Nael K, Weckbach S, Reiser MF, Schoenberg SO. MRA of abdominal vessels: technical advances. Eur Radiol 2006; 16:1637-1650.
28. Dawson P. Functional imaging in CT. Eur J Radiol 2006 Dec; 60(3):331-40.
29. Daldrup-Link HE, Shames DM, Wendland M, et al. Comparison of Gadomer-17 and gadopentetate dimeglumine for differentiation of benign from malignant breast tumors with MR imaging. Acad Radiol 2000; 7:934-944.
30. Morana G, Grazioli L, Testoni M, Caccia P, Procacci C. Contrast agents for hepatic magnetic resonance imaging. Top Magn Reson Imaging 2002; 13:117-150.
31. Grazioli L, Morana G, Caudana R, et al. Hepato-

cellular carcinoma: correlation between gadobenate dimeglumine-enhanced MRI and pathologic findings. Invest Radiol 2000; 35:25-34.
32. Martin DR, Semelka RC, Chung JJ, Balci NC, Wilber K. Sequential use of gadolinium chelate and mangafodipir trisodium for the assessment of focal liver lesions: initial observations. Magn Reson Imaging 2000; 18:955-963.
33. Crossgrove J, Zheng W. Manganese toxicity upon overexposure. NMR Biomed 2004; 17:544-553.
34. Torheim G, Lombardi M, Rinck PA. An independent software system for the analysis of dynamic MR images. Acta Radiol 1997; 38:165-172.
35. Li X, Rooney WD, Springer CS, Jr. A unified magnetic resonance imaging pharmacokinetic theory: intravascular and extracellular contrast reagents. Magn Reson Med 2005; 54:1351-1359.
36. Tofts PS. Modeling tracer kinetics in dynamic gadolinium-DTPA MR imaging. J Magn Reson Imaging 1997; 7:91-101.
37. Kuhl CK, Mielcareck P, Klaschik S, et al. Dynamic breast MR imaging: are signal intensity time course data useful for differential diagnosis of enhancing lesions? Radiology 1999; 211:101-110.
38. Kiessling F, Krix M, Heilmann M, et al. Comparing dynamic parameters of tumor vascularization in nude mice revealed by magnetic resonance imaging and contrast-enhanced intermittent power Doppler sonography. Invest Radiol 2003; 38:516-524.
39. Jackson A, Haroon H, Zhu XP, Li KL, Thacker NA, Jayson G. Breath-hold perfusion and permeability mapping of hepatic malignancies using magnetic resonance imaging and a first-pass leakage profile model. NMR Biomed 2002; 15:164-173.
40. Preda A, van Vliet M, Krestin GP, Brasch RC, van Dijke CF. Magnetic resonance macromolecular agents for monitoring tumor microvessels and angiogenesis inhibition. Invest Radiol 2006; 41:325-331.
41. International Working Party. Terminology of nodular hepatocellular lesions. Hepatology 1995; 22:983-993.
42. Hussain SM, van den Bos IC, Dwarkasing RS, Kuiper JW, den Hollander J. Hepatocellular adenoma: findings at state-of-the-art magnetic resonance imaging, ultrasound, computed tomography and pathologic analysis. Eur Radiol 2006.
43. Terkivatan T, Hussain SM, De Man RA, IJzermans JN. Diagnosis and treatment of benign focal liver lesions. Scand J Gastroenterol Suppl 2006:102-115.
44. Hussain SM, Terkivatan T, Zondervan PE, et al. Focal nodular hyperplasia: findings at state-of-the-art MR imaging, US, CT, and pathologic analysis. Radiographics 2004; 24:3-17; discussion 18-19.
45. Terkivatan T, van den Bos IC, Hussain SM, Wielopolski PA, de Man RA, IJzermans JN. Focal nodular hyperplasia: lesion characteristics on state-of-the-art MRI including dynamic gadolinium-enhancedd and superparamagnetic iron-oxide--uptake sequences in a prospective study. J Magn Reson Imaging 2006; 24:864-872.
46. Wang J, Chen LT, Tsang YM, Liu TW, Shih TT. Dynamic contrast-enhanced MRI analysis of perfusion changes in advanced hepatocellular carcinoma treated with an antiangiogenic agent: a preliminary study. AJR Am J Roentgenol 2004; 183:713-719.
47. Folkman J. Tumor angiogenesis: therapeutic implications. N Engl J Med 1971; 285:1182-1186.
48. Leach MO, Brindle KM, Evelhoch JL, et al. Assessment of antiangiogenic and antivascular therapeutics using MRI: recommendations for appropriate methodology for clinical trials. Br J Radiol 2003; 76 Spec No 1:S87-91.
49. Morgan B, Thomas AL, Drevs J, et al. Dynamic contrast-enhanced magnetic resonance imaging as a biomarker for the pharmacological response of PTK787/ZK 222584, an inhibitor of the vascular endothelial growth factor receptor tyrosine kinases, in patients with advanced colorectal cancer and liver metastases: results from two phase I studies. J Clin Oncol 2003; 21:3955-3964.

chapter7
DISCUSSION

chapter7.1
general discussion

Magnetic resonance imaging is a diagnostic modality THAT HAS BEEN EVOLVING RAPIDLY IN THE PAST TWO DECADES.

The development of advanced software, improved coil technology, and higher magnetic field strength has allowed faster imaging, with increased temporal and spatial resolution[1].

This has resulted in the development of new sequences that have allowed improved visualisation of neoplastic processes, including fat-suppressed T2-weighted sequences and black-blood echo-planar imaging[2]. In addition, improved multiphasic dynamic imaging after intravenous administration of contrast media became feasible, which has resulted in improved timing of the arterial peak enhancement. Since analysis of peak arterial enhancement is essential for diagnosis of especially malignant lesions, time-resolved dynamic MR imaging provided improved tumor characterization possibilities[3].

The radiologic imaging work-up of primary hepatic tumors improved considerably as a result of the developments in MR imaging techniques. MR imaging is an imaging modality that is highly valuable for the differentiation of these tumors, since the combination of several T1- and T2-weighted sequences before and after administration of a gadolinium-chelate allows determination of intrinsic tissue characteristics of the lesion, with possibility to detect neovasculature in an early stage. In addition, liver-specific contrast media may provide additional information on the origin of the tumor. These characteristics make MR imaging an ideal modality for detection and differentiation of focal liver lesions[3].

Primary liver tumors are categorized according to the regenerative or dysplastic nature of the lesion in combination with the anatomic characteristics of adjacent hepatic stroma. Most common lesions are focal nodular hyperplasia (FNH), hepatocellular adenoma (HCA) and hepatocellular carcinoma (HCC)[4].

FNH and HCA most frequently occur in young women, in whom differentiation between FNH and HCA is important, in view of the risk of bleeding and potential malignant transformation in larger HCA[5]. Even though it is rare, malignant transformation has been reported repeatedly in literature. In this context, liver cell dysplasia (LCD) has been proposed as missing link between HCA and HCC, in which HCA is not pre-malignant, whilst LCD is potentially malignant and may proceed to HCC[5] (see chapter 3.1). In the diagnosis of HCA versus FNH, our studies illustrated that HCA has intratumoral fatty infiltration in most lesions whilst this is rare in FNH; HCA has less pronounced arterial enhancement than FNH, and the liver may show co-existing liver abnormalities in case of HCA. In addition, the use of liver-specific iron-oxide contrast agents (SPIO) facilitate the diagnosis of FNH, since the uptake of SPIO within the lesion improves the conspicuity of the central scar and septa which is a characteristic feature of FNH.

In routine clinical care, typically, classic FNH does not require follow-up examinations, whilst in HCA, follow-up imaging is advised every 6-12 months. MR imaging is the modality of choice for imaging of these lesions, since it provides extensive information on the tumor characteristics, has no radiation exposure and enables confident diagnosis of the lesion, including confident assessment of potential complications including hemorrhage or development of HCC[3].

HCC is the most common primary hepatocellular malignancy, and develops in at least 1-2% of patients with longstanding cirrhosis. The incidence is highest in patients with hepatitis B or C related cirrhosis or cirrhosis related to alcohol abuse, hemochromatosis or biliary abnormalities such as primary biliary cirrhosis. Men older than 50 years of age with longstanding cirrhosis and liver cell dysplasia, may develop HCC in as many as 10% of the cases. Recently, the insulin resistance syndrome (obesity, diabetes) has been described as a possible risk factor for development of HCC, but the exact relation to the rising incidence of HCC remains unclear[6]. In cirrhosis, HCC typically occurs in a step-wise fashion, which can be visualized with MR imaging[5] (see chapter 4.1). In this sequence, a regenerative nodule (RN) develops into low grade dysplastic nodule (DN I) – high grade dysplastic nodule (DN II) – small HCC – large HCC, respectively. On the other hand, HCC occurring in a non-cirrhotic liver is typically very large[7].

Early detection of HCC in patients with cirrhosis is important, to improve patient outcome and decision making in therapeutic strategies. Our studies have illustrated the potential value of MR imaging for improved detection of HCC in an early stage. Even though therapeutic possibilities for HCC have expanded greatly in the past two decades, potentially curative surgical therapy for HCC is still limited to approximately 40% of patients only. This is partly caused by an often advanced stage of liver fibrosis, but also because of often advanced HCC at presentation. Therefore, improved patient outcome depends not only on extended therapeutic options, but also on improved imaging information[5].

MR imaging is the modality of choice in the assessment of developing HCC. The MR imaging findings of developing HCC may vary, which is possibly related to the diversity in genetic pathways and a possible polygenic predisposition, but this remains to be determined. As demonstrated in our study, in the transition of a DN to HCC, it is important to assess changes in T2-weighted signal intensity, which may show increasing signal; and arterial enhancement patterns, which often show a transition of portal enhancement to true early arterial enhancement. In addition, detection of delayed phase washout in combination with delayed phase enhancement of a tumor capsule is diagnostic in many cases. However, as demonstrated in our study (chapter 4.2), it is important to realize that in the growth process of HCC, signal intensities may change, which reflects not only the intrinsic tissue characteristics, but also the changing blood supply, distribution and excretion expressed as dynamic enhancement patterns after administration of a gadolinium-chelate[5].

In the development of high magnetic field MR imaging scanners (3.0T), the increased signal-to-noise ratio (SNR, theoretically double as high) provides potential for improved hepatobiliary imaging. The doubled SNR can be utilized to significantly improve the spatial resolution in the same acquisition time, or ½ slice thickness with identical coverage, or 4-fold faster scan time for identical resolution settings[1]. However, there are some associated challenges for imaging at high magnetic field strength (3.0T) as well. These include: 1) the changed relaxation times at higher magnetic field strength, which translate in different signal intensities; 2) increased inhomogeneity of the magnetic field which results in more pronounced B_1-inhomogeneities and dielectric resonance effects that degrade image quality; and 3) increased energy deposition within the scanned subject, expressed as increased specific absorption rate levels (SAR)[1].

Nonetheless, the increased SNR was soon successfully used for markedly improved dynamic MR imaging after contrast administration, with high resolution three-dimensional T1-weighted sequences acquired with parallel imaging. T2-weighted sequences however, in particular the fast spin-echo (FSE) sequences, were limited in anatomic coverage by increased SAR levels. As demonstrated in our studies, the application of a special shape radiofrequency pulse for excitation and refocussing, the "variable-rate selective excitation (VERSE)" provides a solution for this problem, as FSE sequences obtained with VERSE provide markedly increased slice coverage. This is important for patient comfort, as it shortens total scan duration considerably. In this respect, black-blood echo-planar imaging (BBEPI) should be considered as well, as this sequence provides full volume liver coverage within a single breath-hold, with low SAR levels at 3.0T. In addition, this sequence enables improved thin-slice imaging, and high contrast of the lesion compared to the liver which will improve confident lesion detection.

In the future, semi-automated analysis of computed tomography (CT) and MR imaging exams may play an increasingly important role, as the amount of data acquired with these imaging modalities have vastly increased in the past decade and will certainly continue to rise even further. In this respect it is important to aim at acquiring near-isotropic datasets for improved automated analysis. Even though this remains challenging, the implementation of 3.0T MR imaging scanners has provided potential development in this area. Additionally, semi-automated analysis of dynamic contrast-enhanced imaging of the liver by means of color-coded techniques and generation of time-intensity curves facilitates the analysis of often very large datasets. Since hepatic perfusion is essential for analysis and differential diagnosis of either focal or diffuse liver abnormalities, quantification of these parameters may facilitate the evaluation of hepatic diseases, as is demonstrated in chapter 6. The improved visualization of the abnormality within the liver by means of color-coded images provides easy-to-interpret color images for either the less experienced radiologist or involved clinician.

Conclusions and recommendations for future research

It may be concluded that MR imaging is a highly accurate method for the detection and characterization of focal liver lesions. In the near future, spectroscopy, perfusion imaging including high resolution slice imaging and perfusion imaging with tagging, diffusion-weighted imaging and MR elastography will most likely be added to the routine work-up and follow-up of patients with suspected or proven focal liver disease, or for follow-up of treatment including chemoembolization, radiofrequency ablation therapy (RFA), or radiotherapy[8].

Therefore, it is to be expected that MR imaging will continue to expand its possibilities for versatile ab-

dominal imaging. In this context, it should be kept in mind that even though the development of current high-quality multi-slice CT scanners is very promising for the evaluation of the vasculature of the upper abdomen; it is limited for the interpretation of focal liver lesions. Potential health effects from increased radiation exposure resulting from routinely implemented multiphasic CT exams of the liver should therefore not be underestimated[9].

From this thesis, it is concluded that MR imaging can provide a non-invasive differentiation of FNH and HCA in the work-up of young women with focal liver lesions. Even though a predilection was suggested for diffuse liver abnormalities in patients with HCA, this could not be firmly established. To further address this matter, a study including both patient groups is recommended.

In the diagnostic work-up of patients with cirrhosis that are at high risk for development of HCC, MR imaging should be considered as the modality of choice. The results of this thesis show that development and evolution of HCC can be followed safely and non-invasively by means of MR imaging, as the gradual changes within the lesion can be evaluated and monitored by means of a combination of T1- and T2-weighted sequences before and after administration of an intravenous contrast agent. The accurate timing of these follow-up examinations remains to be determined. In order to address this, accurate determination of lesions at low, intermediate, or high risk for malignant transformation is recommended to allow justified follow-up criteria for improved patient care. A large multicenter trial evaluating all lesions that developed in HCC may potentially answer this question.

The main goal for further development and expansion of the potential of MR imaging should be aimed at development of fast, easy-to-apply, one-stop-shop imaging protocols for hepatobiliary imaging. In this perspective, it is possible that further development of imaging at high magnetic field strength will enable this development. Such imaging protocols should aim at prescribing a maximum duration of 5-15 minutes scan time for full work-up of patients with known or suspected liver disease, or for work-up of potential living-related donors for liver transplantation candidates.

In addition, further development and implementation of liver-specific contrast media will most likely add to facilitated diagnosis of primary liver tumors and tumors of biliary origin, or for the follow-up after focal treatment strategies, including chemo-embolization or RFA.

In conclusion, implementation of MR imaging as the primary imaging modality in clinical follow-up protocols for patients with abnormalities of the liver or biliary tree should be considered, aiming at accurate, non-invasive, patient-friendly diagnosis of hepatobiliary diseases.

REFERENCES

1. Hussain SM, Wielopolski PA, Martin DR. Abdominal Magnetic Resonance Imaging at 3.0 T: Problem or a Promise for the Future? Top Magn Reson Imaging 2005; 16:325-335.
2. Hussain SM, De Becker J, Hop WC, Dwarkasing S, Wielopolski PA. Can a single-shot black-blood T2-weighted spin-echo echo-planar imaging sequence with sensitivity encoding replace the respiratory-triggered turbo spin-echo sequence for the liver? An optimization and feasibility study. J Magn Reson Imaging 2005; 21:219-229.
3. Hussain SM, Semelka RC. Hepatic imaging: comparison of modalities. Radiol Clin North Am 2005; 43:929-947, ix.
4. International Working Party. Terminology of nodular hepatocellular lesions. Hepatology 1995; 22:983-993.
5. Van den Bos IC, Hussain SM, Terkivatan T, Zondervan PE, De Man RA. Step-wise carcinogenesis of hepatocellular carcinoma in the cirrhotic liver: demonstration on serial MR imaging. JMRI 2006 Nov; 24(5): 1071-80.
6. El-Serag HB. Hepatocellular carcinoma: recent trends in the United States. Gastroenterology 2004; 127:S27-34.
7. Verhoef C, de Man RA, Zondervan PE, Eijkemans MJ, Tilanus HW, IJzermans JN. Good outcomes after resection of large hepatocellular carcinoma in the non-cirrhotic liver. Dig Surg 2004; 21:380-386.
8. Hyslop WB, Balci NC, Semelka RC. Future horizons in MR imaging. Magn Reson Imaging Clin N Am 2005; 13:211-224.
9. Martin DR, Semelka RC. Health effects of ionising radiation from diagnostic CT. Lancet 2006; 367:1712-1714.

chapter7.2 primary hepatocellular lesions, an overview

Primary hepatocellular lesions:
IMAGING FINDINGS ON STATE-OF-THE-ART MRI;

with pathologic correlation

ABSTRACT

MR imaging is routinely used for the work-up of patients with focal or diffuse liver disease, including primary hepatocellular lesions, storage diseases, metastatic liver disease and diseases of the hepatobiliary tree. The most important MR imaging sequences used for diagnostic imaging of the liver consist of T1-weighted sequences, T2-weighted sequences, and at least the arterial and delayed phases of dynamic gadolinium-enhanced imaging. This paper provides an overview of MR imaging of primary hepatocellular lesions, and will describe: 1) the classification and etiology of primary hepatocellular lesions, including focal nodular hyperplasia, hepatocellular adenoma and hepatocellular carcinoma; 2) the step-wise carcinogenesis of hepatocellular carcinoma in cirrhosis on MR imaging; and 3) the typical imaging findings of primary hepatocellular lesions on MR imaging, with differential diagnoses.

INTRODUCTION

Annually, thousands of patients worldwide undergo an imaging work-up for the evaluation of proven or suspected diffuse or focal liver disease. In most centers, a combination of different imaging modalities is used for detection and characterization, including one or more of the following: ultrasonography (US), computed tomography (CT), positron emission tomography (PET) and magnetic resonance (MR) imaging. These imaging modalities have fundamental differences in the data acquisition, which translates in different accuracy in detecting and characterizing the type of liver disease that they interrogate. Currently, no strict consensus for the optimal imaging work-up for evaluation of the liver exists. Therefore, the choice of the applied imaging modality often depends of the referring physician and the expertise of the local radiologist[1]. MR imaging is often used as a problem-solving modality, and valued for its potency for the evaluation of intrinsic tissue characteristics, the possibility for multiphasic dynamic contrast-enhanced imaging, the possibility to use liver-specific contrast agents, and all without radiation exposure[1].

Current state-of-the-art MR imaging protocols consist of a set of T1-weighted and T2-weighted sequences; and dynamic contrast-enhanced imaging in multiple phases after intravenous administration of a gadolinium-chelate[2]. In our institute, the routine liver imaging protocol consists of single-shot fast spin-echo (SSFSE) images with varying echo-times (TE) in the axial and coronal planes; in- and opposed phase T1-weighted gradient-echo (GRE); either 3D fat-suppressed or 2D non-fat-suppressed dynamic multiphasic gadolinium-enhanced sequences in at least the arterial, portal, venous and delayed phases; and a T2-weighted fast spin-echo (FSE) sequence with fat suppression. The coronal and axial SSFSE sequences can be used for a quick overview of the abdominal anatomy as well as localizers for planning of the other sequences. Our liver protocol contains axial shorter and longer TE SSFSE sequences that are used to make distinction between lesions with high-fluid content and solid lesions[2]. Chemical shift imaging (in- and opposed phase T1-weighted GRE) are essential for the detection of the fatty infiltration of the liver (steatosis) and lesions. Dynamic time-resolved multiphasic imaging gives valuable information on the dual-blood supply of the liver, which consists of inflowing blood from both the hepatic artery (25%) and the portal vein (75%) as well as the enhancement patterns of focal liver lesions[3]. Last, the fat-suppressed T2-weighted FSE sequence with moderate T2-weighting which is routinely performed only after the dynamic gadolinium-enhanced sequence has been performed[4], provides valuable information for the detection of focal liver lesions, since most lesions will be depicted with high liver-to-lesion contrast on this sequence.

This paper provides an overview of MR imaging of primary hepatocellular lesions, and will describe: 1) the classification and etiology of primary hepatocellular lesions, including focal nodular hyperplasia, hepatocellular adenoma and hepatocellular carcinoma; 2) the step-wise carcinogenesis of hepatocellular carcinoma in cirrhosis on MR imaging; and 3) the typical imaging findings of primary hepatocellular lesions on MR imaging and differential diagnoses.

Indra C. van den Bos, MD[1], Shahid M. Hussain, MD, PhD[1,2], Robert A. de Man, MD, PhD[3], Pieter E. Zondervan, MD[4], Jan N.M. IJzermans, MD, PhD[5], Gabriel P. Krestin, MD, PhD[1]

Departments of [1]Radiology, [3]Gastroenterology & Hepatology, [4]Pathology and [5]Surgery, Erasmus MC, University Medical Center Rotterdam, The Netherlands; and [2]Department of Radiology, University of Nebraska Medical Center, Omaha, NE, USA

Current Problems in Diagnostic Radiology, in press

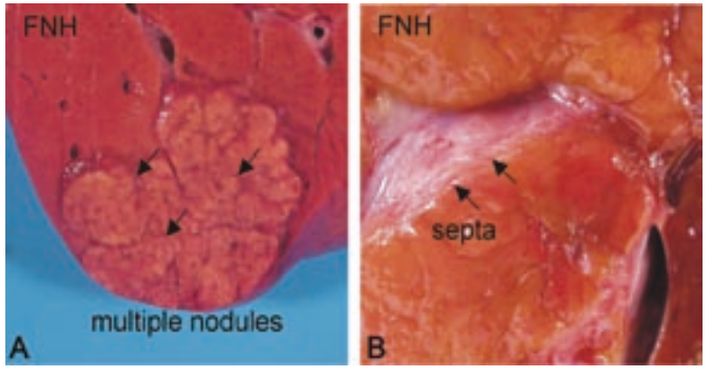

Figure 1: Focal nodular hyperplasia (FNH), illustrating the multinodular appearance of these lesions. (a) Macroscopic image of a subcapsular FNH, with multiple nodules within the lesions. (b) detailed view of the FNH, illustrating fibrous septa surrounding the nodules.

Current terminology and classification

In 1995, an International Working party established a classification system for the evaluation of primary hepatocellular nodules[5]. In this classification, nodular lesions within the liver are classified according to the regenerative or neoplastic nature of the lesions; and the characteristics of adjacent hepatocellular stroma. This results in 1) regenerative; and 2) dysplastic or neoplastic nodules.

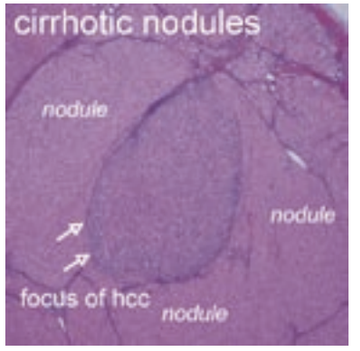

Figure 2: Multiple regenerative cirrhotic nodules in a patient with longstanding cirrhosis, photomicrograph x40, H&E staining. This illustrates the presence of multiple regenerative nodules surrounded by fibrous bands, and a focus of HCC (<1 mm), with high grade atypia, increased nuclear density with mitoses, and hepatocytes organized in >3 plates.

Regenerative nodules

The regenerative nodules consist of a localized proliferation of hepatocytes and supporting hepatic stroma, resulting in the following lesions: monoacinar nodules; multiacinar nodules; lobar or segmental hyperplasia; focal nodular hyperplasia (FNH); and cirrhotic nodules[5].

A monoacinar or multiacinar regenerative nodule contains either only one (monoacinar) or multiple (multiacinar) portal tracts, and are assumed to have developed in response to altered circulation, necrosis, or other stimuli[6]. Lobar or segmental hyperplasia entails a more diffuse hyperplastic reaction, in which a complete or part of the liver lobe has enlarged. This is usually accompanied by atrophy, necrosis, or fibrosis of other areas of the liver[5]. In FNH, the gross appearance consists of multiple nodules composed of hepatocytes, which are surrounded by radiating septa originating in a central fibrous scar[7] (Fig. 1). In cirrhotic regenerative nodules, diffuse nodular changes with micro- (<3 mm) and/or macrodules (>3 mm) are observed within the liver, surrounded by thin fibrous septa. As a rule, within regenerative nodules, no dysplastic or neoplastic pathologic features such as increased cellularity, atypical nuclei and/or chaotic distribution are present.

Dysplastic or neoplastic nodules

The dysplastic and neoplastic hepatocellular nodules consist of hepatocytes that show histological characteristics of abnormal growth caused by genetic alteration. These lesions include: hepatocellular adenoma (HCA), dysplastic foci, dysplastic nodules with or without a focus of HCC, and hepatocellular carcinoma (HCC).

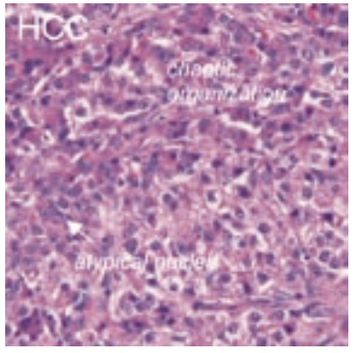

Figure 3: Photomicrograph (x100, H&E stain) of HCC in longstanding cirrhosis, showing a profoundly chaotic organization of the hepatocytes, increased cellular and nuclear density, and atypical nulei with mitoses.

Even though the growth pattern of HCA is relatively

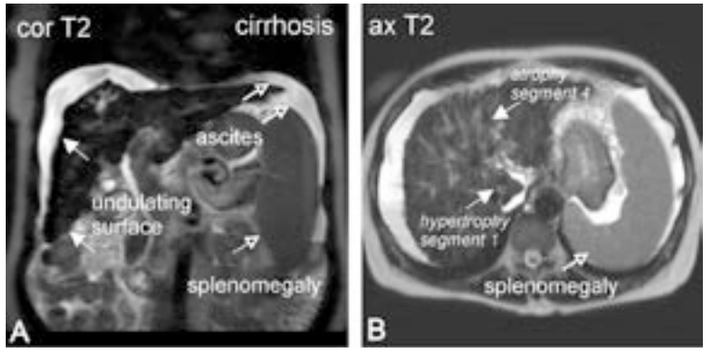

Figure 4: Histology proven cirrhosis in a patient with longstanding hepatitis-B related cirrhosis. (a) Coronal T2-weighted single-shot fast spin-echo (FSE), showing an undulating liver surface, and portal hypertension with splenomegaly and ascites. (b) Axial T2-weighted single-shot FSE, showing a macronodular cirrhotic liver with changed segmental distribution, with a hypertrophic segment 1 (caudate lobe) and an atrophic segment 4.

benign, the International Working Party classified this lesion as neoplastic due to rare reports of malignant transformation into HCC[8]. Dysplasia is defined as presence of cytoplasmic and/or nuclear changes within a cluster of hepatocytes, without definite histologic criteria of malignancy[2]. A dysplastic focus consists of a localized cluster of hepatocytes with dysplastic features, measuring <1 mm in diameter. Dysplastic nodules are often found in cirrhotic liver disease, and can show either low- or high-grade dysplasia. In high-grade dysplastic nodules, the atypia is at least moderate, but insufficient for the diagnosis of malignancy. In addition, microscopic evaluation of these nodules shows increased number of cells, increased nuclei-to-cytoplasm ratios, and increased layers of hepatocytes[5]. HCC is a malignant neoplasm composed of cells with hepatocellular differentiation, and may occur as a focus of HCC in a highly dysplastic nodule (Fig. 2). A small HCC is defined as <2 cm. The differentiation of a highly dysplastic nodule from a small HCC can be challenging, but the following criteria favor malignancy: 1) increased cellularity; 2) loss of normal reticulin structure; 3) plates three or more cells thick; and 4) invasion of stroma or surrounding portal tracts[2] (Fig. 3).

Step-wise carcinogenesis of HCC in cirrhosis

Even though the gold standard for diagnosis of liver cirrhosis is histologic, the following MR imaging criteria are routinely used for the assessment of either presence or absence of cirrhosis[9, 10]:

1) undulating liver surface with nodularity;
2) changed segmental distribution, consisting of hypertrophy of Couinaud's segment 1 (caudate lobe), atrophy of segment 4, enlargement of the periportal spaces and expansion of the gallbladder fossa;
3) secondary signs of portal hypertension, including splenomegaly, collateral formation and/or ascites (Fig. 4).

In cirrhotic livers, HCC typically develops in a step-wise fashion, as described by Sakamoto et al in 1991[11].

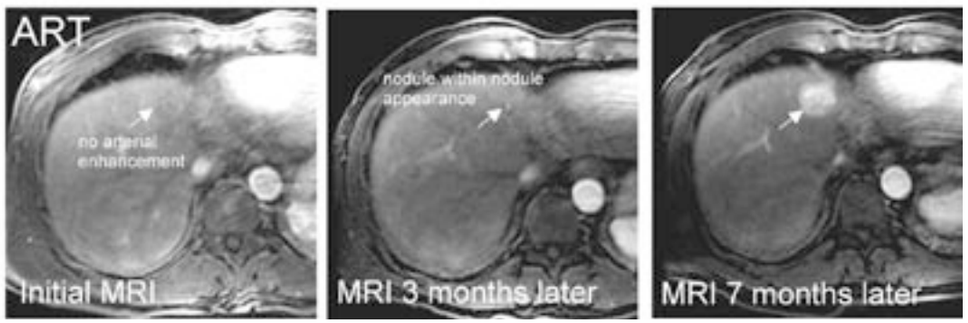

Figure 5: Developing HCC in a patient with hepatitis-B related cirrhosis, in which in developing HCC is visible on arterial phase 3D fat-suppressed T1-weighted gradient-echo. Three months after the initial MRI, HCC with a nodule-within-nodule appearance is visible within a dysplastic nodule. Because patient refused to undergo treatment and regular follow-up, unfortunately, seven month after the second MRI, full-blown HCC had developed, with washout and tumor capsule enhancement in the delayed phase (not shown).

According to their findings, the step-wise carcinogenesis of HCC is based on increasing cellularity, changing vascularity and increasing lesion size. The currently accepted nomenclature in step-wise carcinogenesis of HCC is regenerative nodule (RN) – low grade dysplastic nodule (DN I)) – high grade dysplastic nodule (DN II) – small HCC – large HCC[12]. In this sequence, the nodule shows gradually increasing cellularity, nuclear atypia, and changing vascularity surrounding the lesion, which can be observed as a slow transition from portal vein to hepatic artery inflow[13]. The appearance of these tumor arteries is essential for development and sustained growth of the HCC. When a focus of HCC develops within a dysplastic nodule, this may be observed as a "nodule-within-nodule" appearance on MR imaging, as was described by Mitchell et al in 1995[14].

As demonstrated in a recent study[15], the step-wise development of HCC in cirrhosis may show a spectrum of MR imaging findings, including: 1) localized fatty infiltration within a developing dysplastic nodule that gradually evolved into HCC; 2) development of a focus of HCC with high T2-signal intensity in a dysplastic nodule; 3) prominent neovasculature as initial sign of fast growing HCC. Therefore, on MR imaging, developing HCC in the step-wise carcinogenesis may be associated with fat accumulation; gradual increase in size; increasing signal intensity on T2-weighted images; progressive enhancement in the arterial phase with a nodule-within-nodule appearance (Fig 5); and progressive washout of contrast material in the delayed phase[15].

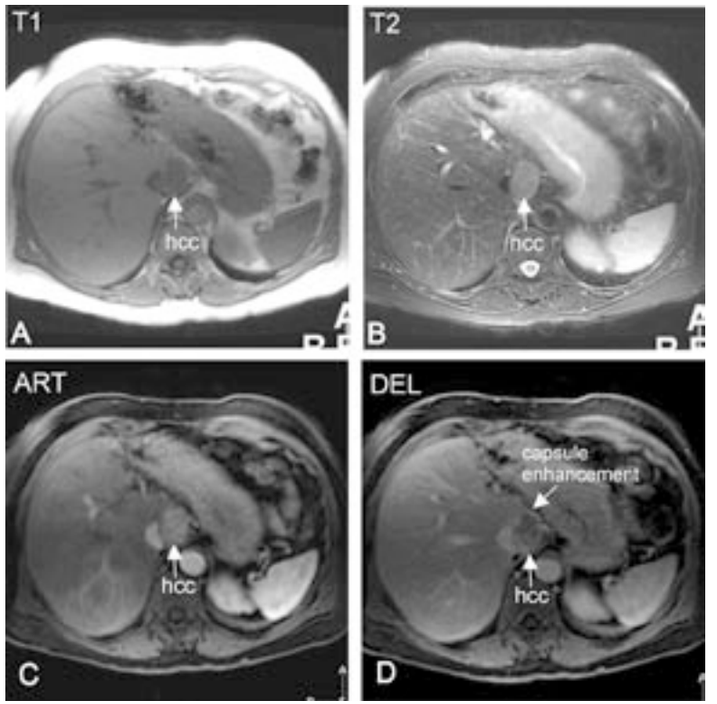

Figure 6: HCC in a patient with hepatitis-B related cirrhosis, showing classical MR imaging findings of HCC. (a) In-phase T1-weighted gradient-echo (GRE), showing a hypointense signal of HCC in segment 1 (caudate lobe). (b) Fat-suppressed T2-weighted FSE, showing hyperintense signal intensity of the HCC. (c) Arterial-phase 3D fat-suppressed T1-weighted GRE, showing marked arterial enhancement of the HCC. (d) Delayed-phase image of the same sequence, illustrating washout of contrast material and delayed enhancement of a fibrous tumor capsule surrounding the HCC.

MR imaging of hepatocellular carcinoma

Hepatocellular carcinoma (HCC) is the most common primary neoplasm of the liver. The incidence is highest in patients with hepatitis B or C related cirrhosis and cirrhosis related to alcohol abuse, metabolic liver diseases and others[16, 17]. The tumor marker for HCC is alpha-fetoprotein (AFP). Even though AFP is not specific for HCC, and can give false-positive results in hepatitis, fibrosis, and cirrhosis, it is useful in monitoring the disease process in combination with imaging results[18]. Currently, treatment of HCC includes liver transplantation, segmental liver resection, percutaneous minimal invasive therapies, such as radiofrequency ablation (RFA), stereotactic radiation therapy[19], transarterial (chemo)-embolization procedures and gene or immune therapies[20]. Curative therapy of HCC is still limited to approximately 40% of cases only, which is partly

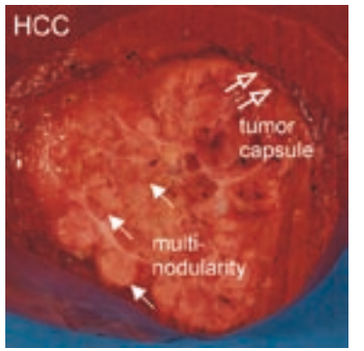

Figure 7: Macroscopic image of a subcapsular HCC in a patient with cirrhosis, illustrating intratumoral multinodularity and a fibrous tumor capsule surrounding the lesion.

related to often advanced HCC at presentation[21]. This makes early detection and characterization of HCC of paramount importance.
Classic MR imaging findings of HCC include a slightly hypointense signal on in-phase T1-weighted sequences; hyperintense signal intensity on T2-weighted sequences; increased heterogeneous arterial enhancement; and washout with fibrous tumor capsule enhancement in the delayed phase[12] (Fig. 6). However, since the introduction of current state-of-the-art MR imaging sequences, HCC can be detected when lesions are still small. According to a recent study, the imaging finding of HCC are related to the size of the tumor[22] (unpublished data). In this study, it is shown that 1) smaller HCC have tendency for hypo- or isointensity on fat-suppressed T2-weighted sequences; 2) smaller HCC show more pronounced arterial enhancement compared to larger HCC; and 3) smaller HCC show less pronounced washout in the delayed phase. Multinodularity or mosaic pattern within the lesion can be observed in especially larger HCC, including intratumoral fatty infiltration. At histology, HCC is often composed of multiple intratumoral nodules with different tissue characteristics (including fatty infiltration, accumulation of iron), surrounded by a fibrous tumor capsule (Fig. 7).

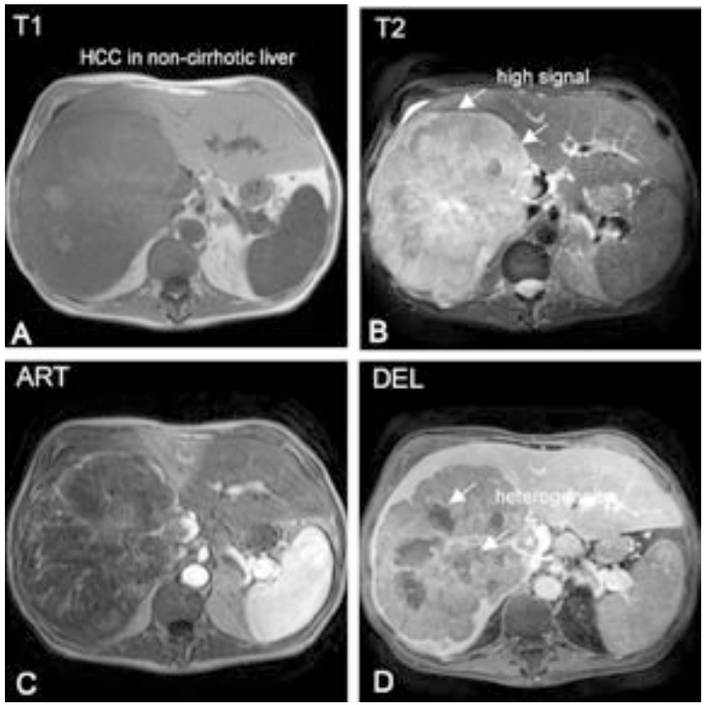

Figure 8: large HCC in a patient with a non-cirrhotic liver. (a) In-phase T1-weighted gradient-echo (GRE), showing a heterogeneous, predominantly hypointense signal intensity of the HCC. (b) Fat-suppressed T2-weighted fast spin-echo, showing a heterogeneous hyperintense signal intensity of the HCC. Note a thin layer of ascites surrounding the liver. (c) Arterial phase 2D T1-weighted GRE, showing heterogeneous arterial enhancement of intratumoral vessels. (d) Delayed phase 3D fat-suppressed T1-weighted GRE, showing washout, marked heterogeneity and enhancement of a fibrous tumor capsule. Note invasion of the tumor in the main portal vein (asterisk).

HCC in non-cirrhotic liver

HCC occurring in non-cirrhotic liver is typically very large (mean size 9 cm), and has a better prognosis compared to HCC occurring in cirrhosis[23]. Often, the lesion has striking heterogeneity, with extensive multinodularity within the lesion. A central scar may occur within the lesion, and a thick fibrous tumor capsule is virtually always present[6]. If the surrounding tumor capsule ruptures, satellite lesions may be observed in proximity to the main tumor. Tumor invasion may be observed in the adjacent venous vessels (most frequently the portal vein) (Fig. 8).
On MR imaging, typically, a hypointense signal intensity is observed on T1-weighted sequences, and intratumoral fatty infiltration may be present (with decrease in signal intensity on the opposed-phase T1-weighted images). On T2-weighted sequences, the lesions are typically hyperintense, with marked heterogeneity. In the arterial phase, the enhancement pattern is usually hypervascular, with marked heterogeneity; whilst delayed phase imaging typically shows marked washout, heterogeneity and enhancement of a thick fibrous tumor capsule[6] (Fig. 8).

Hepatocellular adenoma

HCA occurs mainly in young women, and is strongly related to use of oral contraceptives (OC)[24]. In fact, the incidence of HCA strongly increased since the introduction of OC in the 1960s[25]. Non-OC-related causes of HCA include (glycogen) storage disease, and hormonal stimulation from other sources, such as anabolic steroid use by body builders, pregnancy or hormone production by a (gynecological) neoplastic lesion[26]. Diagnosis of HCA is important, since HCA is associated with a risk of (potentially life-threatening) hemorrhage or rarely, malignant transformation[26, 27]. For differentiation with FNH, it is helpful to realize that HCA: has intratumoral fatty infiltration in up to >70%[28]; has homogeneous, less pronounced, arterial enhancement compared to FNH; may occur with single or multiple lesions (sometimes with liver steatosis); and is associated with hemorrhage. HCA with malignant degeneration into HCC may show more heterogeneity, delayed phase washout and capsule enhancement. Often, HCA occurs with multiple lesions, which is recognized as hepatic adenomatosis. However, it should be kept in mind that these two entities show identical characteristics on histopathology, therefore, presumably, both entities represent the same ongoing disease process[29].
At histology, HCA consists solely of hepatocytes which are organized in plates that are one or three cell layers thick. Typically, HCA lacks bile ductules, which facilitates the distinction from FNH[29]. Intratumoral fatty infiltration is present in >70%, and microscopic areas of previous hemorrhage are often detected (Fig. 9).
On MR imaging, HCA typically does not differ much from the surrounding liver on in-phase T1-weighted GRE and T2-weighted sequences, confirming in fact its primary nature (Fig. 10). Since underlying liver abnormalities are frequent, with steatosis in a majority of cases, most HCA become hyperintense to the surrounding liver on opposed-phase T1-weighted images[30] (unpublished data). In case of intratumoral fatty infiltration, the opposed-phase T1-weighted GRE shows decreased signal intensity of the lesion compared to the signal intensity on the in-phase T1-weighted GRE (Fig. 11). On T2-weighted sequences, the signal intensity may vary from hyperintensity to, rarely, hypointensity, related to the degree of fatty infiltration either within the lesion and/or the surrounding liver[26]. In the arterial phase after gadolinium, HCA typically enhances with a faint blush, typically less intense than FNH, with fading to isointensity in the delayed phase without washout or enhancement of a fibrous tumor capsule (Fig. 10). HCA may be surrounded by a complete or partial pseudocap-

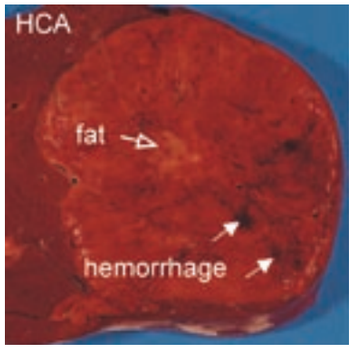

Figure 9: Macroscopic image of resected HCA, showing focal fatty infiltratin and small areas of hemorrhage within the lesion.

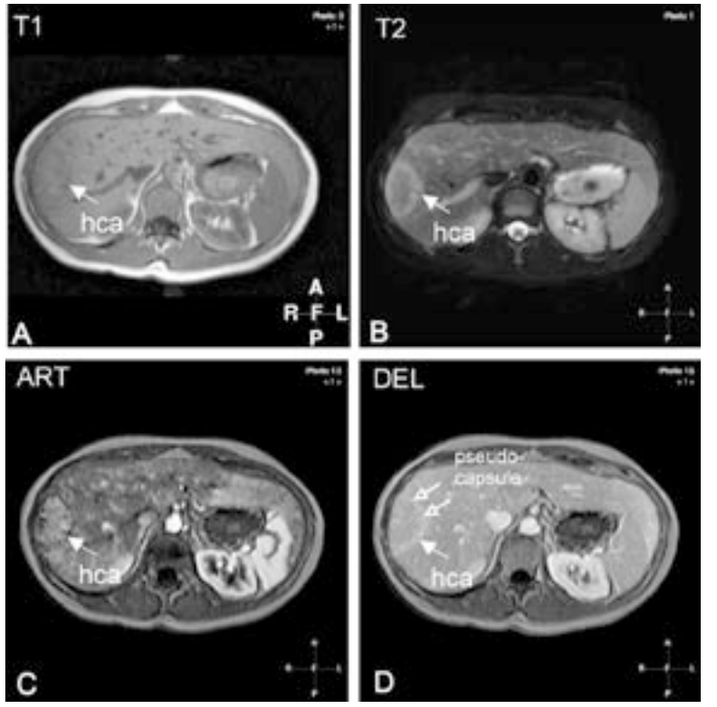

Figure 10: HCA in young female patient. (a) In-phase T1-weighted gradient-echo (GRE), showing isointensity of the HCA. (b) Fat-suppressed T2-weighted fast spin-echo, showing slight hyperintensity of the lesion. Note the hyperintensity of the surrounding pseudocapsule. (c) Arterial-phase 2D T1-weighted GRE, showing a faint blush enhancement pattern. (d) Delayed-phase 2D T1-weighted GRE, showing persistent enhancement with isointensity with the surrounding liver. Note the persistent enhancement of the surrounding pseudocapsule (open arrow).

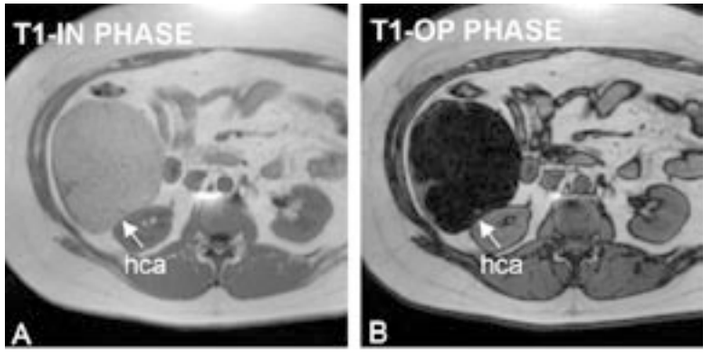

Figure 11: HCA in a female patient. (a) In-phase T1-weighted gradient-echo (GRE) shows isointensity of the HCA. (b) Opposed-phase T1-weighted GRE shows profound decrease in signal of the HCA, indicating intratumoral fatty infiltration.

sule, which consists of compressed hepatic parenchyma and compressed vessels, which typically has high signal intensity on T2-weighted sequences and persistent delayed-phase enhancement (Fig. 10). A relatively thick capsule with low signal intensity on T2-weighted images and delayed enhancement may suggest malignant nature of the lesion.

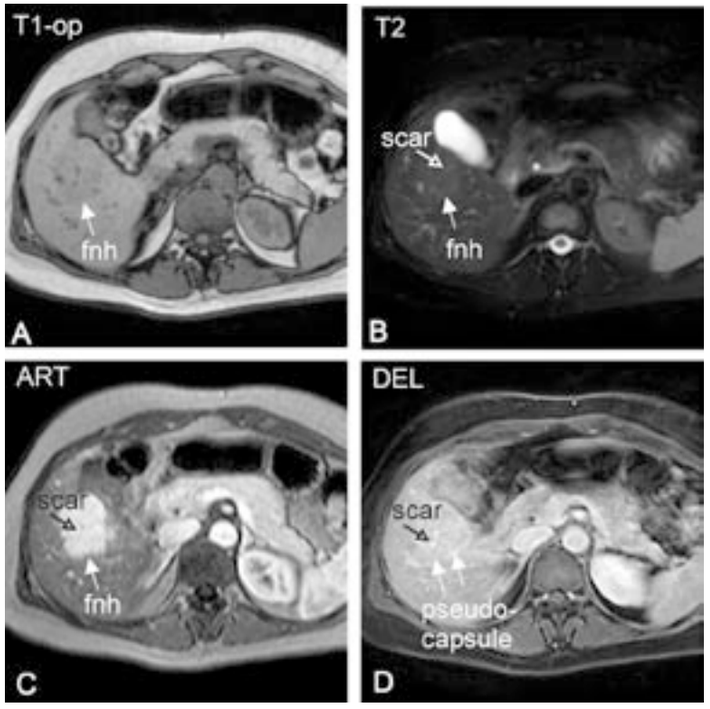

Figure 12: FNH in a young female patient. (a) Opposed-phase T1-weighted gradient-echo (GRE) shows only slight hypointensity compared to the surrounding liver. (b) Fat-suppressed T2-weighted fast spin-echo (FSE) shows isointensity – to slight hyperintensity – of the FNH, with a slightly hyperintense central scar (open arrow). (c) Arterial-phase 2D T1-weighted GRE shows very strong enhancement of the FNH. Note the lobulated contours, and less enhancement of the central scar. (d) Delayed-phase 3D fat-suppressed T1-weighted GRE shows persistent enhancement of the FNH, and enhancement of the central scar, radiating septa and pseudocapsule.

Focal nodular hyperplasia

FNH is the second most common benign liver tumor after hemangioma, the incidence is 0.9%[31]. Underlying vascular malformations have been suggested to explain the underlying pathogenesis, but this is not well understood[7]. FNH occurs mainly in young women (man:women ratio 1:8), and there is no relation with oral contraception use[31]. In approximately 20%, multiple FNHs are found. The combination of multiple FNHs and hemangiomas is considered as multiple FNH syndrome[32]. Since FNH is usually observed in young to middle-aged women and is usually asymptomatic, the distinction between FNH and other hypervascular liver lesions such as HCA, HCC, and hypervascular metastases is essential to ensure proper treatment. In patients with symptoms related to the lesion or in ambiguous cases, transarterial embolization or surgical resection may be considered[32]. At histology, FNH is composed of multiple nodules surrounded by fibrous bands (Fig. 1), and typically, malformed vascular structures are found within the central scar.

On MR imaging, typically, the signal intensity of FNH does not differ much from the surrounding liver on T1- and T2-weighted sequences before the administration of a gadolinium-chelate[33]. Therefore, on T1-weighted sequences, the signal is often only slightly hypointense to the surrounding liver. In a recent study, intratumoral fatty infiltration within FNH was observed in approximately 6%, with decreased signal intensity on the opposed-phase T1-weighted GRE impressed surrounding blood vessels. This pseudocapsule is typically very thin, with low T1-signal, slightly higher T2-signal and may show persistent enhancement in the delayed phase after gadolinium[32] (Fig. 9).

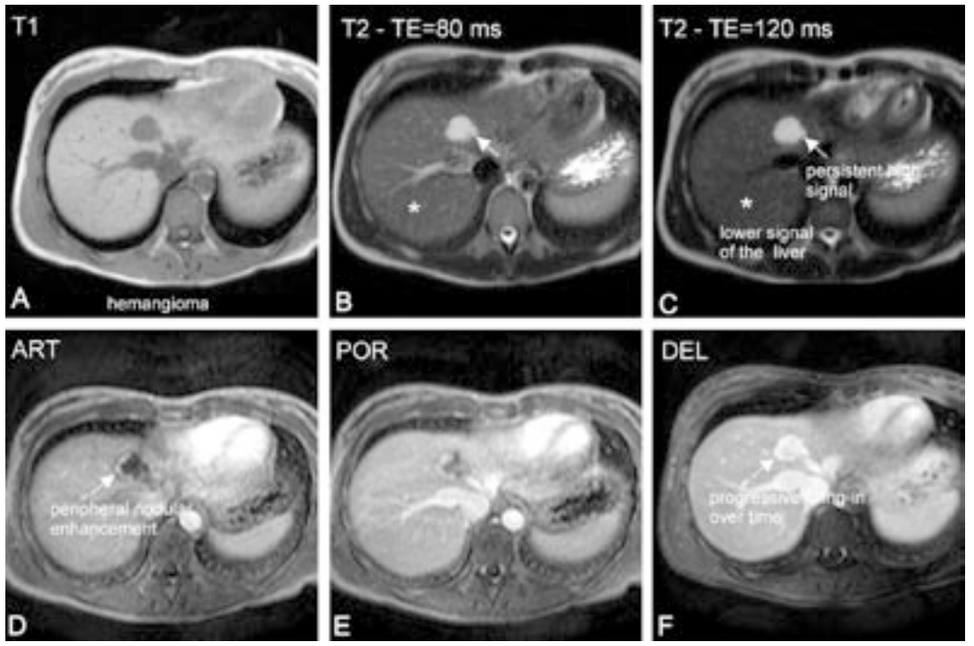

Figure 13: Medium-sized hemangioma in the right liver lobe. (a) In-phase T1-weighted gradient-echo (GRE), showing hypointensity of the lesion. Note that the signal intensity is lower compared to primary liver lesions. (b) Single-shot T2-weighted fast spin-echo (TE 80msec), illustrating very high fluid-like signal intensity of the hemangioma. (c) Single-shot T2-weighted fast spin-echo (TE 120msec), showing persistent high signal of the hemangioma, whilst the liver (a solid organ) has dropped in signal intensity. (d) Arterial-phase 2D T1-weighted GRE, showing peripheral nodular enhancement in a discontinuous ring. (e) Portal-phase 2D T1-weighted GRE, showing progressive filling-in of contrast towards the center of the hemangioma over time l. (f) Delayed-phase fat-suppressed 3D T1-weighed GRE, showing persistent enhancement of the hemangioma.

ages[33]. On T2-weighted sequences, FNH is typically slightly hyperintense. In the arterial phase after administration of gadolinium, FNH typically enhances strongly hypervascular, with persistent enhancement or fading to isointensity with the liver in the delayed phase (Fig. 9). The typical morphology of FNH is a lobulated lesion which consists of multiple nodules, with a central scar and radiating septa that surround these nodules. Typically, the central scar has low signal intensity on T1- and slightly higher signal on the T2-weighted sequences, with delayed enhancement after gadolinium (Fig. 9). In a recent study it was shown that additional administration of a liver-specific iron containing contrast agent (superparamagnetic iron-oxide particles, SPIO), facilitates the visualization of a central scar, since this area within the lesion does not contain any Kupffer cells[33]. Last, FNH is typically surrounded by a thin pseudocapsule, which consists of compressed surrounding hepatic stroma and com-

Differential diagnosis

For improved differential diagnosis of liver lesions, it is important to consider the appearance of the surrounding liver parenchyma. Fibrosis or cirrhosis of the liver can be caused by a variety of exogeneous and endogeneous causes, including: toxic agents (including aftatoxin), obesity, alcoholism, viral infections (hepatitis B and C being the most common infectious agents), and metabolic or genetic disorders, including hemochromatosis[2].

The International Working Party (1995) has advised not to diagnose HCA and FNH in the setting of cirrhosis[5]. Therefore, the differential diagnosis of a nodule or multiple nodules in case of a cirrhotic liver should always include regenerative nodule, dysplastic nodule (low or high grade), or HCC. A hypervascular lesion within a cirrhotic liver will be likely a HCC or high grade dysplastic nodule unless proven otherwise.

Differential diagnoses in case of a non-cirrhotic liver

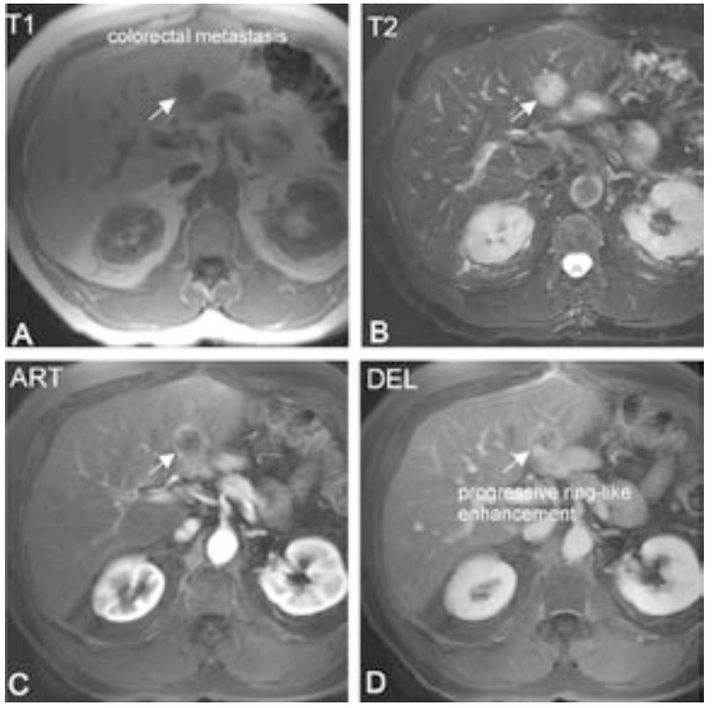

Figure 14: Colorectal metastasis in a patient with sigmoid adenocarcinoma. (a) In-phase T1-weighted gradient-echo (GRE), showing hypointensity of the metastasis. (b) Fat-suppressed T2-weighted fast spin-echo (FSE), showing marked hyperintensity of the lesion. (c) Arterial-phase fat-suppressed 3D T1-weighted GRE, showing ring-like enhancement. (d) Delayed-phase fat-suppressed 3D T1-weighted GRE, showing progressive ring-like enhancement over time with a target appearance. These findings are typical for colorectal liver metastasis.

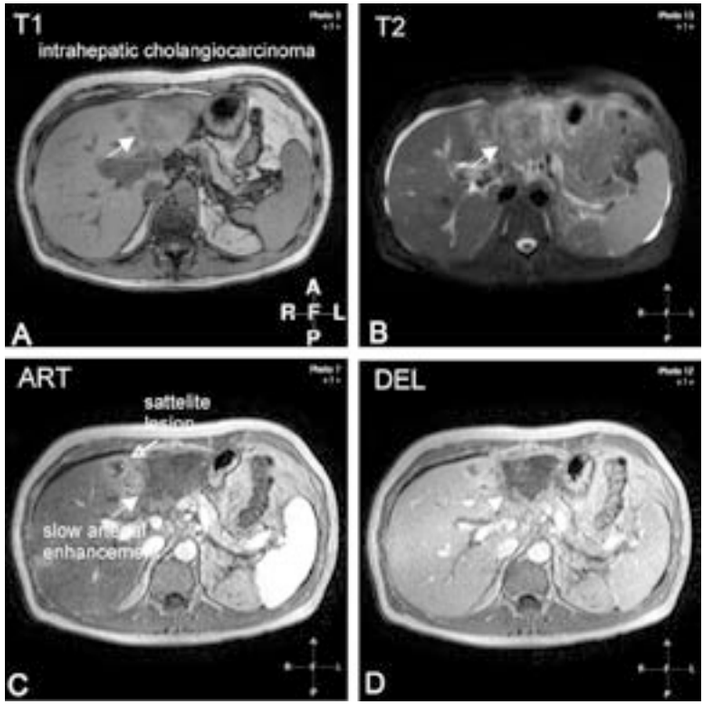

Figure 15: Intrahepatic peripheral cholangiocarcinoma in the left liver lobe. (a) Opposed-phase T1-weighted gradient-echo (GRE), showing a heterogeneous slightly lower signal intensity of the lesion. (b) Fat-suppressed T2-weighted image, showing a heterogeneous higher signal intensity of the lesion Note a small rim of ascites surrounding the liver and spleen. (c) Arterial phase 2D T1-weighted GRE, showing very slow enhancement of the lesion. Note several satellite lesions in proximity to the main tumor. (d) Delayed-phase 2D T1-weighted GRE, showing slow progressive enhancement of the lesion.

should include the following entities: 1) FNH (no washout in the delayed phase, presence of a central scar); 2) HCA (no washout in the delayed phase, often intratumoral fatty infiltration present); 3) HCC (large single lesion, striking heterogeneity in especially larger lesions, washout in the delayed phase, delayed enhancement of a fibrous tumor capsule (note that intratumoral fatty infiltration or central scar may rarely be present)); 4) hypervascular metastasis (ring-like enhancement with target-like appearance); 5) intrahepatic cholangiocarcinoma; 6) vascular abnormalities, such as arterio-portal or porto-venous shunts; 7) flash-filling hemangiomas.

The MR imaging features of these lesions include the following:

Hemangioma: typically shows very high T2-signal intensity, indicating the non-solid nature. In addition, on T2-weighted single-shot FSE images with shorter and longer TE, the T2-signal shows only minimal signal decay indicating the high fluid-content of the lesion. In dynamic gadolinium-enhanced imaging, hemangioma shows a peripheral nodular enhancement in a discontinuous ring in the arterial phase, with filling-in towards the center of the lesion over time (Fig. 13). Large hemangioma may contain a central fibrous scar[12]. Flash-filling hemangioma may show some atypical findings which include rapid (or flash-filling) enhancement, with or without perilesional enhancement or shunting. The appearance in the delayed phase[12] on the other hand, is the same as the classical hemangioma with persistent enhancement in the delayed phase.

Colorectal metastasis: typically shows low signal intensity on T1-weighted sequences, never with intratumoral fatty infiltration. On T2-weighted sequences, the signal is slightly hyperintense compared to the surrounding liver. After gadolinium, the colorectal metastasis shows a progressive ringlike (onion-ringlike) enhancement towards the center of the lesion over time, with hypointense areas in the delayed phase (Fig. 14). Hypervascular metastases, including neuroendocrine tumors (or carcinoids) and islet cell tumors; typically show very high signal intensity on the T2-weighted sequences, which nearly equals the signal intensity of fluid. After gadolinium, the lesions show irregular ring-shaped or heterogeneous enhancement in the arterial phase, with delayed phase washout.

Intrahepatic peripheral cholangiocarcinoma: on T1-weighted sequences, the signal intensity usually is slightly lower, with heterogeneity. On T2-weighted sequences, signal intensity is heterogeneously hyperintense, and typically, dilated bile ducts may be observed both within and in the periphery of the lesion. After gadolinium, the enhancement pattern is usually slow and progressive over time. Pooling of contrast may occur in the delayed phase as a large amount of fibrosis is usually present within the tumor[34] (Fig. 15). Differential diagnosis with HCC may be challenging, but the most important features to consider are: 1) there is usually no liver cirrhosis (although this may rarely occur, such as in underlying primary sclerosing cholangitis); 2) the enhancement is very slow; and 3) there is no fibrous tumor capsule surrounding the lesion[34].

CONCLUSION

Primary hepatocellular tumors are classified according to the nature of the lesion and the characteristics of the surrounding liver. Currently, no strict consensus for the optimal imaging work-up for evaluation of the liver exists, but MR imaging is often used as a problem-solving modality, and is valued for its potency for the evaluation of intrinsic tissue characteristics, and the possibility for multiphasic dynamic contrast-enhanced imaging. The most important MR imaging sequences used for diagnostic imaging of the liver consist of T1-weighted sequences, T2-weighted sequences, and at least the arterial and venous phases of dynamic gadolinium-enhanced imaging. In this review article, the imaging findings of the most important primary liver lesions are discussed, including focal nodular hyperplasia, hepatocellular adenoma and hepatocellular carcinoma; with a variety of other lesions that must be considered in the differential diagnosis of these lesions. This article will enable the reader to understand the classification of primary hepatocellular lesions, to understand the step-wise carcinogenesis of hepatocellular carcinoma, and to evaluate the typical MR imaging findings of the most common lesions.

REFERENCES

1. Hussain SM, Semelka RC. Hepatic imaging: comparison of modalities. Radiol Clin North Am 2005; 43:929-947, ix.
2. Hussain SM. Liver MRI; Correlation with other imaging modalities and histopathology. Heidelberg: Springer-Verlag, 2007.
3. Burt A, Day C. Pathophysiology of the liver. In: MacSween RNM BA, Portmann BC, ed. Pathology of the liver: Churchill Livingstone, 2002; 67-104.
4. Jeong YY, Mitchell DG, Holland GA. Liver lesion conspicuity: T2-weighted breath-hold fast spin-echo MR imaging before and after gadolinium enhancement--initial experience. Radiology 2001; 219:455-460.
5. International Working Party. Terminology of nodular hepatocellular lesions. Hepatology 1995; 22:983-993.
6. Hussain SM, Zondervan PE, IJzermans JN, Schalm

discussionPRIMARY HEPATOCELLULAR LESIONS, AN OVERVIEW

SW, de Man RA, Krestin GP. Benign versus malignant hepatic nodules: MR imaging findings with pathologic correlation. Radiographics 2002; 22: 1023-1036; discussion 1037-1029.
7. Wanless IR, Mawdsley C, Adams R. On the pathogenesis of focal nodular hyperplasia of the liver. Hepatology 1985; 5:1194-1200.
8. Gyorffy EJ, Bredfeldt JE, Black WC. Transformation of hepatic cell adenoma to hepatocellular carcinoma due to oral contraceptive use. Ann Intern Med 1989; 110:489-490.
9. Ito K, Mitchell DG, Hann HW, et al. Viral-induced cirrhosis: grading of severity using MR imaging. AJR Am J Roentgenol 1999; 173:591-596.
10. Ito K, Mitchell DG, Gabata T, Hussain SM. Expanded gallbladder fossa: simple MR imaging sign of cirrhosis. Radiology 1999; 211:723-726.
11. Sakamoto M, Hirohashi S, Shimosato Y. Early stages of multistep hepatocarcinogenesis: adenomatous hyperplasia and early hepatocellular carcinoma. Hum Pathol 1991; 22:172-178.
12. Hussain SM, Semelka RC. Liver masses. Magn Reson Imaging Clin N Am 2005; 13:255-275.
13. Jeong YY, Yim NY, Kang HK. Hepatocellular Carcinoma in the Cirrhotic Liver with Helical CT and MRI: Imaging Spectrum and Pitfalls of Cirrhosis-Related Nodules. AJR Am J Roentgenol 2005; 185:1024-1032.
14. Mitchell DG, Rubin R, Siegelman ES, Burk DL, Jr., Rifkin MD. Hepatocellular carcinoma within siderotic regenerative nodules: appearance as a nodule within a nodule on MR images. Radiology 1991; 178:101-103.
15. van den Bos IC, Hussain SM, Terkivatan T, Zondervan PE, de Man RA. Step-wise carcinogenesis of hepatocellular carcinoma in the cirrhotic liver: demonstration on serial MR imaging. J Magn Reson Imaging 2006; 24:1071-1080.
16. El-Serag HB. Hepatocellular carcinoma: recent trends in the United States. Gastroenterology 2004; 127:S27-34.
17. Fattovich G, Stroffolini T, Zagni I, Donato F. Hepatocellular carcinoma in cirrhosis: incidence and risk factors. Gastroenterology 2004; 127:S35-50.
18. Braga L, Guller U, Semelka RC. Modern hepatic imaging. Surg Clin North Am 2004; 84:375-400.
19. Mendez Romero A, Wunderink W, Hussain SM, et al. Stereotactic body radiation therapy for primary and metastatic liver tumors: A single institution phase i-ii study. Acta Oncol 2006; 45:831-837.
20. Sangro B, Mazzollini G, Prieto J. Future therapies for hepatocellular carcinoma. Eur J Gastroenterol Hepatol 2005; 17:515-521.
21. Bosch FX, Ribes J, Cleries R, Diaz M. Epidemiology of hepatocellular carcinoma. Clin Liver Dis 2005; 9:191-211, v.
22. van den Bos IC, Dwarkasing RS, Hussain SM, Krestin GP, Zondervan PE, De Man RA. Hepatocellular carcinoma: relation between tumour size and diagnostic features at state-of-the-art MR imaging. Radiological Society of North America, 92 nd Scientific Assembly and Annual Meeting, Chicago, USA. 2006:Proc. RSNA, 2007, 2713.
23. Verhoef C, de Man RA, Zondervan PE, Eijkemans MJ, Tilanus HW, IJzermans JN. Good outcomes after resection of large hepatocellular carcinoma in the non-cirrhotic liver. Dig Surg 2004; 21:380-386.
24. Rooks JB, Ory HW, Ishak KG, et al. Epidemiology of hepatocellular adenoma. The role of oral contraceptive use. Jama 1979; 242:644-648.
25. Edmondson HA, Henderson B, Benton B. Liver-cell adenomas associated with use of oral contraceptives. N Engl J Med 1976; 294:470-472.
26. Hussain SM, van den Bos IC, Dwarkasing RS, Kuiper JW, den Hollander J. Hepatocellular adenoma: findings at state-of-the-art magnetic resonance imaging, ultrasound, computed tomography and pathologic analysis. Eur Radiol 2006; 16:1873-1886.
27. Tao LC. Are oral contraceptive-associated liver cell adenomas premalignant? Acta Cytol 1992; 36: 338-344.
28. Prasad SR, Wang H, Rosas H, et al. Fat-containing lesions of the liver: radiologic-pathologic correlation. Radiographics 2005; 25:321-331.
29. Anthony PP. Tumours and tumour-like lesions of the liver and biliary tract: aetiology, epidemiology and pathology. In: MacSween RNM, Burt AD, Portmann BC, ed. Pathology of the liver: Churchill Livingstone, 2002; 711-775.
30. van den Bos IC, Hussain SM, Zondervan PE, Wielopolski PA, IJzermans JN, De Man RA. Hepatocellular adenoma and the surrounding liver: a spectrum of characteristic findings at state-of-the-art MR imaging, with pathologic correlation. International Society for Magnetic Resonance in Medicine, 14th Scientific Meeting and Exhibition, Seattle, Washington, USA. 2006:Proc Intl Soc Mag Reson Med, 2006; 2432.
31. Nguyen BN, Flejou JF, Terris B, Belghiti J, Degott C. Focal nodular hyperplasia of the liver: a comprehensive pathologic study of 305 lesions and recognition of new histologic forms. Am J Surg Pathol 1999; 23:1441-1454.
32. Hussain SM, Terkivatan T, Zondervan PE, et al. Focal nodular hyperplasia: findings at state-of-the-art MR imaging, US, CT, and pathologic analysis. Radiographics 2004; 24:3-17; discussion 18-19.
33. Terkivatan T, van den Bos IC, Hussain SM, Wielopolski PA, de Man RA, IJzermans JN. Focal nodular hyperplasia: lesion characteristics on state-of-the-art MRI including dynamic gadolinium-enhanced and superparamagnetic iron--oxide-uptake sequences in a prospective study. J Magn Reson Imaging 2006; 24:864-872.
34. Manfredi R, Barbaro B, Masselli G, Vecchioli A, Marano P. Magnetic resonance imaging of cholangiocarcinoma. Semin Liver Dis 2004; 24:155-164.

discussionPRIMARY HEPATOCELLULAR LESIONS, AN OVERVIEW

chapter8
SUMMARY

chapter8.1
summary

The purpose of this research project was 1) to improve insight in magnetic resonance (MR) imaging findings of primary hepatocellular lesions; 2) TO INCREASE AWARENESS IN SPECIFIC TUMOR FEATURES ON DIFFERENT MR IMAGING SEQUENCES INCLUDING CONTRAST-ENHANCED IMAGING;

3) to improve non-invasive diagnosis for these lesions through increased diagnostic confidence by the reading radiologist;

and 4) to develop hepatobiliary imaging at high magnetic field strength.

Chapter 1 provides an overview of the anatomy of the liver and the fundamentals of MR imaging in chapter **1.1**.; and an outline of the study in **chapter 1.2**.

Chapter 2 presents the results of a prospective study, which was designed to assess the MR imaging features of focal nodular hyperplasia (FNH) before and after administration of two contrast agents, including gadolinium-chelate and superparamagnetic iron-oxide particles (SPIO). This study indicates that the combination of dynamic gadolinium-enhanced imaging with T1- and T2-weighted imaging after administration of SPIO facilitates detection and characterization of FNH in a large majority of patients. It is shown that signal intensity of FNH prior to contrast differs only slightly from the surrounding liver; accumulation of fat is present in a minority of FNH; dynamic enhancement with a gadolinium-chelate is intense and homogeneous in the arterial phase with fading to near isointensity in the delayed phase; and uptake of SPIO in FNH is pronounced with improved conspicuity of central scar and septa.

Chapter 3 addresses the imaging findings of hepatocellular adenoma (HCA). In **chapter 3.1**, the most recent concepts on HCA are reviewed: the clinical presentation of HCA; the findings at pathology; recent literature on pathogenesis and transformation into HCC; and imaging findings at ultrasonography (US), computed tomography (CT), and MR imaging are discussed. The full spectrum of imaging findings using state-of-the-art MR imaging is shown, in comparison with US and CT. **Chapter 3.2** presents the results of a retrospective study which was designed to assess the spectrum of MR imaging findings of both HCA and the surrounding liver. It is shown that HCA has intratumoral fat in >70%; hyperintense signal intensity on T2-weighted fat-suppressed sequences and early arterial enhancement. The surrounding liver parenchyma shows changed segmental distribution; steatosis and inhomogeneous patchy arterial enhancement. These results indicate that in patients with HCA, both lesions as well as surrounding liver parenchyma show similar soft tissue and vascular abnormalities.

Chapter 4 illustrates three studies addressing the MR imaging findings of hepatocellular carcinoma (HCC), and a report of a rare hepatoid adenocarcinoma of the gallbladder as a mimicker of HCC. In **chapter 4.1**, the detailed imaging findings of developing hepatocellular carcinoma in cirrhosis at sequential MR imaging are described. In this study, state-of-the-art MR imaging displayed a spectrum of findings in the initial detection of developing HCC, including 1) localized fatty infiltration within a developing dysplastic nodule that gradually evolved into HCC in combination with a slowly increasing alpha-fetoprotein (AFP); 2) development of a focus of pathology-proven HCC with high signal intensity at T2-weighted imaging in a dysplastic nodule; 3) prominent neovasculature as the initial sign of developing, fast growing HCC, confirmed at histology after liver explantation. These findings provide insight in various pathways of step-wise carcinogenesis of developing hepatocellular carcinoma in cirrhosis, which may facilitate early detection, improve patient outcome, provide better identification of patients for follow-up and further explain the genetic heterogeneity of hepatocellular carcinoma. In **chapter 4.2**, the relationship between the size of hepatocellular carcinoma and specific MR imaging findings is studied. Related to the improved MR imaging hardware, coils and software, accelerated imaging sequences have become available which allow detection and characterization of smaller (malignant) primary liver lesions. These developments have had their influence on the MR imaging findings, both because of different magnetization properties of the tissues related to changed pulse techniques, but also because lesions are detected when they are still small. In this study it is shown that smaller HCCs often show lower signal on fat-suppressed T2-weighted sequences, more intense enhancement and less pronounced washout compared to larger tumors (typically >2 cm). In **chapter 4.3**, MR imaging findings are described in a young patient, who underwent Kasai portoenterostomy for biliary atresia as a neonate, and developed HCC as a rare complication. Kasai surgery has substantially increased the survival rates of this young patient group since its introduction in 1959, and consequently postpones subsequential liver transplantation. However, almost all patients develop features of end-stage liver disease and biliary cirrhosis. Since they are at risk for development of HCC, repeated sequential MR imaging exams of the native liver is necessary to monitor possible malignant transformation of liver nodules that may develop as a result of chronic cholestatic disease. **Chapter 4.4** illustrates the MR imaging findings of a large gallbladder tumor in a patient with no known liver disease and strongly elevated AFP. Given the combination of tumor morphology and location in the gallbladder, signal intensity, contrast enhancement, high AFP and histology, hepatoid adenocarcinoma (HAC) of the gallbladder was the most likely diagnosis. This is a rare form of adenocarcinoma with hepatoid differentiation of the tumor cells, which behaves and acts like HCC, but occurs in a multitude of organs outside the liver. Knowledge of these tumors is important, since HCC and HAC require a different therapeutic approach, especially in patients with non-cirrhotic liver disease.

Chapter 5 presents two optimization studies which were performed to improve hepatobiliary imaging at higher magnetic field strength. The introduction of 3.0T MRI systems has provided a number of potential advantages for abdominal MR imaging, related to doubled signal-to-noise ratio (SNR) which allows faster imaging and improved resolution. However, imaging at 3.0T posed some challenges as well, including increased inhomogeneity of the magnetic field, changed magnetic tissue characteristics and increased specific absorption rate (SAR) levels, which potentially result in heating effects within the scanned subject. This is most pronounced for SAR-intensive sequences such as T2-weighted fast spin-echo imaging. Since this sequence is essential for detection of focal liver lesions, the following two studies were designed to relieve some of the limitations for imaging at 3.0T whilst making use of the advantages of imaging at higher magnetic field strength.

In **chapter 5.1**, variable-rate-selective excitation (VERSE) radiofrequency (RF) pulses were assessed and compared to standard RF pulses, for fat-suppressed T2-weighted fast spin-echo (FSE) liver MR imaging at 3.0T. The results of this study indicate that the use of VERSE RF pulses provided significantly increased slice coverage with lower SAR. Compared to 1.5T, the increased SNR on 3.0T enabled thin-slice volumetric imaging of the liver within a single breath-hold, with multiplanar reformatting possibilities as post-processing tool. In **chapter 5.2**, breath-hold diffusion-weighted black-blood echo-planar-imaging (BBEPI) was evaluated as potential alternative for SAR-intensive spin-echo sequences at 3.0T. The results of this study indicate that BBEPI can be used for ultrafast, low SAR, thin-slice morphologic imaging of the entire liver in a single breath-hold at 3.0T.

Chapter 6 illustrates the current status of automated and color-coded post-processing techniques for analysis of dynamic multiphasic contrast-enhanced MR imaging of the liver. Post-processing of these images on dedicated workstations allows generation of time-intensity curves (TIC) as well as color-coded images, which provides useful information on (neo-) angiogenesis within a liver lesion, if necessary combined with information on enhancement patterns of surrounding liver parenchyma. Analysis of these images provides an easy to interpret schematic presentation of tumor behavior, providing additional characteristics for adequate differential diagnosis. Inclusion of TIC and color-coded images as part of the routine abdominal MR imaging work-up protocol may help to further improve the specificity of MR imaging findings and may facilitate the diagnostic work-up of disease for detection, staging, and monitoring of anti-tumor therapy.

in **chapter 7.1**; and an overview article discussing the MR imaging findings of primary hepatocellular lesions in **chapter 7.2**.

chapter8.2
samenvatting

Het doel van het in dit proefschrift beschreven onderzoek was om: 1) het inzicht in het aspect van primaire levertumoren bij beeldvorming met magnetische kernspinresonantie (magnetic resonance imaging, MRI) te verdiepen; 2) DE SPECIFIEKE MORFOLOGISCHE KENMERKEN VAN DEZE LESIES OP MRI TE VERDUIDELIJKEN;

3) de non-invasieve diagnostiek van primaire levertumoren met MRI verder te verbeteren door het vertrouwen in de diagnostische waarde van MRI te vergroten;
en 4) beeldvorming van de lever op hogere magnetische veldsterkte verder te ontwikkelen.

Hoofdstuk 1 behandelt de anatomie van de lever en basis principes van MRI in **hoofdstuk 1.1**, en geeft een overzicht van de verrichte studies in **hoofdstuk 1.2.**

Hoofdstuk 2 beschrijft de resultaten van een prospectieve studie, waarbij het doel was de MRI kenmerken van focale nodulaire hyperplasie (FNH) in beeld te brengen, voor en na toediening van twee verschillende contrast middelen. In deze studie werd gebruik gemaakt van een gadolinium-verbinding en een ijzerhoudend contrast middel (SPIO). De resultaten van dit onderzoek tonen dat de detectie en karakterisatie van FNH bevorderd wordt door een dynamisch MRI onderzoek met gadolinium te combineren met T1- en T2-gewogen sequenties na toediening van SPIO. Er wordt aangetoond dat FNH vóór contrast toediening nauwelijks te onderscheiden is van de rest van de lever; dat vetstapeling in FNH slechts in een klein percentage van de lesies aanwezig is; dat de aankleuring na gadolinium toediening in de arteriële fase intens en homogeen is; en dat er een sterke opname van SPIO contrast in FNH is, waarbij het karakteristieke centrale bindweefselschot en de verschillende bindweefselsepta duidelijker in beeld komen.

Hoofdstuk 3 beschrijft de karakteristieken van levercel adenomen (hepatocellular adenoma, HCA) bij beeldvorming. In **hoofdstuk 3.1** wordt een overzicht gegeven van de huidige denkbeelden wat betreft de histologische kenmerken van HCA, de onderliggende pathogenese en maligne degeneratie van HCA in hepatocellulair carcinoom (HCC); en het volledige spectrum van radiologische bevindingen van HCA op basis van de huidige literatuur, inclusief echografie, computer tomografie (CT) en MRI. **Hoofdstuk 3.2** beschrijft de resultaten van een retrospectieve studie die werd opgezet om de kenmerken op MRI van zowel HCA als de omgevende lever te bestuderen. Hierin wordt aangetoond dat vetstapeling aanwezig is in meer dan 70% van de HCA lesies; dat de signaal intensiteit van HCA op vetonderdrukte T2-gewogen sequenties hoog is; en de aankleuring in de arteriële fase vroeg is. Het omgevende leverparenchym vertoont vaak vetstapeling, een inhomogene vlekkige aankleuring in de arteriële fase, en een veranderde morfologie van de verschillende segmenten. Deze bevindingen tonen aan dat in patiënten met HCA zowel de lesies als de omgevende lever gelijksoortige veranderingen vertonen.

Hoofdstuk 4 beschrijft drie studies die de MRI karakteristieken van hepatocellulair carcinoom (HCC) onderzochten, en een rapportage van het zeldzame hepatoid adenocarcinoom van de galblaas als imitator van HCC. In **hoofdstuk 4.1** worden gedetailleerd de kenmerken van HCC in ontwikkeling bij onderliggende levercirrose beschreven, op opeenvolgende MRI onderzoeken. In dit onderzoek werd met behulp van MRI een spectrum van kenmerken van een zich ontwikkelend HCC gevisualiseerd: 1) focale vetinfiltratie in een dysplastische nodule, die langzaam in een HCC ontwikkelde terwijl het alfa-foetoproteine (AFP) gehalte in het bloed langzaam steeg; 2) ontwikkeling van een focus van HCC in een dysplastische nodule, met een hoge signaal intensiteit op de T2-gewogen sequentie; en 3) prominente neovascularisatie als initieel teken van een zich ontwikkelend, zeer snel groeiend HCC (histologisch bevestigd na levertransplantatie). Al deze bevindingen bieden verder inzicht in de verschillende reeksen van stapsgewijze ontwikkeling van HCC in een cirrotische lever. Dit bevordert de vroege diagnostiek van deze tumoren, kan dientengevolge de prognose voor de patiënt verbeteren en maakt het mogelijk om patiënten voor wie korte termijn follow-up noodzakelijk is, beter te herkennen. Verder wordt de genetische heterogeniteit die ten grondslag ligt aan de ontwikkeling van HCC door deze studie bevestigd. In **hoofdstuk 4.2** wordt de relatie tussen de grootte van een HCC en specifieke MRI bevindingen bestudeerd. Door de verbeteringen in MRI hardware, coils en software zijn zeer snelle beeldvormende sequenties ontwikkeld die de detectie en karakterisatie van kleinere (maligne) primaire levertumoren duidelijk hebben verbeterd. Deze ontwikkelingen hebben invloed gehad op de MRI kenmerken van deze tumoren, zowel doordat de magnetische karakteristieken van weefsels kunnen verschillen door het gebruik van andere puls sequentie technieken; maar ook omdat lesies worden ontdekt als ze nog klein zijn. In deze studie wordt aangetoond dat kleinere hepatocellulaire carcinomen (typisch kleiner dan 2 cm) in vergelijking met grotere tumoren vaak een lagere signaal intensiteit hebben op vetonderdrukte T2-gewogen sequenties, een sterkere aankleuring in de arteriële fase, en een minder sterk verlies van contrast in de late fase. In **hoofdstuk 4.3** worden de MRI bevindingen beschreven van een patiënt die als zuigeling een Kasai portoenterostomie voor een aangeboren afsluiting van de galwegen onderging, en die later een HCC ontwikkelde als zeldzame complicatie. Kasai chirurgie heeft sinds de introductie van deze techniek in 1959 de overleving van deze patiënten groep sterk verbeterd, mede doordat de noodzakelijke levertransplantatie vaak lang kan worden uitgesteld. Echter, bijna alle patiënten ontwikkelen eindstadium leverfalen en biliaire cirrose, waarbij ze een verhoogd risico op de ontwikkeling van HCC hebben. Herhaalde MRI vervolg onderzoeken lijken geïndiceerd in deze patiënten groep, om mogelijke kwaadaardige degeneratie binnen de nodules, die zich in de lever ontwikkelen als gevolg van de chronische galstuwing, zo vroeg mogelijk op het spoor te komen. In **hoofdstuk 4.4** worden de MRI bevindingen van een grote galblaastumor bij een patiënt met een blanco voorgeschiedenis en een sterk verhoogd serum AFP gehalte beschreven. De diagnose hepatoid adenocarcinoom (HAC) van de galblaas was in deze patiënt de meest waarschijnlijke diagnose, gezien de combinatie van tumor morfologie, lokalisatie, signaal intensiteit, aankleuring na contrast, AFP gehalte en histologische bevindingen. HAC is een zeldzaam adenocarcinoom met hepatoïde differentiatie van de tumor cellen, dat zich gedraagt als een HCC, maar kan voorkomen op meerdere plaatsen buiten de lever. Kennis van dergelijke tumoren is belangrijk, omdat HCC en HAC een verschillende therapeutische benadering vereisen, vooral in patiënten die een niet-cirrotische lever hebben.

Hoofdstuk 5 beschrijft twee optimalisatie studies die werden uitgevoerd met het doel de beeldvorming van de lever op hogere magnetische veldsterkte (3.0 Tesla (3.0T)) te verbeteren. De introductie van 3.0T MRI systemen heeft een aantal voordelen voor MRI van het abdomen, welke zijn gerelateerd aan een verdubbelde signaal-ruis verhouding (SNR). Deze hogere SNR maakt het mogelijk om in kortere tijd afbeeldingen te maken, met een hogere resolutie. Echter, beeldvorming op 3.0T bracht een aantal uitdagingen met zich mee, waaronder een verhoogde inhomogeniteit van het magnetisch veld, veranderde magnetische karakteristieken van de weefsels en toegenomen SAR (specific absorption rate levels), die mogelijk kunnen resulteren in gevaarlijke temperatuursstijging in weefsels. Het SAR effect is het meest uitgesproken voor T2-gewogen FSE (fast spin-echo) sequenties, welke juist zeer belangrijk zijn voor detectie van focale leverafwijkingen. Om dit probleem verder te bestuderen en oplossingen te genereren, werden de volgende twee studies verricht. In **hoofdstuk 5.1** wordt de VERSE (variable-rate-selective excitation) radiofrequentie (RF) puls techniek geëvalueerd en vergeleken met standaard RF pulsen, en toegepast in vetonderdrukte T2-gewogen FSE voor afbeelding van de lever op 3.0T. De resultaten van deze studie geven aan dat het gebruik van VERSE RF pulsen in een duidelijk verbeterd anatomisch bereik resulteert, en tegelijk in een een lager SAR gehalte. Ook maakte de verhoogde SNR op 3.0T het mogelijk om met gebruik van VERSE RF pulsen afbeeldingen van de lever te maken met zeer dunne coupes, die in verschillende richtingen konden worden gereconstrueerd. In **hoofdstuk 5.2** wordt een andere techniek geëvalueerd als potentieel alternatief voor sequenties met hoog SAR gehalte, voor beeldvorming met een 3.0T magneet, name-

lijk de breath-hold diffusion-weighted black-blood echo-planar-imaging (BBEPI). De resultaten van dit onderzoek geven aan dat BBEPI gebruikt kan worden voor het maken van ultrasnelle afbeeldingen van de gehele lever in een enkele adempauze, waarbij zeer dunne coupes vervaardigd kunnen worden en de SAR laag blijft.

Hoofdstuk 6 illustreert de huidige stand van zaken omtrent de geautomatiseerde en kleur-gecodeerde post-processing technieken voor analyse van dynamische multifasische contrast-versterkte MRI van de lever. Post-processing van deze MRI beelden maakt het mogelijk om zogenaamde "time-intensity curves" (TIC) en kleur-gecodeerde afbeeldingen te vervaardigen op speciale werkstations. Dergelijke afbeeldingen verschaffen aanvullend inzicht in het aankleuringspatroon van een leverlesie, alsmede informatie over het aankleuringspatroon van de omgevende lever. Op deze wijze kunnen makkelijk te interpreteren, schematische representaties worden gegeven van het tumor gedrag, hetgeen verder kan bijdragen aan de differentiële diagnostiek. De routine toepassing van deze post-processing technieken in MRI protocollen kan de MRI diagnostiek van focale leverafwijkingen verbeteren, en de werkwijze omtrent lesie-detectie, tumor stagering en therapie-monitoring vergemakkelijken.

In **hoofdstuk 7.1**; en een overzichtsartikel over de MRI kenmerken van primaire hepatocellulaire tumoren in **hoofdstuk 7.2**.

chapter9
APPENDIX

chapter9.1
dankwoord

Dit proefschrift was nooit tot stand gekomen

ZONDER DE HULP, STEUN EN INSPIRATIE VAN VELEN, VAN WIE IK ENKELEN IN HET BIJZONDER ZOU WILLEN BEDANKEN.

Prof.dr. G.P. Krestin; u bent mijn opleider, ons afdelingshoofd en mijn promotor, een man met vele hoeden op. Dank u voor al uw tijd, alles wat ik van u heb mogen leren, en dank u voor de immer openstaande deur en dat ik u vele malen heb mogen lastigvallen met vragen van diverse aard. Ook wil ik u bedanken voor de extra tijd die ik van u kreeg om dit proefschrift succesvol te kunnen afronden;

Prof.dr. S.M. Hussain; beste Shahid, jouw passie voor het vak Radiologie, en in het bijzonder MRI van hepatobiliaire ziekten heeft mij vanaf het begin van de opleiding beïnvloed. Jouw liefde voor de wetenschap en drang naar verbetering van de patiëntenzorg heeft velen weten te inspireren! Zonder jouw bezielende begeleiding was dit proefschrift niet in deze vorm tot stand gekomen. Dank voor de vele uren brainstormen, dank voor het stroomlijnen van mijn soms overenthousiaste ideeën en dank voor het altijd beschikbaar zijn voor overleg via telefoon of email in de periode nadat je naar de Verenigde Staten verhuisd was;

Dr. R.A. de Man; beste Rob, jouw immers vriendelijke en bescheiden opstelling heeft al velen voor mij geinspireerd. Dank voor de vele waardevolle adviezen die ik van je mocht ontvangen. Je open blik, je grote empathie en je sterk ontwikkeld invoelend vermogen maken je niet alleen tot een exceptionele geneesheer, maar ook een bijzonder gewaardeerde collega. Bedankt;

Dr. P.A. Wielopolski; beste Piotr; jouw passie voor de complexe techniek, fysica en formules die onherroepelijk verbonden zijn met het maken van afbeeldingen met behulp van MRI is belangrijk voor velen. Jouw geduld om te trachten aan Radiologen inzicht te verschaffen in deze complexe materie is bewonderenswaardig, ook omdat dit niet altijd even succesvol is. Dank voor de vele uren achter de MRI scanner, het brainstormen over nieuwe studies, en het bedenken van oplossingen voor afbeeldend onderzoek van de lever op hogere veldsterkte;

Prof.dr. P.M.T. Pattynama, prof.dr. C. van Kuijk, prof.dr. B.E. van Beers, en prof.dr. A.J. van der Lely; dank voor het zitting nemen in de promotiecommissie;

Prof.dr. J.N.M. IJzermans; beste Jan, als chirurg en voorzitter van de Lever Tumor Werkgroep ben je van grote importantie voor het niveau van de leverdiagnostiek en –therapie aan het Erasmus MC. Dank voor je adviezen, de inspiratie en het prettige contact. Dank voor het vertrouwen dat je in mij stelde toen ik na het vertrek van Shahid samen met Roy de wekelijkse leverbespreking mocht gaan verzorgen;

Drs. R.S. Dwarkasing; beste Roy, ik ontmoette je als ouderejaars assistent in opleiding, en had toen al de bewondering voor je die ik nu nog steeds heb. De precisie en toegewijdheid waarmee je je aan studies van diverse aard wijdt pas je ook toe in de gezondheidszorg, en dat maakt je tot een radioloog van bijzonder niveau. Dank voor alles wat ik van je heb geleerd in de uren dat wij de leverbespreking voorbereidden, dank voor je vertrouwen en dank voor je deelname aan enkele van onze studies. Ik wens je heel veel succes toe met de afronding van je eigen promotie;

De leden van de Lever Tumor Werkgroep, voor de steun en prettige samenwerking in de afgelopen anderhalf jaar;

Mijn vader Antonie, mijn moeder Merel, mijn zus Sishta, mijn broer Argh en natuurlijk ook Bas en Petra, voor hun onvoorwaardelijke liefde;

Mijn paranimfen Marion en Meike, voor het naast mij staan tijdens de verdediging van dit proefschrift en voor de vele uren die wij samen hebben doorgebracht in onze promotietijd, op congres, op cursus, tussendoor, of in de koffiebar. Dat is van onschatbare waarde geweest voor mij!;

Mijn lieve vrienden Martine en Jeroen, voor de broodnodige ontspanning en vele uurtjes kletsen;

Marije en Tamar, voor de ouderwetse meidenavonden (“net als vroeger”) die nu hopelijk weer wat veelvuldiger zullen plaatsvinden;

Johanna, voor de inspiratie die je mij altijd geeft, al sinds wij elkaar als tieners ontmoetten. Ik vind het fantastisch dat je helemaal naar Nederland bent gevlogen voor het bijwonen van mijn promotie!;

Maaike, omdat je hier zo van had genoten;

Alle assistenten Radiologie, voor de gezelligheid en steun;

Eva, voor het mogelijk maken van wat onmogelijk leek;

Het stafsecretariaat van de afdeling Radiologie voor de ondersteuning in al het papierwerk dat onherroepelijk verbonden is aan een promotie;

De MRI laboranten, voor hun grenzeloze ondersteuning, enthousiasme en hulp;

Jepke de Berg, voor het introduceren van het vak Radiologie. Jij bent mijn Radiologische vader!;

Ton Everaers, voor het verzorgen van de lay-out van dit boekje. Jij hebt maar een half woord nodig om precies aan te voelen wat iemand wil: dat is een bijzonder talent!;

Het Trialbureau, Caroline en Wibeke, voor het verzorgen van alle ondersteuning;

De medewerkers van “Research Office Radiologie”; Linda, Frans en Erik-Jan, voor de geweldige steun aan alle promovendi. Ook al worden jullie in de wandelgangen soms de research politie genoemd: zonder jullie zou het allemaal een stuk minder leuk en gezellig zijn. Dank! ;

En alle anderen, die ik hier niet bij naam heb kunnen noemen.

India

chapter9.2 publications

Publications

Terkivatan T, **Van den Bos IC**, Hussain SM, Wielopolski PA, De Man RA, IJzermans JNM. Focal nodular hyperplasia: lesion characteristics at state-of-the-art MR imaging including dynamic gadolinium-enhanced and superparamagnetic iron-oxide-uptake sequences in a prospective study. JMRI 2006 Aug 31;24(4): 864-872.

Hussain SM, **Van den Bos IC**, Dwarkasing RS, Kuiper JW, Den Hollander J. Hepatocellular adenoma: findings at ultrasound, computed tomography, MR imaging and pathologic analysis. European Radiology, 2006 Sep; 16(9): 1873-86.

Van den Bos IC, Hussain SM, Zondervan PE, IJzermans JNM, De Man RA. Hepatocellular adenoma and the surrounding liver: a spectrum of characteristic findings at state-of-the-art MR imaging, with pathologic correlation. Submitted.

Van den Bos IC, Hussain SM, Terkivatan T, Zondervan PE, De Man RA. Step-wise carcinogenesis of hepatocellular carcinoma in the cirrhotic liver: demonstration on serial MR imaging. JMRI 2006 Nov; 24(5): 1071-80.

Van den Bos IC, Hussain SM, Dwarkasing RS, Hop WCJ, De Man RA, IJzermans JNM, Walker CW, Krestin GP. MR imaging of hepatocellular carcinoma: relationship between lesion size and imaging findings, including signal intensity and dynamic enhancement patterns. Journal of Magnetic Resonance Imaging, in press.

Hol L, **Van den Bos IC**, Hussain SM, Zondervan PE, De Man RA. Hepatocellular carcinoma complicating biliary atresia after Kasai portoenterostomy. Submitted.

Van den Bos IC, Hussain SM, Dwarkasing RS, Zondervan PE, Metselaar H, De Man RA. Hepatoid adenocarcinoma of the gallbladder: a mimicker of hepatocellular carcinoma. British Journal of Radiology, in press.

Van den Bos IC, Hussain SM, Krestin GP, Wielopolski PA. Extending slice coverage for breath-hold fat-suppressed T2-weighted fast spin-echo of the liver at 3.0T: application of variable-rate selective excitation (VERSE) RF pulses. Submitted.

Van den Bos IC, Hussain SM, Krestin GP, Wielopolski PA. Liver Imaging at 3.0T: Diffusion-induced black-blood echo-planar imaging with large anatomic volumetric coverage as an alternative for specific absorption rate (SAR) -intensive echo-train spin-echo sequences. Submitted.

Wang L, **Van den Bos IC**, Hussain SM, Pattynama PMT, Vogel MW, Krestin GP. Post-processing of dynamic gadolinium-enhanced MRI exams of the liver: explanation and potential clinical applications of color-coded qualitative and quantitative analysis. Accepted for publication in Acta Radiologica.

Van den Bos IC, Hussain SM, De Man RA, Zondervan PE, IJzermans JNM, Krestin GP. Primary hepatocellular lesions: imaging findings on state-of-the-art MRI, with pathologic correlation. Current Problems in Diagnostic Radiology, in press.

Van den Bos IC, Hussain SM, De Man RA, Zondervan PE, IJzermans JNM, Preda A, Krestin GP. MR imaging of liver lesions: exceptions and atypical lesions. Current Problems in Diagnostic Radiology, in press.

Hussain SM, **Van den Bos IC**, Oliveto JM, Martin DR. MR imaging of the female pelvis at 3.0T: Initial Experience. Magnetic Resonance Imaging Clinics of North America, in press.

Van den Bos IC, Khanolkar-Young S, Das PK, Lockwood DNJ. Immunohistochemical detection of PGL-I, LAM, 30 kD and 65 kD antigens in leprosy infected paraffin preserved skin and nerve sections. Leprosy Review, 1999; 70-3: 272-281.

Terkivatan T, **Van den Bos IC**, Hussain SM, De Man RA, IJzermans JNM. Work-up of focal liver lesions: is there still a place for liver biopsy in the era of modern MRI? Submitted.

Weustink AC, Hussain SM, **Van den Bos IC**, Den Bakker MA, Verhoef C. Unusual findings of a liver lesion in a patient with known colorectal malignancy: implications for imaging work-up and patient management. Submitted.

chapter9.3
curriculum vitae

Born on April 11th 1972 in Rotterdam, the Netherlands, INDRA CÉLINE VAN DEN BOS ATTENDED SECONDARY SCHOOL IN HEESWIJK-DINTHER AND WILLEMSTAD, CURAÇAO (DUTCH ANTILLES),

before graduating from the Christelijk Lyceum in Zeist (the Netherlands). She went to medical school at the Erasmus University in Rotterdam, where she graduated in 1996.

During her studies, she interned at the Instituto Tor Vergata in Rome. Her final thesis project involved the development and implementation of a serological test to diagnose leprosy, for which she spent 6 months in Brazil doing field research (Instituto Lauro de Souza Lima, prof.dr. D.V. Opromolla).
Upon graduation, Indra spent one year abroad, including six months doing research at the Institute for Hygiene and Tropical Medicine in London (dr. D.N. Lockwood). The results of her research on leprosy-infected paraffin-embedded tissue samples were published in Leprosy Review. Next, she completed her medical internships at the Sint Elisabeth Hospital in Curaçao (prof.dr. R.A. Royer), under auspices of the Rijksuniversiteit in Groningen, where she graduated cum laude in September of 1999.
In 2000, she moved to Lisbon, Portugal, where she worked as an emergency room physician at the University Hospital Santa Maria (dr. C. França), and completed a post-graduate study in tropical medicine at the Instituto de Higiene e Medicina Tropical (prof. dr. J. Atouguia).
In November 2001, Indra returned to the Netherlands to start a clinical training in radiology at the Erasmus MC, University Medical Center in Rotterdam (prof. dr. G.P. Krestin), which she completed in May 2007. During her training, she spent one year working as a radiologist-in-training at the Albert Schweizer Hospital in Dordrecht (dr. R.A. de Vries).

In 2004, Indra started her doctoral research on magnetic resonance imaging in the work-up of primary hepatocellular tumors (prof.dr. S.M. Hussain). The results of her research are presented in this thesis, and have also resulted in several still ongoing studies.

Financial support WAS GENEROUSLY PROVIDED BY:

Guerbet Nederland BV
Stichting Lever Onderzoek
GE Healthcare
Schering Nederland BV
Siemens Nederland NV
Toshiba Medical Systems Nederland